

Metrics reloaded: Pitfalls and recommendations for image analysis validation

LENA MAIER-HEIN^{*†}, German Cancer Research Center (DKFZ), Germany, Heidelberg University, Germany, and National Center for Tumor Diseases (NCT), Germany
ANNIKA REINKE^{*}, German Cancer Research Center (DKFZ), Germany and Heidelberg University, Germany
EVANGELIA CHRISTODOULOU, German Cancer Research Center (DKFZ), Germany
BEN GLOCKER, Imperial College London, UK
PATRICK GODAU, German Cancer Research Center (DKFZ), Germany and Heidelberg University, Germany
FABIAN ISENSEE, German Cancer Research Center (DKFZ), Germany
JENS KLEESIEK, University Medicine Essen, Germany
MICHAL KOZUBEK, Masaryk University, Czech Republic
MAURICIO REYES, University of Bern, Switzerland
MICHAEL A. RIEGLER, Simula Metropolitan Center for Digital Engineering, Norway and UiT The Arctic University of Norway, Norway
MANUEL WIESENFARTH, German Cancer Research Center (DKFZ), Germany
MICHAEL BAUMGARTNER, German Cancer Research Center (DKFZ), Germany
MATTHIAS EISENMANN, German Cancer Research Center (DKFZ), Germany
DOREEN HECKMANN-NÖTZEL, German Cancer Research Center (DKFZ), Germany and National Center for Tumor Diseases (NCT), Germany
A. EMRE KAVUR, German Cancer Research Center (DKFZ), Germany
TIM RÄDSCH, German Cancer Research Center (DKFZ), Germany
MINU D. TIZABI, German Cancer Research Center (DKFZ), Germany
LAURA ACION, CONICET – Universidad de Buenos Aires, Argentina and University of Iowa, USA
MICHELA ANTONELLI, King's College London, UK and University College London, UK
TAL ARBEL, McGill University, Canada
SPYRIDON BAKAS, University of Pennsylvania, USA and Perelman School of Medicine at the University of Pennsylvania, USA
PETER BANKHEAD, University of Edinburgh, UK
ARRIEL BENIS, Holon Institute of Technology, Israel
M. JORGE CARDOSO, King's College London, UK and University College London, UK
VERONIKA CHEPLYGINA, IT University of Copenhagen, Denmark
BETH CIMINI, Broad Institute of MIT and Harvard, USA
GARY S. COLLINS, University of Oxford, UK
KEYVAN FARAHANI, National Cancer Institute, USA
BRAM VAN GINNEKEN, Fraunhofer MEVIS, Germany and Radboud University Medical Center, The Netherlands
DANIEL A. HASHIMOTO, Case Western Reserve University School of Medicine, USA
MICHAEL M. HOFFMAN, University Health Network, Canada, University of Toronto, Canada, and Vector Institute, Canada
MEREL HUISMAN, Radboud University Medical Center, The Netherlands
PIERRE JANNIN, Université de Rennes 1, Inserm, France
CHARLES E. KAHN, University of Pennsylvania, USA
ALEXANDROS KARARGYRIS, IHU Strasbourg, France
ALAN KARTHIKESALINGAM, Google Health Deepmind, UK
HANNES KENNGOTT, Heidelberg University Hospital, Germany
ANNETTE KOPP-SCHNEIDER, German Cancer Research Center (DKFZ), Germany
ANNA KRESHUK, European Molecular Biology Laboratory (EMBL), Germany
TAHSIN KURC, Stony Brook University, USA
BENNETT A. LANDMAN, Vanderbilt University, USA
GEERT LITJENS, Radboud University Medical Center, The Netherlands
AMIN MADANI, University Health Network, Canada

KLAUS MAIER-HEIN, German Cancer Research Center (DKFZ), Germany
ANNE L. MARTEL, Sunnybrook Research Institute, Canada and University of Toronto, Canada
PETER MATTSON, Google, US
ERIK MEIJERING, University of New South Wales, Australia
BJOERN MENZE, University of Zurich, Switzerland
DAVID MOHER, Ottawa Hospital Research Institute, Canada and University of Ottawa, Canada
KAREL G.M. MOONS, UMC Utrecht, University Utrecht, The Netherlands
HENNING MÜLLER, University of Applied Sciences Western Switzerland (HES-SO), Switzerland and University of Geneva, Switzerland
BRENNAN NICHYPORUK, MILA (Quebec Artificial Intelligence Institute), Canada
FELIX NICKEL, Heidelberg University Hospital, Germany
JENS PETERSEN, German Cancer Research Center (DKFZ), Germany
NASIR RAJPOOT, University of Warwick, UK
NICOLA RIEKE, NVIDIA GmbH, Germany
JULIO SAEZ-RODRIGUEZ, Heidelberg University, Germany, Heidelberg University Hospital, Germany, and BioQuant, Germany
CLARISA SÁNCHEZ GUTIÉRREZ, University of Amsterdam, The Netherlands
SHRAVYA SHETTY, Google, US
MAARTEN VAN SMEDEN, University Medical Center Utrecht, The Netherlands
CAROLE H. SUDRE, University College London, UK and King's College London, UK
RONALD M. SUMMERS, National Institutes of Health, USA
ABDEL A. TAHA,, Austria
SOTIRIOS A. TSAFTARIS, The University of Edinburgh, Scotland
BEN VAN CALSTER, Katholieke Universiteit (KU) Leuven, Belgium and Leiden University Medical Center, The Netherlands
GAËL VAROQUAUX, INRIA Saclay-Île de France, France
PAUL F. JÄGER, German Cancer Research Center (DKFZ), Germany

Disclaimer

This document reflects intermediate results of a multi-stage Delphi process on metrics conducted by an international consortium of more than 60 image analysis experts. By making the current status of the Delphi process publicly accessible, we seek to obtain constructive feedback from the community in order to optimize the best practice recommendations in the final version of the paper. Helpful feedback will be reflected in the acknowledgements (if desired by the community member). In the case of substantial contributions, co-authorship can be considered.

*Shared first authors.

†The complete list of affiliations can be found in App. A.

Abstract: The field of automatic biomedical image analysis crucially depends on robust and meaningful performance metrics for algorithm validation. Current metric usage, however, is often ill-informed and does not reflect the underlying domain interest. Here, we present a comprehensive framework that guides researchers towards choosing performance metrics in a problem-aware manner. Specifically, we focus on biomedical image analysis problems that can be interpreted as a classification task at image, object or pixel level. The framework first compiles domain interest-, target structure-, data set- and algorithm output-related properties of a given problem into a *problem fingerprint*, while also mapping it to the appropriate *problem category*, namely *image-level classification*, *semantic segmentation*, *instance segmentation*, or *object detection*. It then guides users through the process of selecting and applying a set of appropriate validation metrics while making them aware of potential pitfalls related to individual choices. In this paper, we describe the current status of the *Metrics Reloaded* recommendation framework, with the goal of obtaining constructive feedback from the image analysis community. The current version has been developed within an international consortium of more than 60 image analysis experts and will be made openly available as a user-friendly toolkit after community-driven optimization.

Keywords: Challenges, Validation, Metrics, Good Scientific Practice, Biomedical Image Processing, Computer Vision, Classification, Segmentation, Instance Segmentation, Semantic Segmentation, Detection, Localization, Medical Imaging, Biological Imaging

CONTENTS

Abstract	2
1 Introduction	5
2 Metric Recommendation Framework	9
2.1 General Instructions and Terminology	9
2.2 Problem Fingerprinting	13
2.3 Metric Selection	16
3 Recommendations for Image-level Classification	16
4 Recommendations for Semantic Segmentation	20
5 Recommendations for Object Detection	24
6 Recommendations for Instance Segmentation	27
7 Cross-category Recommendations	29
7.1 Selecting Non-Reference-Based Metrics	29
7.2 Determining the Global Decision Threshold	29
7.3 Aggregating Metric Values	29
7.4 Reporting Metric Results	29
8 Current Status and How to Provide Feedback	30
References	30
Appendix	36
A Full Author Affiliations	36
B Symbol References	39
C Acronyms	40
D Problem Category-specific Fingerprints	42
E Decision Guides	50
F Instantiation of the Framework for Concrete Biomedical Problems	57
G Fundamentals of Metrics	61
H Pitfalls of Metrics	87

1 INTRODUCTION

Validation of biological and medical image analysis algorithms is of the utmost importance for making scientific progress and for translating methodological research into practice. Validation metrics¹, the measures according to which performance of algorithms is quantified, constitute the core component of validation design. However, an increasing body of work shows that the metrics used often do not appropriately reflect the underlying biomedical problems, diminishing the validity of the investigated algorithms [26, 33, 39, 51, 52, 57, 58, 94]. This especially holds true for so-called challenges, internationally respected competitions that have over the last few years become the de facto standard for comparative performance assessment in the field. These challenges are often published in prestigious journals [20, 77, 92] and receive tremendous attention from both the scientific community and industry. Despite their crucial importance, a number of shortcomings in design and quality control have recently been unveiled, notably by a multi-center initiative [57] performing the first comprehensive evaluation of biomedical image analysis challenges. Among other things, an international survey performed as part of the study revealed the choice of inappropriate metrics as a core problem related to performance assessment in biomedical image analysis. Common issues with respect to metric choice include (see Fig. 1):

Inappropriate phrasing of the problem: The chosen metrics do not always reflect the biomedical need. For example, the popular segmentation metric Dice Similarity Coefficient (DSC) is frequently chosen as a metric for object detection problems although it does not reflect the critical need of detecting as many structure instances² as possible (Fig. 1b, top).

Poor metric selection: Certain characteristics of a given biomedical problem render particular metrics inadequate. Mathematical metric properties are often neglected, for example when applying the DSC in the presence of particularly small structures (Fig. 1b, middle).

Poor metric application: Applying metrics to a given data set comes with several pitfalls. For example, a common flaw is related to ignoring hierarchical data structure, as in data from multiple hospitals or a variable number of images per patient (Fig. 1b, bottom), when aggregating metric values.

Furthermore, poor validation design choices and even wrong metric definitions are often propagated. One impressive example is the successive modification of the "Segmentation Accuracy" metric proposed by the PascalVOC challenge [31]: A widely-known challenge on cell segmentation [15] substantially altered the originally intended use of pixel-level validation by employing the metric at object level without explicitly commenting on the changes in the manuscript. A subsequent popular competition [81] followed this altered usage and further changed the name to "Average Precision" (AP), a highly confusing change given that this name is already occupied by a fundamentally different and widely accepted metric for object-level validation [31] (Fig. 39). The altered naming and usage have since been adopted by further prominent studies and competitions [49, 87], indicating that the cell segmentation community currently broadly relies on a metric with inappropriate naming and unreflected properties.³

¹Not to be confused with distance metrics in the pure mathematical sense.

²An instance refers to an object or structure in an image.

³In the meantime, [15] corrected their primary metric to F₁ Score and [81] corrected the name of their metric to "Accuracy".

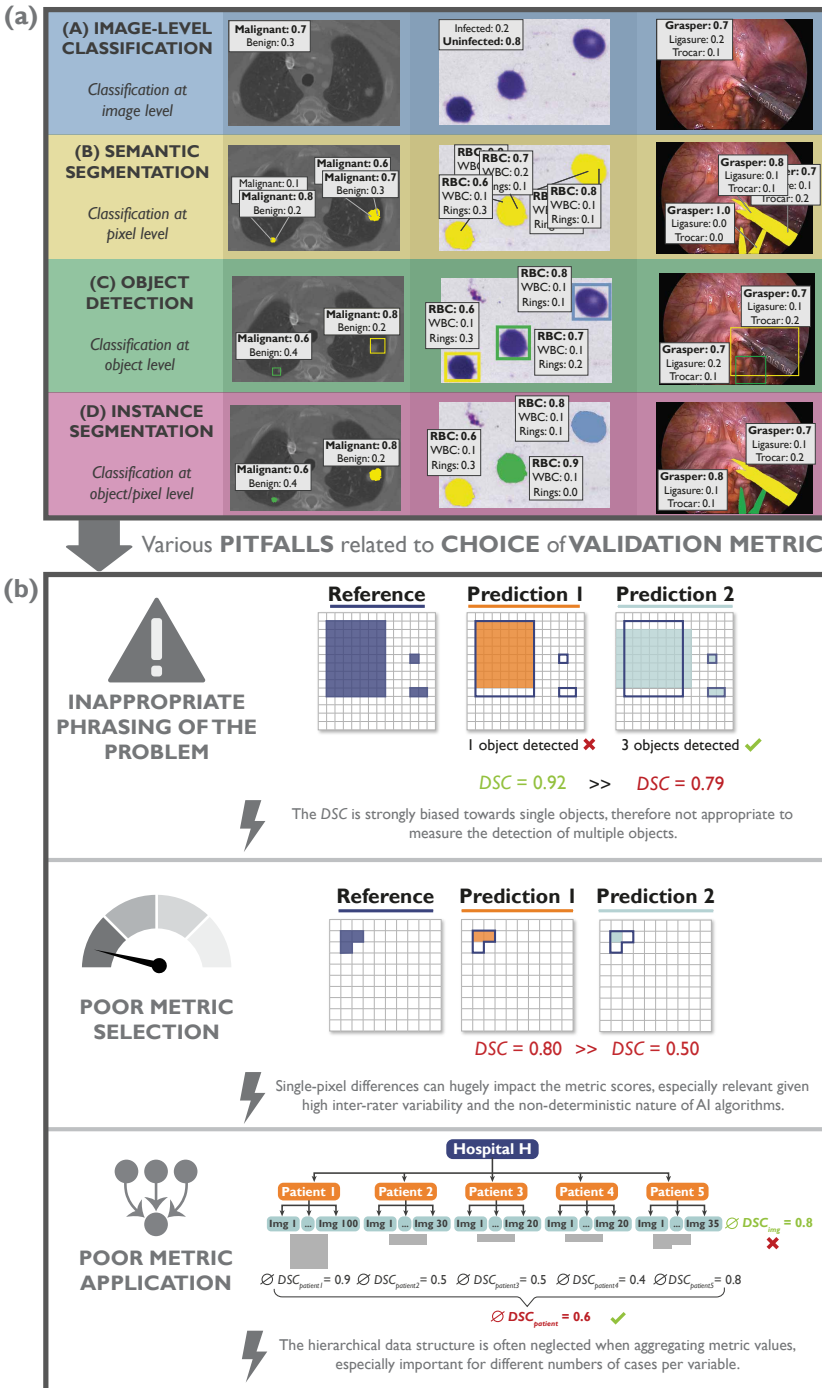


Fig. 1. Pitfalls related to validation metrics in image analysis. a) This paper addresses biomedical problems that can be interpreted as a classification task. Specifically, we focus on problems with categorical labels at various scales (image level vs. pixel level vs. object level). b) Common problems typically arise from (top) inappropriate phrasing of the problem (here: object detection confused with semantic segmentation), (middle) poor metric selection (here: neglecting the small size of structures) and (bottom) poor metric application (here: inappropriate aggregation scheme).

As a result of all of these flaws related to metric selection and application, the scientific community requests a priority to be set on best practice recommendations for metrics [57]. To address this community need, we have compiled an international consortium of more than 60 image analysis experts and representing a large number of relevant biomedical imaging initiatives and societies. The core mission is to provide researchers with guidelines and tools to choose the performance metrics in a problem-aware manner. For the present work, we focused on biomedical problems that can be interpreted as a classification task and are thus mathematically closely related. Specifically, we included problems with categorical labels at various scales, as illustrated in Fig. 1. Based on a kickoff workshop held in December 2020, the framework for metric recommendations was developed with the help of a multi-stage Delphi process [13] for consensus building.

The core of our framework is the *problem fingerprinting*, which is the generation of a structured representation of the given biomedical problem that captures all properties that are relevant for the purpose of metric selection (Fig. 3). Specifically, the fingerprint comprises *domain interest-related* properties, such as the particular importance of structure boundaries, *target structure-related* properties, such as the size of the structures relative to the image grid size, *data set-related* properties, such as class imbalance, as well as *algorithm output-related* properties, such as the theoretical possibility of the algorithm output not containing any target structure. Based on the problem fingerprint, the user is then guided through the process of selecting an appropriate set of metrics while considering potential pitfalls related to the specific characteristics of the underlying biomedical problem (Fig. 2). In this paper, we consider problems in which categorical output for a given n -dimensional input image (possibly enhanced with context information) is sought at pixel, object or image level. More specifically, we put a focus on problems that can be assigned to one of the following four problem categories: image-level classification, semantic segmentation, object detection or instance segmentation problem. Examples for the fields of radiology, biology and surgery, respectively, are provided in Fig. 1.

The following section 2 presents the general concept of the recommendation framework, while sections 3-6 present the specific recommendations for the four problem categories. Cross-topic recommendations are then summarized in section 7.

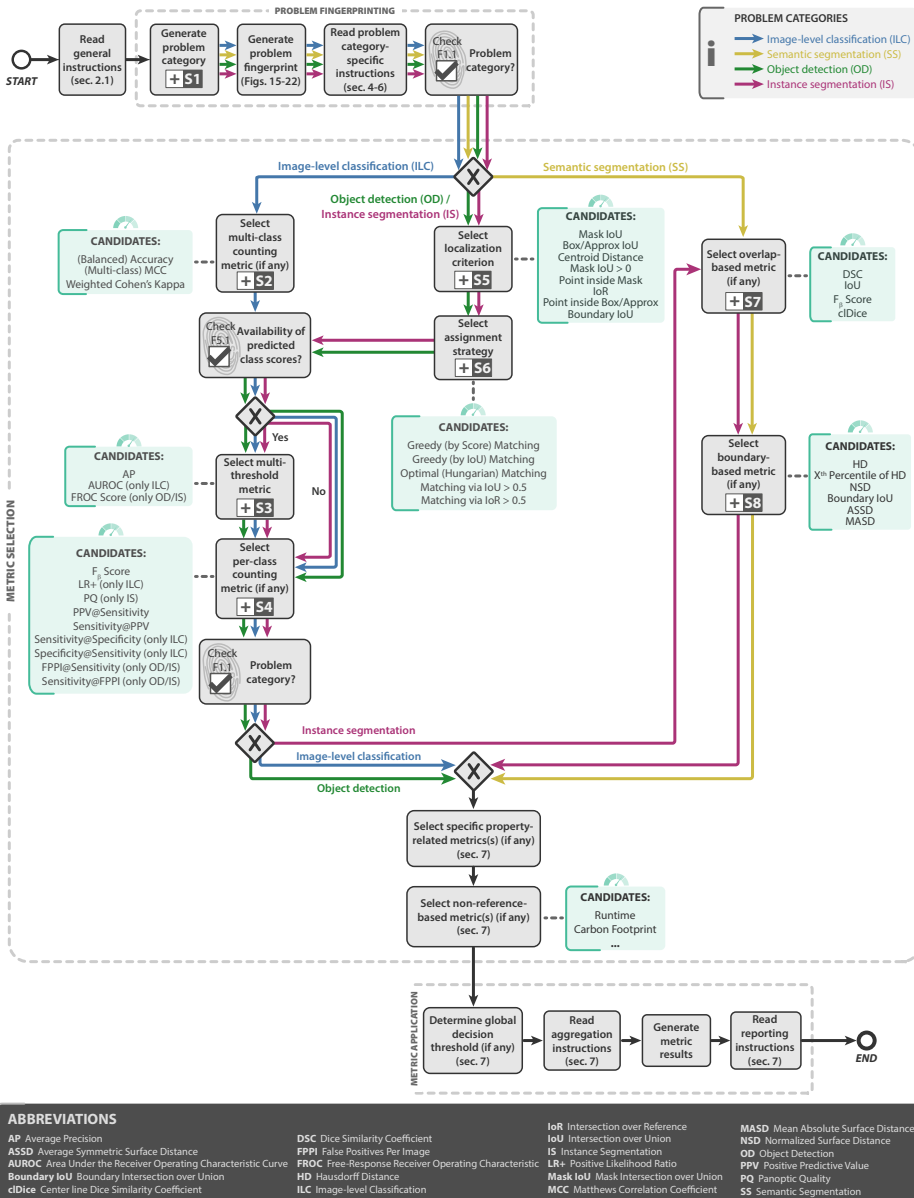


Fig. 2. **Metrics Reloaded** recommendation framework from a user’s perspective. Initially, the characteristics of the given biomedical problem are captured in a *problem fingerprint*, which is a structured representation of the given biomedical problem. The problem fingerprinting further comprises a step of mapping the given biomedical image analysis problem to the appropriate image *problem category*, namely *image-level classification (ILC)* (blue arrows →), *semantic segmentation (SS)* (yellow arrows →), *instance segmentation (IS)* (pink arrows →), or *object detection (OD)* (green arrows →). Based on the problem fingerprint (referred to with “FX.Y”, where F indicates a fingerprint and X and Y are placeholders for numbers, see App. D), the user is guided through the process of selecting and applying an appropriate set of validation metrics while being made aware of potential pitfalls related to individual choices. All subprocesses, indicated by the \boxplus -symbol, are provided in dedicated figures or sections. An overview of the symbols used in the process diagram is provided in Fig. 13.

2 METRIC RECOMMENDATION FRAMEWORK

The purpose of our framework is to enable users to make educated decisions on which validation metrics to select for a given biomedical problem. The overall process is depicted in Fig. 2. A user should begin by reading the general instructions of the recommendation framework, provided in Sec. 2.1. Next, a *problem fingerprint* should be generated as a structured representation of the given biomedical, as detailed in Sec. 2.2. Based on the problem fingerprint, the user is then guided through the process of selecting an appropriate set of metrics as summarized in Sec. 2.3. The problem category-specific recommendations are provided separately in Sec. 3-6. Finally, the user is supported in applying the metrics and reporting the results according to cross-topic recommendations, summarized in Sec. 7).

2.1 General Instructions and Terminology

A user of our recommendation framework should begin by reading the following instructions, which present fundamental terminology as well as the guiding principles that the framework is based on.

2.1.1 Fundamentals.

Problem categories. In this paper, we consider problems of the following four categories (see Figs. 1a and 12 for examples).

Image-level classification refers to the assignment of one or multiple category labels to the entire image. Deciding on the presence or absence of a certain condition/pathology would be a typical example, such as disease classification in dermoscopic images, or fracture detection on X-ray images.

Semantic segmentation refers to the assignment of one or multiple category labels to each pixel. Common examples include organ segmentation in Computed Tomography (CT) images and labeling full laparoscopic image frames with all structures/organs/pathologies that appear (e.g. for the purpose of surgical scene understanding or autonomous robotics).

Object detection refers to the detection and localization of structures of one or multiple categories. The detection and bounding box-based localization of polyps in colonoscopy sequences is a popular example.

Instance segmentation refers to the detection and delineation of each distinct object of a particular class. It can be regarded as delivering the tasks of object detection and semantic segmentation at the same time. In contrast to object detection, instance segmentation also involves the accurate marking of the object boundary. In contrast to semantic segmentation, it distinguishes different instances of the same class. Cell nuclei segmentation with a subsequent goal of cell tracking or counting is a common example.

Notably, the four different categories are mathematically closely related as illustrated in Fig. 27. A comprehensive description of the problem categories can be found in App. G.

Table 1. Overview of recommended reference-based metrics. For each metric, a name, acronym, synonyms, reference to the definition and illustration, range, related limitations and corresponding problem categories are provided. The direction of each green arrow in the column *range* indicates whether higher (up) or lower scores (down) are better. ILS: image-level classification; SS: semantic segmentation; OD: object detection; IS: instance segmentation.

Metric	Acronym	Synonyms	Definition	Illustration	Range	Related Limitations	Recommended for			
							ILC	SS	OD	IS
Counting Metrics										
Accuracy			[34]	Fig. 29	[0, 1] ↑	Figs. 48, 49, 50	x			
Balanced Accuracy	BA		[34]	Fig. 29	[0, 1] ↑	Figs. 49, 50	x			
Center line Dice Similarity Coefficient	cDice		[83]	Fig. 35	[0, 1] ↑	Fig. 57, 60, 83		x		x
Dice Similarity Coefficient	DSC	Sørensen–Dice Coefficient, F ₁ Score, Balanced F Score	[28]	Fig. 31	[0, 1] ↑	Figs. 56, 58, 59, 60, 61, 64, 66, 68, 83		x		x
F _β Score			[23]	Fig. 28	[0, 1] ↑	Figs. 49, 56, 58, 59, 60, 61, 66, 77, 83	x	x	x	x
False Positives per Image@Sensitivity	FPPI@Sensitivity	Sensitivity: Recall, Hit Rate, True Positive Rate	[12, 34]	Fig. 40	[0, ∞) ↓				x	x
Intersection over Union	IoU	Jaccard Index, Tanimoto Coefficient	[42]	Fig. 31	[0, 1] ↑	Figs. 56, 58, 59, 60, 61, 64, 66, 68, 72, 73, 74, 75, 83		x		x
(Multi-class) Matthews Correlation Coefficient	MCC	Phi Coefficient	[59]	Fig. 29	[-1, 1] ↑		x			
Panoptic Quality	PQ		[50]	Fig. 42	[0, 1] ↑	Fig. 70				x
Positive Likelihood Ratio	LR+	Likelihood Ratio Positive, Likelihood Ratio for Positive Results	[5]	Fig. 28	[0, ∞) ↑		x			
Positive Predictive Value@Sensitivity	PPV@Sensitivity	PPV: Precision; Sensitivity: Recall, Hit Rate, True Positive Rate	[12, 34]	Fig. 30	[0, 1] ↑	Figs. 48, 49, 50, 53, 66, 77, 83	x		x	x
Sensitivity@Positive Predictive Value	Sensitivity@PPV	Sensitivity: Recall, Hit Rate, True Positive Rate; PPV: Precision	[12, 34]	Fig. 30	[0, 1] ↑	Figs. 48, 49, 50, 66, 77, 83	x		x	x
Specificity@Sensitivity		Specificity: Selectivity, True Negative Rate; Sensitivity: Recall, Hit Rate, True Positive Rate	[12, 34]	Fig. 30	[0, 1] ↑	Figs. 48, 49, 50, 66, 77, 83	x			
Sensitivity@False Positives per Image	Sensitivity@FPPI	Sensitivity: Recall, Hit Rate, True Positive Rate	[12, 34]	Fig. 40	[0, 1] ↑	Figs. 48, 49, 50, 66, 77, 83			x	x
Sensitivity@Specificity		Sensitivity: Recall, Hit Rate, True Positive Rate; Specificity: Selectivity, True Negative Rate	[12, 34]	Fig. 30	[0, 1] ↑	Figs. 48, 49, 50, 66, 77, 83	x			
Youden’s Index	J	Youden’s J Statistic, Youden’s J, Bookmaker Informedness (BM)	[102]	Fig. 29	[-1, 1] ↑		x			
Multi-threshold Metrics										
Area under the Receiver Operating Characteristic Curve	AUROC	Area under the curve (AUC), AUC Receiver Operating Characteristic (ROC), C-Index, C-Statistics	[37]	Fig. 30	[0, 1] ↑	Figs. 46, 48, 54, 79, 80, 81	x			
Average Precision	AP		[54]	Fig. 39	[0, 1] ↑	Figs. 78, 79, 80, 81	x		x	x
Free-Response Receiver Operating Characteristic Score	FROC Score		[7, 95]	Fig. 40	[0, 1] ↑				x	x
Distance-based Metrics										
Average Symmetric Surface Distance	ASSD		[100]	Fig. 33	[0, ∞) ↓	Figs. 58, 62, 64, 66, 84		x		x
Boundary Intersection over Union	Boundary IoU		[19]	Fig. 36	[0, 1] ↑	Fig. 76		x		x

Metric	Acronym	Synonyms	Definition	Illustration	Range	Related Limitations	Recommended for			
							ILC	SS	OD	IS
Hausdorff Distance	HD	Hausdorff Metric, Pompeiu–Hausdorff Distance, Maximum Symmetric Surface Distance	[41]	Fig. 32	$[0, \infty)$ ↓	Figs. 58, 62, 64, 65, 66, 84		x		x
Mean Average Surface Distance	MASD		[10]	Fig. 33	$[0, \infty)$ ↓	Figs. 58, 62, 64, 66, 84		x		x
Normalized Surface Distance	NSD	Normalized Surface Dice, Surface Surface Dice	[68]	Fig. 34	$[0, 1]$ ↑	Figs. 58, 62, 66, 83		x		x
X^{th} Percentile Hausdorff Distance	X^{th} Percentile HD		[41]	Fig. 32	$[0, \infty)$ ↓	Figs. 58, 62, 64, 66, 84		x		x

Metric families. As an important prerequisite for the development of the recommendation framework, the expert panel identified the most relevant reference-based metrics for the image analysis categories addressed in this paper (Tab. 1). All of these metrics are directly or indirectly based on the cardinalities of the so-called *confusion matrix* (i.e., the true (T)/false (F) positives (P)/negatives (N) in binary problems). They are typically computed by comparing the algorithm’s prediction to a reference annotation. Modern neural network-based approaches commonly require a threshold to be set in order to convert the algorithm output comprising predicted class scores⁴ to a confusion matrix, as illustrated in Fig. 27. For the purpose of metric recommendation, we classify the identified metrics into **counting metrics** that operate directly on the confusion matrix and express the metric value as a function of the cardinalities (see Figs. 28, 29 and 31), **multi-threshold metrics** that operate on a dynamic confusion matrix, such as *Area under the Receiver Operating Characteristic Curve (AUROC)* (see Fig. 30), and *Average Precision (AP)* (see Fig. 39) and **distance-based metrics** that typically rely on the explicit definition of object boundaries (see Figs. 32 and 34).

Reference versus ground truth: We assume that the validation process is based on the comparison of the algorithm output and a **reference** (sometimes called **gold standard**), which is assumed to be close or equal to the correct result; the (often forever unknown) **ground truth**. In terms of metrics, we distinguish between *reference-based metrics* [45], which use the image-based reference, and *non-reference-based metrics* that assess complementary properties, such as runtime, memory consumption, or carbon footprint.

Conflicting terminology. Terminology may differ substantially across communities. For example, the statistics community prefers the term Positive Predictive Value (PPV) over *Precision*, as the latter can be confused with the confidence of an output. In the medical domain, the term *validation* is used for an independent assessment (untouched test set) of an algorithm, while the machine learning community commonly uses a *validation set* for hyperparameter tuning. To avoid confusion resulting from unclear terminology, the final version of this manuscript will provide a glossary in the Appendix.

2.1.2 Guiding principles. Our framework is based on the following guiding principles:

Phrasing of the biomedical task. The recommendation framework has been designed in a way to support the metric selection and application process for one specific driving biomedical question. In practice, multiple questions are often addressed with one given data set. For example, a clinician may have the ultimate interest of diagnosing brain cancer in a patient based on a given Magnetic

⁴Sometimes referred to as predicted class probabilities, continuous class scores or pseudo-probabilities.

Resonance Imaging (MRI) data set. While this would be phrased as an image-level classification task, an interesting *surrogate task* could be that of segmentation to assess the quality of tumor delineation. In the case of multiple different driving biomedical questions, a recommendation is generated separately for each question.

Dealing with multiple classes. In non-binary problems, a per-class validation is always recommended. As problem properties may differ from class to class (e.g. the size or size variability of target structures), the problem fingerprint needs to be generated separately for each class. In consequence, each subprocess (denoted by the \boxplus -symbol in the framework overview shown in Fig. 2) needs to be traversed separately for each class in case the fingerprint properties relevant for the respective subprocess differ. Although not common in current validation practice, this may - in theory - lead to different validation metrics for different classes. Note that in addition to metrics applied to individual classes ("One versus rest" setting), a multi-class metric operating on the entire confusion matrix (e.g. Matthews Correlation Coefficient (MCC)) may be applied, as detailed in the problem category-specific instructions.

Model-agnostic metric recommendation. Metrics should be chosen based solely on the driving biomedical problem and not be effected by algorithm design choices. For example, the error functions applied in common neural network architectures do not justify the use of corresponding metrics (e.g. validating with DSC to match the Dice loss [29] used for training a U-net [74]).

Comparative benchmarking versus diagnostics. In general, the biomedical interest cannot be captured with a single metric. In segmentation tasks, for example, the popular DSC (which measures the overlap between the prediction and the reference) is typically complemented by a contour-based metric to explicitly assess the quality of boundaries. The framework has therefore been designed to recommend multiple complementary metrics for a given task. We assume two primary use cases of metrics in this paper. In comparative benchmarking studies (e.g. competitive challenges), multiple algorithms or algorithm variants are compared on identical data sets. This requires the ranking of the competing algorithms according to performance. Typically multiple complementary validation metrics are applied in this use case, resulting in either multiple rankings or a merged ranking that takes all or several metric values into account, as detailed in Sec. 7. We refer to the metrics that contribute to the (primary) ranking(s) as *primary metrics*. *Secondary metrics* can additionally be applied for comprehensive reporting, for example because they reflect complementary properties of interest (e.g. compute time, carbon footprint), or for providing performance measures that are comparable across publications. The computer vision community, for example, typically reports the Intersection over Union (IoU) rather than the DSC. While our mappings focus on the recommendation of primary metrics, users are invited to complement them by further secondary metrics according to their specific needs. The second use case of metrics addressed by our framework are validation studies centered around a single algorithm that focus on comprehensive diagnostics rather than comparative assessment. In this case, it is often desired to report as many complementary metrics as possible in order to comprehensively analyse the properties of an algorithm. If a user of our framework is interested in this second type of study, the notion of primary and secondary metrics can be ignored.

Predefined target values. Modern algorithms output (continuous) predicted class scores. To classify cases in an actual biomedical application (e.g. in a screening tool), however, it is required to set a cutoff value on the scores. Sometimes, the underlying problem provides a specific target metric value to be reached (e.g. a certain Sensitivity or a certain ratio of false detections (False

Positive (FP) versus misses (False Negative (FN))), requiring a corresponding cutoff value. If this is not the case, there are two widely-adapted coping strategies that are not transparently motivated or distinguished in current practice: 1) determining a cutoff based on default values (e.g. "argmax" operation in semantic segmentation, or "0.5" in binary image classification) or based on optimizing a primary metric (e.g. F₁ Score) using a validation set; 2) abstaining from validating algorithms at a certain cutoff and exclusively reporting results on multi-threshold metrics (averaging over various cutoffs) instead. The deciding factor between the two strategies should be how much focus is to be put on a certain application at hand versus general and application-agnostic algorithm assessment. While some communities seem to have converged on cutoff-based validation (e.g. cell instance segmentation [15]), recent clinical initiatives advocate for cutoff-agnostic validation arguing that cutoffs are often over-optimized on a specific data set and that associated results are not transferable across study cohorts (e.g. with differing disease prevalence) and clinical applications (e.g. with differing cost-benefit trade-offs for patients) [9, 64, 97]. We handle this controversy in current practices by making validation at certain cutoffs optional (for all tasks except semantic segmentation).

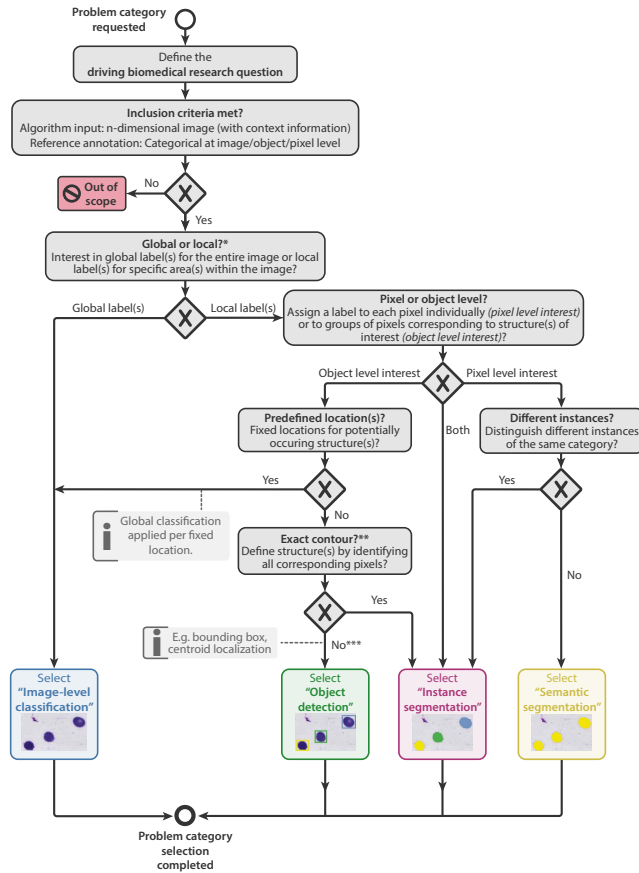
Notation: The notation for our recommendations have been based on Business Process Model and Notation (BPMN). The individual components used in the recommendation diagrams are explained in Fig. 13.

2.2 Problem Fingerprinting

As an important foundation for the metric recommendation framework, the expert panel identified common and rare failure cases of metrics in a community-powered process process. The results are provided in App. H and include a wide variety of pitfalls ranging from those related to domain interest, data set and properties of the target structure all the way to mathematical considerations with respect to analyses and post-processing. These pitfalls served as a foundation for developing the *problem fingerprint*, whose purpose is to capture all properties of the underlying biomedical problem that are relevant for selecting appropriate validation metrics. Common problems often relate to selecting metrics from the wrong problem category, as illustrated in App. H.1. To avoid such problems, the problem fingerprinting comprises the step of mapping a given problem with all its intrinsic and data set-related properties to the corresponding problem category via the *category mapping* (Fig. 4).

Image processing category identified by category mapping ⇒ ILC, SS, OD, IS		ILC Class 1 Class 2	SS	OD	IS
Domain interest-related properties					
Particular importance of structure boundaries ⇒ SS, IS			Unequal handling of classes requested ⇒ ILC, SS, OD, IS		
Particular importance of structure volume ⇒ SS, IS	 V = ...		Handling of spatial outliers ⇒ SS, IS		
Particular importance of structure center (e.g. in cells, vessels) ⇒ SS, OD, IS			Required granularity of localization ⇒ OD		
Target structure-related properties					
Small size of structures relative to pixel size ⇒ SS, OD, IS			Possibility of overlapping or touching target structures (e.g. medical instruments or cells) ⇒ SS, OD, IS		
High variability of structure sizes (within one image, across images) ⇒ SS, OD, IS			Possibility of disconnected target structure(s) ⇒ SS, OD, IS		
Target structures feature tubular shape ⇒ SS, OD, IS			Possibility of multiple labels per unit (pixel or image) ⇒ ILC, SS, IS		
Data set-related properties					
High class imbalance ⇒ ILC, SS, OD, IS			Non-independence of test cases ⇒ ILC, SS, OD, IS		
High inter-/intra-rater variability ⇒ SS, OD, IS	Ref 1 Ref 2 	Ref 1 Ref 2 	Possibility of reference without target structure(s) ⇒ SS, OD, IS	Ref 	Ref
Possibility of spatial outliers in reference annotation ⇒ SS, OD, IS	Ref 	Ref 	Granularity of provided reference annotations ⇒ OD		
Algorithm output-related properties					
Possibility of invalid algorithm output (e.g. Prediction is NaN) ⇒ ILC, SS, OD, IS	Ref Pred 	Ref Pred 	Possibility of algorithm output not containing the target structure(s) ⇒ SS, OD, IS	Pred 	Pred

Fig. 3. **Relevant properties of a driving biomedical image analysis problem are captured by the *problem fingerprint*** (selection shown here). Besides the problem category, the fingerprint comprises (1) domain interest-related properties, (2) target structure-related properties, (3) data set-related properties and (4) algorithm output-related properties. The relevance of the properties for the problem categories image-level classification (ILC), semantic segmentation (SS), object detection (OD) and instance segmentation (IS) is indicated by a ⇒. A comprehensive version of the fingerprint for the individual problem categories can be found in Fig. 15 (ILC), Figs. 16/17 (SS), Figs. 18/19 (OD) and Figs. 20 - 22 (IS).



* We define the scale of validation according to the confusion matrix, i.e. the scale at which predictions are matched with reference labels. **Global labels** refer to reference annotations on image level, **local labels** to reference annotations on object or pixel level.

** If a substantial fraction of objects is tiny (F3.1), any outline-based definition becomes very brittle/noisy and experimenters might want to consider alternatives such as a center point-based definitions (→ Object detection).

*** If the number of structures per category and image is known, the task would be considered as an image-level regression problem and thus defined as **out of scope**.

Fig. 4. **Subprocess S1 for selecting a problem category.** The *Category Mapping* maps a given research problem to the appropriate problem category with the goal of **grouping problems by similarity of validation**. The leaf nodes represent the categories: image-level classification, object detection, instance segmentation or semantic segmentation). F3.1 refers to fingerprint 3.1 (see Fig. 17). An overview of the symbols used in the process diagram is provided in Fig. 13.

Finally, a structured representation of the biomedical problem is generated, which not only includes the appropriate problem category, but also comprises (1) *domain interest-related* properties, such as the unequal importance of classes or the particular importance of structure boundaries, (2) *target structure-related* properties, such as the size of the structures relative to the image grid size or the shape complexity, (3) *data set-related* properties, such as class imbalance and annotation quality, as well as (4) *algorithm output-related* properties, such as the theoretical possibility of the algorithm output not containing any target structure. The category-specific fingerprints are provided in Fig. 15 (image-level classification), Figs. 16/17 (semantic segmentation), Figs. 18/19 (object detection) and

Figs. 20/21 (instance segmentation). Individual fingerprints are from hereon referred to with the prefix F (e.g. $F2.2$: *Particular importance of structure volume*) The metric recommendation is then performed with a BPMN-based flowchart (see Fig. 13), in which conditional operations are based on one or multiple fingerprint properties, as detailed in the following sections.

2.3 Metric Selection

The fingerprint is leveraged to enable the guided selection of a suitable set of metrics for the driving biomedical problem, as illustrated in Fig. 2. While the selection of the primary reference-based metrics is performed in a problem category-specific manner, a common routine is applied for selecting further property-specific metrics as well as non-reference-based metrics. The latter include metrics for assessing speed, memory consumption or carbon footprint, for example. The following sections present the category-specific selection process for the reference-based metrics. Exemplary traversals through the recommendation framework for four different biomedical scenarios can be found in App. F with the resulting metric recommendations summarized in Fig. 12.

3 RECOMMENDATIONS FOR IMAGE-LEVEL CLASSIFICATION

Image-level classification refers to the process of assigning one or multiple labels, or *classes*, to an image. Modern algorithms usually output continuous scores between 0 and 1 for every image and class, which are often interpreted as predicted class probabilities. By introducing a threshold (e.g. 0.5), predictions are considered as positive (e.g. cancer = true) if they are above the threshold or negative if they are below the threshold. Subsequently, a confusion matrix can be determined based on matching predictions with reference labels. The most common pitfalls related to metric selection in classification are summarized in App. H.2 and include pitfalls related to class imbalance, unequal importance of classes, missing prevalence correction as well as the hierarchical structure of the classes and/or the data. The identified pitfalls served as a basis for the generation of the category-specific fingerprint (Fig. 15) and metric mapping (dark blue path in Fig. 2). The following information is relevant as a basis for traversing the mapping:

Recommendation at a glance: We recommend picking one multi-class counting metric (subprocess S2, Fig. 5) and complementing it with a multi-threshold metric (subprocess S3, Fig. 6) and (optionally) a per-class counting metric (subprocess S4, Fig. 7). Multi-class metrics have the unique advantage that they capture the performance of all classes in a single value. By taking into account all entries of the multi-class confusion matrix, they provide a holistic measure for the problem in a single score without the need for customized class-aggregation schemes. On the other hand, detailed class-specific analyses are not possible with multi-class metrics. To address this weakness, we recommend an additional per-class validation based on multi-threshold metrics and/or per-class counting metrics, where each class is separately assessed in a "One-vs-the-Rest" fashion (merging remaining other classes together), although other variants are also possible [36]. If desired, further customized metrics and non-reference-based metrics can be added to the metric pool.

Output Calibration: In application scenarios that involve interpreting the raw algorithm output (specifically the predicted class scores), *output calibration* can be used to obtain a reliable measure of confidence associated with the decision. Please check decision guide D3.3 in App. E.2 and Fig. 54 for further information.

Expected format of reference and algorithm output: The metric mapping expects the following format for image-level classification with C classes: For each image I there is a

reference annotation y_I that is either indicating the class for the image ($y_I \in \{1, \dots, C\}$) or in the case of multi-label classification indicating presence for each class ($y_I \in \{0, 1\}^C$). Similarly the algorithm is expected for each image I to output continuous class scores for each of the classes ($\hat{y}_I \in [0, 1]^C$), indicating the predicted class probability. In case the provided reference annotations deviate from the expected format, matching can be achieved via various measures (e.g. aggregation of pixel-level reference to required image-level reference).

The traversal through the decision tree of our framework for the specific task of disease classification in dermoscopic images is illustrated in Fig. 23. The resulting metric recommendation can be found in Fig. 12.

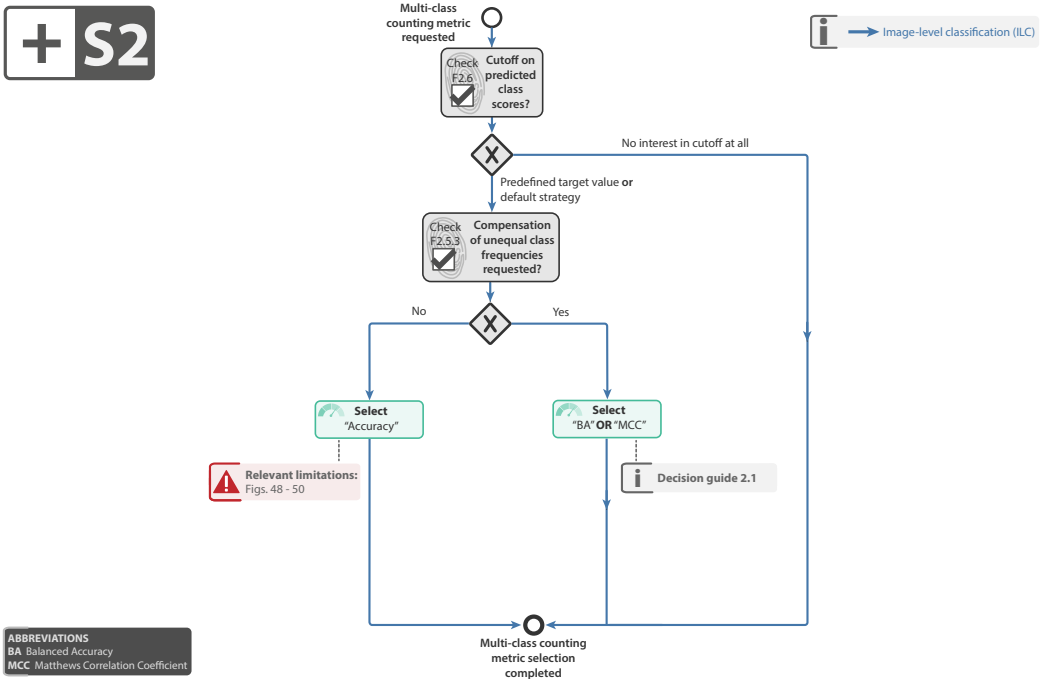


Fig. 5. **Subprocess S2 for selecting multi-class metrics (if any).** Applies to: Image-level classification (ILC). Based on the problem fingerprint (referred to as "FX.Y"), the user is guided through the process of selecting a multi-class counting metric from the family of counting metrics while being made aware of potential pitfalls related to individual choices. Metric definitions can be found in Tab. 1 and App. G.1. Decision guides are provided in App. E.1. Detailed descriptions of the problem fingerprint are provided in Fig. 15. An overview of the symbols used in the process diagram is provided in Fig. 13.

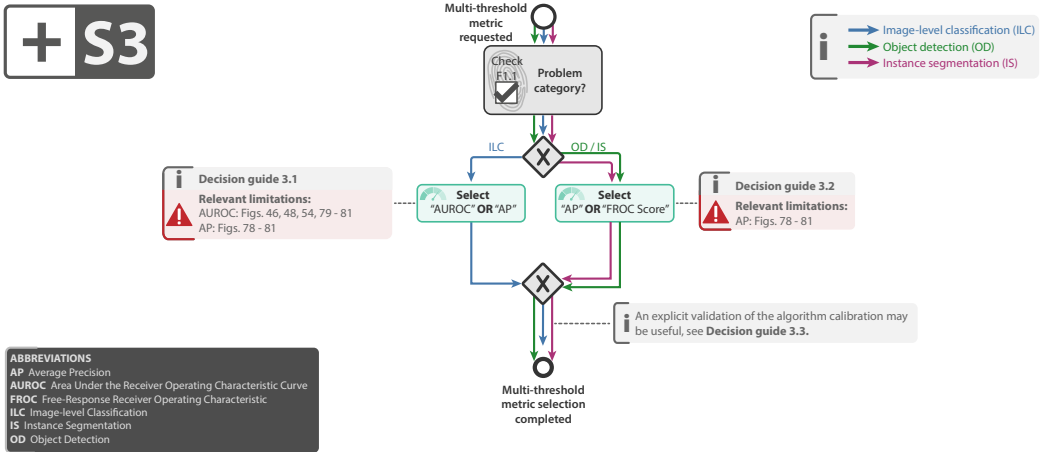


Fig. 6. **Subprocess S3 for selecting a multi-threshold metric (if any).** Applies to: Image-level classification (ILC), object detection (OD) and instance segmentation (IS). Based on the problem fingerprint (referred to as "FX.Y"), the user is guided through the process of selecting a multi-threshold metric while being made aware of potential pitfalls related to individual choices. Metric definitions can be found in Tab. 1 and App. G.1 and G.3. Decision guides are provided in App. E.2. Detailed descriptions of the problem fingerprint are provided in Figs. 15, 18 - 22. An overview of the symbols used in the process diagram is provided in Fig. 13.

+ S4

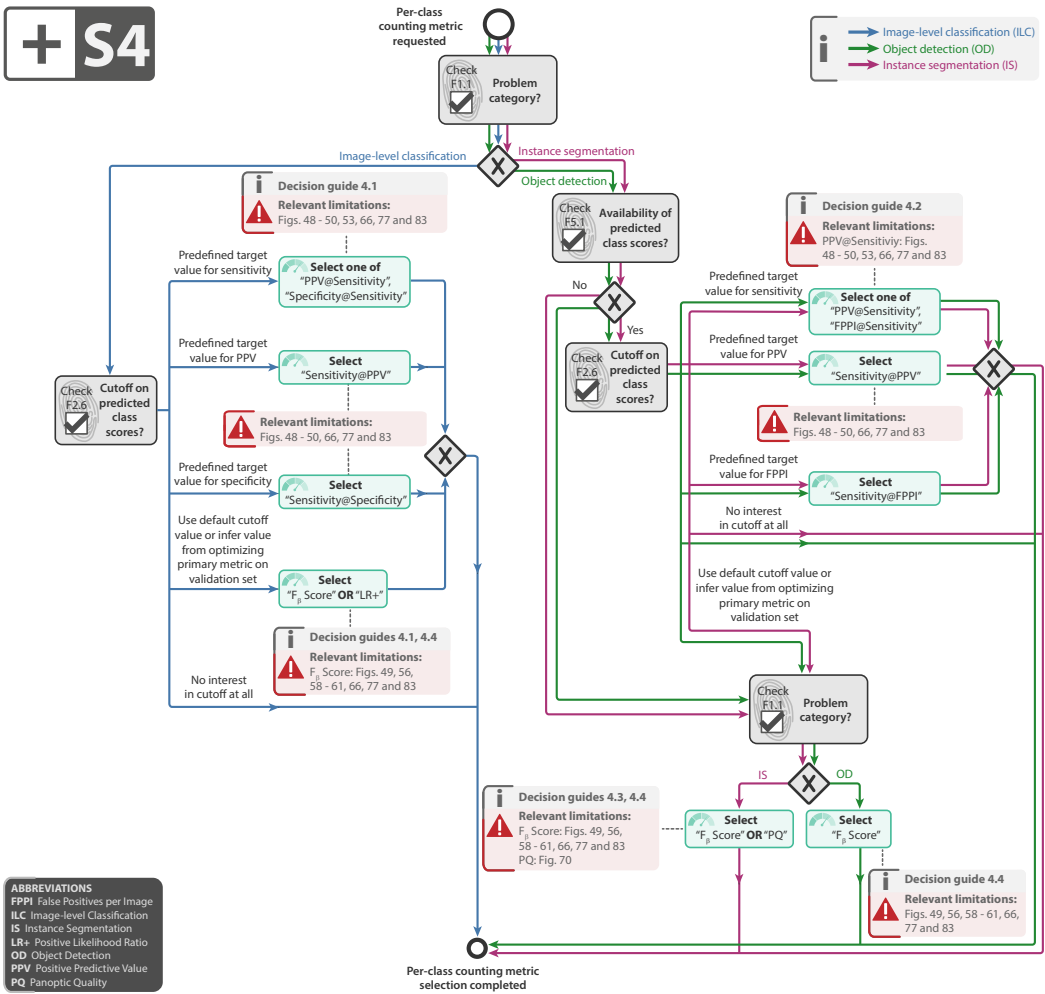


Fig. 7. Subprocess S4 for selecting a per-class counting metric (if any). Applies to: Image-level classification (ILC), object detection (OD) and instance segmentation (IS). Based on the problem fingerprint (referred to as "FX.Y"), the user is guided through the process of selecting an appropriate validation metrics from the family of counting metrics while being made aware of potential pitfalls related to individual choices. Metric definitions can be found in Tab. 1 and App. G.1, G.3 and G.4. Decision guides are provided in App. E.3. Detailed descriptions of the problem fingerprint are provided in Figs. 15, 18 - 22. An overview of the symbols used in the process diagram is provided in Fig. 13.

4 RECOMMENDATIONS FOR SEMANTIC SEGMENTATION

In semantic image segmentation, classification is performed at pixel level, i.e. each pixel is assigned to one or multiple categories. For many segmentation problems, object boundaries are generated in addition to the pixel-wise classification images. This enables the computation of distance-based metrics, such as the Normalized Surface Distance (NSD). Common pitfalls in segmentation problems are summarized in App. H.3 and are primarily related to the small size, shape and size variability of target structures as well as data set-related properties, such as the uncertainties in reference annotation. The pitfalls served as a basis for generating the category-specific fingerprint (Figs. 16 and 17) and metric mapping (orange path in Fig. 2) for semantic segmentation. The following information is relevant as a basis for traversing the mapping:

Recommendation at a glance: The semantic segmentation mapping for reference-based metrics comprises three parts: First, a per-class counting metric (subprocess S7, Fig. 8) – in segmentation tasks referred to as an *overlap-based metric* – is selected. Overlap-based metrics, such as the DSC or IoU, measure the overlap between the reference annotation and the prediction of the algorithm and provide powerful insights into algorithm performance. Key weaknesses, however, include shape unawareness (Fig. 59) and limitations when dealing with small structures (Fig. 56) or high size variability (Fig. 58). A general recommendation is therefore to complement an overlap-based metric with a boundary-based metric (subprocess S8, Fig. 9). Finally, specific property-related metrics may be selected to assess additional algorithm properties. A popular example are volume-based metrics, which explicitly measure absolute or relative volume differences of structures as these are of key relevance from a domain perspective. The reference-based metrics can then be complemented by non-reference-based metrics.

Requirements for distance-based metrics: While overlap-based metrics, such as the DSC are almost always recommended in segmentation problems (see subprocess S7, Fig. 8), distance-based metrics are not appropriate under several circumstances. In scenarios in which multiple structures of the same type can be seen within the same image (e.g. in multiple sclerosis lesion segmentation), for example, a potential pitfall is related to comparing a given structure boundary to the boundary of the wrong instance in the reference. Similar problems arise in the case of completely missed instances. In such scenarios, we recommend reconsideration to phrase the problem as an instance segmentation problem. If semantic segmentation remains the chosen category, we advise against the use of distance-based metrics, as these are not designed for cases where mix-up of contours across different instances can occur.

Multi-threshold metrics for semantic segmentation: Empirically, segmentation networks are very confident for most pixels of the image (close to 0 and 1). Only at the boundary of objects, changing the threshold would have an impact, essentially controlling over- and undersegmentation. Cases, where threshold variations affect whether or not entire smaller objects are found, and there is an inherent interest in identifying these objects (as opposed to the entirety of all pixels), are better formulated as instance segmentation tasks (see subprocess S1, Fig. 4).

Specific property-related metrics: Overlap-based and contour-based metrics can be complemented with further reference-based metrics that assess additional properties that are relevant from a domain perspective. They can, for example, address the particular importance of structure volume (F2.2) with the Relative Volume Difference [65], Volume Similarity [65]

or the Relative Symmetric Volume Difference [99] metrics. Similarly, the compliance with prior knowledge, such as hierarchical label structure (F3.4) can be measured.

Expected format of reference and algorithm output: We assume the reference annotation and the algorithm output to be in the same coordinate system with identical spacing. The metric mapping expects the following format for semantic segmentation with C classes: For each pixel P there is a reference annotation y_P that either assigns a single class to P ($y_P \in \{1, \dots, C\}$) or, in case of possible multiple labels per pixel, indicates assignment for each class ($y_P \in \{0, 1\}^C$). As for the algorithm output, for each pixel P there is expected to be either a single prediction ($\hat{y}_P \in \{1, \dots, C\}$) or, in case of multiple possible labels per pixel, a prediction for each class ($\hat{y}_P \in \{0, 1\}^C$). Some segmentation metrics are defined only on the border pixels of the reference and predicted segmentation. Border pixels are defined as the set of all pixels of class c that have an immediate neighbor not containing the class c .

The traversal through the decision tree of our framework for the specific task of liver segmentation in computed tomography images is illustrated in Fig. 24. The resulting metric recommendation can be found in Fig. 12.

+ S7

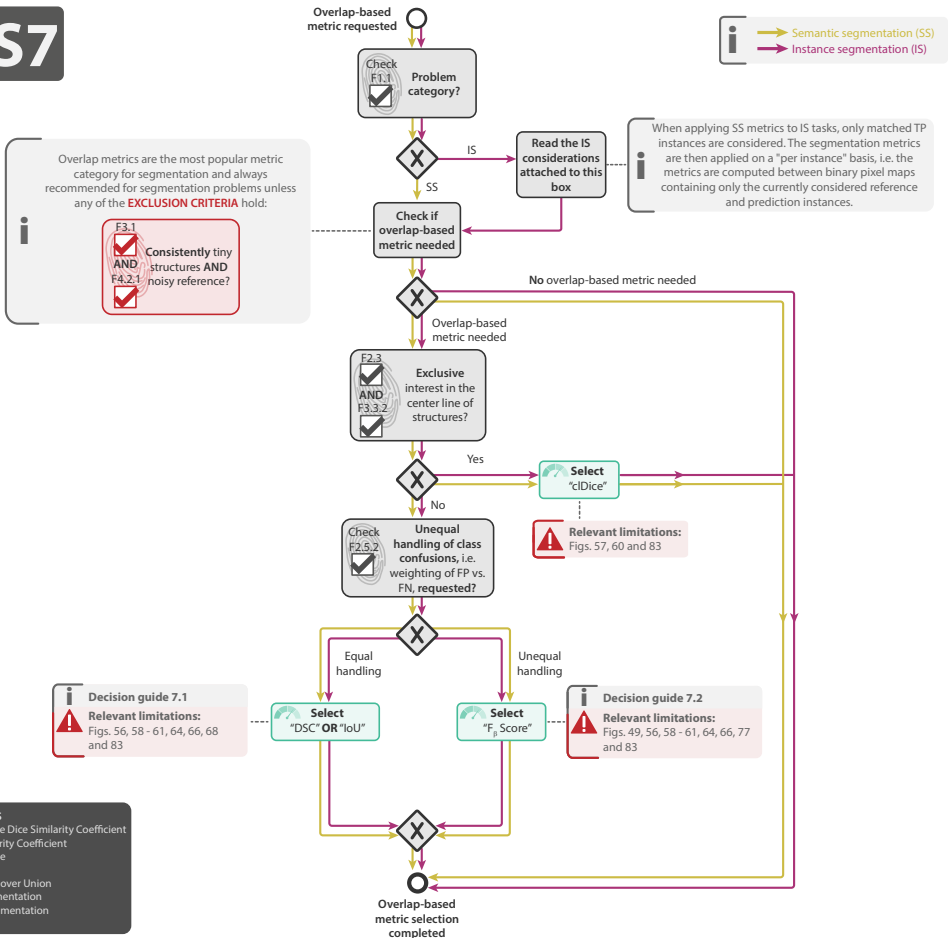


Fig. 8. **Subprocess S7 for selecting overlap-based segmentation metrics (if any).** Applies to semantic segmentation (SS) and instance segmentation (IS). Based on the problem fingerprint (referred to as "FX.Y"), the user is guided through the process of selecting an appropriate set of overlap-based validation metrics from the family of counting metrics while being made aware of potential pitfalls related to individual choices. Metric definitions can be found in Tab. 1 and App. G.2. Decision guides are provided in App. E.6. Detailed descriptions of the problem fingerprint are provided in Figs. 16 - 17 and 20 - 22. An overview of the symbols used in the process diagram is provided in Fig. 13.

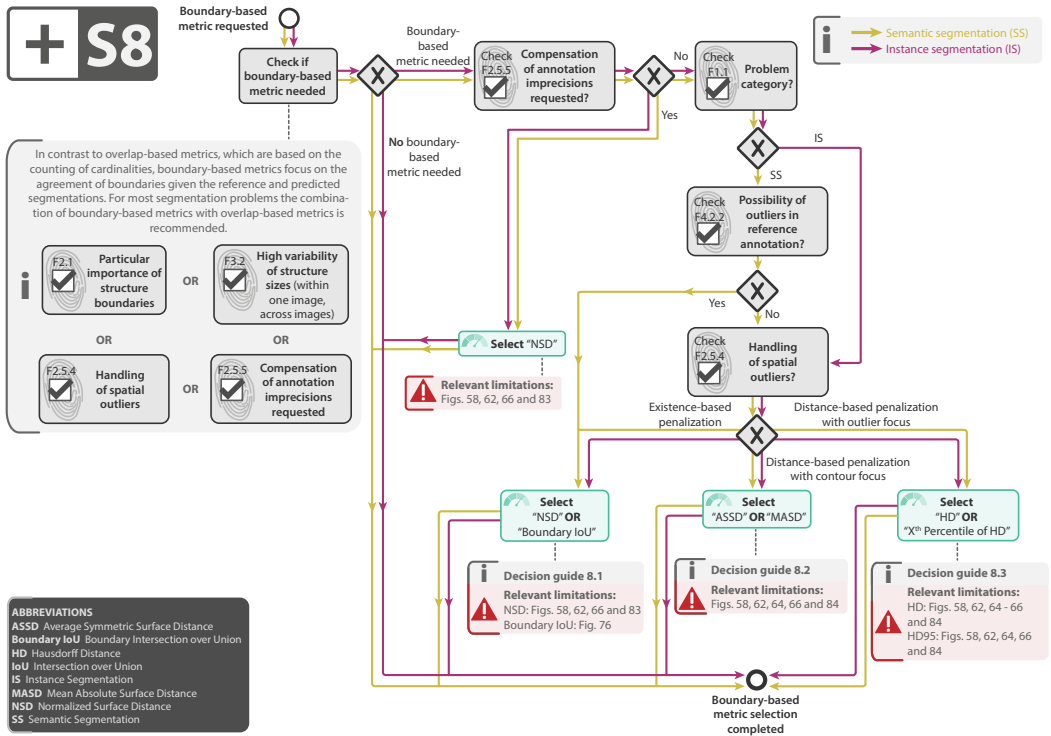


Fig. 9. Subprocess S8 for selecting a boundary-based segmentation metric (if any). Applies to semantic segmentation (SS) and instance segmentation (IS). Based on the problem fingerprint (referred to as "FX.Y"), the user is guided through the process of selecting an appropriate boundary-based segmentation metric from the family of distance-based metrics while being made aware of potential pitfalls related to individual choices. Metric definitions can be found in Tab. 1 and App. G.2. Decision guides are provided in App. E.7. Detailed descriptions of the problem fingerprint are provided in Figs. 16 - 17 and 20- 22. An overview of the symbols used in the process diagram is provided in Fig. 13.

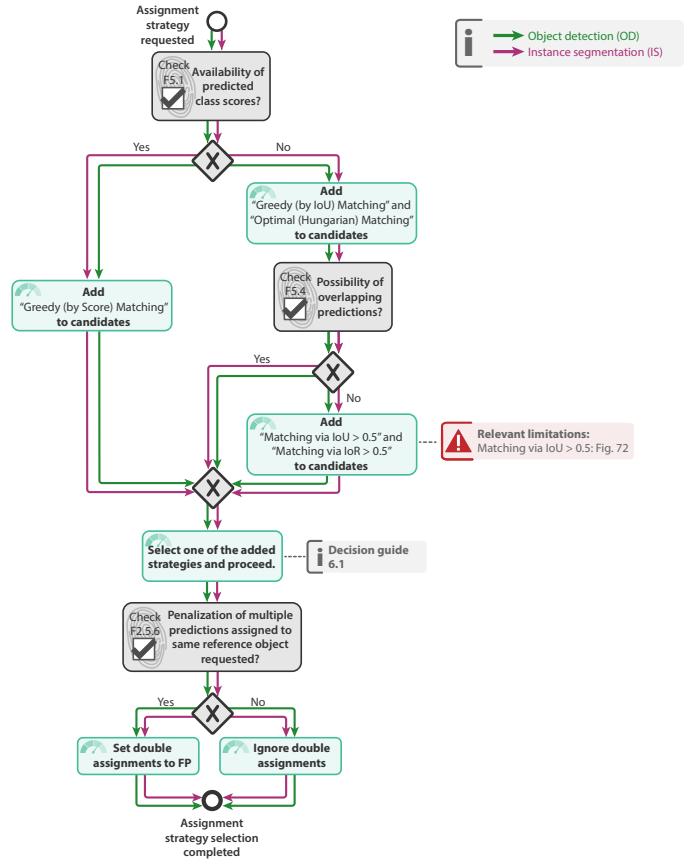
5 RECOMMENDATIONS FOR OBJECT DETECTION

Object detection refers to the detection of one or multiple objects, or instances, of a particular class (e.g. lesion) in an image [54]. The following description assumes single-class problems, but generalization to multi-class problems is straightforward, as validation for multiple classes on object level is performed individually per class. Notably, as multiple predictions and reference instances may be present in one image, the predictions need to include localization information, such that a matching between reference and predicted objects can be performed. The validation process in object detection comprises three parts (see also G.3: 1) localization of objects (i.e. matching of prediction and reference objects), 2) final assignment (i.e. resolving ambiguities that occurred during localization) to enable determining the confusion matrix, and 3) actual method assessment given a set of suitable validation metrics. Note that the entire process is performed on a per-class basis and that a key characteristic of object detection problems is the absence of True Negative (TN), which renders many popular classification metrics invalid. Suitable counting metrics can only be based on three of the four entries of the confusion matrix. Relevant pitfalls identified for object detection problems are summarized in H.4 and are mainly related to these three aspects. The identified pitfalls served as the foundation for the generation of the category-specific fingerprint (Figs. 18 and 19) and metric mapping (light blue path in Fig. 2) for object detection. The following information is relevant as a basis for traversing the mapping:

Recommendation at a glance: Following the three-step process for object detection validation described above, the associated metric selection process is divided into three parts: First, a criterion for deciding whether a predicted object matches a reference object ("localization") is selected (subprocess S5, Fig. 10). Second, a strategy for handling ambiguous assignments is chosen (subprocess S6, Fig. 11). Finally, the validation metrics are selected, which comprise a multi-threshold metric (subprocess S3, Fig. 7) and (optionally) a single-threshold counting metric (subprocess S4, Fig. 7). These standard reference-based metrics can then be complemented by customized metrics and non-reference-based metrics.

Strictness of localization criterion: Determining whether an object is detected requires deciding on a threshold on the selected localization criterion (e.g. IoU > 0.5 counts as detected). However, such cutoff renders the validity of results limited to the specific threshold. To increase robustness of reported metrics, it is common practice in the computer vision community to average metrics over multiple cutoff values (default for IoU criteria: from 0.5 until 0.9 in steps of 0.05). On the other hand, certain properties of the problem at hand may limit the relevance of evaluated cutoff values to lower or higher values. The following properties might warrant validation with lower thresholds: interest in the existence of objects rather than their precise localization, small size of structures (F3.1), high variability of structure sizes (F3.2), 3D input images (as volume increases cubically with size, the desired overlap ratio might require adaptation), uncertainties in the reference (F4.2.1). Conversely, these properties typically warrant validation at higher thresholds: interest in precise localization, dense distribution of structures in images (F3.5).

Expected format of reference and algorithm output: The metric mapping expects the following format for object detection with C classes: For each object O the reference consists of a tuple (y_O, l_O) , where $y_O \in \{1, \dots, C\}$ indicates the class of the object and l_O is some location information (box, center point, radius, etc.). The algorithm output for an object prediction O is expected to comprise a tuple (\hat{y}_O, \hat{l}_O) as well, where \hat{y}_O indicates a single predicted class ($\hat{y}_O \in \{1, \dots, C\}$) optionally accompanied by an associated predicted class score ($\hat{c}_O \in [0, 1]$).



ABBREVIATIONS
 FP False Positive
 IoR Intersection over Reference
 IoU Intersection over Union

Fig. 11. **Subprocess S6 for selecting the assignment strategy.** Applies to object detection (OD) and instance segmentation (IS). Based on the problem fingerprint (referred to as "FX.Y"), the user is guided through the process of selecting an appropriate assignment criterion while being made aware of potential pitfalls related to individual choices. Assignment strategies are defined in App. G.3. Decision guides are provided in App. E.5. Detailed descriptions of the problem fingerprint are provided in Figs. 18- 22. An overview of the symbols used in the process diagram is provided in Fig. 13.

6 RECOMMENDATIONS FOR INSTANCE SEGMENTATION

In contrast to semantic segmentation, instance segmentation problems distinguish different instances of the same class (i.e. different lesions). Similarly as in object detection problems, the task is to detect individual instances of the same class, but detection performance is measured by pixel-level correspondences, as in semantic segmentation problems. Instances can be optionally assigned to one of multiple classes. Validation metrics in instance segmentation problems often combine common detection metrics with segmentation metrics applied per instance. Thus, their pitfalls are the combination of identified pitfalls in object detection (App. H.4) and semantic segmentation (App. H.3). The identified pitfalls served as a foundation for the generation of the category-specific fingerprint (Figs. 20 - 22) and metric mapping (purple path in Fig. 2) for instance segmentation. The following information is relevant as a basis for traversing the mapping:

Recommendation at a glance: The metric selection process for instance segmentation first traverses the same path as in object detection (subprocesses S5, Fig. 10, S6, Fig. 11, S3, Fig. 6, S4, Fig. 7). One main difference to object detection is the fact that localization criteria in S5 are based on pixel correspondence. Furthermore, an instance segmentation-specific metric, referred to as Panoptic Quality (PQ) (see subprocess S4) can be selected to reflect the hybrid nature of the task; more specifically, the metric combines the assessment of overall detection performance and segmentation quality of successfully matched (True Positive (TP)) instances in a single score. If, instead, a separate assessment of segmentation quality for TP instances is desired, additionally to selected detection metrics, the semantic segmentation path (subprocesses S7, Fig. 8 and S8, Fig. 9) can be traversed to select corresponding metrics. The segmentation metrics are then applied per instance. These resulting set of standard reference-based metrics can finally be complemented by customized metrics and non-reference-based metrics.

Metrics avoiding reference matching: While we have found our generic recommendation to match the majority of biomedical problems, the standard reference-based metrics are not well-suited for some applications. In such cases, specialized metrics targeted to the specific problem may be required, as discussed in Sec. 7. Metrics such as Rand Index (RI) [71] and Variation of Information (VoI) [61], for example, allow to skip the steps of matching predicted instances with reference instances (subprocesses S5, Fig. 10 and S6, Fig. 11). This is crucial for tasks with extremely dense and at the same time complex shapes (e.g. tissue images in electron microscopy) that feature similar size scales, where overlap-based localization criteria fail miserably. These metrics are further useful in cases where changes in topology are important which cannot be evaluated based on overlap-based criteria. On the downside, RI and VoI are based on counting pixel pairs and are thus not normalized on object size (large objects will dominate validation compared to smaller objects; see Fig. 56). Finally, as shown in [3], both RI and VoI, while conceptually very different, potentially lead to the same ranking of predicted segmentations if the boundaries of the reference are thinned.

Expected format of reference and algorithm output The metric mapping expects the following format for instance segmentation with C classes: For each object O the reference consists of a tuple (y_O, m_O) , where $y_O \in \{1, \dots, C\}$ indicates the class of the object and $m_O \in \{0, 1\}^{H \times W}$ is a binary pixel map per instance matching the size of the image (height H and width W) and indicating pixel-wise location. The algorithm output for an object prediction O is expected to comprise a tuple (\hat{y}_O, \hat{m}_O) , where, similarly to object detection, \hat{y}_O indicates a single predicted class ($\hat{y}_O \in \{1, \dots, C\}$) optionally accompanied by an associated predicted class score ($\hat{y}_O \in [0, 1]$). See F5.1 in case no predicted class probability is provided.

\hat{m}_O denotes a binary pixel map per instance analogously to m_O . Note that annotations from semantic segmentation (not distinguishing instances of the same class) can be transformed to the instance segmentation format via connected component analysis (in case of purely non-touching instances).

The traversal through the decision tree of our framework for the specific task of cell nuclei instance segmentation in time-lapse light microscopy is illustrated in Fig. 25. The resulting recommendations for localization/assignment strategies and metrics can be found in Fig. 12.

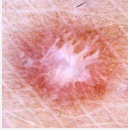
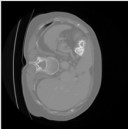
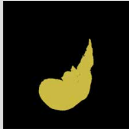
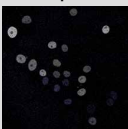
PROBLEM CATEGORY	SCENARIO	EXAMPLE IMAGE	RECOMMENDATION
Image-level classification	Disease classification in dermoscopic images	Input	Requested output
			
Semantic segmentation	Liver segmentation in computed tomography images	Input	Requested output
			
Object detection	Polyp detection in colonoscopy videos with predefined sensitivity of 0.98	Input	Requested output
			
Instance segmentation	Cell nuclei instance segmentation in time-lapse light microscopy with a subsequent goal of cell tracking	Input	Requested output
			
<p>Multi-class counting metric (S2): BA</p> <p>Multi-threshold metric (S3): AUROC, output calibration needed</p> <p>Per-class counting metric (S4): LR+</p>			
<p>Overlap-based metric (S7): DSC</p> <p>Boundary-based metric (S8): NSD</p> <p>Specific property-related metric: Absolute Volume Difference</p>			
<p>Localization criterion (S5): Box IoU</p> <p>Assignment strategy (S6): Greedy (by Score) Matching, set double assignments to FP</p> <p>Multi-threshold metric (S3): FROC Score</p> <p>Per-class counting metric (S4): FPPI¹@Sensitivity = 0.98</p> <p>¹ The false positives are determined per video = patient, not per frame = image level, reflecting clinical interest.</p>			
<p>Localization criterion (S5): IoR</p> <p>Assignment strategy (S6): Matching via IoR > 0.5, set double assignments to FP</p> <p>No multi-threshold metric (S4) needed (predicted class scores not available)</p> <p>Multi-threshold metric (S4): F_β Score</p> <p>Overlap-based metric (S7): IoU (per each cell)</p> <p>No boundary-based metric (S8) needed (no interest in structure boundaries)</p>			

Fig. 12. **Instantiation of the framework with recommendations for concrete biomedical questions.** a) Disease classification in dermoscopic images [24], b) liver segmentation in computed tomography images [2, 85], c) polyp detection in colonoscopy videos with predefined sensitivity of 0.98 [11, 80] and d) cell nuclei instance segmentation in time-lapse light microscopy with a subsequent goal of cell tracking [92]. The corresponding traversals through the decision trees are shown in App. F.

7 CROSS-CATEGORY RECOMMENDATIONS

The consortium is currently compiling the cross-category recommendations on the following topics:

7.1 Selecting Non-Reference-Based Metrics

For a given biomedical application, properties beyond the agreement of the algorithm output and a reference may be of crucial importance. This section will therefore give recommendations on how to assess common complementary properties, namely run time, memory consumption and carbon footprint.

7.2 Determining the Global Decision Threshold

Metrics from the families of counting metrics and distance-based metrics require a threshold to be set on the predicted class scores in order to generate the confusion matrix or the structure boundaries. Importantly, this threshold needs to be globally used for all validation metrics. This paragraph will give recommendations with respect to setting the global decision threshold.

7.3 Aggregating Metric Values

Aggregating metric values from multiple test cases of a given test set is not necessarily trivial and multiple pitfalls exist, as demonstrated in App. H.5. This section will therefore provide recommendations with respect to metric aggregation.

7.4 Reporting Metric Results

Finally, several pitfalls exist with respect to reporting metrics results (see e.g. Fig. 82). This section will therefore give recommendations with respect to result reporting.

8 CURRENT STATUS AND HOW TO PROVIDE FEEDBACK

The most important intermediate results of the international Delphi process have been summarized in the previous section. The consortium is currently working on (1) cross-category recommendations with a specific focus on how to apply selected metrics appropriately to a given data set as well as on (2) a toolkit implementing the entire framework in a user-friendly manner. At this stage, we explicitly invite the research community to challenge our current proposal and provide constructive feedback by replying to this questionnaire: <https://onlinesurvey.dkfz.de/index.php/454312?lang=en>; both short one-click and comprehensive feedback is possible. The final recommendation will be made publicly available once the Delphi process has been completed.

ACKNOWLEDGEMENTS

This work was initiated by the Helmholtz Association of German Research Centers in the scope of the Helmholtz Imaging Incubator (HI), the MICCAI special interest group on biomedical image analysis challenges and the benchmarking working group of the MONAI initiative. It was further supported in part by the Intramural Research Program of the National Institutes of Health Clinical Center as well as by the National Cancer Institute (NCI) and the National Institute of Neurological Disorders and Stroke (NINDS) of the National Institutes of Health (NIH), under award numbers NCI:U01CA242871 and NINDS:R01NS042645. The content of this publication is solely the responsibility of the authors and does not represent the official views of the NIH. S.A. Tsafaris acknowledges the support of Canon Medical and the Royal Academy of Engineering and the Research Chairs and Senior Research Fellowships scheme (grant RCSR1819\825).

We would like to thank Silvia D. Almeida, Michael Baumgartner, Ahmad Bin Qasim, Dimitrios Bounias, Till Bungert, Kris Dreher, Maximilian Fischer, Niklas Holzwarth, Marco Hübner, Lukas Klein, Gregor Köhler, Bálint Kovács, Xiao Liu, Dominik Michael, Lucas-Raphael Müller, Tobias Norajitra, Maike Rees, Melanie Schellenberg, Silvia Seidlitz, Jan Sellner, Akriti Srivastava, Andrea Marheim Storås, Vajira Thambawita, Constantin Ulrich and Tassilo Wald for testing the metric mappings.

REFERENCES

- [1] Shadi AlZu'bi, Mohammed Shehab, Mahmoud Al-Ayyoub, Yaser Jararweh, and Brij Gupta. 2020. Parallel implementation for 3d medical volume fuzzy segmentation. *Pattern Recognition Letters* 130 (2020), 312–318.
- [2] Michela Antonelli, Annika Reinke, Spyridon Bakas, Keyvan Farahani, Bennett A Landman, Geert Litjens, Bjoern Menze, Olaf Ronneberger, Ronald M Summers, Bram van Ginneken, et al. 2021. The medical segmentation decathlon. *arXiv preprint arXiv:2106.05735* (2021).
- [3] Ignacio Arganda-Carreras, Srinivas C Turaga, Daniel R Berger, Dan Cireşan, Alessandro Giusti, Luca M Gambardella, Jürgen Schmidhuber, Dmitry Laptev, Sarvesh Dwivedi, Joachim M Buhmann, et al. 2015. Crowdsourcing the creation of image segmentation algorithms for connectomics. *Frontiers in neuroanatomy* (2015), 142.
- [4] Saeid Asgari Taghanaki, Kumar Abhishek, Joseph Paul Cohen, Julien Cohen-Adad, and Ghassan Hamarneh. 2021. Deep semantic segmentation of natural and medical images: a review. *Artificial Intelligence Review* 54, 1 (2021), 137–178.
- [5] John Attia. 2003. Moving beyond sensitivity and specificity: using likelihood ratios to help interpret diagnostic tests. *Australian prescriber* 26, 5 (2003), 111–113.
- [6] D Bamira and MH Picard. 2018. Imaging: Echocardiology—Assessment of Cardiac Structure and Function. (2018).
- [7] Andriy I Bandos, Howard E Rockette, Tao Song, and David Gur. 2009. Area under the free-response ROC curve (FROC) and a related summary index. *Biometrics* 65, 1 (2009), 247–256.
- [8] Solon Barocas, Moritz Hardt, and Arvind Narayanan. 2017. Fairness in machine learning. *Nips tutorial* 1 (2017), 2.
- [9] Babak Ehteshami Bejnordi, Mitko Veta, Paul Johannes Van Diest, Bram Van Ginneken, Nico Karssemeijer, Geert Litjens, Jeroen AWM Van Der Laak, Meyke Hermsen, Quirine F Manson, Maschenka Balkenhol, et al. 2017. Diagnostic

assessment of deep learning algorithms for detection of lymph node metastases in women with breast cancer. *Jama* 318, 22 (2017), 2199–2210.

- [10] Miroslav Beneš and Barbara Zitová. 2015. Performance evaluation of image segmentation algorithms on microscopic image data. *Journal of microscopy* 257, 1 (2015), 65–85.
- [11] Jorge Bernal, Aymeric Histace, Marc Masana, Quentin Angermann, Cristina Sánchez-Montes, Cristina Rodríguez de Miguel, Maroua Hammami, Ana García-Rodríguez, Henry Córdova, Olivier Romain, et al. 2019. GTCreator: a flexible annotation tool for image-based datasets. *International journal of computer assisted radiology and surgery* 14, 2 (2019), 191–201.
- [12] Sebastian Bickelhaupt, Paul Ferdinand Jaeger, Frederik Bernd Laun, Wolfgang Lederer, Heidi Daniel, Tristan Anselm Kuder, Lorenz Wuesthof, Daniel Paech, David Bonekamp, Alexander Radbruch, et al. 2018. Radiomics based on adapted diffusion kurtosis imaging helps to clarify most mammographic findings suspicious for cancer. *Radiology* 287, 3 (2018), 761–770.
- [13] Bernice B Brown. 1968. *Delphi process: a methodology used for the elicitation of opinions of experts*. Technical Report. Rand Corp Santa Monica CA.
- [14] Neil G Burnet, Simon J Thomas, Kate E Burton, and Sarah J Jefferies. 2004. Defining the tumour and target volumes for radiotherapy. *Cancer Imaging* 4, 2 (2004), 153.
- [15] Juan C Caicedo, Allen Goodman, Kyle W Karhohs, Beth A Cimini, Jeanelle Ackerman, Marzieh Haghighi, CherKeng Heng, Tim Becker, Minh Doan, Claire McQuin, et al. 2019. Nucleus segmentation across imaging experiments: the 2018 Data Science Bowl. *Nature methods* 16, 12 (2019), 1247–1253.
- [16] Juan C Caicedo, Jonathan Roth, Allen Goodman, Tim Becker, Kyle W Karhohs, Matthieu Broisin, Csaba Molnar, Claire McQuin, Shantanu Singh, Fabian J Theis, et al. 2019. Evaluation of deep learning strategies for nucleus segmentation in fluorescence images. *Cytometry Part A* 95, 9 (2019), 952–965.
- [17] Aaron Carass, Snehashis Roy, Adrian Gherman, Jacob C Reinhold, Andrew Jesson, Tal Arbel, Oskar Maier, Heinz Handels, Mohsen Ghafourian, Bram Platel, et al. 2020. Evaluating white matter lesion segmentations with refined Sørensen–Dice analysis. *Scientific reports* 10, 1 (2020), 1–19.
- [18] Dev P Chakraborty and Xuetong Zhai. 2019. Analysis of data acquired using ROC paradigm and its extensions.
- [19] Bowen Cheng, Ross Girshick, Piotr Dollár, Alexander C Berg, and Alexander Kirillov. 2021. Boundary IoU: Improving Object-Centric Image Segmentation Evaluation. In *Proceedings of the IEEE/CVF Conference on Computer Vision and Pattern Recognition*. 15334–15342.
- [20] Nicolas Chenouard, Ihor Smal, Fabrice De Chaumont, Martin Maška, Ivo F Sbalzarini, Yuanhao Gong, Janick Cardinale, Craig Carthel, Stefano Coraluppi, Mark Winter, et al. 2014. Objective comparison of particle tracking methods. *Nature methods* 11, 3 (2014), 281–289.
- [21] Davide Chicco and Giuseppe Jurman. 2020. The advantages of the Matthews correlation coefficient (MCC) over F1 score and accuracy in binary classification evaluation. *BMC genomics* 21, 1 (2020), 1–13.
- [22] Davide Chicco, Niklas Tötsch, and Giuseppe Jurman. 2021. The Matthews correlation coefficient (MCC) is more reliable than balanced accuracy, bookmaker informedness, and markedness in two-class confusion matrix evaluation. *BioData mining* 14, 1 (2021), 1–22.
- [23] Nancy Chinchor. 1992. MUC-4 Evaluation Metrics. In *Proceedings of the 4th Conference on Message Understanding (McLean, Virginia) (MUC4 '92)*. Association for Computational Linguistics, USA, 22–29. <https://doi.org/10.3115/1072064.1072067>
- [24] Noel Codella, Veronica Rotemberg, Philipp Tschandl, M Emre Celebi, Stephen Dusza, David Gutman, Brian Helba, Aadi Kallou, Konstantinos Liopyris, Michael Marchetti, et al. 2019. Skin lesion analysis toward melanoma detection 2018: A challenge hosted by the international skin imaging collaboration (isic). *arXiv preprint arXiv:1902.03368* (2019).
- [25] Nancy R Cook. 2007. Use and misuse of the receiver operating characteristic curve in risk prediction. *Circulation* 115, 7 (2007), 928–935.
- [26] Paulo Correia and Fernando Pereira. 2006. Video object relevance metrics for overall segmentation quality evaluation. *EURASIP Journal on Advances in Signal Processing* 2006 (2006), 1–11.
- [27] Jesse Davis and Mark Goadrich. 2006. The relationship between Precision-Recall and ROC curves. In *Proceedings of the 23rd international conference on Machine learning*. 233–240.
- [28] Lee R Dice. 1945. Measures of the amount of ecologic association between species. *Ecology* 26, 3 (1945), 297–302.
- [29] Michal Drozdal, Eugene Vorontsov, Gabriel Chartrand, Samuel Kadoury, and Chris Pal. 2016. The importance of skip connections in biomedical image segmentation. In *Deep learning and data labeling for medical applications*. Springer, 179–187.
- [30] Mark Everingham, SM Ali Eslami, Luc Van Gool, Christopher KI Williams, John Winn, and Andrew Zisserman. 2015. The pascal visual object classes challenge: A retrospective. *International journal of computer vision* 111, 1 (2015), 98–136.

- [31] Mark Everingham, Luc Van Gool, Christopher KI Williams, John Winn, and Andrew Zisserman. 2010. The pascal visual object classes (voc) challenge. *International journal of computer vision* 88, 2 (2010), 303–338.
- [32] Tilmann Gneiting and Adrian E. Raftery. 2007. Strictly Proper Scoring Rules, Prediction, and Estimation. *J. Amer. Statist. Assoc.* 102, 477 (March 2007), 359–378. <https://doi.org/10.1198/016214506000001437>
- [33] Mark J Gooding, Annamarie J Smith, Maira Tariq, Paul Aljabar, Devis Peressutti, Judith van der Stoep, Bart Reymen, Daisy Emans, Djoya Hattu, Judith van Loon, et al. 2018. Comparative evaluation of autocontouring in clinical practice: a practical method using the Turing test. *Medical physics* 45, 11 (2018), 5105–5115.
- [34] Margherita Grandini, Enrico Bagli, and Giorgio Visani. 2020. Metrics for multi-class classification: an overview. *arXiv preprint arXiv:2008.05756* (2020).
- [35] Chuan Guo, Geoff Pleiss, Yu Sun, and Kilian Q Weinberger. 2017. On Calibration of Modern Neural Networks. *ICML* (2017), 10.
- [36] David J Hand and Robert J Till. 2001. A simple generalisation of the area under the ROC curve for multiple class classification problems. *Machine learning* 45, 2 (2001), 171–186.
- [37] James A Hanley and Barbara J McNeil. 1982. The meaning and use of the area under a receiver operating characteristic (ROC) curve. *Radiology* 143, 1 (1982), 29–36.
- [38] Steven Hicks, Inga Strüke, Vajira Thambawita, Malek Hammou, Pål Halvorsen, Michael Riegler, and Sravanthi Parasa. 2021. On evaluation metrics for medical applications of artificial intelligence. *medRxiv* (2021).
- [39] Katrin Honauer, Lena Maier-Hein, and Daniel Kondermann. 2015. The hci stereo metrics: Geometry-aware performance analysis of stereo algorithms. In *Proceedings of the IEEE International Conference on Computer Vision*. 2120–2128.
- [40] Mohammad Hossin and Md Nasir Sulaiman. 2015. A review on evaluation metrics for data classification evaluations. *International journal of data mining & knowledge management process* 5, 2 (2015), 1.
- [41] Daniel P Huttenlocher, Gregory A. Klanderman, and William J Rucklidge. 1993. Comparing images using the Hausdorff distance. *IEEE Transactions on pattern analysis and machine intelligence* 15, 9 (1993), 850–863.
- [42] Paul Jaccard. 1912. The distribution of the flora in the alpine zone. 1. *New phytologist* 11, 2 (1912), 37–50.
- [43] Paul F Jaeger, Simon AA Kohl, Sebastian Bickelhaupt, Fabian Isensee, Tristan Anselm Kuder, Heinz-Peter Schlemmer, and Klaus H Maier-Hein. 2020. Retina U-Net: Embarrassingly simple exploitation of segmentation supervision for medical object detection. In *Machine Learning for Health Workshop*. PMLR, 171–183.
- [44] Paul Ferdinand Jäger. 2020. Challenges and Opportunities of End-to-End Learning in Medical Image Classification. (2020).
- [45] Pierre Jannin, Christophe Grova, and Calvin R Maurer. 2006. Model for defining and reporting reference-based validation protocols in medical image processing. *International Journal of Computer Assisted Radiology and Surgery* 1, 2 (2006), 63–73.
- [46] Liang Jin, Jiancheng Yang, Kaiming Kuang, Bingbing Ni, Yiyi Gao, Yingli Sun, Pan Gao, Weiling Ma, Mingyu Tan, Hui Kang, et al. 2020. Deep-learning-assisted detection and segmentation of rib fractures from CT scans: Development and validation of FracNet. *EBioMedicine* 62 (2020), 103106.
- [47] Leo Joskowicz, D Cohen, N Caplan, and J Sosna. 2019. Inter-observer variability of manual contour delineation of structures in CT. *European radiology* 29, 3 (2019), 1391–1399.
- [48] Jens N Kaftan, Atilla P Kiraly, Annemarie Bakai, Marco Das, Carol L Novak, and Til Aach. 2008. Fuzzy pulmonary vessel segmentation in contrast enhanced CT data. In *Medical Imaging 2008: Image Processing*, Vol. 6914. International Society for Optics and Photonics, 69141Q.
- [49] Kaggle. 2021. Satorius Cell Instance Segmentation 2021. <https://www.kaggle.com/c/sartorius-cell-instance-segmentation>. [Online; accessed 25-April-2022].
- [50] Alexander Kirillov, Kaiming He, Ross Girshick, Carsten Rother, and Piotr Dollár. 2019. Panoptic segmentation. In *Proceedings of the IEEE/CVF Conference on Computer Vision and Pattern Recognition*. 9404–9413.
- [51] Florian Kofler, Ivan Ezhov, Fabian Isensee, Christoph Berger, Maximilian Korner, Johannes Paetzold, Hongwei Li, Suprosanna Shit, Richard McKinley, Spyridon Bakas, et al. 2021. Are we using appropriate segmentation metrics? Identifying correlates of human expert perception for CNN training beyond rolling the DICE coefficient. *arXiv preprint arXiv:2103.06205v1* (2021).
- [52] Ender Konukoglu, Ben Glocker, Dong Hye Ye, Antonio Criminisi, and Kilian M Pohl. 2012. Discriminative segmentation-based evaluation through shape dissimilarity. *IEEE transactions on medical imaging* 31, 12 (2012), 2278–2289.
- [53] Harold W Kuhn. 1955. The Hungarian method for the assignment problem. *Naval research logistics quarterly* 2, 1-2 (1955), 83–97.
- [54] Tsung-Yi Lin, Michael Maire, Serge Belongie, James Hays, Pietro Perona, Deva Ramanan, Piotr Dollár, and C Lawrence Zitnick. 2014. Microsoft coco: Common objects in context. In *European conference on computer vision*. Springer, 740–755.

- [55] Hua Ma, Andriy I Bandos, Howard E Rockette, and David Gur. 2013. On use of partial area under the ROC curve for evaluation of diagnostic performance. *Statistics in medicine* 32, 20 (2013), 3449–3458.
- [56] Aouatef Mahani and Ahmed Riad Baba Ali. 2019. Classification problem in imbalanced datasets. *Recent Trends in Computational Intelligence* (2019), 1–23.
- [57] Lena Maier-Hein, Matthias Eisenmann, Annika Reinke, Sinan Onogur, Marko Stankovic, Patrick Scholz, Tal Arbel, Hrvoje Bogunovic, Andrew P Bradley, Aaron Carass, et al. 2018. Why rankings of biomedical image analysis competitions should be interpreted with care. *Nature communications* 9, 1 (2018), 1–13.
- [58] Ran Margolin, Lihi Zelnik-Manor, and Ayellet Tal. 2014. How to evaluate foreground maps?. In *Proceedings of the IEEE conference on computer vision and pattern recognition*. 248–255.
- [59] Brian W Matthews. 1975. Comparison of the predicted and observed secondary structure of T4 phage lysozyme. *Biochimica et Biophysica Acta (BBA)-Protein Structure* 405, 2 (1975), 442–451.
- [60] Pavel Matula, Martin Maška, Dmitry V Sorokin, Petr Matula, Carlos Ortiz-de Solórzano, and Michal Kozubek. 2015. Cell tracking accuracy measurement based on comparison of acyclic oriented graphs. *PLoS one* 10, 12 (2015), e0144959.
- [61] Marina Meilă. 2003. Comparing clusterings by the variation of information. In *Learning theory and kernel machines*. Springer, 173–187.
- [62] Bjoern H Menze, Andras Jakab, Stefan Bauer, Jayashree Kalpathy-Cramer, Keyvan Farahani, Justin Kirby, Yuliya Burren, Nicole Porz, Johannes Slotboom, Roland Wiest, et al. 2014. The multimodal brain tumor image segmentation benchmark (BRATS). *IEEE transactions on medical imaging* 34, 10 (2014), 1993–2024.
- [63] Pawel Mlynarski, Hervé Delingette, Hamza Alghamdi, Pierre-Yves Bondiaud, and Nicholas Ayache. 2020. Anatomically consistent CNN-based segmentation of organs-at-risk in cranial radiotherapy. *Journal of Medical Imaging* 7, 1 (2020), 014502.
- [64] Karel GM Moons, Douglas G Altman, Johannes B Reitsma, John PA Ioannidis, Petra Macaskill, Ewout W Steyerberg, Andrew J Vickers, David F Ransohoff, and Gary S Collins. 2015. Transparent Reporting of a multivariable prediction model for Individual Prognosis or Diagnosis (TRIPOD): explanation and elaboration. *Annals of internal medicine* 162, 1 (2015), W1–W73.
- [65] Ying-Hwey Nai, Bernice W Teo, Nadya L Tan, Sophie O’Doherty, Mary C Stephenson, Yee Liang Thian, Edmund Chiong, and Anthonin Reilhac. 2021. Comparison of metrics for the evaluation of medical segmentations using prostate MRI dataset. *Computers in Biology and Medicine* 134 (2021), 104497.
- [66] Tanya Nair. 2018. *Exploring uncertainty measures in deep networks for multiple sclerosis lesion detection and segmentation*. Ph.D. Dissertation. McGill University.
- [67] Nudrat Nida, Aun Irtaza, Ali Javed, Muhammad Haroon Yousaf, and Muhammad Tariq Mahmood. 2019. Melanoma lesion detection and segmentation using deep region based convolutional neural network and fuzzy C-means clustering. *International journal of medical informatics* 124 (2019), 37–48.
- [68] Stanislav Nikolov, Sam Blackwell, Alexei Zverovitch, Ruheena Mendes, Michelle Livne, Jeffrey De Fauw, Yojan Patel, Clemens Meyer, Harry Askham, Bernadino Romera-Paredes, et al. 2021. Clinically applicable segmentation of head and neck anatomy for radiotherapy: deep learning algorithm development and validation study. *Journal of Medical Internet Research* 23, 7 (2021), e26151.
- [69] Kemal Oksuz, Baris Can Cam, Emre Akbas, and Sinan Kalkan. 2018. Localization recall precision (LRP): A new performance metric for object detection. In *Proceedings of the European Conference on Computer Vision (ECCV)*. 504–519.
- [70] David MW Powers. 2020. Evaluation: from precision, recall and F-measure to ROC, informedness, markedness and correlation. *arXiv preprint arXiv:2010.16061* (2020).
- [71] William M Rand. 1971. Objective criteria for the evaluation of clustering methods. *Journal of the American Statistical Association* 66, 336 (1971), 846–850.
- [72] Annika Reinke, Matthias Eisenmann, Sinan Onogur, Marko Stankovic, Patrick Scholz, Peter M Full, Hrvoje Bogunovic, Bennett A Landman, Oskar Maier, Bjoern Menze, et al. 2018. How to exploit weaknesses in biomedical challenge design and organization. In *International Conference on Medical Image Computing and Computer-Assisted Intervention*. Springer, 388–395.
- [73] Annika Reinke, Matthias Eisenmann, Minu D Tizabi, Carole H Sudre, Tim Rädtsch, Michela Antonelli, Tal Arbel, Spyridon Bakas, M Jorge Cardoso, Veronika Cheplygina, et al. 2021. Common limitations of image processing metrics: A picture story. *arXiv preprint arXiv:2104.05642* (2021).
- [74] Olaf Ronneberger, Philipp Fischer, and Thomas Brox. 2015. U-Net: Convolutional Networks for Biomedical Image Segmentation. In *Medical Image Computing and Computer-Assisted Intervention – MICCAI 2015 (Lecture Notes in Computer Science)*, Nassir Navab, Joachim Hornegger, William M. Wells, and Alejandro F. Frangi (Eds.). Springer International Publishing, Cham, 234–241. https://doi.org/10.1007/978-3-319-24574-4_28
- [75] Azriel Rosenfeld and John L Pfaltz. 1966. Sequential operations in digital picture processing. *Journal of the ACM (JACM)* 13, 4 (1966), 471–494.

- [76] Tobias Roß, Annika Reinke, Peter M Full, Martin Wagner, Hannes Kenngott, Martin Aplitz, Hellena Hempe, Diana Mindroc-Filimon, Patrick Scholz, Thuy Nuong Tran, et al. 2021. Comparative validation of multi-instance instrument segmentation in endoscopy: results of the ROBUST-MIS 2019 challenge. *Medical image analysis* 70 (2021), 101920.
- [77] Daniel Sage, Hagai Kirshner, Thomas Pengo, Nico Stuurman, Junhong Min, Suliana Manley, and Michael Unser. 2015. Quantitative evaluation of software packages for single-molecule localization microscopy. *Nature methods* 12, 8 (2015), 717–724.
- [78] Anindo Saha, Joeran Bosma, Jasper Linmans, Matin Hosseinzadeh, and Henkjan Huisman. 2021. Anatomical and Diagnostic Bayesian Segmentation in Prostate MRI – Should Different Clinical Objectives Mandate Different Loss Functions? *arXiv preprint arXiv:2110.12889* (2021).
- [79] Frank W Samuelson and Nicholas Petrick. 2006. Comparing image detection algorithms using resampling. In *3rd IEEE International Symposium on Biomedical Imaging: Nano to Macro*, 2006. IEEE, 1312–1315.
- [80] Cristina Sánchez-Montes, Francisco Javier Sánchez, Jorge Córdova, María López-Cerón, Miriam Cuatrecasas, Cristina Rodríguez De Miguel, Ana García-Rodríguez, Rodrigo Garcés-Durán, María Pellisé, et al. 2019. Computer-aided prediction of polyp histology on white light colonoscopy using surface pattern analysis. *Endoscopy* 51, 03 (2019), 261–265.
- [81] Uwe Schmidt, Martin Weigert, Coleman Broaddus, and Gene Myers. 2018. Cell detection with star-convex polygons. In *International Conference on Medical Image Computing and Computer-Assisted Intervention*. Springer, 265–273.
- [82] Arnaud Arindra Adiyoso Setio, Alberto Traverso, Thomas De Bel, Moira SN Berens, Cas Van Den Bogaard, Piergiorgio Cerello, Hao Chen, Qi Dou, Maria Evelina Fantacci, Bram Geurts, et al. 2017. Validation, comparison, and combination of algorithms for automatic detection of pulmonary nodules in computed tomography images: the LUNA16 challenge. *Medical image analysis* 42 (2017), 1–13.
- [83] Suprosanna Shit, Johannes C Paetzold, Anjany Sekuboyina, Ivan Ezhov, Alexander Unger, Andrey Zhylyka, Josien PW Pluim, Ulrich Bauer, and Bjoern H Menze. 2021. cDice-a novel topology-preserving loss function for tubular structure segmentation. In *Proceedings of the IEEE/CVF Conference on Computer Vision and Pattern Recognition*. 16560–16569.
- [84] Jacob Shreffler and Martin R Huecker. 2020. Diagnostic testing accuracy: Sensitivity, specificity, predictive values and likelihood ratios. (2020).
- [85] Amber L Simpson, Michela Antonelli, Spyridon Bakas, Michel Billelo, Keyvan Farahani, Bram Van Ginneken, Annette Kopp-Schneider, Bennett A Landman, Geert Litjens, Bjoern Menze, et al. 2019. A large annotated medical image dataset for the development and evaluation of segmentation algorithms. *arXiv preprint arXiv:1902.09063* (2019).
- [86] Ana-Maria Simundić. 2009. Measures of diagnostic accuracy: basic definitions. *ejifcc* 19, 4 (2009), 203.
- [87] Carsen Stringer, Tim Wang, Michalis Michaelos, and Marius Pachitariu. 2021. Cellpose: a generalist algorithm for cellular segmentation. *Nature methods* 18, 1 (2021), 100–106.
- [88] Carole H Sudre, Wenqi Li, Tom Vercauteren, Sebastien Ourselin, and M Jorge Cardoso. 2017. Generalised dice overlap as a deep learning loss function for highly unbalanced segmentations. In *Deep learning in medical image analysis and multimodal learning for clinical decision support*. Springer, 240–248.
- [89] Yanmin Sun, Andrew K. C. Wong, and Mohamed S. Kamel. 2009. Classification of Imbalanced Data: a Review. *Int. J. Pattern Recognit. Artif. Intell.* 23 (2009), 687–719.
- [90] Abdel Aziz Taha and Allan Hanbury. 2015. Metrics for evaluating 3D medical image segmentation: analysis, selection, and tool. *BMC medical imaging* 15, 1 (2015), 1–28.
- [91] Abdel Aziz Taha, Allan Hanbury, and Oscar A Jimenez del Toro. 2014. A formal method for selecting evaluation metrics for image segmentation. In *2014 IEEE international conference on image processing (ICIP)*. IEEE, 932–936.
- [92] Vladimir Ulman, Martin Maška, Klas EG Magnusson, Olaf Ronneberger, Carsten Haubold, Nathalie Harder, Pavel Matula, Petr Matula, David Svoboda, Miroslav Radojevic, et al. 2017. An objective comparison of cell-tracking algorithms. *Nature methods* 14, 12 (2017), 1141–1152.
- [93] Uchila N Umesh, Robert A Peterson, and Matthew H Sauber. 1989. Interjudge agreement and the maximum value of kappa. *Educational and Psychological Measurement* 49, 4 (1989), 835–850.
- [94] Femke Vaassen, Colien Hazelaar, Ana Vaniqui, Mark Gooding, Brent van der Heyden, Richard Canters, and Wouter van Elmpt. 2020. Evaluation of measures for assessing time-saving of automatic organ-at-risk segmentation in radiotherapy. *Physics and Imaging in Radiation Oncology* 13 (2020), 1–6.
- [95] Bram Van Ginneken, Samuel G Armato III, Bartjan de Hoop, Saskia van Amelsvoort-van de Vorst, Thomas Duindam, Meindert Niemeijer, Keelin Murphy, Arnold Schilham, Alessandra Retico, Maria Evelina Fantacci, et al. 2010. Comparing and combining algorithms for computer-aided detection of pulmonary nodules in computed tomography scans: the ANODE09 study. *Medical image analysis* 14, 6 (2010), 707–722.
- [96] Bram Van Ginneken, Tobias Heimann, and Martin Styner. 2007. 3D segmentation in the clinic: A grand challenge. In *MICCAI Workshop on 3D Segmentation in the Clinic: A Grand Challenge*, Vol. 1. 7–15.
- [97] Andrew J Vickers, Ben Van Calster, and Ewout W Steyerberg. 2016. Net benefit approaches to the evaluation of prediction models, molecular markers, and diagnostic tests. *bmj* 352 (2016).

- [98] Pauli Virtanen, Ralf Gommers, Travis E Oliphant, Matt Haberland, Tyler Reddy, David Cournapeau, Evgeni Burovski, Pearu Peterson, Warren Weckesser, Jonathan Bright, et al. 2020. SciPy 1.0: fundamental algorithms for scientific computing in Python. *Nature methods* 17, 3 (2020), 261–272.
- [99] Peter L Warburton, Jenna L Wang, and Paul G Mezey. 2008. On the balance of simplification and reality in molecular modeling of the electron density. *Journal of Chemical Theory and Computation* 4, 10 (2008), 1627–1636.
- [100] Varduhi Yeghiazaryan and Irina Voiculescu. 2015. An overview of current evaluation methods used in medical image segmentation. *Department of Computer Science, University of Oxford* (2015).
- [101] Varduhi Yeghiazaryan and Irina D Voiculescu. 2018. Family of boundary overlap metrics for the evaluation of medical image segmentation. *Journal of Medical Imaging* 5, 1 (2018), 015006.
- [102] William J Youden. 1950. Index for rating diagnostic tests. *Cancer* 3, 1 (1950), 32–35.

APPENDIX

A Full Author Affiliations

Lena Maier-Hein, l.maier-hein@dkfz.de, German Cancer Research Center (DKFZ), Div. Intelligent Medical Systems and HI Helmholtz Imaging, Heidelberg, Germany and Heidelberg University, Faculty of Mathematics and Computer Science and Medical Faculty, Heidelberg, Germany and National Center for Tumor Diseases (NCT), Heidelberg, Germany

Annika Reinke*, German Cancer Research Center (DKFZ), Div. Intelligent Medical Systems and HI Helmholtz Imaging, Heidelberg, Germany and Heidelberg University, Faculty of Mathematics and Computer Science, Heidelberg, Germany

Evangelia Christodoulou, German Cancer Research Center (DKFZ), Division of Cancer Epidemiology, Heidelberg, Germany

Ben Glocker, Imperial College London, Biomedical Image Analysis Group, Department of Computing, London, UK

Patrick Godau, German Cancer Research Center (DKFZ), Div. Intelligent Medical Systems, Heidelberg, Germany and Heidelberg University, Faculty of Mathematics and Computer Science, Heidelberg, Germany

Fabian Isensee, German Cancer Research Center (DKFZ), HI Applied Computer Vision Lab, Division of Medical Image Computing, Heidelberg, Germany

Jens Kleesiek, University Medicine Essen, Translational Image-guided Oncology (TIO), Institute for AI in Medicine (IKIM), Essen, Germany

Michal Kozubek, Masaryk University, Centre for Biomedical Image Analysis, Brno, Czech Republic

Mauricio Reyes, University of Bern, ARTORG Center for Biomedical Engineering Research, Bern, Switzerland

Michael A. Riegler, Simula Metropolitan Center for Digital Engineering, Oslo, Norway and UiT The Arctic University of Norway, Oslo, Norway

Manuel Wiesenfarth, German Cancer Research Center (DKFZ), Div. Biostatistics, Heidelberg, Germany

Michael Baumgartner, German Cancer Research Center (DKFZ), Div. Medical Image Computing, Heidelberg, Germany

Matthias Eisenmann, German Cancer Research Center (DKFZ), Div. Intelligent Medical Systems and HI Helmholtz Imaging, Heidelberg, Germany

Doreen Heckmann-Nötzel, German Cancer Research Center (DKFZ), Div. Intelligent Medical Systems, Heidelberg, Germany and National Center for Tumor Diseases (NCT), Heidelberg, Germany

A. Emre Kavur, German Cancer Research Center (DKFZ), HI Applied Computer Vision Lab, Division of Medical Image Computing; Div. Intelligent Medical Systems, Heidelberg, Germany

Tim Rüdtsch, German Cancer Research Center (DKFZ), Div. Intelligent Medical Systems and HI Helmholtz Imaging, Heidelberg, Germany

Minu D. Tizabi, German Cancer Research Center (DKFZ), Div. Intelligent Medical Systems and HI Helmholtz Imaging, Heidelberg, Germany

Laura Acion, CONICET – Universidad de Buenos Aires, Instituto de Cálculo, Buenos Aires, Argentina and University of Iowa, Department of Psychiatry, Iowa City, Iowa, USA

Michela Antonelli, King's College London, School of Biomedical Engineering and Imaging Science, London, UK and University College London, Centre for Medical Image Computing, London, UK

Tal Arbel, McGill University, Centre for Intelligent Machines and MILA (Quebec Artificial Intelligence Institute), Montreal, Canada

Spyridon Bakas, University of Pennsylvania, Center for Biomedical Image Computing & Analytics, Philadelphia, Pennsylvania, USA and Perelman School of Medicine at the University of Pennsylvania, Department of Pathology & Laboratory Medicine and Department of Radiology, Philadelphia, Pennsylvania, USA

Peter Bankhead, University of Edinburgh, Institute of Genetics and Cancer, Edinburgh, UK

Arriel Benis, Holon Institute of Technology, Faculty of Industrial Engineering and Technology Management, Faculty of Digital Technologies in Medicine, Holon, Israel

M. Jorge Cardoso, King's College London, School of Biomedical Engineering and Imaging Science, London, UK and University College London, Department of Medical Physics and Biomedical Engineering, London, UK

Veronika Cheplygina, IT University of Copenhagen, Copenhagen, Denmark
Beth Cimini, Broad Institute of MIT and Harvard, Imaging Platform, Cambridge, Massachusetts, USA
Gary S. Collins, University of Oxford, Centre for Statistics in Medicine, Oxford, UK
Keyvan Farahani, National Cancer Institute, Center for Biomedical Informatics and Information Technology, USA
Bram van Ginneken, Fraunhofer MEVIS, Bremen, Germany and Radboud University Medical Center, Radboud Institute for Health Sciences, Nijmegen, The Netherlands
Daniel A. Hashimoto, Case Western Reserve University School of Medicine, University Hospitals Cleveland Medical Center, Cleveland, Ohio, USA
Michael M. Hoffman, University Health Network, Princess Margaret Cancer Centre, Toronto, Canada and University of Toronto, Department of Medical Biophysics, Department of Computer Science, Toronto, Canada and Vector Institute, Toronto, Canada
Merel Huisman, Radboud University Medical Center, Department of Radiology, Nijmegen, The Netherlands
Pierre Jannin, Université de Rennes 1, Inserm, Laboratoire Traitement du Signal et de l'Image – UMR_S 1099, Rennes, France
Charles E. Kahn, University of Pennsylvania, Perelman School of Medicine, Philadelphia, Pennsylvania, USA
Alexandros Karargyris, IHU Strasbourg, Strasbourg, France
Alan Karthikesalingam, Google Health Deepmind, London, UK
Hannes Kenngott, Heidelberg University Hospital, Department of General, Visceral and Transplantation Surgery, Heidelberg, Germany
Annette Kopp-Schneider, German Cancer Research Center (DKFZ), Div. Biostatistics, Heidelberg, Germany
Anna Kreshuk, European Molecular Biology Laboratory (EMBL), Cell Biology and Biophysics Unit, Heidelberg, Germany
Tahsin Kurc, Stony Brook University, Stony Brook Cancer Center, Stony Brook, New York, USA
Bennett A. Landman, Vanderbilt University, Electrical Engineering, Nashville, Tennessee, USA
Geert Litjens, Radboud University Medical Center, Department of Pathology and Radboud Institute for Health Sciences, Nijmegen, The Netherlands
Amin Madani, University Health Network, Department of Surgery, Toronto, Canada
Klaus Maier-Hein, German Cancer Research Center (DKFZ), Div. Medical Image Computing, Heidelberg, Germany
Anne L. Martel, Sunnybrook Research Institute, Physical Sciences, Toronto, Canada and University of Toronto, Department of Medical Biophysics, Toronto, Canada
Peter Mattson, Google, Mountain View, US
Erik Meijering, University of New South Wales, School of Computer Science and Engineering, New South Wales, Australia
Bjoern Menze, University of Zurich, Department of Quantitative Biomedicine, Zurich, Switzerland
David Moher, Ottawa Hospital Research Institute, Centre for Journalology, Clinical Epidemiology Program, Ottawa, Canada and University of Ottawa, School of Epidemiology and Public Health, Faculty of Medicine, Ottawa, Canada
Karel G.M. Moons, UMC Utrecht, University Utrecht, Julius Center for Health Sciences and Primary Care, Utrecht, The Netherlands
Henning Müller, University of Applied Sciences Western Switzerland (HES-SO), Information Systems Institute, Sierre, Switzerland and University of Geneva, Medical Faculty, Geneva, Switzerland
Brennan Nichyporuk, MILA (Quebec Artificial Intelligence Institute), Montreal, Canada
Felix Nickel, Heidelberg University Hospital, Department of General, Visceral and Transplantation Surgery, Heidelberg, Germany
Jens Petersen, German Cancer Research Center (DKFZ), Div. Medical Image Computing, Heidelberg, Germany
Nasir Rajpoot, University of Warwick, Tissue Image Analytics Laboratory, Department of Computer Science, Coventry, West Midlands, UK
Nicola Rieke, NVIDIA GmbH, Munich, Germany
Julio Saez-Rodriguez, Heidelberg University, Institute for Computational Biomedicine, Heidelberg, Germany,

Faculty of Medicine and Heidelberg University Hospital, Heidelberg, Germany and BioQuant, Heidelberg, Germany

Clarisa Sánchez Gutiérrez, University of Amsterdam, Informatics Institute, Faculty of Science, Amsterdam, The Netherlands

Shravya Shetty, Google, Google Health, Palo Alto, US

Maarten van Smeden, University Medical Center Utrecht, Julius Center for Health Sciences and Primary Care, Utrecht, The Netherlands

Carole H. Sudre, University College London, Centre for Medical Image Computing and Medical Research Council Unit for Lifelong Health and Ageing at UCL, London, UK and King's College London, School of Biomedical Engineering and Imaging Science, London, UK

Ronald M. Summers, National Institutes of Health, Radiology and Imaging Sciences, Clinical Center, Bethesda, Maryland, USA

Abdel A. Taha, Scigility International GmbH, Vienna, Austria

Sotirios A. Tsaftaris, The University of Edinburgh, School of Engineering, Edinburgh, Scotland

Ben Van Calster, Katholieke Universiteit (KU) Leuven, Department of Development and Regeneration and EPI-centre, Leuven, Belgium and Leiden University Medical Center, Department of Biomedical Data Sciences, Leiden, The Netherlands

Gaël Varoquaux, INRIA Saclay-Île de France, Parietal Project-team, Palaiseau, France

Paul F. Jäger, German Cancer Research Center (DKFZ), Interactive Machine Learning Group and HI Helmholtz Imaging, Heidelberg, Germany.

B Symbol References

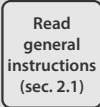
Symbol	Explanation
	Start of a process
	End of a process
	Task to be performed by the user
	Subtask/Subprocess
	Task with reference to problem fingerprint
	A metric/criterion/strategy is added to the collection of relevant candidates to choose from
	A metric/criterion/strategy is selected
	Group
	<p>Exclusive gateway: An exclusive gateway (or XOR-gateway) allows you to make a decision. It can have multiple outgoing sequence flows. It is used when several conditions are mutually exclusive and only one selection is possible.</p> <p>An exclusive gateway is also used to join multiple incoming flows together and improve the readability of the diagram.</p>
	Notes
	Warning
	Further information

Fig. 13. **Overview of symbols used in the process diagrams.** The notation used in the process diagrams originates from Business Process Model and Notation (BPMN).

C Acronyms

AP Average Precision
ASSD Average Symmetric Surface Distance
AUC Area under the curve
AUROC Area under the Receiver Operating Characteristic Curve
BA Balanced Accuracy
Boundary IoU Boundary Intersection over Union
BM Bookmaker Informedness
BPMN Business Process Model and Notation
cIDice Center line Dice Similarity Coefficient
CT Computed Tomography
DSC Dice Similarity Coefficient
FN False Negative
FP False Positive
FPPI False Positives per Image
FPR False Positive Rate
FROC Free-Response Receiver Operating Characteristic
HD Hausdorff Distance
HD95 Hausdorff Distance 95% Percentile
IoU Intersection over Union
IoR Intersection over Reference
LR+ Positive Likelihood Ratio
MASD Mean Average Surface Distance
MCC Matthews Correlation Coefficient
MRI Magnetic Resonance Imaging
NaN Not a Number
NPV Negative Predictive Value
NSD Normalized Surface Distance
PPV Positive Predictive Value
PQ Panoptic Quality
PR Precision-Recall
RI Rand Index
ROC Receiver Operating Characteristic
TN True Negative
TNR True Negative Rate
TP True Positive
TPR True Positive Rate
VoI Variation of Information
Xth Percentile HD Xth Percentile Hausdorff Distance

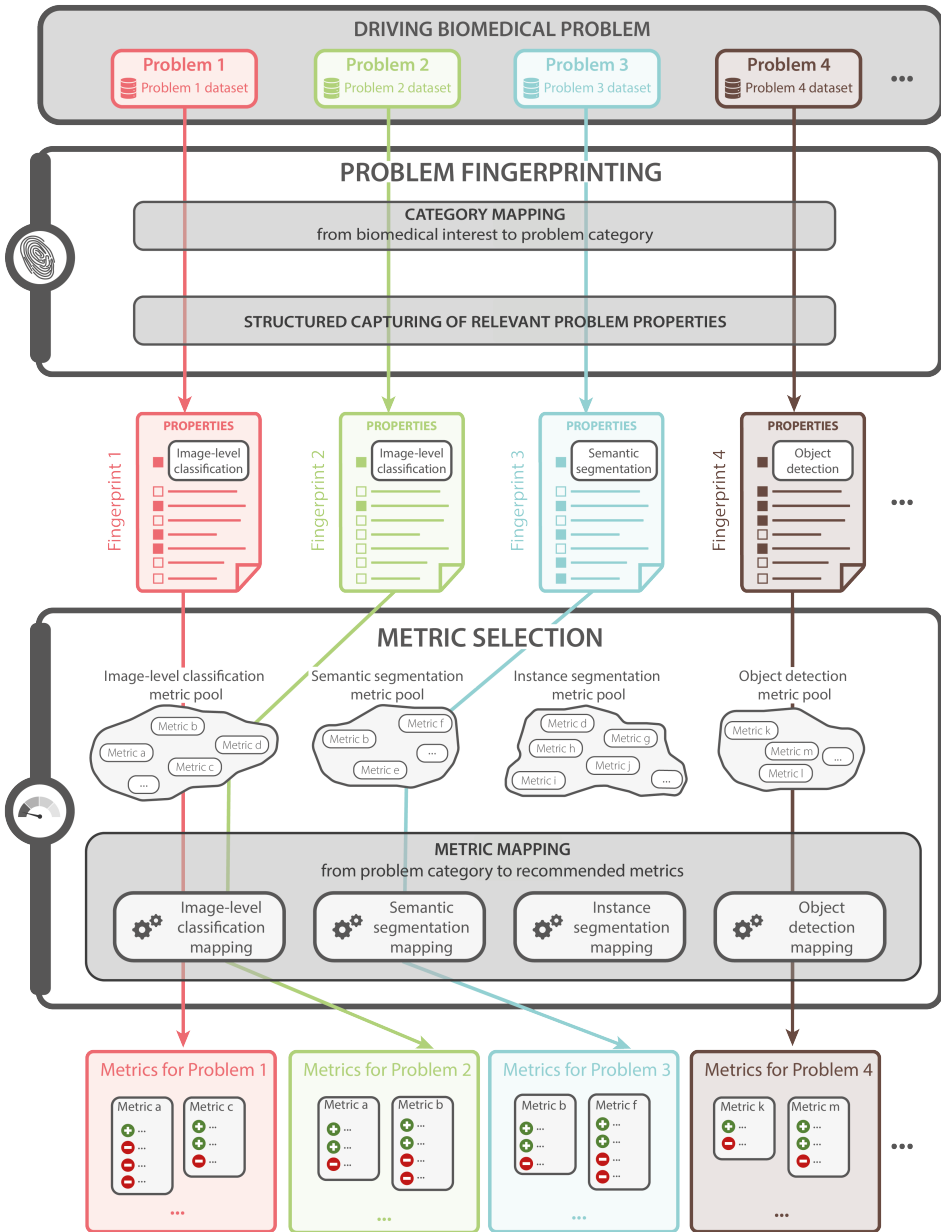


Fig. 14. **Metric recommendation framework.** Choosing metrics for a driving biomedical question is achieved in two main steps. *Problem fingerprinting* refers to the step of capturing the characteristics of the driving biomedical problem relevant for metric selection. This includes the mapping of the given problem to the appropriate image processing category (see also Fig. 4), namely *image-level classification*, *semantic segmentation*, *instance segmentation* and *object detection*. Next, the *metric mapping* generates a set of suitable metrics, including problem-specific strength-weaknesses profiles, from a category-specific pool of metrics.

D Problem Category-specific Fingerprints

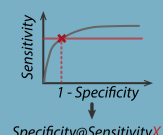
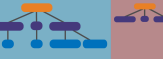
<p>1.1 Image processing category identified by category mapping</p>	<p>Applied in S3 and S4</p>		<p>Image-level classification (ILC): assignment of one or multiple category labels to the entire image. <i>Example: disease screening; deciding on the presence or absence of a certain condition/pathology without localizing the phenomenon.</i></p>
<p>Domain interest-related properties</p>			
<p>2.5 Penalization of errors There may be a preference for certain types of errors from a domain perspective.</p>			
<p>2.5.1 Unequal handling of classes requested</p>	<p>Applied in D2.1</p>		<p>There is a preference for one or several of the classes. As a consequence, it may be desirable to give more weight to the more important classes when aggregating class-specific scores. <i>Example: full surgical scene segmentation for autonomous robotics; critical structures, such as nerves or vessels, should be more accurately localized compared to fatty tissue.</i></p>
<p>2.5.2 Unequal handling of class confusions requested</p>	<p>Applied in S2, D3.1, D4.1 and D4.4</p>		<p>Any class can be confused with another, but certain mismatches are more severe than others, from a domain point of view. <i>Example 1 (binary): polyp detection; a FN (missed polyp) is clinically much more severe than a FP.</i> <i>Example 2 (multi-class): lung tumor categorization T1-T5 depends largely on structure size, implying an ordinal scale of classes.</i></p>
<p>2.5.3 Compensation of unequal class frequencies requested</p>	<p>Applied in S2 and Sec. 7</p>		<p>The test data may (1) feature a balanced class distribution, (2) reflect the class distribution of the real-world population, or (3) feature a rather arbitrary distribution of classes. If (2) and (3) are undesired, unequal class frequencies may be compensated.</p>
<p>2.6 Cutoff on predicted class scores Options: - Predefined target value - Default strategy - No interest in cutoff at all</p>	<p>Applied in S2, S4 and D3.3</p>		<p>Modern algorithms output continuous class scores. Setting a cutoff value on the scores enables the generation of a (cutoff-specific) confusion matrix and thus the computation of popular single-threshold counting metrics, such as sensitivity, precision and F1 score. The cutoff can be set in a way that a specific target metric value is reached (e.g. a certain sensitivity) or based on a default value/strategy (e.g. 0.5 in the binary case, argmax for more classes). Some communities argue that no cutoff value at all is needed for comprehensive validation. Based on the biomedical interest, the following options are available: - Use predefined target value for sensitivity/ specificity/PPV/FPI - Use default cutoff value or infer value from optimizing primary metric on validation set. The Youden Index, for example, is commonly maximized to determine an optimal cutoff. - No interest in cutoff at all Once a cutoff value for the predicted class probabilities has been set in such a way that the target metric value is achieved (if any), other metric values are then obtained from the corresponding fixed confusion matrix, e.g. PPV@Sensitivity.</p>
<p>Target structure-related properties</p>			
<p>3.4 Possibility of multiple labels per unit (pixel or image)</p>	<p>Applied in Sec. 7</p>		<p>Multiple categories may be assigned to one image. <i>Examples: image classified with multiple pathologies during a screening process.</i></p>
<p>Data set-related properties</p>			
<p>4.1 High class imbalance</p>	<p>Applied in D3.1, D4.1 and Sec. 7</p>		<p>The class frequencies differ substantially. Further reading: [Mahani & Ali, 2019].</p>
<p>4.4 Non-independence of test cases</p>	<p>Applied in Sec. 7</p>		<p>The test cases are hierarchically structured, indicating non-independence of test cases. <i>Examples: multiple images of the same patient, hospital or video.</i></p>
<p>Algorithm output-related properties</p>			
<p>5.1 Availability of predicted class scores</p>	<p>Applied in S4</p>		<p>Modern algorithms in biomedical image classification output continuous class scores, which are often interpreted as predicted class probabilities. These scores contain relevant information about the performance of a model and are thus crucial for comprehensive and meaningful validation. If no predicted class probabilities are available, this property is set to false.</p>
<p>5.3 Possibility of invalid algorithm output (e.g. Prediction is NaN)</p>	<p>Applied in Sec. 7</p>		<p>The files representing the algorithm output can contain invalid output.</p>

Fig. 15. **Fingerprint for image-level classification.** In the case of binary fingerprints, the blue column shows examples for which the property is true while the red column shows counterexamples. Categorical fingerprints are only shown in blue.

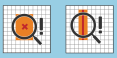
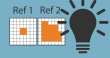
<p>1.1 Image processing category identified by category mapping</p>	<p>Applied in S7</p>		<p>Semantic segmentation (SS): assignment of one or multiple category labels to each pixel. <i>Example: surgical scene segmentation for autonomous robotics; assigning each pixel the corresponding structure/organ/pathology label.</i></p>
Domain interest-related properties			
<p>2.1 Particular importance of structure boundaries</p>	<p>Applied in S8</p>		<p>The biomedical application requires exact structure boundaries. <i>Example: segmentation for radiotherapy planning; knowledge of exact structure boundaries is crucial to destroy the tumor while sparing healthy tissue.</i></p> <p>Important: Overlap-based metrics do not measure shape agreement. In the cases of complex shapes (high boundary-to-volume ratio) it is therefore typically advisable to set this property to true.</p>
<p>2.2 Particular importance of structure volume</p>	<p>Applied in Sec. 7</p>		<p>The biomedical application requires accurate knowledge of structure volumes. <i>Example: liver segmentation as basis for remnant liver volume computation in surgical resection planning.</i></p>
<p>2.3 Particular importance of structure center (e.g. in cells, vessels)</p>	<p>Applied in S7</p>		<p>The biomedical application requires accurate knowledge of structure centers. <i>Example: cell centers are subsequently used for cell tracking and cell motion characterisation, so false center movement should be suppressed.</i></p>
<p>2.5 Penalization of errors</p>	<p>There may be a preference for certain types of errors from a domain perspective.</p>		
<p>2.5.1 Unequal handling of classes requested</p>	<p>Applied in Sec. 7</p>		<p>There is a preference for one or several of the classes. As a consequence, it may be desirable to give more weight to the more important classes when aggregating class-specific scores. <i>Example: full surgical scene segmentation for autonomous robotics; critical structures, such as nerves or vessels, should be more accurately localized compared to fatty tissue.</i></p>
<p>2.5.2 Unequal handling of class confusions requested</p>	<p>Applied in S7 and S8</p>		<p>Any class can be confused with another, but certain mismatches are more severe than others, from a domain point of view. <i>Example 1 (binary): polyp detection; a FN (missed polyp) is clinically much more severe than a FP.</i> <i>Example 2 (multi-class): Lung tumor categorization T1-T5 depends largely on structure size implying an ordinal scale of classes.</i></p>
<p>2.5.3 Compensation of unequal class frequencies requested</p>	<p>Applied in Sec. 7</p>		<p>The test data may (1) feature a balanced class distribution, (2) reflect the class distribution of the real-world population, or (3) feature a rather arbitrary distribution of classes. If (2) and (3) are undesired, unequal class frequencies may be compensated.</p>
<p>2.5.4 Handling of spatial outliers</p>	<p>Applied in S8 and D8.3</p>		<p>Spatial outliers are FP predictions that feature a large distance to the reference. They can be handled in three different ways: Distance-based penalization with outlier focus: Outliers should be heavily penalized as a function of the distance to the reference. Distance-based penalization with contour focus: Outliers should be penalized as a function of the distance to the reference, but the assessment should focus on the general contour agreement rather than individual outliers. Existence-based penalization: The existence of spatial outliers should be penalized irrespective of their distance to the reference.</p> <p>Distance-based penalization is not possible when either the reference or the prediction is empty. In applications, in which many of such cases potentially occur, we therefore recommend an existence-based penalization.</p>
<p>2.5.5 Compensation for annotation imprecisions requested</p>	<p>Applied in S8</p>		<p>The reference annotation is typically only an approximation of the (forever unknown) ground truth. It may be desirable to compensate for known uncertainties, such as intra-rater or inter-rater variability, by configuring the metric accordingly. This is only possible for some metrics.</p>

Fig. 16. **Fingerprint for semantic segmentation (Part 1).** In the case of binary fingerprints, the blue column shows examples for which the property is true while the red column shows counterexamples. Categorical fingerprints are only shown in blue.

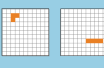
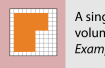
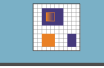
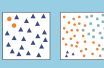
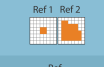
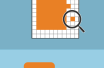
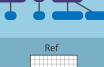
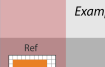
Target structure-related properties				
3.1 Small size of structures relative to pixel size	Applied in S7			A single pixel makes up at least several percentage points of the structure volume. <i>Example: multiple sclerosis lesions in magnetic resonance imaging (MRI) scans.</i>
3.2 High variability of structure sizes (within one image, across images)	Applied in S8			The target structures vary substantially in size, such that some structures are several times the sizes of others. <i>Example: polyps in colonoscopy screening, where some polyps are several times the size of others.</i> <i>Counterexample: large organs, such as the liver or the kidneys, which are relatively comparable in size across individuals.</i>
3.3 Target structures feature tubular shape	Applied in S7			The target structures feature a tubular shape. <i>Examples: vessels, fibers.</i>
3.4 Possibility of multiple labels per unit (pixel or image)	Applied in Sec. 7			Multiple categories may be assigned to one pixel. <i>Examples: labels "tumor core" and "tumor" assigned to the same pixel.</i>
Data set-related properties				
4.1 High class imbalance	Applied in Sec. 7			The class frequencies differ substantially. Further reading: [Mahani & Ali, 2019].
4.2 Uncertainties in the reference		The reference is typically only an approximation of the (forever unknown) ground truth. Various sources and types of errors exist, which require special treatment in the context of metric selection.		
4.2.1 High inter-/intra-rater variability	Applied in S7			The reference can be assumed to be noisy due to high inter-rater variability.
4.2.2 Possibility of spatial outliers in reference annotation	Applied in S8			The reference may feature spatial outliers that are distant from the (unknown) ground truth.
4.4 Non-independence of test cases	Applied in Sec. 7			The test cases are hierarchically structured, indicating non-independence of test cases. <i>Examples: multiple images of the same patient, hospital or video.</i>
4.5 Possibility of reference without target structure(s)	Applied in Sec. 7			There are test cases in which the reference comprises only the background class.
Algorithm output-related properties				
5.2 Possibility of algorithm output not containing the target structure(s)	Applied in S8			The algorithm may yield output images only comprising the background class.
5.3 Possibility of invalid algorithm output (e.g. Prediction is NaN)	Applied in Sec. 7			The files representing the algorithm output can contain invalid output.

Fig. 17. **Fingerprint for semantic segmentation (Part 2).** In the case of binary fingerprints, the blue column shows examples for which the property is true while the red column shows counterexamples. Categorical fingerprints are only shown in blue.

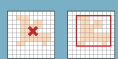
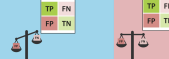
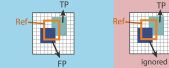
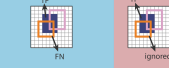
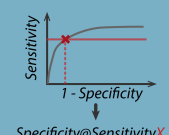
<p>1.1 Image processing category identified by category mapping</p>	<p>Applied in S3, S4 and S5</p>		<p>Object detection (OD): detection and localization of structures of one or multiple categories. <i>Example: detection and bounding box-based localization of polyps in colonoscopy sequences.</i></p>
Domain interest-related properties			
<p>2.3 Particular importance of structure center (e.g. in cells, vessels)</p>	<p>Applied in D5.3</p>		<p>The biomedical application requires accurate knowledge of structure centers. <i>Example: cell centers are subsequently used for cell tracking and cell motion characterisation, so false center movement should be suppressed.</i></p>
<p>2.4 Required granularity of localization</p>	<p>Applied in S5</p>		<p>The granularity of required localization can vary in object detection tasks. We distinguish two main categories: Only position: given an n-dimensional image, the object is represented by its position, encoded in n degrees of freedom (e.g. xyz coordinates of center point). Rough outline: a rough outline of the object is provided, typically given by simple geometric approximations such as bounding boxes or ellipsoids. It should be noted that if a substantial fraction of objects are tiny (F3.1), any outline-based localization becomes very noisy. In such cases, users might want to consider alternative localization strategies, such as a center point-based localization.</p>
<p>2.5 Penalization of errors</p> <p style="text-align: center;">There may be a preference for certain types of errors from a domain perspective.</p>			
<p>2.5.1 Unequal handling of classes requested</p>	<p>Applied in D5.1</p>		<p>There is a preference for one or several of the classes. As a consequence, it may be desirable to give more weight to the more important classes when aggregating class-specific scores. <i>Example: full surgical scene segmentation for autonomous robotics; critical structures, such as nerves or vessels, should be more accurately localized compared to fatty tissue.</i></p>
<p>2.5.2 Unequal handling of class confusions requested</p>	<p>Applied in D3.1, D4.1 and D4.4</p>		<p>Any class can be confused with another, but certain mismatches are more severe than others, from a domain point of view. <i>Example 1 (binary): polyp detection; a FN (missed polyp) is clinically much more severe than a FP.</i> <i>Example 2 (multi-class): Lung tumor categorization T1-T5 depends largely on structure size implying an ordinal scale of classes.</i></p>
<p>2.5.3 Compensation of unequal class frequencies requested</p>	<p>Applied in Sec. 7</p>		<p>The test data may (1) feature a balanced class distribution, (2) reflect the class distribution of the real-world population, or (3) feature a rather arbitrary distribution of classes. If (2) and (3) are undesired, unequal class frequencies may be compensated.</p>
<p>2.5.6 Penalization of multiple predictions assigned to the same reference object requested</p>	<p>Applied in S6 and D6.1</p>		<p>Object detection algorithms involve the step of assigning predicted objects to reference objects. This may result in more than one prediction being assigned to the same reference. This fingerprint should be set to true if all but one prediction of such an assignment should be penalized as FP and set to false if these spare predictions should be ignored during validation.</p>
<p>2.5.7 Penalization of multiple reference objects assigned to same prediction requested</p>	<p>Applied in D5.1</p>		<p>Object detection algorithms involve the step of assigning reference objects to predicted objects. This may result in more than one reference being assigned to the same prediction. If such an assignment should be penalized, this fingerprint should be set to true.</p>
<p>2.6 Cutoff on predicted class scores</p> <p>Options:</p> <ul style="list-style-type: none"> - Predefined target value - Default strategy - No interest in cutoff at all 	<p>Applied in S4 and D3.3</p>	 <p style="text-align: center;"><i>Specificity@Sensitivity_X</i></p>	<p>Modern algorithms output continuous class scores. Setting a cutoff value on the scores enables the generation of a (cutoff-specific) confusion matrix and thus the computation of popular single-threshold counting metrics, such as sensitivity, precision and F1 score. The cutoff can be set in a way that a specific target metric value is reached (e.g. a certain sensitivity) or based on a default value/strategy (e.g. 0.5 in the binary case, argmax for more classes). Some communities argue that no cutoff value at all is needed for comprehensive validation. Based on the biomedical interest, the following options are available:</p> <ul style="list-style-type: none"> - Use predefined target value for sensitivity/ specificity/PPV/FPPV - Use default cutoff value or infer value from optimizing primary metric on validation set. The Youden Index, for example, is commonly maximized to determine an optimal cutoff. - No interest in cutoff at all <p>Once a cutoff value for the predicted class probabilities has been set in such a way that the target metric value is achieved (if any), other metric values are then obtained from the corresponding fixed confusion matrix, e.g. PPV@Sensitivity.</p>

Fig. 18. **Fingerprint for object detection (Part 1)**. In the case of binary fingerprints, the blue column shows examples for which the property is true while the red column shows counterexamples. Categorical fingerprints are only shown in blue.

Target structure-related properties			
3.1 Small size of structures relative to pixel size	Applied in S1 and Sec. 5		A single pixel makes up at least several percentage points of the structure volume. <i>Example: multiple sclerosis lesions in magnetic resonance imaging (MRI) scans.</i>
3.2 High variability of structure sizes (within one image, across images)	Applied in D5.1 and Sec. 5		The target structures vary substantially in size, such that some structures are several times the sizes of others. <i>Example: polyps in colonoscopy screening, where some polyps are several times the size of others.</i> <i>Counterexample: large organs, such as the liver or the kidneys, which are relatively comparable in size across individuals.</i>
3.3 Target structures feature tubular shape	Applied in D5.3 and Sec. 5		The target structures feature a tubular shape. <i>Examples: vessels, fibers.</i>
3.5 Possibility of overlapping or touching target structures (e.g. medical instruments or cells)	Applied in D5.2 and Sec. 5		Different instances of a class can overlap or touch each other. <i>Examples: touching cells, overlapping medical instruments in laparoscopy.</i>
3.6 Possibility of disconnected target structure(s)	Applied in D5.3 and Sec. 5		A given structure appears disconnected in the given image. <i>Examples: single tomographic image slice depicting complex vessel, partially occluded by a medical instrument.</i>
Data set-related properties			
4.1 High class imbalance	Applied in D3.1, D4.1 and Sec. 7		The class frequencies differ substantially. Further reading: [Mahani & Ali, 2019].
4.2 Uncertainties in the reference		The reference is typically only an approximation of the (forever unknown) ground truth. Various sources and types of errors exist, which require special treatment in the context of metric selection.	
4.2.1 High inter-/intra-rater variability	Applied in Sec. 5		The reference can be assumed to be noisy due to high inter-rater variability.
4.3 Granularity of provided reference annotations	Applied in S5 and D5.2		The granularity of the reference can vary in object detection problems. We distinguish three main categories: <u>Only position:</u> Given an n-dimensional image, the object is represented by its position, encoded in n degrees of freedom (e.g. xy/xyz coordinates of center point) <u>Rough outline:</u> A rough outline of the object is provided, typically given by simple geometric objects such as bounding boxes or ellipsoids. <u>Exact outline:</u> The object is outlined exactly.
4.4 Non-independence of test cases	Applied in Sec. 7		The test cases are hierarchically structured, indicating non-independence of test cases. <i>Examples: multiple images of the same patient, hospital or video.</i>
4.5 Possibility of reference without target structure(s)	Applied in Sec. 7		There are test cases in which the reference comprises only the background class.
Algorithm output-related properties			
5.1 Availability of predicted class scores	Applied in S4, S6 and Sec. 5		Modern algorithms in biomedical image classification output continuous class scores, which are often interpreted as predicted class probabilities. These scores contain relevant information about the performance of a model and are thus crucial for comprehensive and meaningful validation. In object detection, predicted class probabilities are typically available for each detected object. If no predicted class probabilities are available, this property is set to false.
5.2 Possibility of algorithm output not containing the target structure(s)	Applied in Sec. 7		The algorithm may yield output images only comprising the background class.
5.3 Possibility of invalid algorithm output (e.g. Prediction is NaN)	Applied in Sec. 7		The files representing the algorithm output can contain invalid output.
5.4 Possibility of overlapping predictions	Applied in S6		Predictions of the algorithm can potentially overlap.

Fig. 19. **Fingerprint for object detection (Part 2).** In the case of binary fingerprints, the blue column shows examples for which the property is true while the red column shows counterexamples. Categorical fingerprints are only shown in blue.

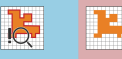
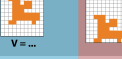
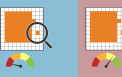
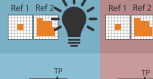
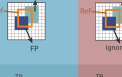
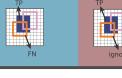
<p>1.1 Image processing category identified by category mapping</p>	<p>Applied in S3, S4, S5 and S7</p>		<p>Instance segmentation (IS): detection and delineation of each distinct object of a particular class. It can be regarded as delivering the tasks of object detection and semantic segmentation at the same time. In contrast to object detection, instance segmentation also involves the accurate marking of the object boundary. In contrast to semantic segmentation, it distinguishes different instances of the same class. <i>Example: cell segmentation with a subsequent goal of cell counting.</i></p>
<p>Domain interest-related properties (part 1)</p>			
<p>2.1 Particular importance of structure boundaries</p>	<p>Applied in S8 and D5.1</p>		<p>The biomedical application requires exact structure boundaries. <i>Example: segmentation for radiotherapy planning; knowledge of exact structure boundaries is crucial to destroy the tumor while sparing healthy tissue.</i></p> <p>Important: Overlap-based metrics do not measure shape agreement. In the cases of complex shapes (high boundary-to-volume ratio) it is therefore typically advisable to set this property to true.</p>
<p>2.2 Particular importance of structure volume</p>	<p>Applied in Sec. 7</p>	 <p>V = ...</p>	<p>The biomedical application requires accurate knowledge of structure volumes. <i>Example: liver segmentation as basis for remnant liver volume computation in surgical resection planning.</i></p>
<p>2.3 Particular importance of structure center (e.g. in cells, vessels)</p>	<p>Applied in S7 and D5.3</p>		<p>The biomedical application requires accurate knowledge of structure centers. <i>Example: cell centers are subsequently used for cell tracking and cell motion characterization, so false center movement should be suppressed.</i></p>
<p>2.5 Penalization of errors</p> <p style="text-align: center;">There may be a preference for certain types of errors from a domain perspective.</p>			
<p>2.5.1 Unequal handling of classes requested</p>	<p>Applied in D5.1</p>		<p>There is a preference for one or several of the classes. As a consequence, it may be desirable to give more weight to the more important classes when aggregating class-specific scores. <i>Example: full surgical scene segmentation for autonomous robotics; critical structures, such as nerves or vessels, should be more accurately localized compared to fatty tissue.</i></p>
<p>2.5.2 Unequal handling of class confusions requested</p> <p>a) for detection b) for segmentation (per instance)</p>	<p>Applied in S7, S8, D4.1 and D4.4</p>		<p>Any class can be confused with another, but certain mismatches are more severe than others, from a domain point of view. <i>Example 1 (binary): polyp detection; a FN (missed polyp) is clinically much more severe than a FP.</i></p> <p>Specifically in instance segmentation problems, the property needs to be set separately for the validation of the (a) detection (relevant decision guide: D4.4) and (b) segmentation performance (relevant subprocesses: S7 and S8). At object level, FNs (missed instances) are typically more severe than FPs, while FNs (e.g. undersegmentation) and FPs (e.g. oversegmentation) may be equally important at pixel level.</p>
<p>2.5.3 Compensation of unequal class frequencies requested</p>	<p>Applied in Sec. 7</p>		<p>The test data may (1) feature a balanced class distribution, (2) reflect the class distribution of the real-world population, or (3) feature a rather arbitrary distribution of classes. If (2) and (3) are undesired, unequal class frequencies may be compensated.</p>
<p>2.5.4 Handling of spatial outliers</p>	<p>Applied in S8 and D8.3</p>		<p>Spatial outliers are FP predictions that feature a large distance to the reference. They can be handled in three different ways: Distance-based penalization with outlier focus: Outliers should be heavily penalized as a function of the distance to the reference. Distance-based penalization with contour focus: Outliers should be penalized as a function of the distance to the reference, but the assessment should focus on the general contour agreement rather than individual outliers. Existence-based penalization: The existence of spatial outliers should be penalized irrespective of their distance to the reference.</p> <p>Distance-based penalization is not possible when either the reference or the prediction is empty. In applications, in which many of such cases potentially occur, we therefore recommend an existence-based penalization.</p>
<p>2.5.5 Compensation of for annotation imprecisions requested</p>	<p>Applied in S8</p>		<p>The reference annotation is typically only an approximation of the (forever unknown) ground truth. It may be desirable to compensate for known uncertainties, such as intra-rater or inter-rater variability, by configuring the metric accordingly. This is only possible for some metrics.</p>
<p>2.5.6 Penalization of multiple predictions assigned to the same reference object requested</p>	<p>Applied in S6 and D6.1</p>		<p>Object detection algorithms involve the step of assigning predicted objects to reference objects. This may result in more than one prediction being assigned to the same reference. This fingerprint should be set to true if all but one prediction of such an assignment should be penalized as FP, and set to false if these spare predictions should be ignored during validation.</p>
<p>2.5.7 Penalization of multiple reference objects assigned to same prediction requested</p>	<p>Applied in D5.1</p>		<p>Object detection algorithms involve the step of assigning reference objects to predicted objects. This may result in more than one reference being assigned to the same prediction. If such an assignment should be penalized, this fingerprint should be set to true.</p>

Fig. 20. **Fingerprint for instance segmentation (Part 1).** In the case of binary fingerprints, the blue column shows examples for which the property is true while the red column shows counterexamples. Categorical fingerprints are only shown in blue.

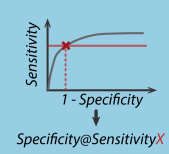
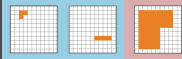
Domain interest-related properties (part 2)			
<p>2.6 Cutoff on predicted class scores</p> <p>Options:</p> <ul style="list-style-type: none"> - Predefined target value - Default strategy - No interest in cutoff at all 	<p>Applied in S4 and D3.3</p>	 <p style="text-align: center;">$\text{Specificity@Sensitivity}_X$</p>	<p>Modern algorithms output continuous class scores. Setting a cutoff value on the scores enables the generation of a (cutoff-specific) confusion matrix and thus the computation of popular single-threshold counting metrics, such as sensitivity, precision and F1 score. The cutoff can be set in a way that a specific target metric value is reached (e.g. a certain sensitivity) or based on a default value/strategy (e.g. 0.5 in the binary case, argmax for more classes). Some communities argue that no cutoff value at all is needed for comprehensive validation. Based on the biomedical interest, the following options are available:</p> <ul style="list-style-type: none"> - Use predefined target value for sensitivity/ specificity/PPV/FPPI - Use default cutoff value or infer value from optimizing primary metric on validation set. The Youden Index, for example, is commonly maximized to determine an optimal cutoff. - No interest in cutoff at all <p>Once a cutoff value for the predicted class probabilities has been set in such a way that the target metric value is achieved (if any), other metric values are then obtained from the corresponding fixed confusion matrix, e.g. PPV@sensitivity.</p>
Target structure-related properties			
<p>3.1 Small size of structures relative to pixel size</p>	<p>Applied in S7</p>		<p>A single pixel makes up at least several percentage points of the structure volume. <i>Example: multiple sclerosis lesions in magnetic resonance imaging (MRI) scans.</i></p>
<p>3.2 High variability of structure sizes (within one image, across images)</p>	<p>Applied in S8 and D5.1</p>		<p>The target structures vary substantially in size, such that some structures are several times the sizes of others. <i>Example: polyps in colonoscopy screening, where some polyps are several times the size of others.</i> <i>Counterexample: large organs, such as the liver or the kidneys, which are relatively comparable in size across individuals.</i></p>
<p>3.3 Target structures feature tubular shape</p>	<p>Applied in S7 and D5.3</p>		<p>The target structures feature a tubular shape. <i>Examples: vessels, fibers.</i></p>
<p>3.4 Possibility of multiple labels per unit (pixel or image)</p>	<p>Applied in Sec. 7</p>		<p>Multiple categories may be assigned to one pixel. <i>Examples: labels "tumor core" and "tumor" assigned to the same pixel.</i></p>
<p>3.5 Possibility of overlapping or touching target structures (e.g. medical instruments or cells)</p>	<p>Applied in DG 5.2</p>		<p>Different instances of a class can overlap or touch each other. <i>Examples: touching cells, overlapping medical instruments in laparoscopy.</i></p>
<p>3.6 Possibility of disconnected target structure(s)</p>	<p>Applied in TODO</p>		<p>A given structure appears disconnected in the given image. <i>Examples: single tomographic image slice depicting complex vessel, partially occluded by a medical instrument.</i></p>

Fig. 21. **Fingerprint for instance segmentation (Part 2)**. In the case of binary fingerprints, the blue column shows examples for which the property is true while the red column shows counterexamples. Categorical fingerprints are only shown in blue.

Data set-related properties			
4.1 High class imbalance	Applied in D3.1, D4.1 and Sec. 7		The class frequencies differ substantially. Further reading: [Mahani & Ali, 2019].
4.2 Uncertainties in the reference		The reference is typically only an approximation of the (forever unknown) ground truth. Various sources and types of errors exist, which require special treatment in the context of metric selection.	
4.2.1 High inter-/intra-rater variability	Applied in S7		The reference can be assumed to be noisy due to high inter-rater variability.
4.2.2 Possibility of spatial outliers in reference annotation	Applied in S8		The reference may feature spatial outliers that are distant from the (unknown) ground truth.
4.4 Non-independence of test cases	Applied in Sec. 7		The test cases are hierarchically structured, indicating non-independence of test cases. <i>Examples: multiple images of the same patient, hospital or video.</i>
4.5 Possibility of reference without target structure(s)	Applied in Sec. 7		There are test cases in which the reference comprises only the background class.
Algorithm output-related properties			
5.1 Availability of predicted class scores	Applied in S4, S6 and Sec. 6		Modern algorithms in biomedical image classification output continuous class scores, which are often interpreted as predicted class probabilities. These scores contain relevant information about the performance of a model and are thus crucial for comprehensive and meaningful validation. Instance segmentation problems in the biomedical domain are often approached by adding a post-processing step (e.g. connected component analysis) to a semantic segmentation algorithm. In this process, predicted class probabilities often get lost in practice. This can be avoided, as illustrated in Figure 43. If no predicted class probabilities are available, this property is set to false.
5.2 Possibility of algorithm output not containing the target structure(s)	Applied in S7		The algorithm may yield output images only comprising the background class.
5.3 Possibility of invalid algorithm output (e.g. Prediction is NaN)	Applied in Sec. 7		The files representing the algorithm output can contain invalid output.
5.4 Possibility of overlapping predictions	Applied in S6		Predictions of the algorithm can potentially overlap.

Fig. 22. **Fingerprint for instance segmentation (Part 3)**. In the case of binary fingerprints, the blue column shows examples for which the property is true while the red column shows counterexamples. Categorical fingerprints are only shown in blue.

E Decision Guides

E.1 Decision guide S2.

D2.1: MCC versus Balanced Accuracy (BA)

We follow the recommendations of Chicco et al. [22], who suggest MCC as the default metric to assess classification performance with a single score. In binary classification problems, a high MCC value implies good results for all four basic rates of the confusion matrix (True Positive Rate (TPR), True Negative Rate (TNR), PPV, Negative Predictive Value (NPV)) as well as a high F_1 Score, Accuracy and BA [22]. Furthermore, MCC is insensitive to which class is defined as the positive class, and its values are relatively well-interpretable with 0 indicating the performance of a random classifier and 1 reflecting perfect performance. On the other hand, the achievable MCC values depend crucially on the prevalence [22]. Furthermore, MCC is generally not suitable if an unequal treatment of classes is requested (see F2.5.1). The weighted versions of BA or the (mathematically almost identical) Youden's Index can be used to address these issues. An open research question, however, is how to best assess the accuracy of multi-class algorithms in the presence of ordinal data (i.e. when an unequal handling of class confusions is requested; F2.5.2). Note that weighted Cohen's Kappa has been proposed to address this issue. However, Kappa statistics in general have originally been proposed for assessing inter-rater reliability and come with various problems in the context of performance assessment [22]. Despite their popularity as chance-corrected alternatives to accuracy we thus do not recommend them in our framework. Furthermore, the properties of all of the multi-class metrics have not been studied well for non-binary classification problems.

E.2 Decision guide S3.

D3.1: TN-based metrics versus non-TN-based metrics

The following aspects should be taken into account when deciding between AUROC (operating on the full confusion matrix) and AP (disregarding TN):

- Problem statement:** Whether or not to validate classification tasks with TN-based metrics is among the most controversial issues in metric selection, currently resulting in heterogeneous practices across the biomedical image analysis community. This is because typical validation combines the aspect of Sensitivity with the aspect of either Specificity (TN-based), or PPV (non-TN-based). Often, the two aspects are not reported individually, but combined into a single score. Thus, the choice between Specificity and PPV (or TN-based versus non-TN-based) represents the basis for further choices, e.g. between common per-class counting metrics such as F_β Score (PPV-based / non-TN-based) and Positive Likelihood Ratio (LR+) (Specificity-based / TN-based) or common multi-threshold metrics such as AUROC (Specificity-based / TN-based) and AP (PPV-based / non-TN-based)⁵. The crucial differences between these pairs are often reported to be in regard to tangible pitfalls such as dealing with class imbalance (e.g. AP responding better to class imbalance than AUROC). However, it is necessary to keep in mind that all these differences can in fact be traced back to whether a metric is based on TN.
- How to decide whether to validate with TN or not?** As this discussion is limited to per-class validation (either binary classification, or "One versus Rest" / "One versus One" schemes for multi-class classification [36]), associated metrics define a positive (P) and a negative class (N) and a subsequent two-class confusion matrix (TP, FP, TN, FN). The fundamental difference between TN-based and non-TN-based metrics boils down to the question: Is there a focus on the positive class or are the two classes of equal interest (F2.5.2)? TN-based metrics (Sensitivity + Specificity, LR+, AUROC) consider the entire confusion matrix and thus reflect a symmetric interest in both classes. Non-TN-based metrics (Sensitivity + PPV, F_β Score, AP) only consider three quarters of the confusion matrix and thus reflect an asymmetric interest shifted towards the positive class. In practice, information retrieval tasks (special interest in the queried class) are often distinguished from classification tasks (interest in both classes). A retrieval task could be to query images featuring a certain phenomenon from a large database. In this case, the focus is on low FP in the queried images, i.e. on PPV, which is a non-TN-based metric. As an

⁵Other relevant TN-based metrics include Accuracy, BA and MCC while other non-TN-based metrics include Free-Response Receiver Operating Characteristic (FROC) score and PQ

example that can be interpreted both ways, consider the task of cancer detection on image level (“cancer or no cancer?”). While the interest in the two errors FP (false alarm) and FN (missed cancer) is obvious, the question is: Should the metric score of the classifier increase when an image without cancer is added to the data set and the classifier predicts that correctly (TN)? In favour of TN-based metrics one could argue that any correct decision should increase the validation score, while in favour of non-TN-based metrics (information retrieval perspective) one could argue that the task is to detect cancer and not to detect non-cancer. The second argument becomes stronger in the case of highly imbalanced data sets, where the aspect of cancer detection performance shrinks in comparison to the aspect of correctly identifying non-cancer. For “One versus Rest” settings in multi-class scenarios, one could argue to employ non-TN-based metrics, since there is an inherent focus on the class defined as positive, and the “rest” often outweighs the single positive class in number of data cases (class imbalance, F4.1 [56]).

- **Dependencies on prevalence:** Prevalence is the ratio of the positive class $P/(P+N)$ occurring in the data set. PPV-based metrics such as F_β Score and AP depend on prevalence, whereas *Specificity*-based metrics such as AUROC and LR+ do not depend on prevalence. Thus, the former might be closer to quantities of interest for practitioners in the context of specific applications, while the latter exclusively represents the inherent properties of the classifier *irrespective of prevalence in the data set* and might thus be more interesting to developers. Note that the independence of prevalence is often portrayed as a pitfall of *Specificity*-based metrics because, counter-intuitively, they may yield high scores in scenarios with low prevalence and thus low PPV. However, in certain cases independence of prevalence can be desired, e.g. when high variations in prevalence are expected in future applications of the model (e.g. due to varying data cohorts).

D3.2: AP versus FROC Score

The following aspects should be taken into account when deciding between AP and FROC Score:

- **Community preferences:** While AP constitutes the undisputed standard metric for object detection and instance segmentation in the computer vision community, the FROC Score is often favoured in the clinical context due to its easier interpretability despite its lack of standardization (employed False Positives per Image (FPPI) Scores vary across studies [9, 46, 82]). Thus, the decision between the two metrics often boils down to a decision between a standardized and technical validation versus an interpretable and application-focused validation.
- **Data set size awareness:** In contrast to AP, the FROC Score takes into account the total number of images in the data set (see also Fig. 78). This property does not affect relative method comparison and can be related to the underlying question “at which scale are matched objects (cardinalities) aggregated / counted?”. We discuss this question and implication for associated metrics in Sec. G.3 (see also Fig. 41). While AP originally (i.e. in the computer vision community) counts matched objects over the entire data set (as opposed to per image), Sec. G.3 demonstrates how to apply AP and other object detection metrics to (e.g. clinical) scenarios requiring per image aggregation. FROC score is a hybrid metric in this context, where *Sensitivity* is computed per data set while FP are averaged over single images (FPPI).
- **Dealing with low-confidence predictions:** It is often desired to filter low confidence predictions (e.g. objects with high confidence of being background) prior to metric computation. For AP computation this requires a cutoff on the confidence score or upper limits of considered predictions per image or per data set. For FROC, however, with typical values of FPPI, such low-confidence predictions naturally go unconsidered, thus allowing to avoid additional filtering measures.
- **FPPI:** Different FPPI values are used in the field for computing the FROC Score. A potential default are the values 1/8, 1/4, 1/2, 1, 2, 4, 8, as used for multiple popular benchmarks [82, 95]. Here, lower FPPI values (smaller than one) are weighted equally to higher FPPI values (greater than 1; four values each). Deviation from this weighting might be appropriate depending on the application, but should be explained. In the biostatistics community, areas under the curve are sometimes computed constraining the FPPI range to [0,1] [79].

D3.3: Predicted confidence scores and calibration

A *calibrated model* outputs predicted class scores (in this context interpreted as “confidence scores”) that match

the empirical success rate (e.g. outputs with score 0.8 for a specific class empirically belong to this class in 80% of the cases). Since this requirement is defined over the entire data set, calibration represents a weaker requirement compared to requiring correct confidence outputs at the individual level. The latter corresponds to estimating the true posterior probability of the output label given the input data. The following aspects should be taken into account when deciding whether control on confidence values is required and at which level:

- **When to validate predicted confidence scores?** In the given context, we distinguish two primary use cases:
 - Classification tasks where a cutoff on the predicted class scores is optimized on a validation set according to a predefined target value (or a predefined trade-off between FP and FN) to induce a concrete decision rule (see Fingerprint F2.6 in Fig. 15). Associated model validation will be based on the confusion matrix resulting from the decision rule while raw values of predicted class scores are not considered. Thus, **validation of predicted confidence scores is no hard requirement for these scenarios.**
 - Tasks where no specific decision rule is set (F2.6: "no interest in cutoff at all") and classification is instead validated through general class discrimination (as measured by multi-threshold metrics). In these cases, the final decision is left to an interpretable rule based on predicted class scores, e.g. "risk < 0.05". In order to ensure meaningful decision rules, it is typically of **importance that predicted confidence scores are validated.** There are, however, exceptions for this requirement, e.g., when a cutoff is not set at the time of validation (implying general interest in algorithm performance across many tasks), but will instead be optimized later upon potential applications.
- **Data set-wise versus individual validation of confidence scores:** Whether a risk as described in the example above must be controlled across all predictions of a given confidence score (calibration) or at the individual level (true posterior probabilities) depends on whether the cost-benefit trade-off is fixed across the data set or varies at the individual level.
- **How to validate predicted confidence scores?** We refer the reader to two common metric families: 1) calibration errors [35], where deviations from the described matching are computed for multiple bins of the continuous confidence scale [0,1] (computed per data set), and 2) proper scoring rules [32], e.g. the Brier Score, which assess whether the classifier outputs are close to the true probability per class given the reference. In contrast to combining calibration errors with a classification metric, proper scoring rules validate confidence scores in a single score. Further, proper scoring rules operate on an individual level, while calibration errors are determined in relation to the entire data set.
- **Calibration plots:** So-called calibration plots [35] allow for quick and interpretable examination of how well predicted confidence scores are classified. They allow for controlling calibration – but not individual-level probabilities – and should be reported in addition to curve plots on which the discrimination metrics are based [64].

E.3 Decision guide S4.

D4.1: TN-based metrics versus non-TN-based metrics

The following aspects should be taken into account when deciding between LR+ (operating on the full confusion matrix) and F_β Score (disregarding TN):

- **Problem statement:** Whether or not to validate classification tasks with TN-based metrics is among the most controversial issues in metric selection, currently resulting in heterogeneous practices across the biomedical image analysis community. This is because typical validation combines the aspect of Sensitivity with the aspect of either Specificity (TN-based), or PPV (non-TN-based). Often, the two aspects are not reported individually, but combined into a single score. Thus, the choice between Specificity and PPV (or TN-based versus non-TN-based) represents the basis for further choices, e.g. between common per-class counting metrics such as F_β Score (PPV-based / non-TN-based) and LR+ (Specificity-based / TN-based) or common multi-threshold metrics such as AUROC (Specificity-based /

TN-based) and AP (PPV-based / non-TN-based) ⁶. The crucial differences between these pairs are often reported to be in regard to dealing with class imbalance (e.g. AP responding better to class imbalance than AUROC). However, it is necessary to keep in mind that all these differences can in fact be traced back to whether a metric is based on TN.

- How to decide whether to validate with TN or not?** As this discussion is limited to per-class validation (either binary classification, or “One versus Rest” / “One versus One” schemes for multi-class classification [36]), associated metrics define a positive (P) and a negative class (N) and a subsequent two-class confusion matrix (TP, FP, TN, FN). The fundamental difference between TN-based and non-TN-based metrics boils down to the question: Is there a focus on the positive class or are the two classes of equal interest (F2.5.2)? TN-based metrics (Sensitivity + Specificity, LR+, AUROC) consider the entire confusion matrix and thus reflect a symmetric interest in both classes. Non-TN-based metrics (Sensitivity + PPV, F_β Score, AP) only consider three quarters of the confusion matrix and thus reflect an asymmetric interest shifted towards the positive class. In practice, information retrieval tasks (special interest in the queried class) are often distinguished from classification tasks (equal interest in both classes). As an example, consider the task of cancer detection on image level (“cancer or no cancer?”). While the interest in the two errors FP (false alarm) and FN (missed cancer) is obvious, the question is: Should the metric score of the classifier increase when an image without cancer is added to the data set and the classifier predicts that correctly (TN)? In favour of TN-based metrics one could argue that any correct decision should increase the validation score, while in favour of non-TN-based metrics (information retrieval perspective) one could argue that the task is to detect cancer and not to detect non-cancer. The second argument becomes stronger in the case of highly imbalanced data sets, where the aspect of cancer detection performance shrinks in comparison to the aspect of correctly identifying non-cancer. For “One versus Rest” settings in multi-class scenarios, one could argue to employ non-TN-based metrics, since there is an inherent focus on the class defined as positive, and the “rest” often outweighs the single positive class in number of data cases (class imbalance, F4.1 [56]).
- Interpretability as an additional aspect for selection:** While the conceptual pros and cons of TN-based metrics have been described above, in practice, the medical community has a strong preference towards TN-based metrics. One reason might be the notion of superior interpretability enabled by the symmetric focus on the positive and negative classes. For instance, in keeping with the above example, LR+ can be interpreted as “the likelihood of cancer being predicted as positive divided by the likelihood of a non-cancer case being predicted as positive” [5].

D4.2: PPV@Sensitivity versus FPPI@Sensitivity

The decision between PPV@Sensitivity and FPPI@Sensitivity relates to most aspects described in D3.2 (AP versus FROC Score): While PPV is a generic metric applied in various communities, FPPI originated in the medical community and features improved interpretability. One important difference is that PPV is typically computed once over the entire data set, while FPPI counts FP per image and subsequently averages over the data set. In Sec. G.3 we discuss the implications of these two aggregation strategies and further present an approach on how to apply various object detection metrics (including PPV) in the context of per-image aggregation.

D4.3: F_β Score versus PQ

The F_β Score is a pure detection metric counting TP, FP, and FN detections on instance level (specifically, it represents the harmonic mean of PPV and Sensitivity, see also Sec. G). The “segmentation aspect” of IS is here only incorporated via a prior cutoff on the localization criterion operating on pixel level (e.g. “IoU > 0.5”). In case shifting the focus of validation more towards the segmentation quality of successfully matched (TP) instances is desired, there are two options:

- Complementary segmentation metric:** One option is to select separate segmentation metrics (in addition to object detection metrics such as F_β Score) on a per-instance basis (e.g. “DSC per TP-instance”).

⁶Other relevant TN-based) metrics include Accuracy, BA and MCC while other non-TN-based metrics include FROC score and PQ

This selection is enabled by following the IS path in Fig. 2 traversing the SS subroutines S7 (Fig. 8) and S8 (Fig. 9).

- (2) **Hybrid metric:** An alternative is to select PQ instead of F_β Score, which allows expressing both interests (detection performance and segmentation quality) in a single score. Essentially, PQ is a modified F_1 Score, where TP instances do not count as “1” in the calculation, but the “1” is replaced with the associated DSC score (range [0,1]) of the instance. While combining the two aspects in a single score might be desirable, e.g. for method benchmarking or ranking, on the downside, such combined metrics make it harder to trace back performance to individual aspects (in this case: object detection versus segmentation).

D4.4: How to determine β in F_β Score

The F_β Score is defined as:

$$F_\beta = (1 + \beta^2) \cdot \frac{\text{PPV} \cdot \text{Sensitivity}}{(\beta^2 \cdot \text{PPV}) + \text{Sensitivity}} = \frac{(1 + \beta^2) \cdot \text{TP}}{(1 + \beta^2) \cdot \text{TP} + \beta^2 \cdot \text{FN} + \text{FP}} \quad (1)$$

The most common choice is to set β to 1 resulting in equal weighting of FP and FN penalties. Higher values of β result in higher weights on FN penalties compared to FP penalties and thus imply a focus on Sensitivity compared to PPV.

E.4 Decision guide S5.

D5.1: Mask IoU versus Boundary Intersection over Union (Boundary IoU) versus Intersection over Reference (IoR)

The following aspects should be taken into account when deciding between Mask and Boundary IoU:

- **Small structures:** Mask IoU over-penalizes small structures in tasks with high variability of structure sizes (F3.2) because boundary pixels increase linearly (or quadratically) with size, while total pixels increase quadratically (or cubically) with size. Boundary IoU [19] addresses this issue by selecting only pixels with a maximum distance of “d” with regard to the boundary for validation (see Fig. 75).
- **Hyperparameters:** However, for the computation of Boundary IoU, the distance “d” constitutes an additional and sensitive hyperparameter to be determined by the experimenter. Reference points are the degree of inconsistency if annotations from two raters are available, or qualitative assessment of general annotation quality. Note that the Boundary IoU can be fooled to result in a perfect value of 1.0 (see Fig. 76).
- **Boundary focus:** While Mask IoU measures the overlap of structures in general, Boundary IoU allows to focus on the correctness of boundaries (F2.1, see Fig. 75).
- **Popularity:** While Mask IoU represents an established concept that is well-known to the community, Boundary IoU is a recently proposed modification that might require careful introduction when used for validation.
- **Touching structures:** In the case of a high ratio of touching reference objects, “non-split errors” (one prediction overlaps with multiple reference objects) might occur frequently. While the IoU criterion might heavily penalize this scenario resulting in FN and multiple FP, a more differentiated penalization might be desired (check F2.5.7), e.g. by explicitly separating such errors into “split errors” as well as “merge errors” [16], or in the form of the Intersection over Reference (IoR) [60], where only the ratio of a reference object’s area covered by a prediction is measured (see Fig. 73).

D5.2: Discarding information of provided annotations

Selecting a localization criterion operating on a lower/coarser resolution with regard to provided reference annotations effectively discards spatial information and should be well motivated by the given task (see Fig. 37). For instance, Box IoU is sometimes employed despite access to pixel-mask annotations (F4.3) because associated models (object detectors) are considered simpler approaches (compared to instance segmentation models). Such simplification may cause problems if structures are not well-approximated by a box shape (especially for 3D shapes, boxes usually constitute poor approximations), or if structures can overlap (F3.5), causing multi-component masks (see Fig. 74).

D5.3: Localization without outlining of structures

When choosing a localization criterion for tasks where the mere existence of objects is of interest (as opposed to the outlining of objects), the following aspects should be considered:

- **Loose criterion:** The intuitive choice of a very loose IoU criterion (e.g. “IoU > 0” or “at least one pixel overlap”) comes with the pitfall that the size of the predicted structure is in theory unbounded, i.e. the predicted location can be ambiguous (see Fig. 72b).
- **Point-based criteria:** A preferable alternative for the case of pure localization (without interest in outlines) is to constrain the prediction to a single coordinate. A common criterion for this scenario is the distance to the center point of the structure (which can also be of explicit interest, see F2.3, Fig. 71). The center point⁷, however, might not be a good reference for tubular structures (check F3.3) or disconnected structures (check F3.6). In such cases (and if annotations are provided in the form of masks), a binary “Point inside Mask” criterion might be the better choice. On the other hand, the “Point inside Mask” criterion does not allow for a variation of the criterion’s strictness (i.e. threshold). Application despite this shortcoming should be well-justified.

D5.4: Box IoU versus IoR

The following aspects should be taken into account when deciding between Box IoU and IoR:

- **Default choice:** The default choice in this setting is Box IoU.
- **Touching structures:** In the case of a high ratio of touching reference objects, “non-split errors” (one prediction overlaps with multiple reference objects) might occur frequently. In this case, the Intersection over Reference (IoR) [60], where only the ratio of a reference object’s area covered by a prediction is measured, might be considered as an alternative to IoU (see Fig. 73).

E.5 Decision guide S6.

D6.1: Assignment without predicted class probabilities on instance level

The following aspects should be considered when selecting the assignment strategy:

- **Common practice:** In the biomedical domain, more sophisticated matching strategies are often avoided by setting the localization criterion to IoU > 0.5 (IoU being any of Mask IoU, Boundary IoU, or IoR as selected in S5; for IoR see also D5.1) and only allowing non-overlapping object predictions (which inherently precludes matching conflicts). However, this setting substantially constrains the space of suitable methods as well as the strictness of the localization criterion.
- **Cost function-based optimization:** The Hungarian algorithm optimizes the matching between predictions and reference objects while minimizing a given cost function, such as the average overlap for all matched pairs. Notably, this optimization generally leads to optimistic interpretation/validation of ambiguous model outputs, but might not represent the most realistic approximation of model performance upon applications.
- **New proposal:** Greedy IoU – instead of sorting predictions per reference object by class score, one can also sort them by IoU score and match the prediction with the highest score while dealing with double assignments according to F2.5.6.

E.6 Decision guide S7.

D7.1: Dice vs IoU

The DSC is identical to the F_1 Score on pixel level and closely related to the IoU, which, in turn, is identical to the Jaccard Index (see equations 5 and 6). The two metrics will yield the same ranking (of aggregated metric values) in most applications (theoretically, deviations are possible), such that there is no value in combining

⁷Depending on what kind of information the center point is derived from, different definitions are possible, for instance: (1) geometric center of the box/approximation shape, (2) geometric center of a binary mask (i.e. average of positions of all pixels), (3) center of mass of a binary mask overlaid with the original image, i.e. weighted average of positions of all pixels with weight equal to (or derived from) the intensity of a particular pixel.

them. Commonly, the computer vision community prefers the IoU, while the medical image community favors the DSC.

D7.2: How to determine β in F_β Score

The F_β Score is defined as:

$$F_\beta = (1 + \beta^2) \cdot \frac{\text{PPV} \cdot \text{Sensitivity}}{(\beta^2 \cdot \text{PPV}) + \text{Sensitivity}} = \frac{(1 + \beta^2) \cdot \text{TP}}{(1 + \beta^2) \cdot \text{TP} + \beta^2 \cdot \text{FN} + \text{FP}} \quad (2)$$

The most common choice is to set β to 1 resulting in equal weighting of FP and FN penalties. Higher values of β result in higher weights on FN penalties (undersegmentation) compared to FP penalties (oversegmentation) and thus imply a focus on Sensitivity compared to PPV.

E.7 Decision guide S8.

D8.1: NSD and Boundary IoU

The following aspects should be considered when deciding between NSD and Boundary IoU:

- **Different research questions:** Both metrics set the focus on the boundary/contour of structures, but fundamentally differ in what they measure: NSD measures the DSC score on the surface voxels (often interpreted as the ratio of correctly predicted contour), where the strictness for what constitutes a correct boundary is controlled by a tolerance parameter. This way, noise in the image, limited resolution (propagating to noise in the reference annotations) or imprecise reference annotations can be accounted for. Boundary IoU directly measures the overlap between predicted and reference contours (without tolerance) up to a certain width (which is controlled by a width parameter). Thus, NSD is preferable if a tolerance accounting for imprecise annotations is requested. Boundary IoU, on the other hand, is preferable if errors at the contour are thought of as crucial inconsistencies that should be assessed, or if a wider area around the contour line is of interest (dynamic transition to the classical IoU).
- **Setting the hyperparameter:** The NSD and Boundary IoU both require users to manually set a hyperparameter. NSD: Boundary distances below the tolerance threshold will be considered TP (deviations do not count as errors). This parameter can be set according to the inter-rater variability or, if not available, heuristics. **Boundary IoU:** The distance parameter determines the thickness of the considered boundary and thus also influences the sensitivity to contour errors (the smaller the distance, the higher the sensitivity). This parameter can also be set according to the inter-rater variability (here in order to capture potential inconsistencies as opposed to disregarding noise like in NSD or, if not available, heuristics).

D8.2: Mean Average Surface Distance (MASD) vs Average Symmetric Surface Distance (ASSD)

The ASSD puts all boundary distances (all distances from boundary A to boundary B and all distances from boundary B to boundary A) in a list, then takes the mean. Thus, if one boundary is much larger than the other, this boundary will impact the mean much more. The MASD computes the sum of the mean distances from boundary A to boundary B and the mean distances from boundary B to boundary A. Therefore, the reference and prediction boundaries contribute equally. While there are corner cases, in which MASD features disadvantages compared to ASSD as well we generally recommend MASD because of the aforementioned advantage.

D8.3: Hausdorff Distance (HD) versus X^{th} Percentile Hausdorff Distance (X^{th} Percentile HD)

The HD calculates the maximum of all shortest distances for all points from one object boundary to the other, which is why it is also known as the Maximum Symmetric Surface Distance [101]. The X^{th} Percentile HD calculates the X^{th} percentile (e.g. 95% percentile for Hausdorff Distance 95% Percentile (HD95)) instead of the maximum, and should therefore be used instead if spatial outliers should be disregarded (F2.5.4, see Fig. 65).

F Instantiation of the Framework for Concrete Biomedical Problems

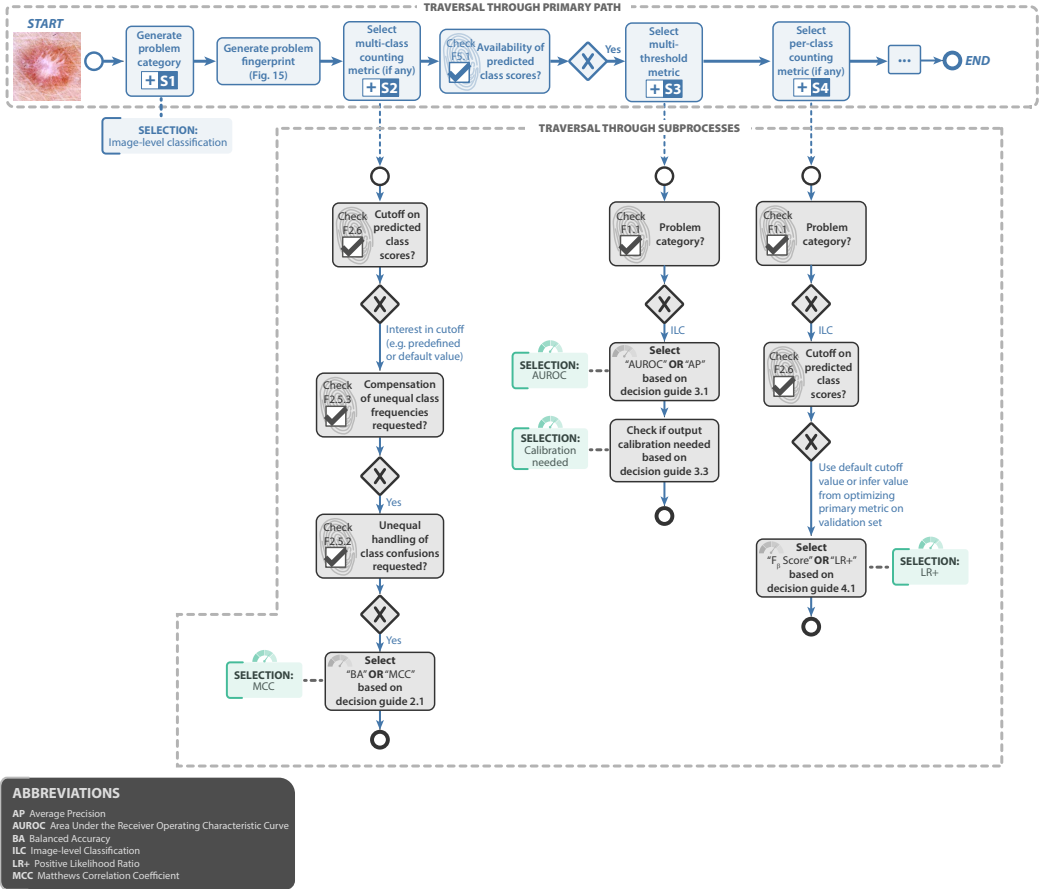


Fig. 23. Instantiation of the framework for the problem of disease classification in dermoscopic images [24]. The upper part shows the traversal through the main path of Fig. 2 based on the generated fingerprint for the specific problem. The lower part shows the traversal through the subprocesses S2 (Fig. 5), S3 (Fig. 6) and S4 (Fig. 7) and the resulting recommended metrics for the problem of disease classification in dermoscopic images.

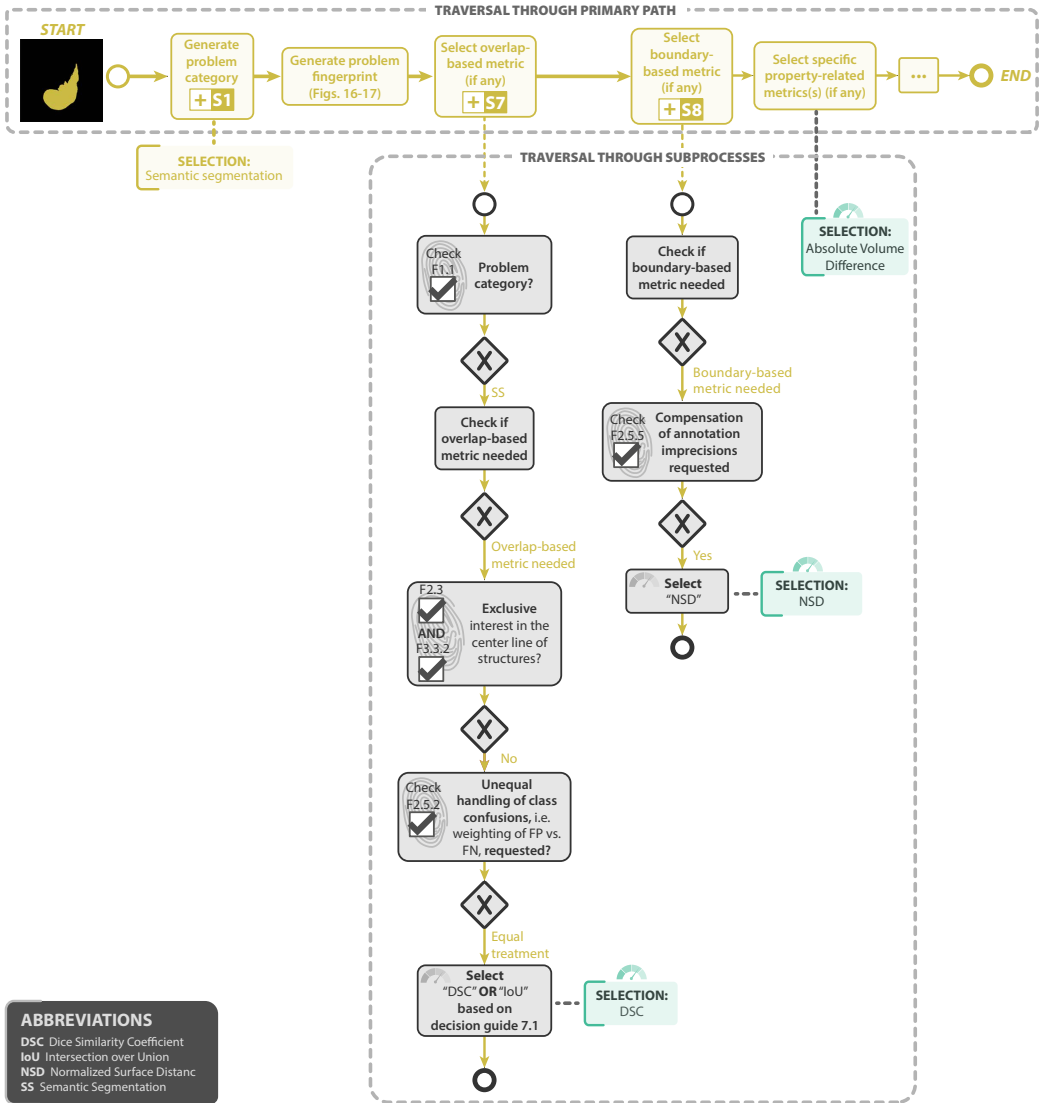


Fig. 24. Instantiation of the framework for the problem of liver segmentation in computed tomography images [2, 85]. The upper part shows the traversal through the main path of Fig. 2 based on the generated fingerprint for the specific problem. The lower part shows the traversal through the subprocesses S7 (Fig. 8) and S8 (Fig. 9) and the resulting recommended metrics for the problem of liver segmentation in computed tomography images.

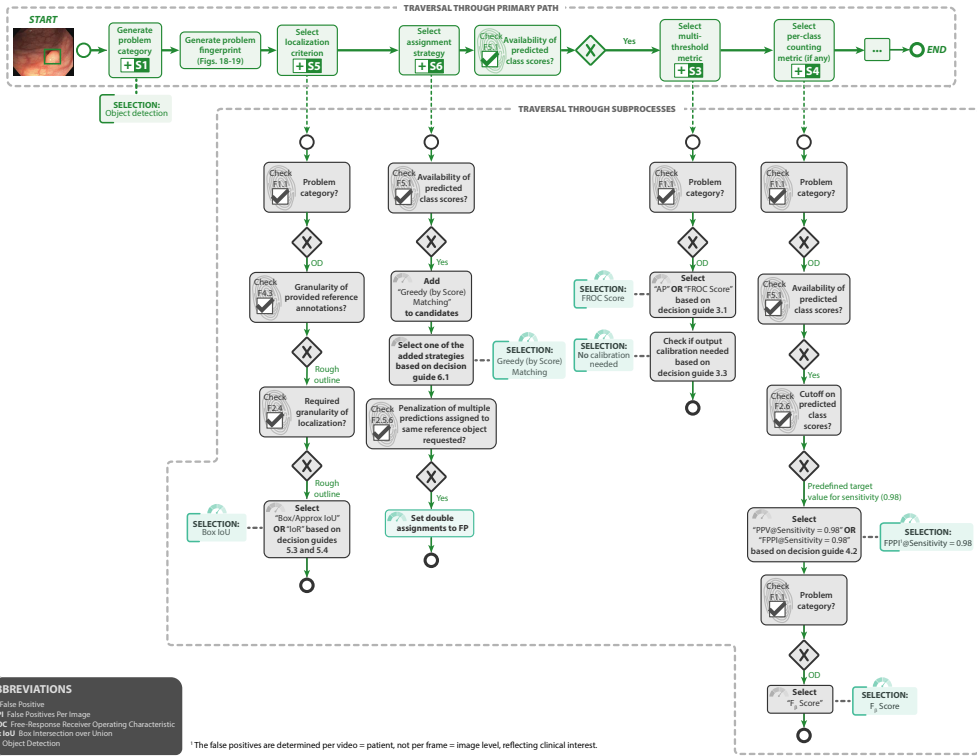


Fig. 25. Instantiation of the framework for the problem of polyp detection in colonoscopy videos with predefined sensitivity of 0.98 [11, 80]. The upper part shows the traversal through the main path of Fig. 2 based on the generated fingerprint for the specific problem. The lower part shows the traversal through the subprocesses S5 (Fig. 10), S6 (Fig. 11), S3 (Fig. 6) and S4 (Fig. 7) as well as the resulting recommended localization/assignment methods and metrics for the problem of polyp detection in colonoscopy videos with a predefined sensitivity of 0.98.

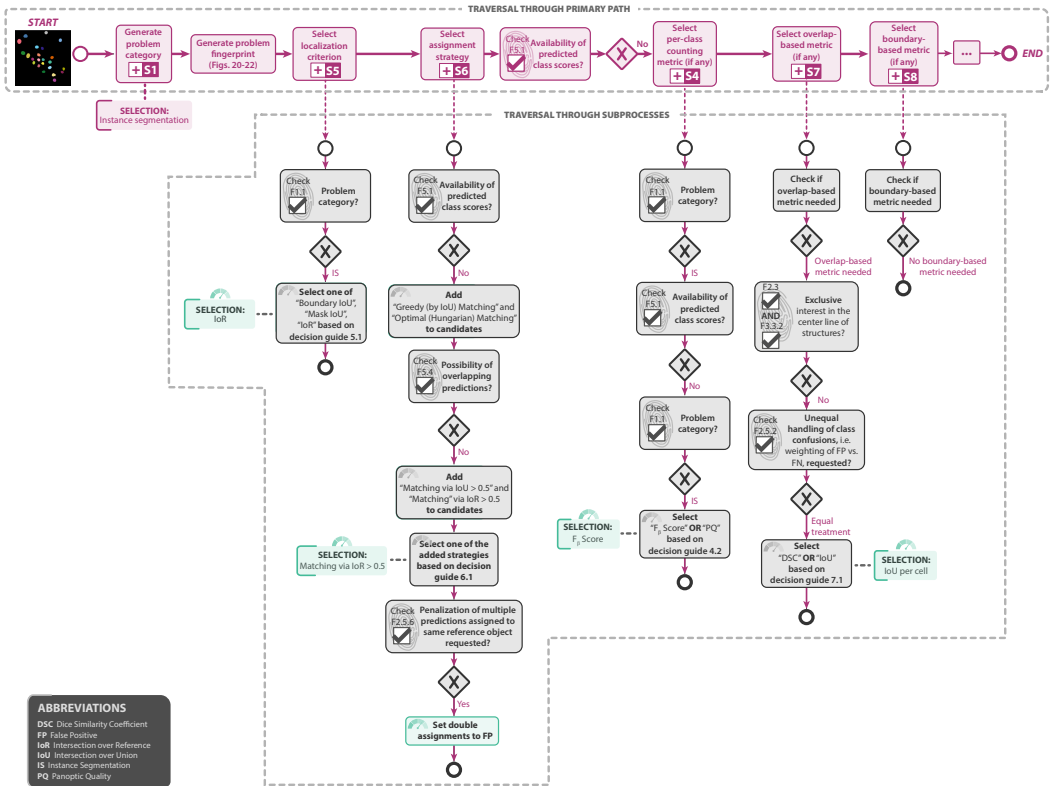


Fig. 26. Instantiation of the framework for the problem of cell nuclei instance segmentation in time-lapse light microscopy with a subsequent goal of cell tracking [92]. The upper part shows the traversal through the main path of Fig. 2 based on the generated fingerprint for the specific problem. The lower part shows the traversal through the subprocesses S5 (Fig. 10), S6 (Fig. 11), S4 (Fig. 7), S7 (Fig. 8) and S8 (Fig. 9) as well as the resulting recommended localization/assignment methods and metrics for the problem of cell nuclei instance segmentation in time-lapse light microscopy with a subsequent goal of cell tracking.

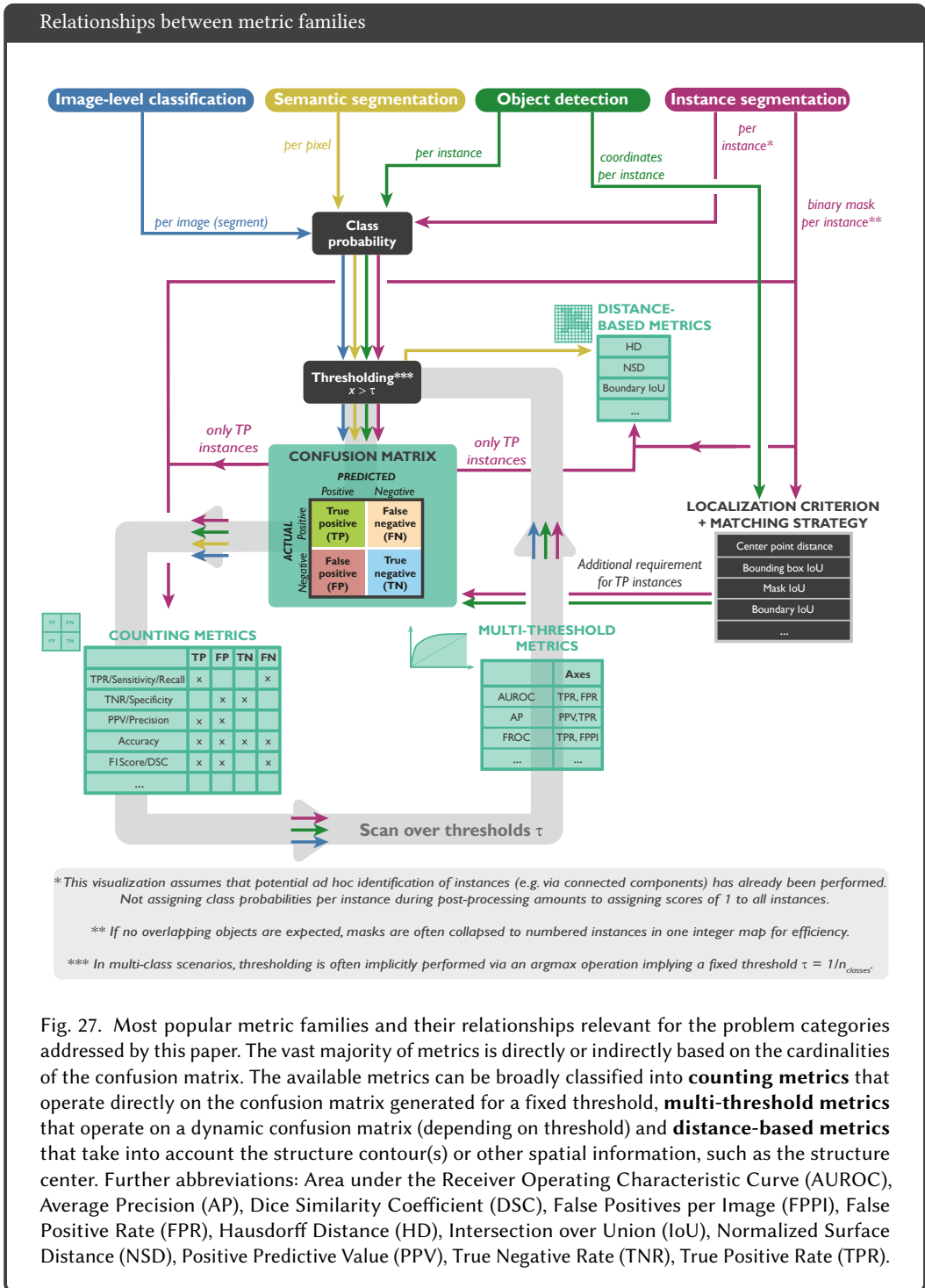
G Fundamentals of Metrics

The present work focuses on biomedical image analysis problems that can be interpreted as a classification task at image, object or pixel level. The vast majority of metrics for these problem categories is directly or indirectly based on epidemiological principles of True Positive (TP), False Negative (FN), False Positive (FP), True Negative (TN), i.e. the *cardinalities* of the so-called confusion matrix, depicted in Fig. 27. The TP/FN/FP/TN, from now on referred to as cardinalities. In the case of more than two classes C we also refer to the entries of the $C \times C$ confusion matrix as cardinalities. For simplicity and clarity in notation, we restrict ourselves to the binary case in most examples. Cardinalities can be computed for image (segment), object or pixel level. They are typically computed by comparing the prediction of the algorithm to a reference annotation. Modern neural network-based approaches typically require a threshold to be set in order to convert the algorithm output comprising predicted class scores (also referred to as continuous class scores) to a confusion matrix, as illustrated in Fig. 27. For the purpose of metric recommendation, the available metrics can be broadly classified as follows:

- **Counting metrics** operate directly on the confusion matrix and express the metric value as a function of the cardinalities (see Figs. 28, 29 and 31). In the context of segmentation, they have typically been referred to as **overlap-based** metrics [90]. We distinguish **multi-class counting metrics**, which are defined for an arbitrary number of classes and invariant under class order, from **per-class counting metrics**, which are computed by treating one class as foreground/positive class and all other classes as background. Popular examples for the former include *MCC*, *Accuracy*, and *Cohen's Kappa* κ , while examples for the latter are *Sensitivity*, *Specificity*, *PPV*, *DSC* and *IoU*.
- **Multi-threshold metrics** operate on a dynamic confusion matrix, reflecting the conflicting properties of interest, such as high *Sensitivity* and high *Specificity*. Popular examples include the *AUROC* (see Fig. 30) and *AP* (see Fig. 39).
- **Distance-based metrics** have been designed for semantic and instance segmentation tasks. They operate exclusively on the TP and rely on the explicit definition of object boundaries (see Figs. 32 and 34). Popular examples are the *HD* and the *NSD* (see Fig. 34).

Depending on the context (e.g. image-level classification vs. semantic segmentation task) and the community (e.g. medical imaging community vs. computer vision community), identical metrics are referred to with different terminology. For example, *Sensitivity*, *TPR* and *Recall* refer to the same concept. The same holds true for the *DSC* and the *F₁ Score*. The most relevant metrics for the problem categories in the scope of this paper are introduced in the following.

Most metrics are recommended to be applied per class (except the multi-class counting metrics), meaning that a potential multi-class problem is converted to multiple binary classification problems, such that each relevant class serves as the positive class once. This results in different confusion matrices depending on which class is used as the positive class.



G.1 Image-level Classification.

Image-level classification refers to the process of assigning one or multiple labels, or *classes*, to an image. If there is only one class of interest (e.g. cancer vs. no cancer), we speak of *binary classification*, otherwise of *categorical classification*. Modern algorithms usually output **predicted class probabilities** (or continuous class scores) between 0 and 1 for every image and class, indicating the probability of the image belonging to a specific class. By introducing a threshold (e.g. 0.5), predictions are considered as positive (e.g. cancer = true) if they are above the threshold or negative if they are below the threshold. Afterwards, predictions are assigned to the cardinalities (e.g. a cancer patient with prediction cancer = true is considered as TP) [27]. The most popular classification metrics are counting metrics, operating on a confusion matrix with fixed threshold on the class probabilities, and multi-threshold metrics, as detailed in the following.

Counting metrics. The most common binary counting metrics used for image-level classification are presented in Figs. 28 (per-class) and 29 (multi-class). Please note that these metrics are also commonly used in segmentation and object detection tasks. For segmentation tasks, they are often referred to as overlap-based metrics. Each of the presented metrics covers specific properties.

The *Sensitivity* (also referred to as *Recall*, *TPR* or *Hit rate*) focuses on the actual positives (TP and FN) and represents the fraction of positives that were correctly detected as such. In contrast, *PPV* (or *Precision*) divides the TP by the total number of predicted positive cases, thus aiming to represent the probability of a positive prediction corresponding to an actual positive. A value of 1 would imply that all positive predicted cases are actually positives, but it might still be the case that positive cases were missed. Please note that the term *PPV* has multiple meanings. In the context of computer assisted interventions, for example, it typically refers to the measured variance. Hence, the usage of its synonym *PPV* may be preferred.

In analogy to the *Sensitivity* for positives, *Specificity* (also referred to as *Selectivity* or *TNR*) focuses on the negative cases by computing the fraction of negatives that were correctly detected as such. Similarly to the *PPV*, the *NPV* divides the TN by the total number of predicted negative cases and measures how many of the predicted negative samples were actually negative. *Specificity* and *NPV* require the definition of TN cases, which is not always possible. In object detection tasks, for example (see App. G.3), TN are typically ill-defined and not provided. Therefore, these measures can not be computed in those cases.

PPV and *NPV* provide quantities of direct interest to the medical practitioner, namely the probability of a certain event given the prediction of the classifier. However, unlike *Sensitivity* and *Specificity*, they are not only functions of the classifier but also of the study population. Hence, one cannot extrapolate from one population (e.g. from a case-control study) to another (general population without correcting for prevalence). In the case of the prevalence being unequal to 0.5, prevalence correction should be applied (see Fig. 53):

$$PPV = \frac{Sensitivity \cdot Prevalence}{Sensitivity \cdot Prevalence + (1 - Specificity) \cdot (1 - Prevalence)} \quad (3)$$

$$NPV = \frac{Specificity \cdot (1 - Prevalence)}{Specificity \cdot (1 - Prevalence) + (1 - Sensitivity) \cdot Prevalence} \quad (4)$$

As illustrated in Fig. 48, reporting of a single metric such as *Sensitivity*, *PPV* or *Specificity* can be highly misleading because, for example, non-informative classifiers can achieve high values on imbalanced classes. The *F₁ Score* (also known as *DSC* in the context of segmentation), overcomes this issue by representing the harmonic mean of *PPV* and *Sensitivity* and therefore penalizing extreme values of either metric [38], while being relatively robust against imbalanced data sets [89]. The *F₁ Score* is a specification of the *F β score*, which adds a weighting between *PPV* and *Sensitivity*. For higher values of β , *Sensitivity* is given a higher weight over *PPV*, which might be desired depending on the application. More specifically, the *F β Score* weights between FP and FN samples. Another metric which combines the metrics above is the *LR+*, which is the ratio of the *Sensitivity* and *1-Specificity* (*FPR*). This metric is described as the "probability that a positive test would be expected in a patient divided by the probability that a positive test would be expected in a patient without a disease" [84]. It is defined as odds ratio and therefore invariant to the prevalence [86].

All of the metrics presented so far are bounded between 0 and 1 with 1 representing a perfect value and 0 the worst possible prediction of this metric. However, all of them rely on the definition of the positive class, which may be straightforward in some cases but can be based on a rather arbitrary choice in others. Notably, metric values may be completely different depending on the choice of positive class [70].

To overcome the need for selecting one class as the positive class, other metrics have been suggested that can be based on all entries of a *multi-class* confusion matrix, in which each class is assigned a row and a column of the matrix. The *Accuracy* is one of the most commonly used metrics and measures the ratio between all correct predictions (TP and TN) and the total number of samples. *Accuracy* is not robust against imbalanced data sets (see Fig. 48), and is therefore often replaced by the more robust *BA* that averages the *Sensitivity* over all classes [34]. For two classes, the metric averages *Sensitivity* and *Specificity*. An alternative is *Youden's Index \bar{J}* or *BM*, similarly summing up *Sensitivity* per class (or for two classes, summing up *Sensitivity* and *Specificity*). Note that *Youden's Index \bar{J}* and *BA* are closely related and can directly be calculated from the other as $\bar{J} = 2BA - 1$ and $BA = (\bar{J} + 1)/2$.

The *MCC*, also known as *Phi Coefficient*, measures the correlation between the actual and predicted class. The metric is bounded between -1 and 1, with high positive values referring to a good prediction which can only be achieved when all cardinalities are good, i.e. with a low number of FP/FN and high TP/TN. Another popular metric is *Cohen's Kappa κ* , which calculates the agreement between the reference and prediction while incorporating information on the agreement by chance. It is therefore a form of chance-corrected *Accuracy*. Similarly to *MCC*, it incorporates all values of the confusion matrix and is bounded between -1 and 1. In contrast to *MCC*, negative values do not indicate anti-correlation, but less agreement than expected by chance. *Cohen's Kappa κ* can be generalized by introducing a weighting scheme for the cardinalities in the *Weighted Cohen's Kappa κ* metric. For those three metrics, a value of 0 refers to a prediction which is not better than random guessing.

All of the presented binary counting metrics can be transferred to the multi-class case [34, 40], where *MCC* and (*Weighted*) *Cohen's Kappa κ* have explicit definitions, whereas the others become the implicit result of an aggregation across a rotating one-versus-the-rest binary perspective for each of the classes.

Multi-threshold metrics. The classical counting metrics presented above rely on fixed thresholds to be set on the predicted class probabilities (if available), resulting in them being based on the cardinalities of the confusion matrix. **Multi-threshold metrics** overcome this limitation by calculating metric scores based on multiple thresholds. For instance, to emphasize how well a prediction distinguishes between the positive and negative class, the *AUROC* can be utilized. The *Receiver Operating Characteristic (ROC)* curve plots the *FPR*, which is equal to $1 - \textit{Specificity}$, against the *Sensitivity* for multiple thresholds of the predicted class probabilities, contrarily to just choosing one fixed threshold. For computation of the ROC curve, the class scores can be ordered in descending order and each score regarded as a potential threshold. For each threshold, the resulting *Sensitivity* and *Specificity* are computed, and the resulting tuple is added to the ROC curve as one point (cf. Fig. 30); note that the lower the threshold, the higher the *Sensitivity* but the lower (potentially) the *Specificity*. This leads to a monotonic increase of the curve. To interpolate between all points, i.e. to approximate the values between the calculated *Sensitivity* and *Specificity* tuples, a simple linear interpolation can be employed by drawing a line between each pair of points [27]. An optimal classifier would lead to *Sensitivity* and *Specificity* of 1 ($1 - \textit{Specificity}$ of 0), therefore corresponding to a single point (0, 1) on the ROC curve. In contrast, a classifier with no skill level (random guessing) would result in a diagonal line from (0, 0) to (1, 1) (dashed line in Fig. 30). The area under the ROC curve is referred to as *AUROC*, also called *AUC ROC* or simply *AUC*.

AUROC comes with two advantages: threshold and scale invariance. *AUROC* measures the quality of the predictions regardless of the threshold, as it is calculated over a number of thresholds. Furthermore, *AUROC* does not focus on the absolute values of predictions, but rather on how well they are ranked. However, those properties are not always desired. If a specific penalization of FP or FN is desired (cf. Fig. 50), *AUROC* is not the best metric choice as it is invariant to the threshold. If the predicted class probabilities are intended to be well calibrated, the scale invariance feature will prevent from doing so.

Per definition, *AUROC* measures the complete area under the *ROC* curve. If only a specific range is of interest, a partial or ranged *AUROC* can also be computed [55]. Similarly, metrics can be assessed at a certain point of the *ROC* curve, for example the *Sensitivity* value at a specific score of the *Specificity* (e.g. 0.9), also referred to as *Sensitivity@Specificity*. This approach can similarly be used for other curve measures, e.g. the *Precision-Recall (PR)* curve, introduced in App. G.3, and is illustrated in Fig. 30.

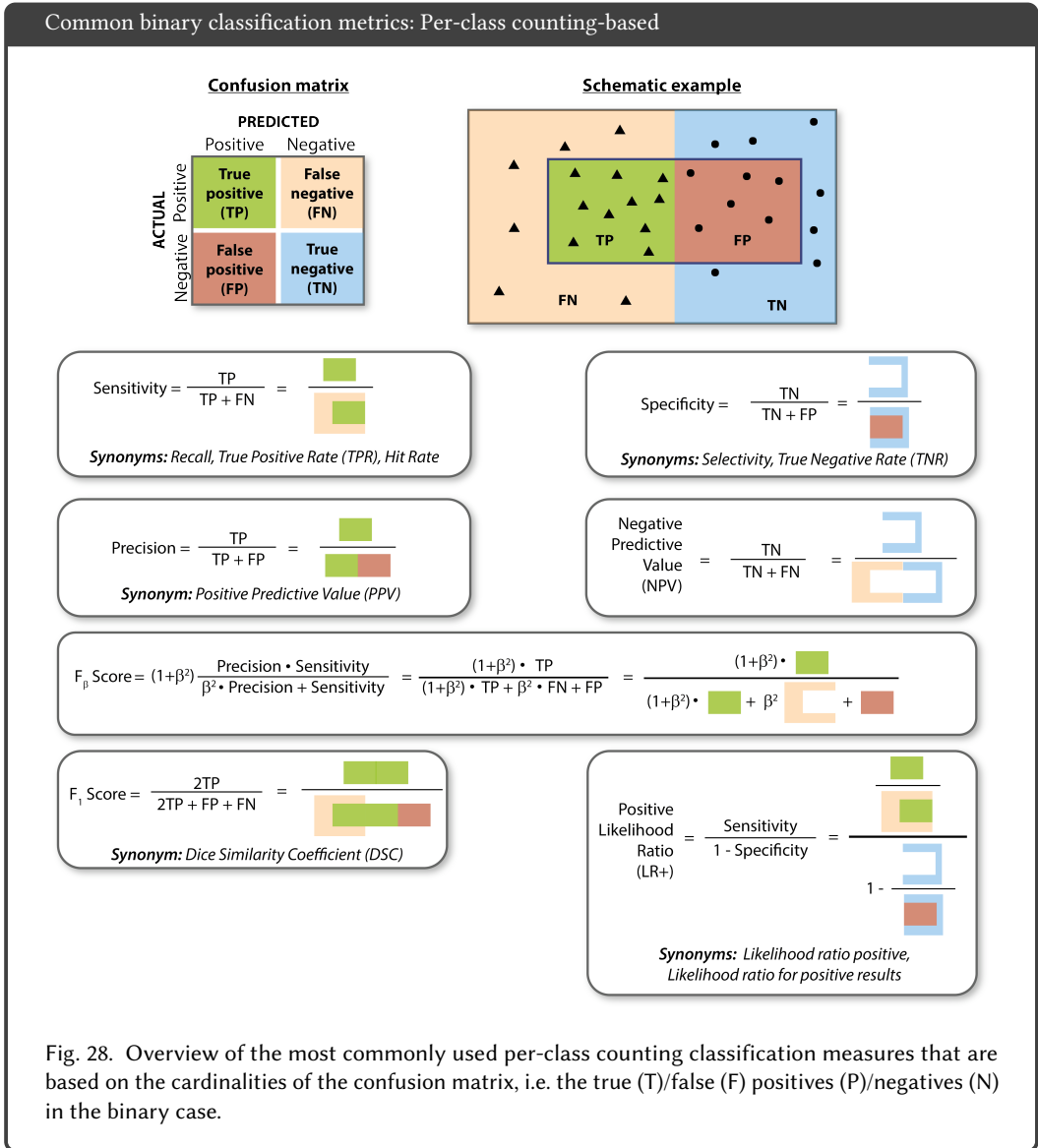
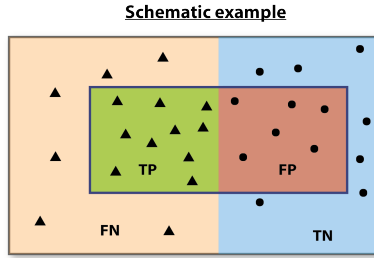


Fig. 28. Overview of the most commonly used per-class counting classification measures that are based on the cardinalities of the confusion matrix, i.e. the true (T)/false (F) positives (P)/negatives (N) in the binary case.

Common binary classification metrics: Multi-class counting-based

Confusion matrix

		PREDICTED	
		Positive	Negative
ACTUAL	Positive	True positive (TP)	False negative (FN)
	Negative	False positive (FP)	True negative (TN)



$$\text{Accuracy} = \frac{TP + TN}{TP + TN + FP + FN} = \frac{\text{Green} + \text{Blue}}{\text{Green} + \text{Blue} + \text{Orange} + \text{Red}}$$

$$\text{Balanced Accuracy} = \frac{1}{2} (\text{Sensitivity} + \text{Specificity}) = \frac{1}{2} \left(\frac{TP}{TP + FN} + \frac{TN}{TN + FP} \right) = \frac{1}{2} \left(\frac{\text{Green}}{\text{Green} + \text{Orange}} + \frac{\text{Blue}}{\text{Blue} + \text{Red}} \right)$$

$$\text{Youden's Index (J)} = \text{Sensitivity} + \text{Specificity} - 1 = \frac{TP}{TP + FN} + \frac{TN}{TN + FP} - 1 = \frac{\text{Green}}{\text{Green} + \text{Orange}} + \frac{\text{Blue}}{\text{Blue} + \text{Red}} - 1$$

Synonym: Youdens' J

$$\text{Matthews Correlation Coefficient (MCC)} = \frac{TP \cdot TN - FP \cdot FN}{\sqrt{(TP + FP)(TP + FN)(TN + FP)(TN + FN)}} = \frac{\text{Green} \cdot \text{Blue} - \text{Red} \cdot \text{Orange}}{\sqrt{(\text{Green} + \text{Red})(\text{Green} + \text{Orange})(\text{Blue} + \text{Red})(\text{Blue} + \text{Orange})}}$$

Synonym: Phi Coefficient

$$\text{Cohen's Kappa} = \frac{p_o - p_e}{1 - p_e} = \frac{2(TP \cdot TN - FN \cdot FP)}{(TP + FP)(FP + TN) + (TP + FN)(FN + TN)} = \frac{2(\text{Green} \cdot \text{Blue} - \text{Red} \cdot \text{Orange})}{(\text{Green} + \text{Red})(\text{Blue} + \text{Orange}) + (\text{Green} + \text{Orange})(\text{Blue} + \text{Red})}$$

$p_o = \text{Accuracy}$

$$p_e = \frac{(TP + FP)(TP + FN)}{TP + TN + FP + FN} + \frac{(TN + FP)(TN + FN)}{TP + TN + FP + FN} = \frac{\text{Green} + \text{Orange}}{\text{Total}} \cdot \frac{\text{Green} + \text{Orange}}{\text{Total}} + \frac{\text{Blue} + \text{Red}}{\text{Total}} \cdot \frac{\text{Blue} + \text{Red}}{\text{Total}}$$

Synonyms: Cohen's Kappa Coefficient, Kappa Statistic, Kappa Score

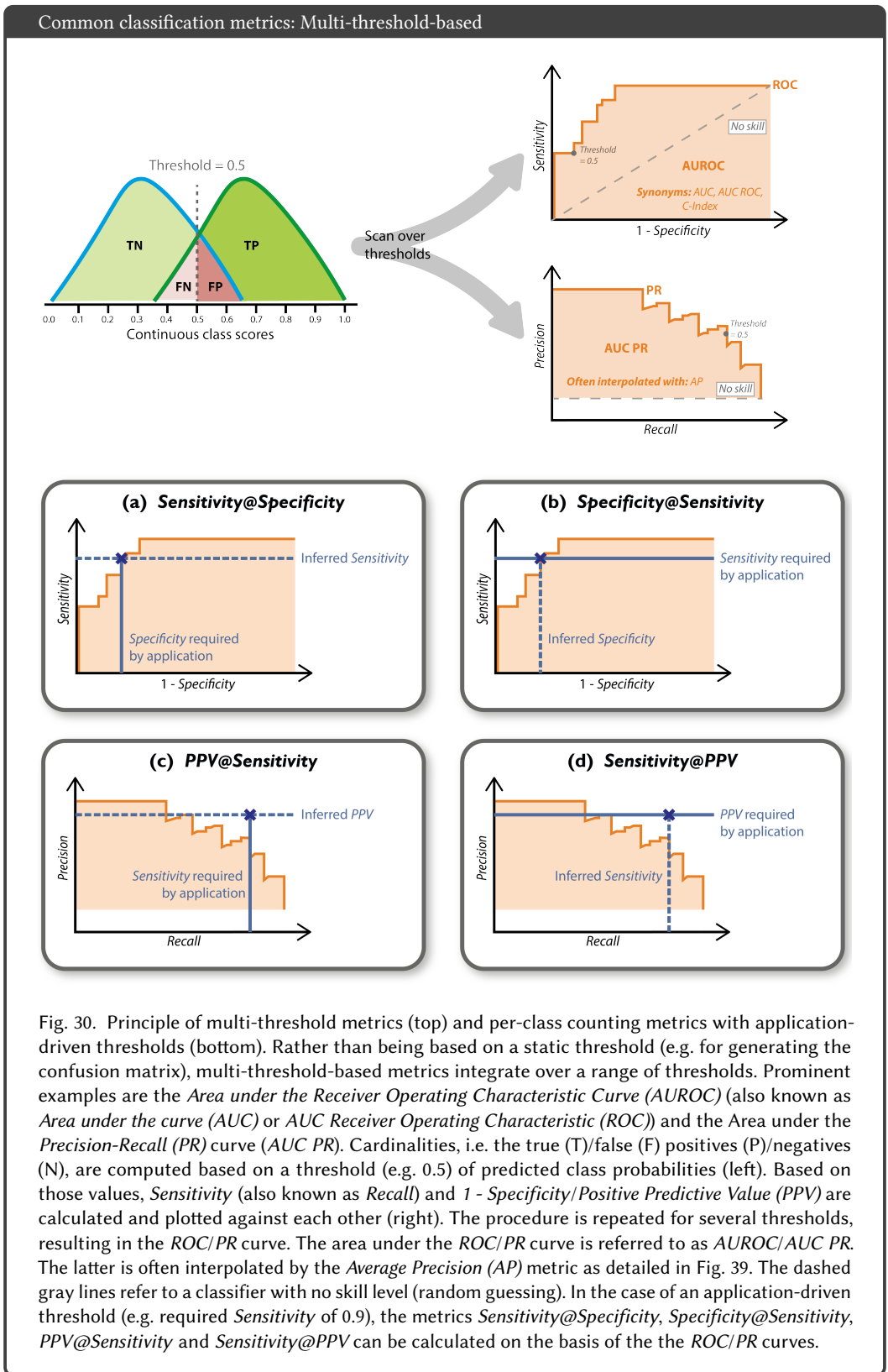
$$\text{Weighted Cohen's Kappa} = \frac{p_o^w - p_e^w}{1 - p_e^w}, p_o^w = \frac{w_{TP} \cdot TP + w_{TN} \cdot TN + w_{FP} \cdot FP + w_{FN} \cdot FN}{TP + TN + FP + FN} = \frac{w_{TP} \cdot \text{Green} + w_{TN} \cdot \text{Blue} + w_{FP} \cdot \text{Red} + w_{FN} \cdot \text{Orange}}{\text{Total}}$$

$$p_e^w = w_{TP} \frac{(TP + FP)(TP + FN)}{TP + TN + FP + FN} + w_{TN} \frac{(TN + FP)(TN + FN)}{TP + TN + FP + FN} + w_{FN} \frac{(FN + FP)(FN + TN)}{TP + TN + FP + FN} + w_{FP} \frac{(FP + TP)(FP + TN)}{TP + TN + FP + FN}$$

$$= w_{TP} \frac{\text{Green} + \text{Orange}}{\text{Total}} \cdot \frac{\text{Green} + \text{Orange}}{\text{Total}} + w_{TN} \frac{\text{Blue} + \text{Orange}}{\text{Total}} \cdot \frac{\text{Blue} + \text{Orange}}{\text{Total}} + w_{FN} \frac{\text{Orange} + \text{Red}}{\text{Total}} \cdot \frac{\text{Orange} + \text{Red}}{\text{Total}} + w_{FP} \frac{\text{Red} + \text{Green}}{\text{Total}} \cdot \frac{\text{Red} + \text{Green}}{\text{Total}}$$

Synonyms: Weighted Cohen's Kappa Coefficient, Weighted Kappa Statistic, Weighted Kappa Score

Fig. 29. Overview of the most commonly used multi-class counting classification measures that are based on the cardinalities of the confusion matrix, i.e. the true (T)/false (F) positives (P)/negatives (N) in the binary case.



G.2 Semantic Segmentation.

Semantic segmentation Semantic segmentation is commonly defined as the process of partitioning an image into multiple segments/regions. To this end, one or multiple labels are assigned to every pixel such that pixels with the same label share certain characteristics. Semantic segmentation can therefore also be regarded as pixel-level classification. As in image-classification problems, predicted class probabilities are typically calculated for each pixel deciding on the class affiliation based on a threshold over the class scores [4]. In semantic segmentation problems, the pixel-level classification is typically followed by a post-processing step, in which connected components are defined as objects, and object boundaries are created accordingly. Semantic segmentation metrics can roughly be classified into three classes: (1) counting metrics or overlap-based metrics, for measuring the overlap between the reference annotation and the prediction of the algorithm, (2) distance-based metrics, for measuring the distance between object boundaries, and (3) problem-specific metrics, measuring, for example, the volume of objects.

Counting metrics. The most frequently used segmentation metrics are **counting metrics**. In the context of segmentation they are also referred to as **overlap metrics**, as they essentially measure the overlap between a reference mask and the algorithm prediction. According to a comprehensive analysis of biomedical image analysis challenges [57], the *DSC* [28] is the by far most widely used metric in the field of medical image analysis. As illustrated in Fig. 31, it yields a value between 0 (no overlap) and 1 (full overlap). The *DSC* is identical to the F_1 Score and closely related to the *IoU*, which is identical to the *Jaccard Index*:

$$IoU = \frac{DSC}{2 - DSC} \quad (5)$$

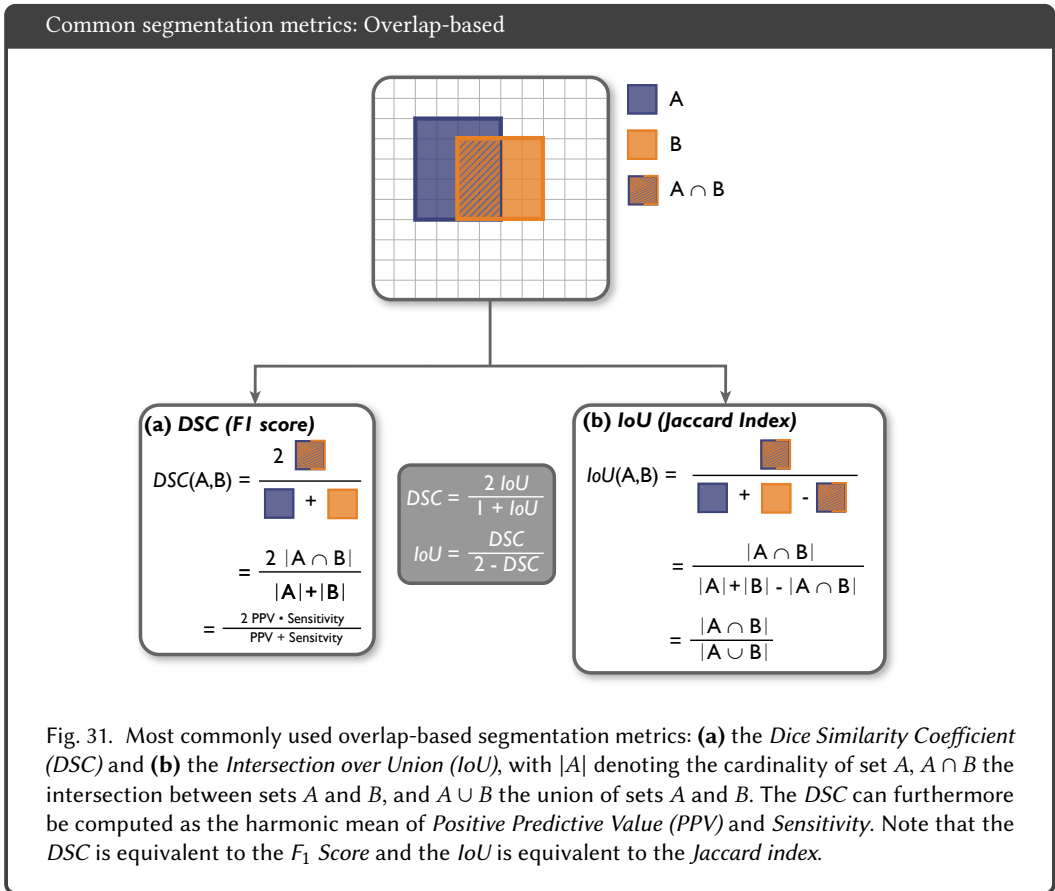
$$DSC = \frac{2IoU}{1 + IoU} \quad (6)$$

Distance-based metrics. Overlap-based metrics are often complemented by **distance-based metrics** that operate exclusively on the TP and compute one or several distances between the reference and the prediction. Apart from a few exceptions, distance-based metrics are often **boundary-based metrics** which focus on assessing the accuracy of object boundaries. According to [57], the *HD* and its 95% percentile variant (*HD95*) [41] are the most commonly used boundary-based metrics. The *HD* calculates the maximum of all shortest distances for all points from one object boundary to the other, which is why it is also known as the *Maximum Symmetric Surface Distance* [101]. The *HD95* calculates the 95% percentile instead of the maximum, therefore disregarding outliers (see Fig. 32). Another popular metric is the *ASSD*, measuring the average of all distances for every point from one object to the other and vice versa [96, 101]. However, if one boundary is much larger than the other, it will impact the score much more. This is avoided by the *MASD* [10], which treats both structures equally by computing the average distance from structure *A* to structure *B* and the average distance from structure *B* to structure *A* and averaging both (see Fig. 33). For the *HD(95)*, *MASD* and *ASSD* metrics, a value of 0 refers to a perfect prediction (distance of 0 to the reference boundary), while there exists no fixed upper bound. The *Boundary IoU* (cf. Fig. 36) is another option for measuring the boundary quality of a prediction. It measures the overlap between prediction and reference up to a certain width (which is controlled by the width parameter *d*) (see App. G.3 for details) and is bounded between 0 and 1.

A major problem related to boundary-based metrics are the error-prone reference annotations (see Figs. 64 and 65). In fact, domain experts often disagree on the definition and annotation of objects and their boundaries [47]. While the *HD(95)* and *ASSD* are not robust with respect to uncertain reference annotations, the *NSD* was explicitly designed for this purpose as a hybrid metric between boundary-based and counting-based approaches. Known uncertainties in the reference as well as acceptable deviations of the predicted boundary from the reference are captured by a threshold τ [68], as shown in Fig. 34. Only boundary parts within the border regions defined by τ are counted as TP. The metric is bounded between 0 (no boundary overlap) and 1 (full boundary overlap), so that it can be interpreted similarly to the classical *DSC* (though restricted to the boundary). Please note that τ is another important hyperparameter which should be chosen wisely, based on inter-rater agreement, for example.

Problem-specific segmentation metrics. While overlap-based metrics and distance-based metrics are the standard metrics used by the general computer vision community, biomedical applications often have special

domain-specific requirements. In medical imaging, for example, the actual volume of an object may be of particular interest (for example tumor volume). In this case, **volume metrics** such as the *Absolute* or *Relative Volume Error* and the *Symmetric Relative Volume Difference* can be computed [65]. However, they are less common than overlap metrics, as the location of objects is not considered at all (see Fig. 61). If the structure center or center line is of particular interest (e.g. in cells or vessels), **connectivity metrics** come into play, which measure the agreement of the center line between two objects. This is of special interest if linear or tube-like objects are present in a data set, for example in brain vascular analysis. In these cases, over- or undersegmentation are typically not of special interest, with the focus rather being on connectivity or network topology. For this purpose, the *Center line Dice Similarity Coefficient (clDice)* [83] has been designed. For computation, the reference and prediction skeletons need to be extracted from the binary masks. Multiple approaches have been proposed, as described in [83]. As shown in Fig. 35, the *clDice* is then defined as the harmonic mean of *Topology Precision* and *Topology Sensitivity*. The *Topology Precision* measures the ratio of the overlap of the skeleton of the prediction skeleton and the reference mask and the skeleton of the prediction. Similarly to *Precision*, it measures the FP samples. On the other hand, *Topology Sensitivity* incorporates FN samples by measuring the ratio of the overlap of the skeleton of the reference and the prediction mask and the reference skeleton.



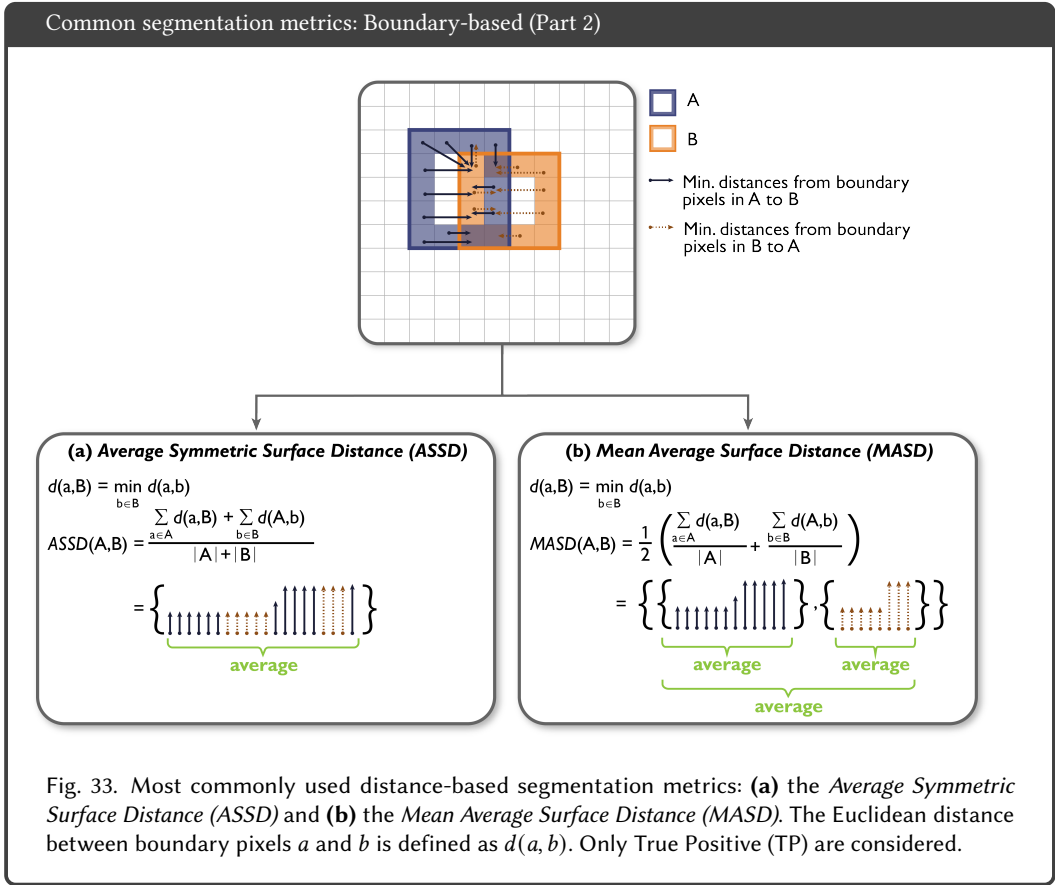


Fig. 33. Most commonly used distance-based segmentation metrics: **(a)** the *Average Symmetric Surface Distance (ASSD)* and **(b)** the *Mean Average Surface Distance (MASD)*. The Euclidean distance between boundary pixels a and b is defined as $d(a, b)$. Only True Positive (TP) are considered.

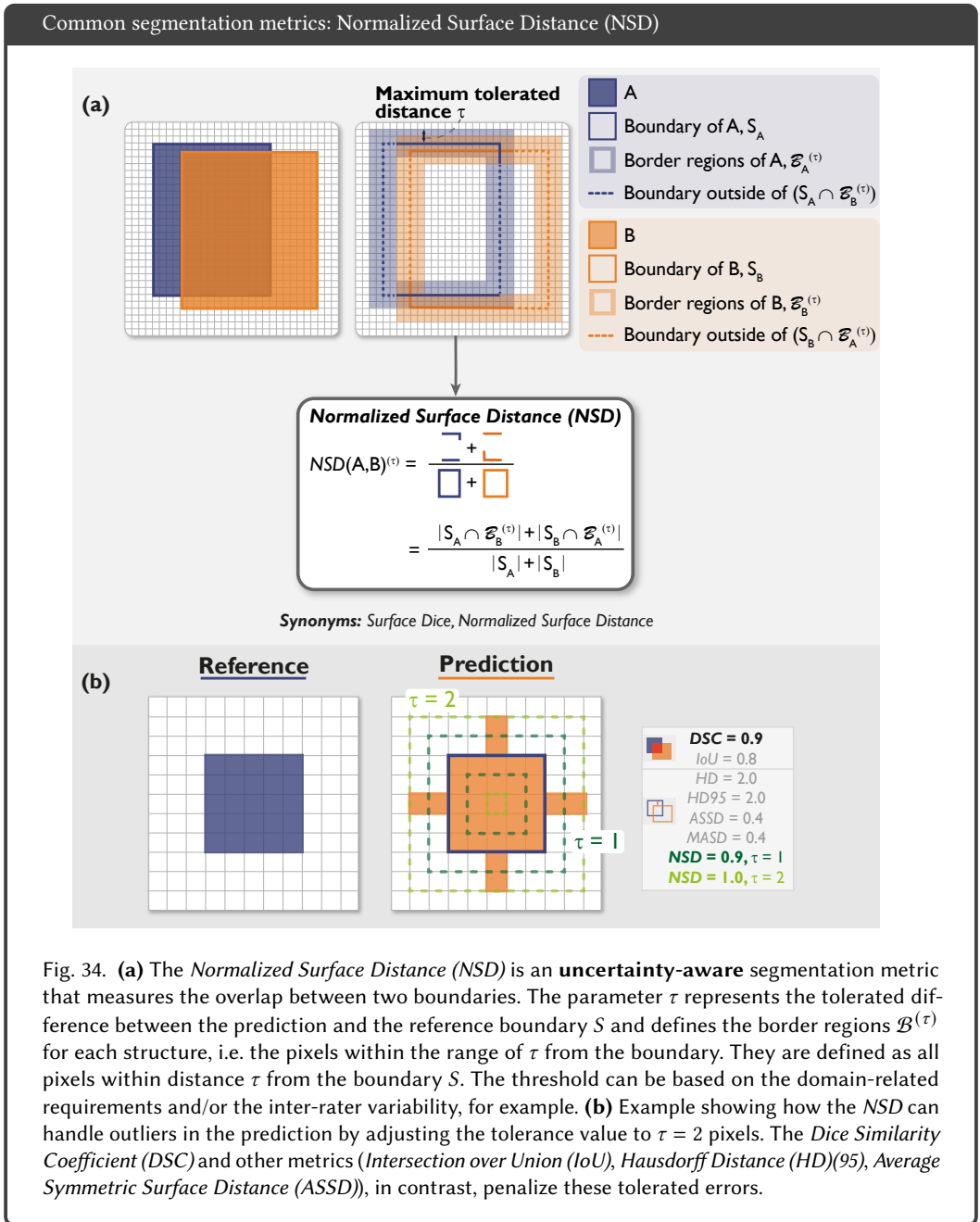
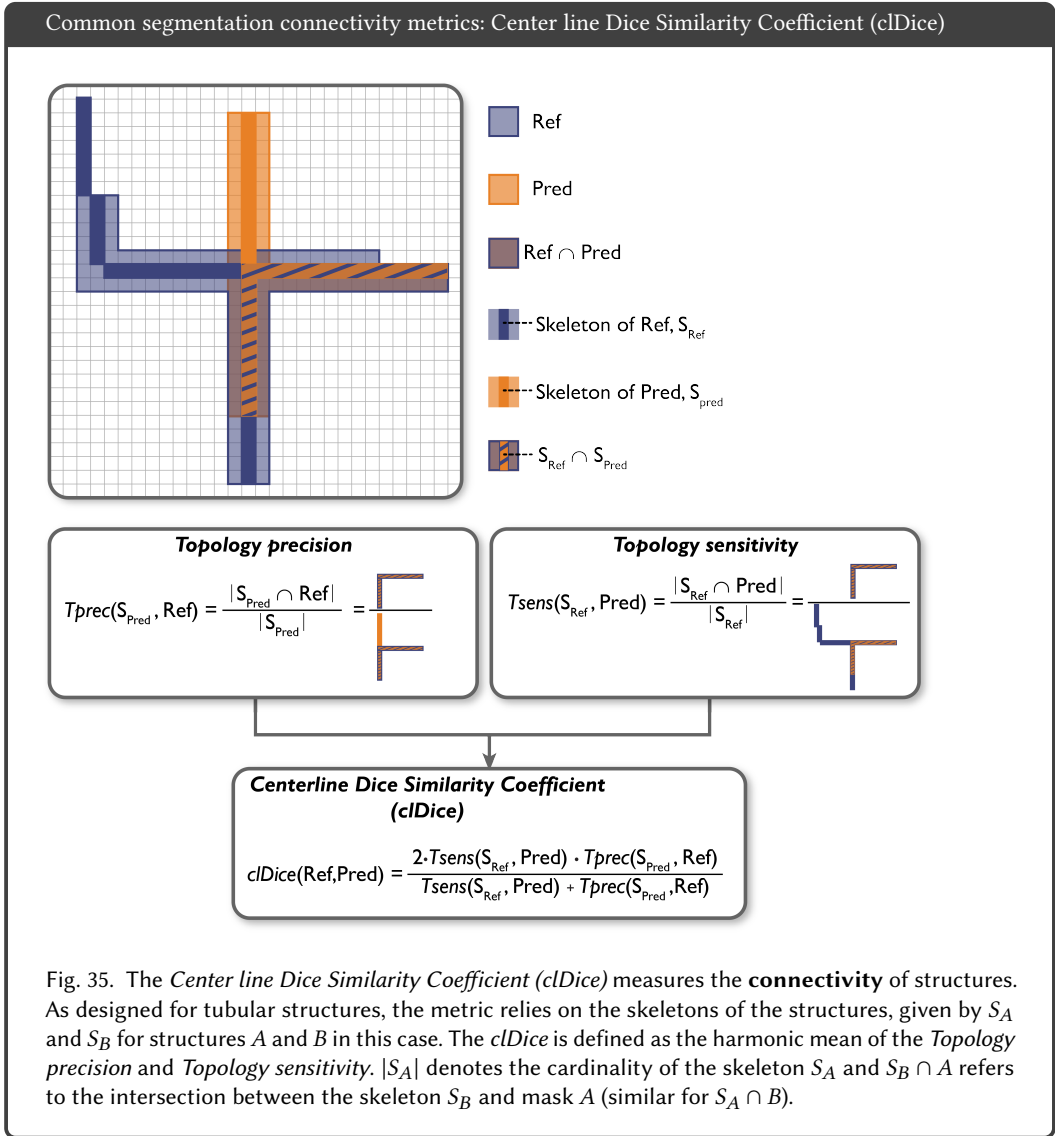


Fig. 34. **(a)** The *Normalized Surface Distance (NSD)* is an **uncertainty-aware** segmentation metric that measures the overlap between two boundaries. The parameter τ represents the tolerated difference between the prediction and the reference boundary S and defines the border regions $\mathcal{B}^{(\tau)}$ for each structure, i.e. the pixels within the range of τ from the boundary S . They are defined as all pixels within distance τ from the boundary S . The threshold can be based on the domain-related requirements and/or the inter-rater variability, for example. **(b)** Example showing how the *NSD* can handle outliers in the prediction by adjusting the tolerance value to $\tau = 2$ pixels. The *Dice Similarity Coefficient (DSC)* and other metrics (*Intersection over Union (IoU)*, *Hausdorff Distance (HD)*(95), *Average Symmetric Surface Distance (ASSD)*), in contrast, penalize these tolerated errors.



G.3 Object Detection.

Object detection refers to the detection of one or multiple objects (or: instances) of a particular class (e.g. lesion) in an image [54]. The following description assumes single-class problems, but translation to multi-class problems is straightforward, as validation for multiple classes on object level is performed individually per class. Notably, as multiple predictions and reference instances may be present in one image, the predictions need to include localization information, such that a matching between reference and predicted objects can be performed. Important design choices with respect to the validation of object detection methods include:

- (1) *How to represent an object?* Representation is typically composed of location information and a class affiliation. The former may take the form of a bounding box (i.e. a list of coordinates), a pixel mask, or the object's center point. Additionally, modern algorithms typically assign a confidence value to each object, representing the probability of a prediction corresponding to an actual object of the respective class. Note that a confusion matrix is later computed for a fixed threshold on the predicted class probabilities.⁸
- (2) *How to decide whether a reference instance was correctly detected?* This step is achieved by applying the *localization criterion*. This may, for example, be based on comparing the object centers of the reference and prediction or computing their overlap (Figs. 71 and 72).
- (3) *How to resolve assignment ambiguities?* The above step might lead to ambiguous matchings, such as two predictions being assigned to the same reference object. Several strategies exist for resolving such cases.

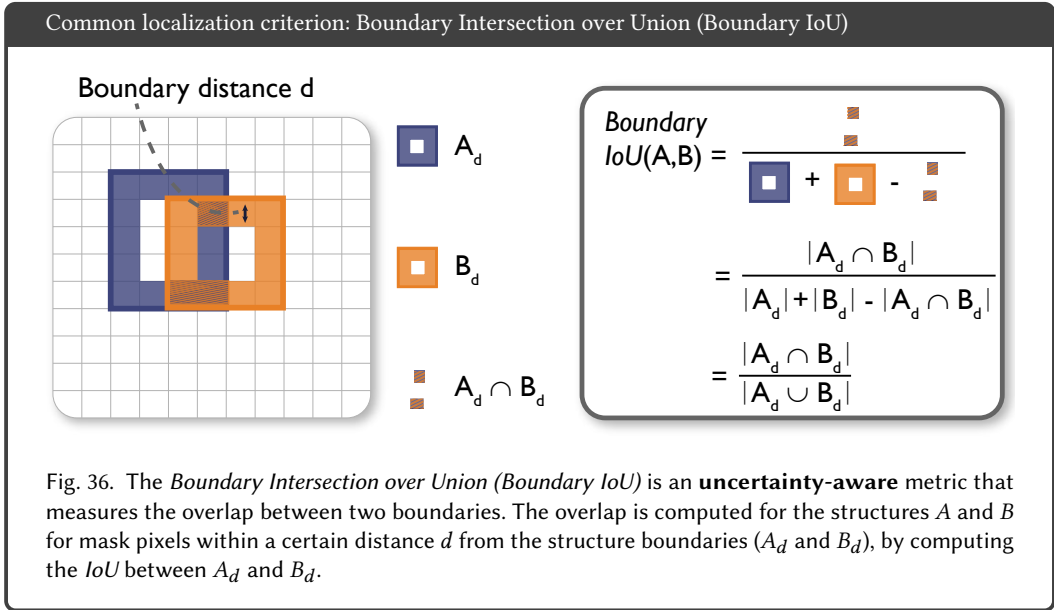
The following sections provide details on (1) applying the localization criterion, (2) applying the assignment strategy and (3) computing the actual performance metrics. Please note that localization performance does not regard anatomical constraints. A tumor growing invasively into neighboring structures might have good metric scores, while clinically the localization/classification/impact for the patient might be disastrous.

Localization criterion. As one image may contain multiple objects or no object at all, the **localization criterion** or **hit criterion** measures the (spatial) similarity between a prediction (represented by a bounding box, pixel mask, center point or similar) and a reference object. It defines whether the prediction *hit/detected* (TP) or *missed* (FP) the reference. Any reference object not detected by the algorithm is defined as FN. Please note that TN are not defined for object detection tasks, which has several implications on the applicable metrics, as detailed below.

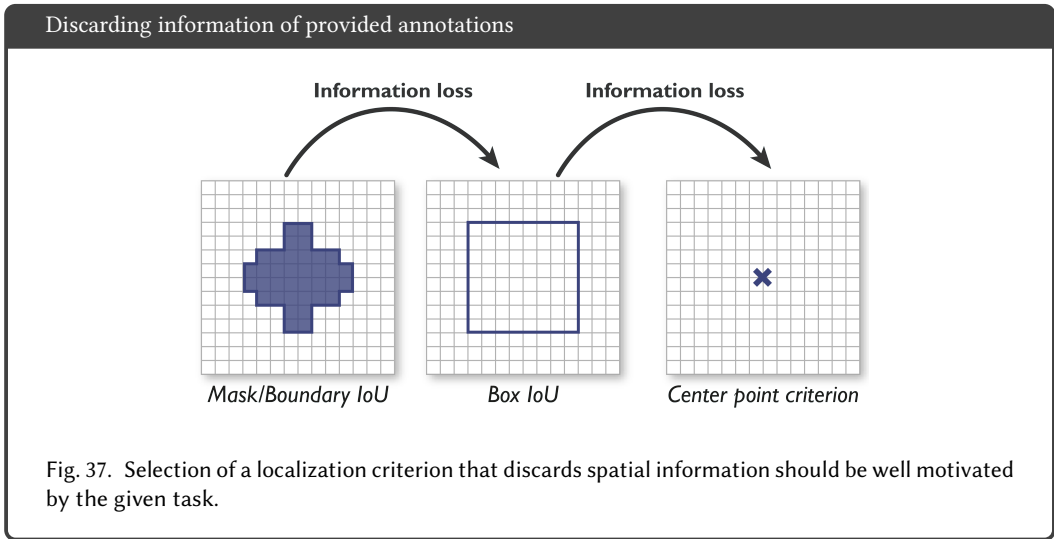
There are multiple ways to define the localization or hit criterion (see Figs. 31, 36 and 71). Popular center-based localization criteria are (a) *the center-cover criterion*, for which the reference object is considered hit if the center of the reference object is inside the predicted detection, (b) *the distance-based hit criterion*, which considers a TP if the distance d between the center of the reference and the detected object is smaller than a certain threshold τ and (c) *the center-hit criterion*, which holds true if the center of the predicted object is inside the reference bounding box or mask.

The most commonly used overlap-based hit criterion is determined by computing the *IoU* [42] (cf. Fig. 31b). The prediction is considered as TP if the overlap is larger than a certain threshold (e.g. 0.3 or 0.5) and as FP otherwise. If bounding boxes are considered, the *IoU* is computed between the reference and predicted bounding boxes (*Box IoU*). For more fine-grained annotations in form of a pixel mask, the *IoU* may be computed for the complete mask (*Mask IoU*). The *Mask IoU* is less sensitive to structure boundary quality in larger objects (cf. App. H.3). This is due to the fact that boundary pixels will increase linearly while pixels inside the structure will increase quadratically with an increase in structure size. The *Boundary IoU* measures the *IoU* of two structures for mask pixels within a certain distance d from the structure boundaries [19], as illustrated in Fig. 36.

⁸Please note that we will use the term confidence scores analogously to predicted class probabilities in the context of object detection and instance segmentation.



The localization criterion should be carefully chosen according to the underlying motivation and research question and depending on the available coarseness of annotations. However, it should be noted that annotations of a lower resolution will result in an information loss, as illustrated in Fig. 37. For example, the *Box IoU* is sometimes used although pixel-mask annotations are available because algorithms are expected to output rough localization in the shape of boxes. Such a simplification might cause problems if structures are not well-approximated by a box shape, or if structures can overlap causing multi-component masks (cf. App. H.4, Fig. 74). Lastly, it should be noted that the decision for a cutoff value on the localization criterion leads to instabilities in the validation (e.g. see Fig. 72). For this reason, it is common practice in the computer vision community to average metrics over multiple cutoff values (default for *IoU* criteria: 0.50:0.05:0.95 [54]). Generally speaking, the cutoff values should be chosen according to the driving biomedical question. For example, if particular interest lies on the exact outlines, higher thresholds should be chosen. On the other hand, for noisy reference standards, a low cutoff value is preferable.



Assignment strategy. The localization criterion alone is not sufficient to extract the final confusion matrix based on a fixed threshold for the predicted class probabilities (confidence scores), as ambiguities can occur. For example, two predictions may have been assigned to the same reference object in the localization step, or vice versa. These ambiguities need to be resolved in a further **assignment step**, as exemplarily shown in Fig. 38.

This assignment and thus the resolving of potential assignment ambiguities can be done via different strategies. The most common strategy in the computer vision community is the *Greedy by Score* strategy [30]. All predictions in an image are ranked by their predicted class probability and iteratively (starting with the highest probability) assigned to the reference object with the highest localization criterion for this prediction. The selected reference object is subsequently removed from the process since it can not be matched to any other prediction (unless double assignments are allowed). The *Hungarian Matching* [53] is associated with a cost function, usually depending on the localization criterion, which is minimized to find the optimal assignment of predictions and reference. In the biomedical domain, more sophisticated matching strategies are often avoided by setting the localization criterion threshold to $IoU > 0.5$ and only allowing non-overlapping object predictions (which inherently avoids matching conflicts). In the case of a high ratio of touching reference objects and common non-split errors, meaning that one prediction overlaps with multiple reference objects, the Intersection over Reference (IoR) [60] might be considered as an alternative to IoU [60] (see Fig. 73).

Example process of resolving a matching ambiguity

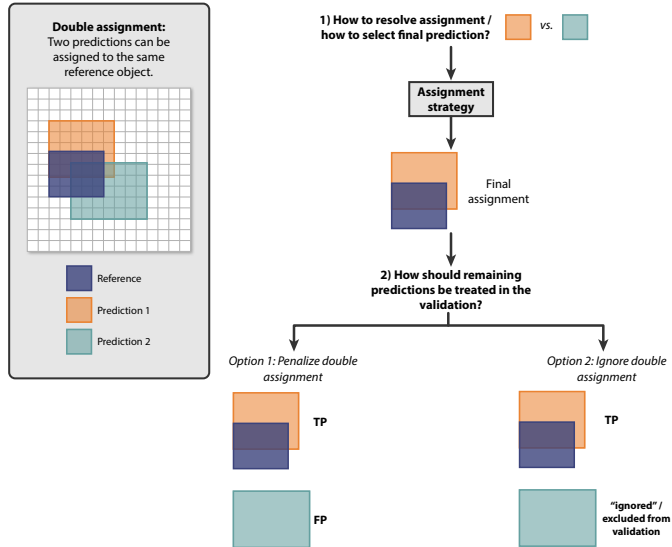


Fig. 38. In case of multiple predictions that may be assigned to the same reference object, an assignment strategy needs to be chosen. This includes a decision on how to treat the remaining predictions. For example, they can be penalized with a False Positive (FP) assignment or may be ignored. Used abbreviations: *Intersection over Union (IoU)*, *Intersection over Reference (IoR)* and True Positive (TP).

Metric computation. Similar to image-level classification and semantic segmentation algorithms, object detection algorithms are commonly assessed with counting metrics, assuming a fixed confusion matrix, (cf. Figs. 28 and 29). However, one of the most popular object detection metrics is the multi-threshold metric *Average Precision (AP)* [54], which is the area under the *Precision-Recall (PR)* curve for a certain interpolation scheme. The *PR* curve is computed similarly to the *ROC* curve by scanning over confidence thresholds and computing the *Precision (PPV)* and *Recall (Sensitivity)* for every threshold (cf. Fig. 30). Note in this context that the popular *ROC* curve is not applicable in object detection tasks because *TN* are not available. Also, while the *ROC* curve is monotonically rising, this behaviour may not be expected from the *PR* curve, which typically features a zigzag shape, as illustrated in Fig. 39. Specifically "as the level of *Recall* varies, the *Precision* does not necessarily change linearly due to the fact that *FP* replaces *FN* in the denominator of the *Precision* metric." [27]. A linear interpolation would therefore be overly optimistic, which is why more complex interpolation is needed, as detailed in [27].

The area under the *PR* curve is typically calculated as the *AP* implying a conservative simplification of curve interpolation,

$$AP = \sum_n (R_n - R_{n-1})P_n, \quad (7)$$

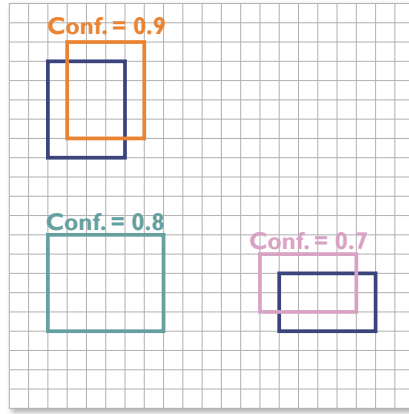
with R_n and P_n denoting the *Recall* and *Precision* at the n th threshold⁹ (cf. dashed gray line in Fig. 39). For the *PR* curve, an optimal model would lead to *Recall (Sensitivity)* and *Precision (PPV)* of 1, therefore being the point (1, 1) on the *PR* curve. Conversely, a model with no skill level (random guessing) would result in a horizontal line with a precision proportional to the portion of positive samples, i.e. the prevalence (dashed line in Fig. 30). For computation of the metric (for a given class), the predictions are sorted in descending order of the confidence for each prediction (for that class). For each possible confidence threshold, the cardinalities are computed and the resulting tuple of *Recall (Sensitivity)* and *Precision* is added to the curve (cf. Fig. 39).

In contrast to drawing the *PR* curve and computing the *AP*, *FROC* curve is often favoured in the clinical context due to its easier interpretability. It operates at object level and plots the average number of *FPPI* (in contrast to the *FPR*) against the *Sensitivity* [18, 95] (cf. Fig. 40). The *FROC Score*, measured as the area under the *FROC* curve, however, is not bounded between 0 and 1 and the employed *FPPI* scores vary across studies, such that there exists no standardized definition of an area under the respective curve. Overall, the decision between the two metrics often boils down to a decision between a standardized and technical validation versus an interpretable and application-focused validation.

⁹https://scikit-learn.org/stable/modules/generated/sklearn.metrics.average_precision_score.html

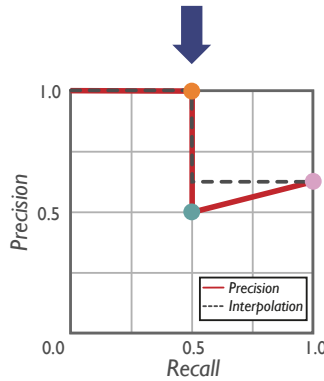
Common object detection metrics: Average Precision (AP)

Localization criterion:
 $IoU > 0.3$



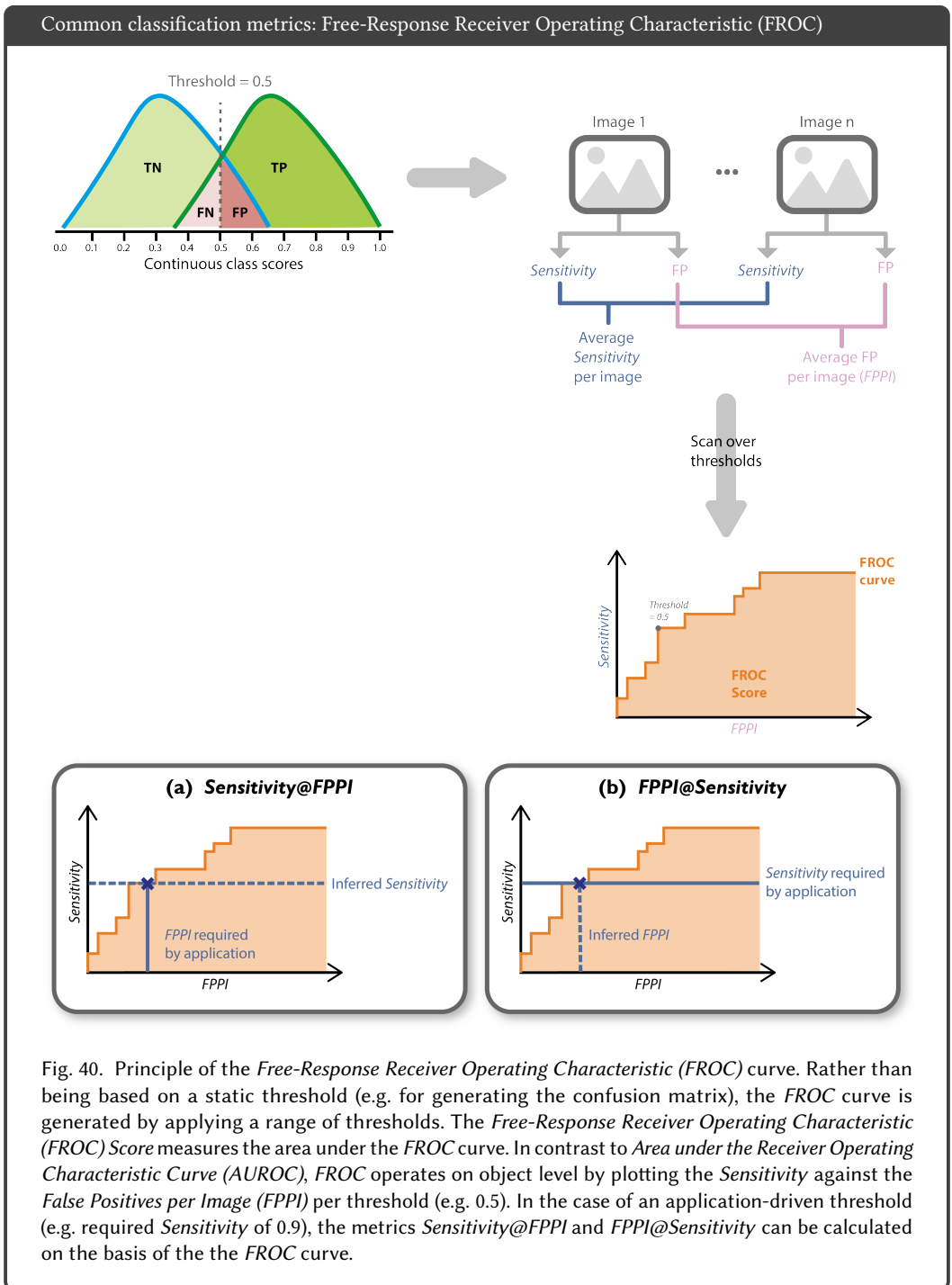
Reference bounding boxes
Prediction bounding boxes

Rank	Conf.	IoU	TP / FP?	Cumulative TP	Cumulative FP	Recall	Precision
1	0.9	0.43	TP	1	0	0.50	1.00
2	0.8	0.00	FP	1	1	0.50	0.50
3	0.7	0.36	TP	2	1	1.00	0.67



$$AP = \sum_n (R_n - R_{n-1}) P_n \approx 0.83$$

Fig. 39. Exemplary computation of the Average Precision (AP) in object detection tasks. Predictions are ranked according to their predicted class probabilities, represented by the confidence (conf.). Based on the Intersection over Union (IoU) or a similar localization/hit criterion, it is determined whether the prediction is a True Positive (TP) or False Positive (FP) (here: $IoU > 0.3$). For the creation of the Precision-Recall (PR) curve, Precision and Recall are computed for the accumulated TP and FP for every confidence score (conf.). The AP interpolates the points of the PR curve as shown by the dashed gray line.



Counting cardinalities at different scales. In image-level classification problems, validation is naturally performed on the entire data set, while segmentation typically relies on computing metrics for each image and then aggregating metric values. This latter approach is not applicable in object detection in a straightforward manner because of the relatively small amount of samples per image (typically a few objects rather than thousands of pixels). Fig. 41 illustrates the per-image and the per-data set validation of objects. In the per-image aggregation approach, special care needs to be taken in the case of an empty reference or prediction, as detailed in App. H.4 (Fig. 77).

A few comments on how to compute evaluation metrics while aggregating matched objects per image:

- **Counting metrics:** Computing per-class metrics such as Sensitivity, PPV, or F_1 Score (see Fig. 28) works intuitively (as depicted in Fig. 41) by computing a score per image and averaging scores over the data set while considering the Not a Number (NaN) conventions shown in Fig. 77.
- **Multi-threshold metrics:** While scanning over all thresholds in the data set (analogously to per data set evaluation), for every threshold the Precision (PPV) and Recall (Sensitivity) scores are computed per image/patient (while considering the NaN conventions in Fig. 77) and averaged over the data set. The averaged Precision and Recall score pairs per threshold form the PR curve. The AP (see Fig. 39) can be computed for this curve analogously to the per-data set evaluation. The FROC curve computation works analogously while replacing Precision per image with FPPI.
- **Single working point evaluation:** A single working point (e.g. PPV@Sensitivity) can be retrieved based on the curves resulting from multi-threshold evaluation described above.

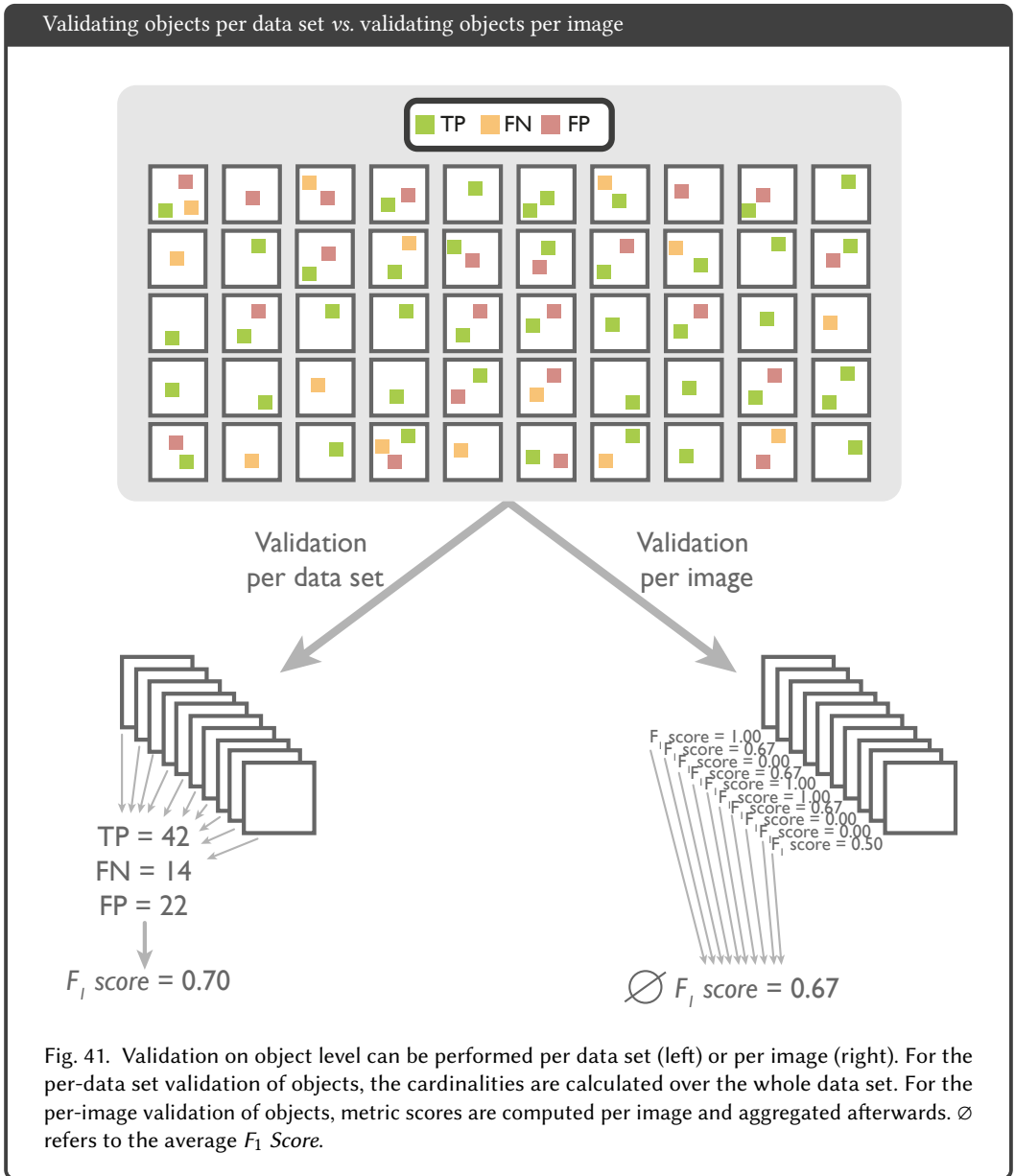
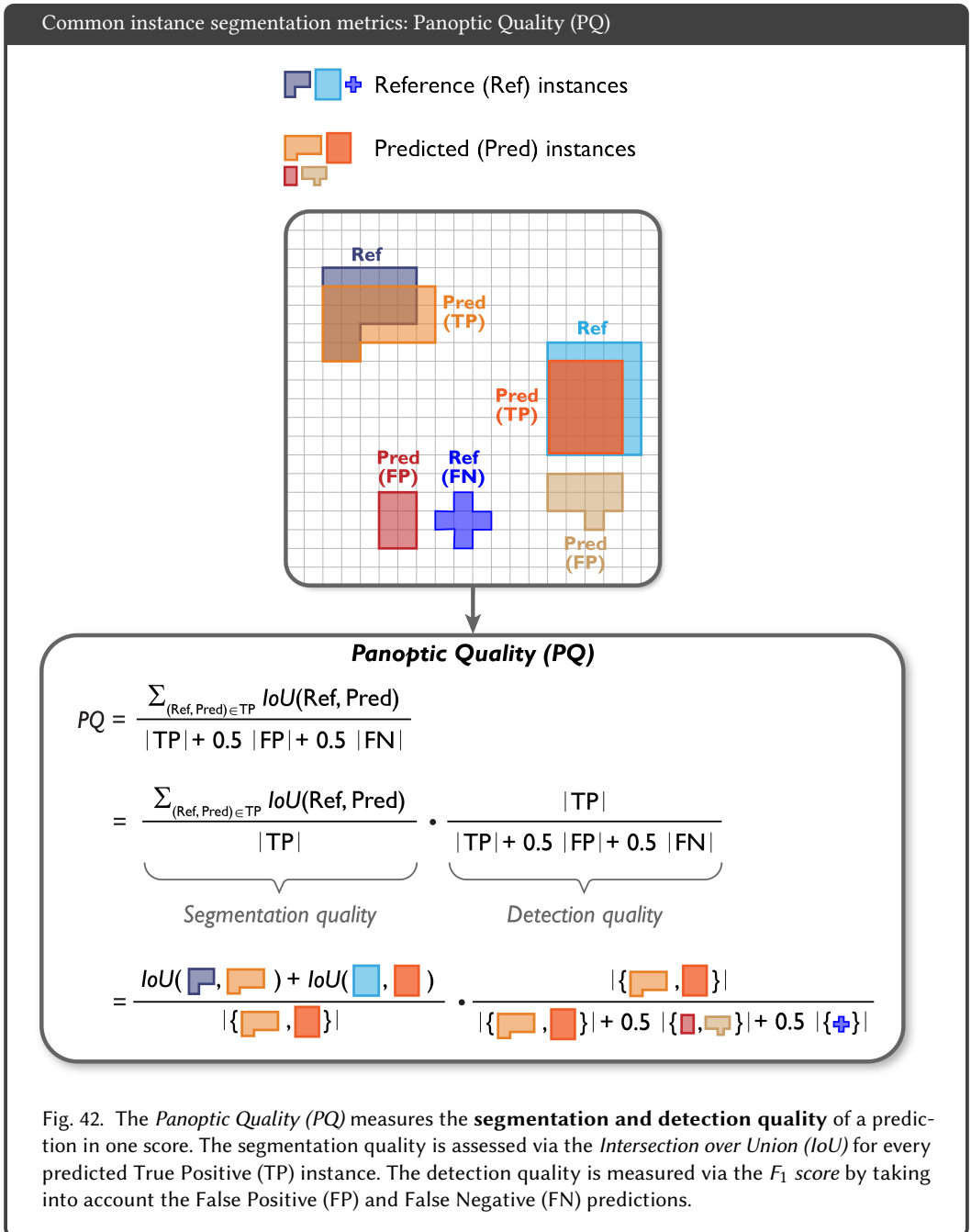


Fig. 41. Validation on object level can be performed per data set (left) or per image (right). For the per-data set validation of objects, the cardinalities are calculated over the whole data set. For the per-image validation of objects, metric scores are computed per image and aggregated afterwards. \emptyset refers to the average F_1 Score.

G.4 Instance Segmentation.

In contrast to semantic segmentation, instance segmentation problems distinguish different instances of the same class (e.g. different lesions). Similarly to object detection problems, the task is to detect individual instances of the same class, but detection performance is measured by pixel-level correspondences (as in semantic segmentation problems). Optionally, instances can be applied to one of multiple classes. Validation metrics in instance segmentation problems often combine common detection metrics with segmentation metrics applied per instance.

If detection and segmentation performance should be assessed simultaneously in a single score, the PQ metric can be utilized [50]. As shown in Fig. 42, the segmentation quality is assessed by averaging the IoU scores for all TP instances. While this part alone would neglect FP and FN predictions, it is multiplied with the detection quality, which is equal to the F_1 score. For perfect segmentation results, i.e. an average IoU of 1, the PQ would simply equal the F_1 Score. In other words, while segmentation quality in the F_1 Score is merely integrated via a hard cutoff during localisation (e.g. $IoU > 0.5$) affecting the counts of TP versus FP and FN, PQ allows for a continuous measurement of segmentation quality by 1) employing a loose prior localization criterion (e.g. $IoU > 0$, i.e. any prediction overlapping with a reference instance is treated as TP) and 2) replacing the simple counting of TP by adding up the continuous IoU scores per TP. PQ was introduced for panoptic segmentation problems that are a combination of semantic and instance segmentation [50]. It is computed per class (including background classes) and can therefore be directly used for instance segmentation problems by only assessing the foreground instances. If needed, the background quality can also be assessed.



It should be noted that instance segmentation problems are often phrased as semantic segmentation problems with an additional post-processing step, such as connected component analysis [75]. In practice, predicted class probabilities, yielded by modern segmentation algorithms, are often discarded in the post-processing step and are thus not available for subsequent validation. Fig. 43 illustrates how to overcome this potential problem.

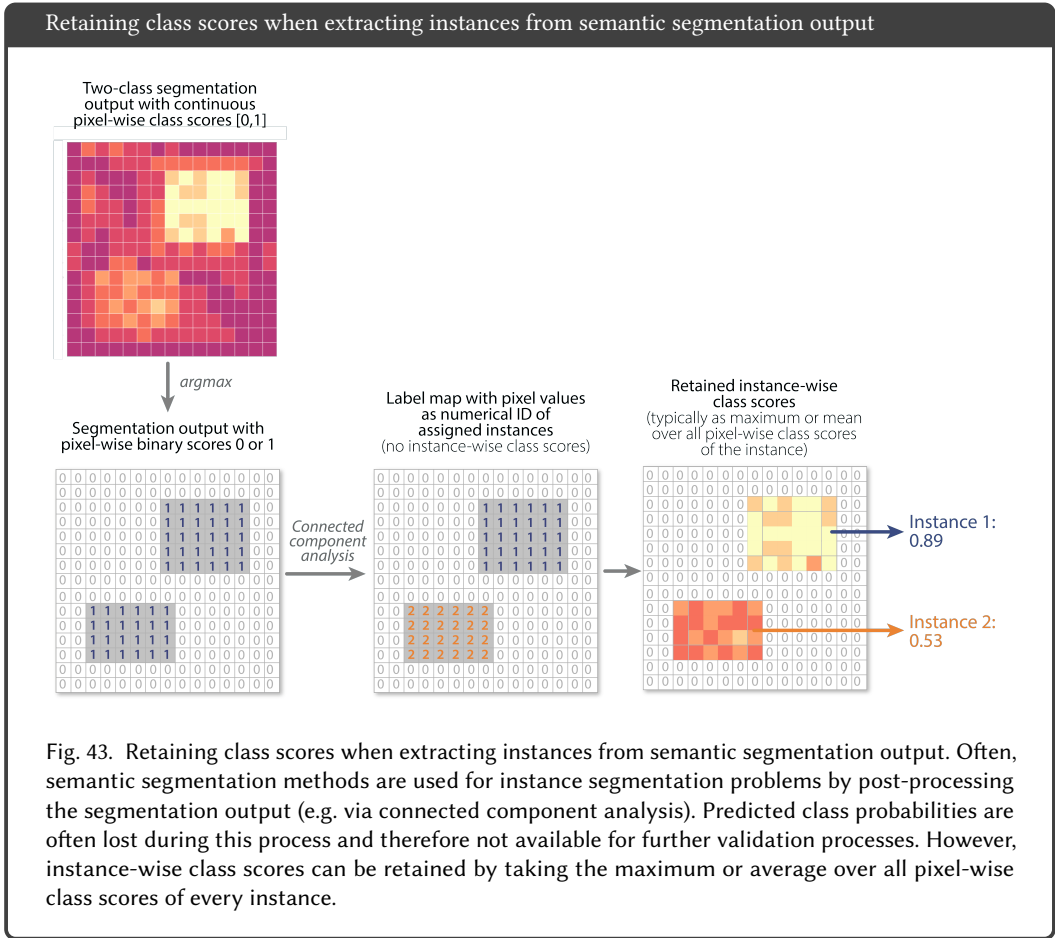


Fig. 43. Retaining class scores when extracting instances from semantic segmentation output. Often, semantic segmentation methods are used for instance segmentation problems by post-processing the segmentation output (e.g. via connected component analysis). Predicted class probabilities are often lost during this process and therefore not available for further validation processes. However, instance-wise class scores can be retained by taking the maximum or average over all pixel-wise class scores of every instance.

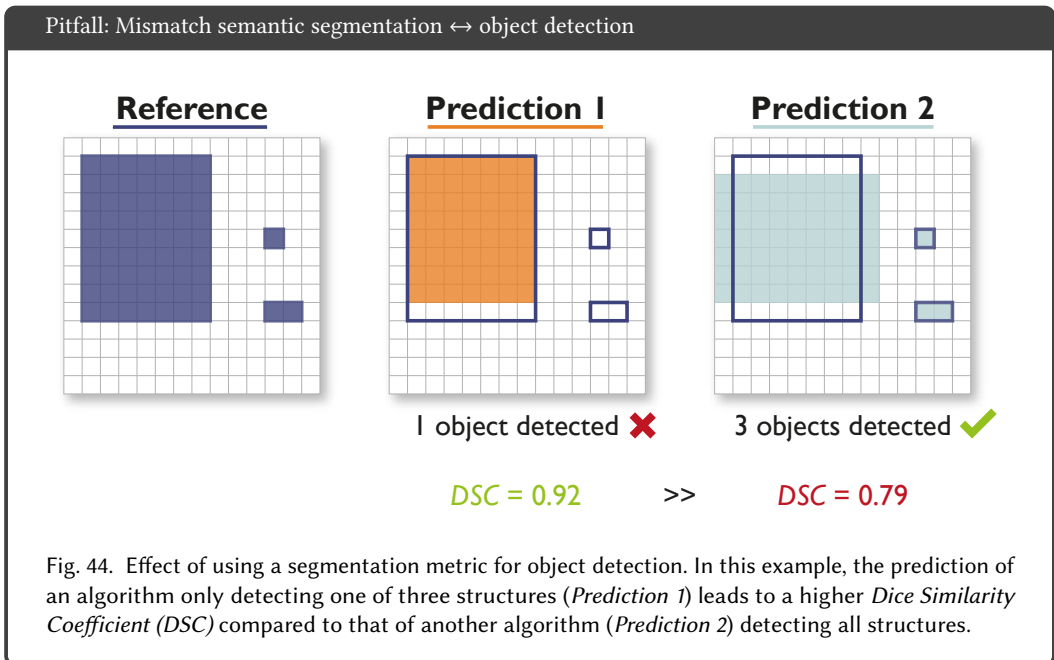
H Pitfalls of Metrics

This section presents common limitations of image processing metrics related to category-metric mismatch (App. H.1), image-level classification (App. H.2), segmentation (App. H.3), object detection (App. H.4) and analyses and post-processing (App. H.5). A dynamically updated and more comprehensive document on the metric pitfalls identified is available in a dedicated arXiv paper [73].

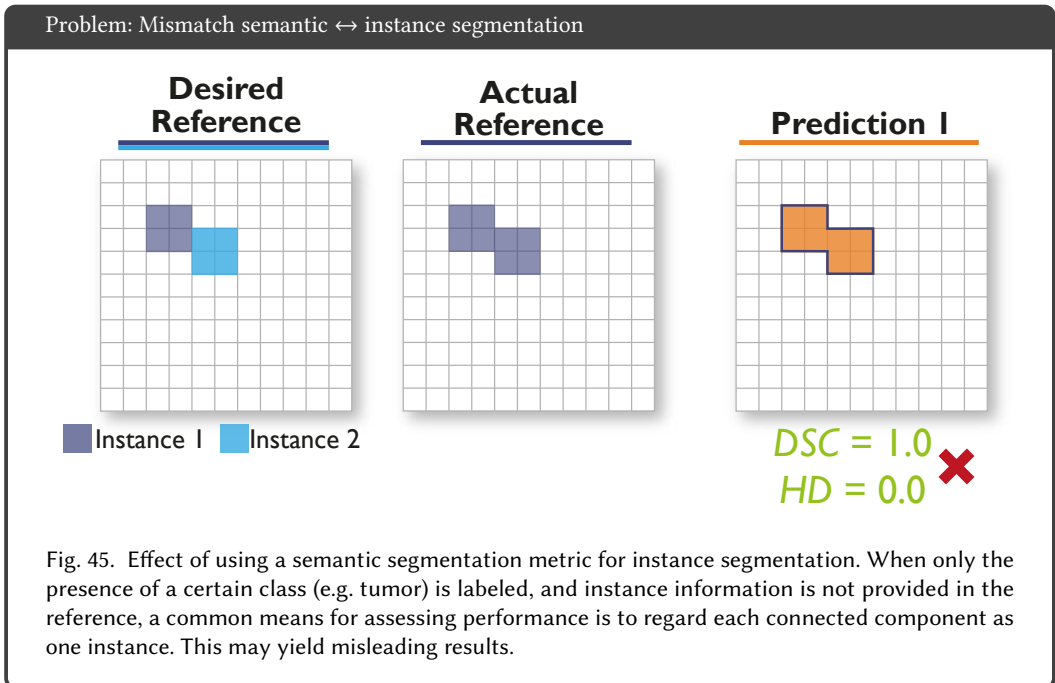
H.1 Pitfalls due to category-metric mismatch.

Performance metrics are typically expected to reflect a domain-specific validation goal (e.g. clinical goal). Previous research, however, suggests, that this is often not the case [78]. Before choosing validation metrics, the correct problem category needs to be defined. In the following, we will describe pitfalls related to metrics not being applied to the appropriate problem category.

Mismatch semantic segmentation \leftrightarrow object detection. A common problem is that segmentation metrics, such as the *DSC*, are applied to *object detection* tasks [17, 44], as illustrated in Fig. 44. From a clinical perspective, for example, the algorithm producing *Prediction 2* and covering all three structures of interest (e.g. tumors) would be clinically much more valuable compared to the one producing a highly accurate segmentation for one structure but missing the other two in *Prediction 1*. This is not reflected in the metric values, which are substantially higher for *Prediction 1*. In general, the *DSC* is strongly biased against single objects, therefore not appropriate for the detection of multiple structures [50, 101].



Mismatch semantic \leftrightarrow instance segmentation. In segmentation problems, the driving research question should decide whether semantic or instance segmentation should be chosen for validation. This is particularly relevant when multiple objects within one image overlap or touch, as often occurring in cell images. For semantic segmentation problems, overlapping or touching objects (see F3.5 and F5.4) may end up merged into a single object without clear boundaries or distinction between the single objects. Instance segmentation problems, on the other hand, ensure that the borders of touching or overlapping structures can be accurately assigned and that objects can be differentiated. If instance segmentation is preferred, the labels need to be chosen accordingly. An example is shown in Fig. 45: The desired annotation consists of two different instances, but only semantic labels are available (middle). A prediction will only be as accurate as the reference, hence detecting only one instance but yielding a perfect metric score although the desired task is not solved.



Mismatch image-level classification ↔ object detection. Tasks that should be validated at image level are sometimes erroneously approached with object detection models instead of image-level classification models [43]. Object detection models are designed to handle different objects in an image rather than the complete image and will naturally introduce problems in a validation setting on image level. Object detection tasks are dependent on choosing a proper localization criterion, which is not needed for an image-level classification problem. For example, a *ROC* curve, typically used for assessing the performance of image-level classification algorithms, does not consider the localization step needed in object detection tasks, as it was designed to validate at image rather than object level. It therefore does not take into account whether a detected object is at the correct location in the image. Moreover, when validation on image level is conducted by using an object detection model, the detection with the largest class probability (confidence score) of all detections in one image is usually taken, neglecting all other predictions. This does not capture the performance of the model accurately. Fig. 46 illustrates some of the resulting problems:

- (1) The image-level *ROC* curve **does not measure the localization performance**. As can be seen from Fig. 46a, the validation is performed per image, not per object, therefore not considering whether an object is actually hit (see *Prediction 2*).
- (2) The image-level *ROC* curve is **invariant to the number of annotated objects**. As can be seen from Fig. 46b, the curve can not discriminate between a model detecting all objects in an image (*Prediction 1*) or just detecting one object (*Prediction 2*), as long as the largest score is the same across predictions.
- (3) The image-level *ROC* curve is **invariant to the number of detected objects**. As can be seen from Fig. 46c, the curve can not discriminate between a model detecting many FP objects in an image (*Prediction 2*) or only detecting one FP (*Prediction 1*), as long as the largest score is the same.

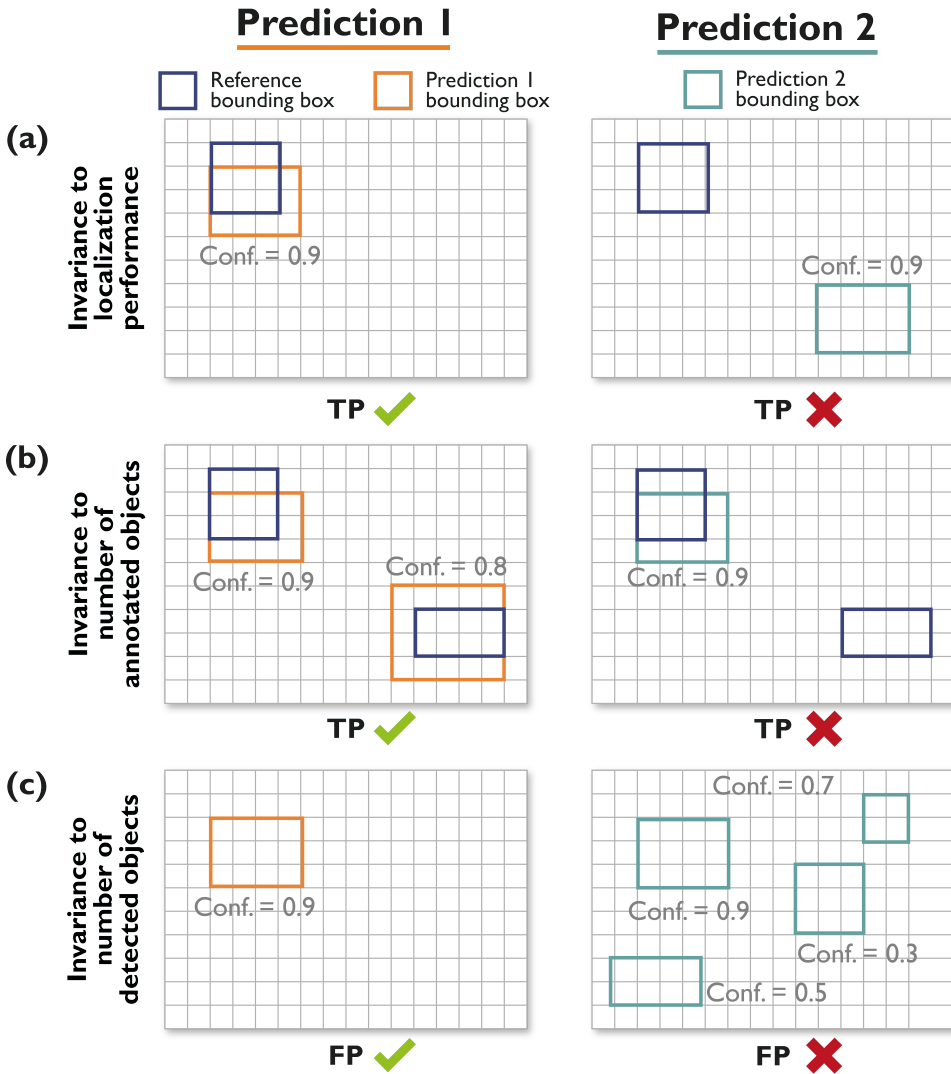
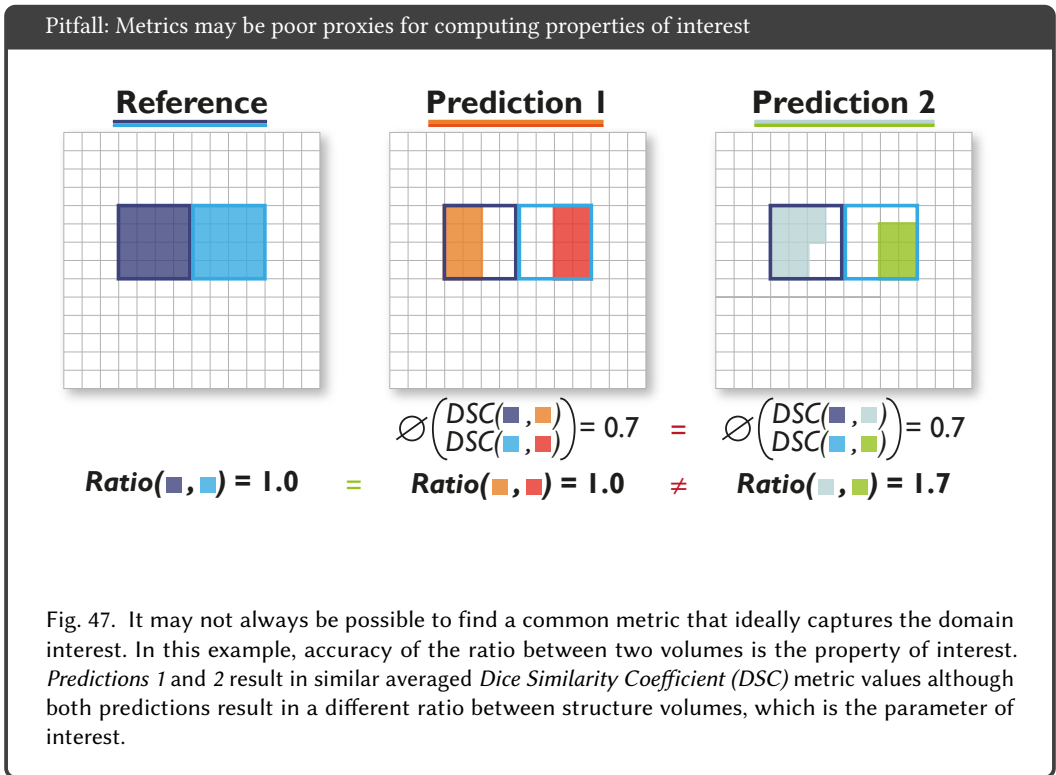
Pitfall: Mismatch image-level classification \leftrightarrow object detection

Fig. 46. When image-level classification metrics such as the area under the *Receiver Operating Characteristic* (ROC) curve are used to validate object detection models, (1) information on the object matching (localization, number of objects etc.) is lost and typically (2) only one detection per image (the one with the highest confidence) is considered. This leads to several problems: **(a)** The image-level ROC curve does not measure the localization performance. Both *Prediction 1* and *2* are considered as True Positive (TP) due to their score being very high, although *Prediction 2* is not hitting the annotated object. **(b)** The image-level ROC is invariant to the number of annotated objects in an image. The curve does not discriminate between a model detecting all positives (*Prediction 1*) and a model detecting only one of the positives (*Prediction 2*), as long as the maximum score is the same. **(c)** The image-level ROC is invariant to the number of detections in an image. The curve does not discriminate between a model with many False Positives (FP), (*Prediction 2*) and a model with just one FP (*Prediction 1*), as long as the maximum score is the same. The class probabilities are represented by confidence scores (conf.).

No matching problem category. Metrics should reflect a domain-specific validation goal. This goal may not align with commonly used technical measures like the *DSC*. Fig. 47 shows an example with the property of interest being the accuracy of the ratio between two structure volumes, indicating, for example, the percentage of blood volume ejected in each cardiac cycle [6]. Both predictions will result in similar averaged *DSC* scores, although the ratio of the volumes vastly differs. A common segmentation metric thus does not reflect the actual research question in this case.



H.2 Pitfalls related to image-level classification.

Most issues related to classification metrics are related to one of the following properties of the underlying biomedical problem:

- High class imbalance (Fig. 48, F4.1)
- Presence of more than two classes (Fig. 49)
- Unequal handling of classes (Fig. 50, F2.5.1 and F2.5.3)
- Interdependencies between classes (Fig. 51)
- Lack of stratification (Fig. 52)
- Missing prevalence correction (Fig. 53)
- Discrimination vs. calibration (Fig. 54)

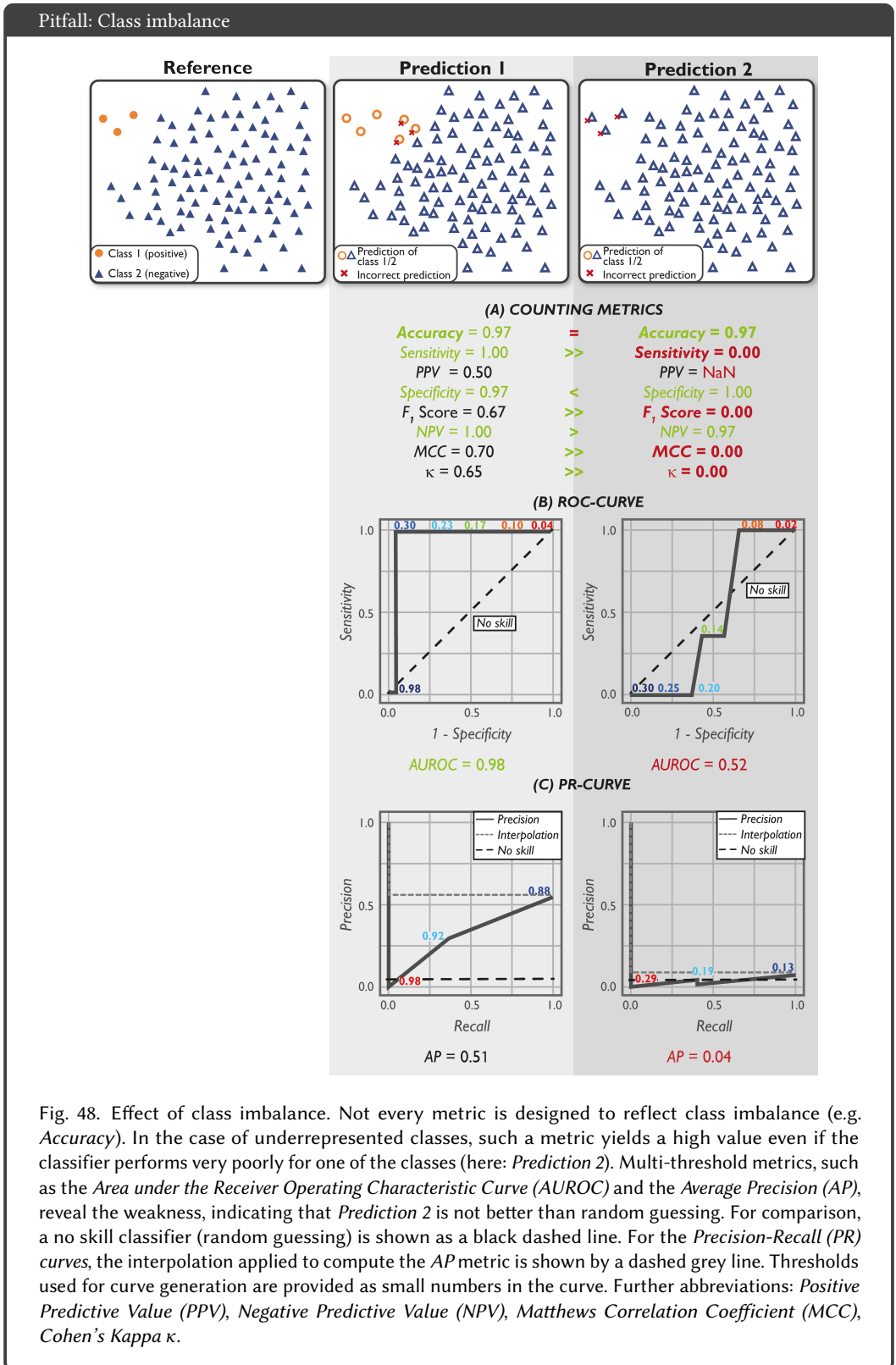
Furthermore, metric-specific limitations may arise (Fig. 55) Please note that all of these also apply to semantic/instance segmentation or object detection problems. The discourse focuses on the most commonly used image-level classification metrics, as presented in Figs. 28, 29 and 30. For most of the problems, it focuses on the *Accuracy*, *Sensitivity* or *PPV*, because those are the most common metrics for image-level classification in biomedical image analysis. Please note that we do not recommend their indiscriminate use, as they come with limitations (discussed in the following paragraphs), but rather wish to spotlight the problems and pitfalls of those most commonly used metrics.

To preserve the clarity of the illustrations, the most important of the presented metric values may be highlighted with color. Green metric values correspond to a "good" metric value (e.g. a high *Sensitivity* score), whereas red values correspond to a "bad" value (e.g. a low *Sensitivity*). Green check marks indicate desirable behaviour of metrics, red crosses indicate undesirable behaviour. Please note that a low metric value is not automatically a "bad" score. A metric value should always be put into perspective and compared to inter-rater variability. For simplicity, we still use the terms "good" and "bad/poor" throughout the section. Finally, our illustrations do not provide the concrete class probabilities of the presented classifiers.

High class imbalance. *Accuracy* is one of the commonly applied metrics in classification problems, presumably because it is particularly straightforward to interpret. However, the metric is not designed to handle imbalanced data sets, which often occur across all domains. Fig. 48 provides an example in which the positive class (orange circle) is heavily underrepresented. While *Prediction 1* gives a reasonable separation of the classes, *Prediction 2* results in the same *Accuracy* value (0.97) although the algorithm only provides the majority vote as a result. In this specific example, *Sensitivity*, *PPV* and *F1 score* reveal the issue, as does *Matthews correlation coefficient (MCC)*, a metric designed to handle class imbalance which reflects that *Prediction 2* is not better than a random guess (0.00) [21]. As many classification measures are easily computable using the number of TP, TN, FP and FN samples, it is highly recommended to report these TP, TN, FP and FN values explicitly and then compute multiple metrics [38].

Plotting the *ROC* and *PR* curves (Figs. 48b and c) also reveals the limitations of *Prediction 2*, which yields an *AUROC* of 0.52 and *AP* of 0.04, indicating that the prediction is not better than random guessing.

Some metrics inherently address the problem of performance overestimation or distortion caused by class imbalance. *Matthews Correlation Coefficient (MCC)* and *Cohen's Kappa κ* , for example, are designed in such a way that they assign a (prevalence-aware) random guessing algorithm the value 0. Similarly, *Area under the Receiver Operating Characteristic Curve (AUROC)* assigns the value 0.5 and *Balanced Accuracy* yields a value of $\frac{1}{C}$, where C is the number of classes. For all other metrics (see Fig. 48), it is recommended in general to put the resulting values into perspective of a (prevalence-aware) random guessing algorithm baseline.



More than two classes available. Many binary metrics can directly be translated to the multi-class case by expanding the confusion matrix to all classes. These classes are often hierarchically structured, for example in the shape of one negative class (e.g. no pathology) and multiple positive classes (e.g. different types of pathologies). Fig. 49 shows an example of a classification into triangles and circles, for which the circle class is further separated into two distinct classes (green and orange). The binary performance into triangle vs. circle, shown in the middle, is good (*Accuracy* of 0.88). But when considering the three classes separately, the prediction struggles to identify the color of the circles, causing their per-class accuracy scores to drop significantly (0.63 each).

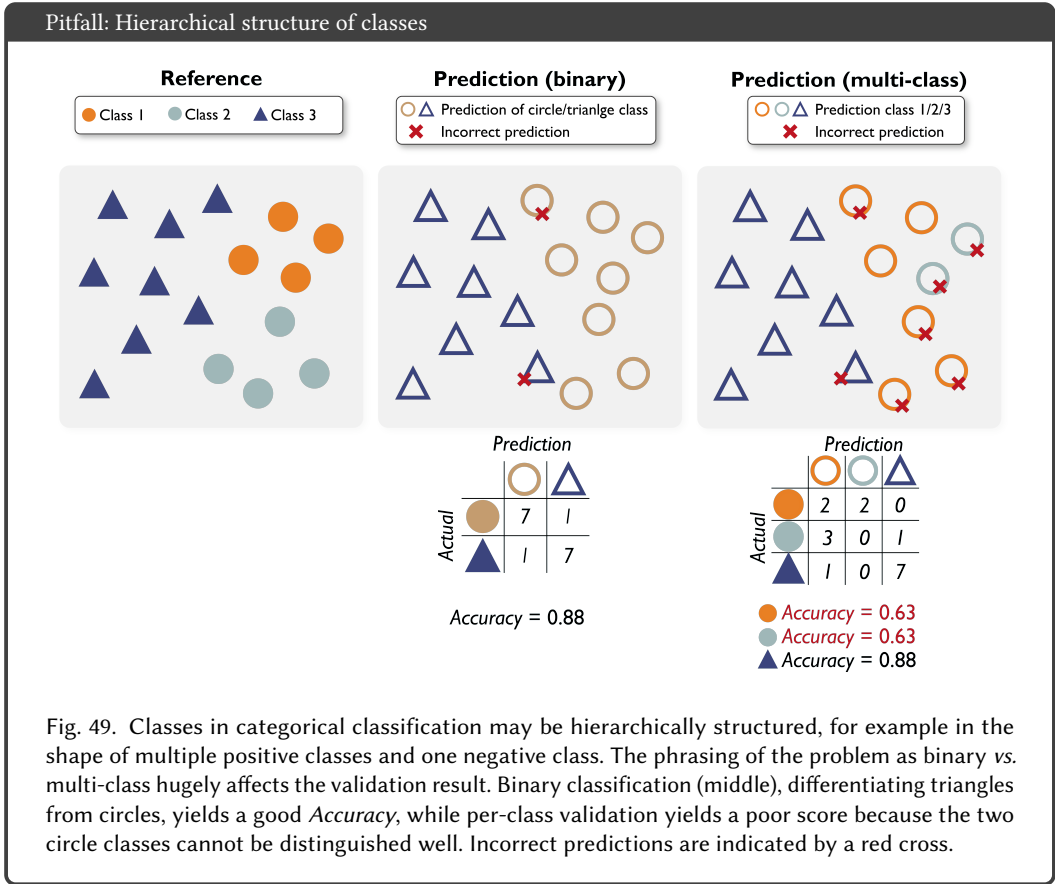


Fig. 49. Classes in categorical classification may be hierarchically structured, for example in the shape of multiple positive classes and one negative class. The phrasing of the problem as binary vs. multi-class hugely affects the validation result. Binary classification (middle), differentiating triangles from circles, yields a good *Accuracy*, while per-class validation yields a poor score because the two circle classes cannot be distinguished well. Incorrect predictions are indicated by a red cross.

Unequal handling of classes. In biomedical applications, classes are often not equally important. Consider the task of colon polyp detection in the gastrointestinal tract, for example. To provide the patient with the best care, it is crucial to detect all of these precancerous lesions. This requires a particular penalization of those samples containing a polyp which have been marked as 'no polyp' (FN), and the metrics need to be chosen accordingly. The *PPV*, for example, does not include the FN in its definition, hence would not be appropriate for this research question. *Sensitivity*, on the other hand, would show the desired poor performance in the presence of many FN predictions, as seen in the top row of Fig. 50a.

For image retrieval, the task of finding images for a specific content, it is not important to find every single existing image, but the images found should be correct. In this setting, the FP (assigning an incorrect image as correct) need to be penalized. Since it includes the computation of FP, in this case, the *PPV* would be a good metric. In contrast, *Sensitivity* does not consider FP, therefore being inappropriate in this context (see bottom row of Fig. 50a). Penalization in both cases is especially important in cases of imbalanced data sets (see Fig. 48).

When it comes to multi-class problems, different approaches may be chosen to compute the metric values. One possibility is to first compute the metric values per class and aggregate them subsequently. Special care has to be taken in the case of unequal importance of the different classes. For example, identifying whether a patient harbors a pathology in general might be more important than identifying the specific type of pathology. In this case, one should not just average over all class metric scores, but instead apply a sufficient weighting scheme. In the example of Fig. 50b, the triangle class is the most important class but also the one with the lowest per-class *Accuracy*. Simple averaging, so-called macro-averaging, would ignore that property and thus result in a higher aggregated *Accuracy* than merited. This effect can be compensated with the *Weighted Accuracy*.

Pitfall: Unequal handling of classes or misclassifications

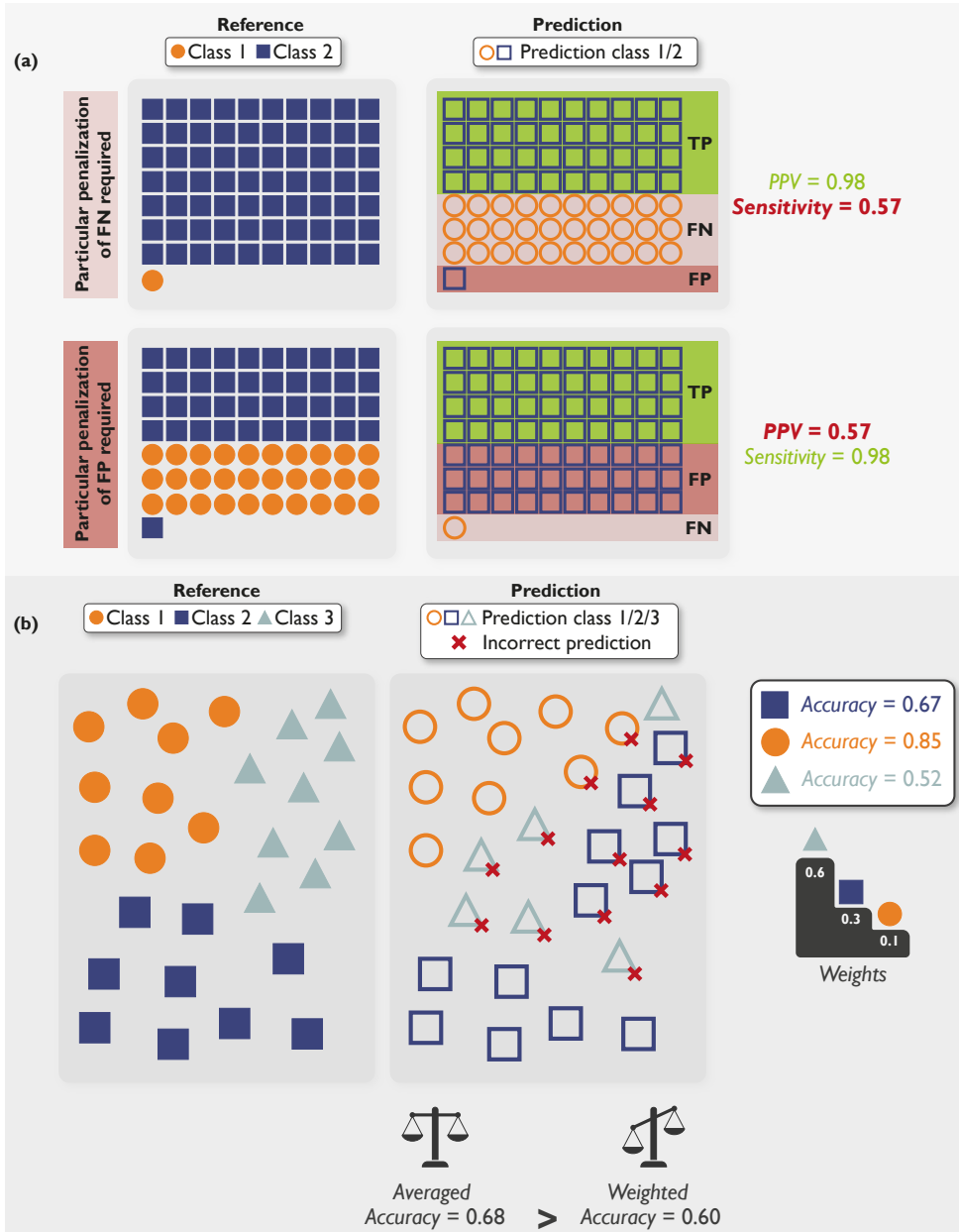
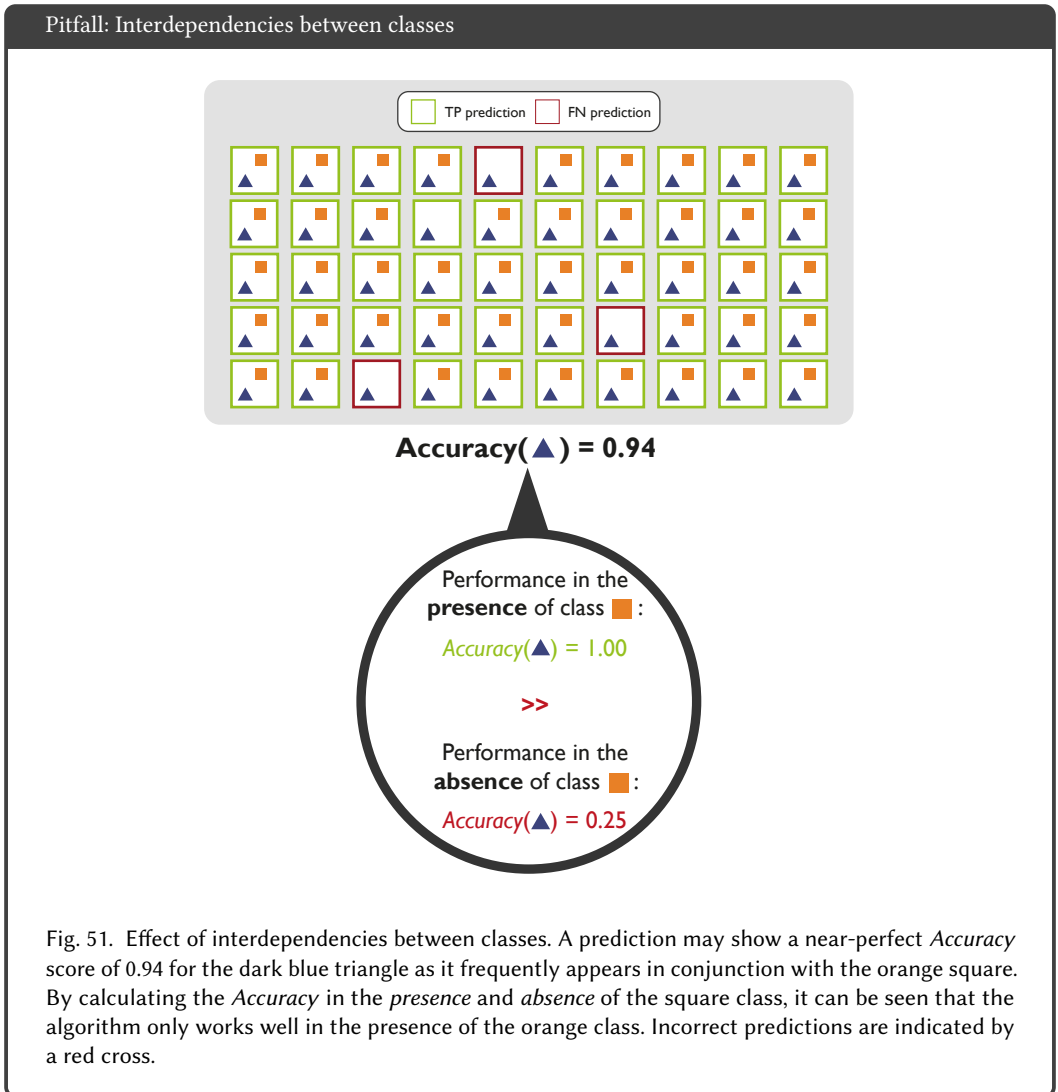
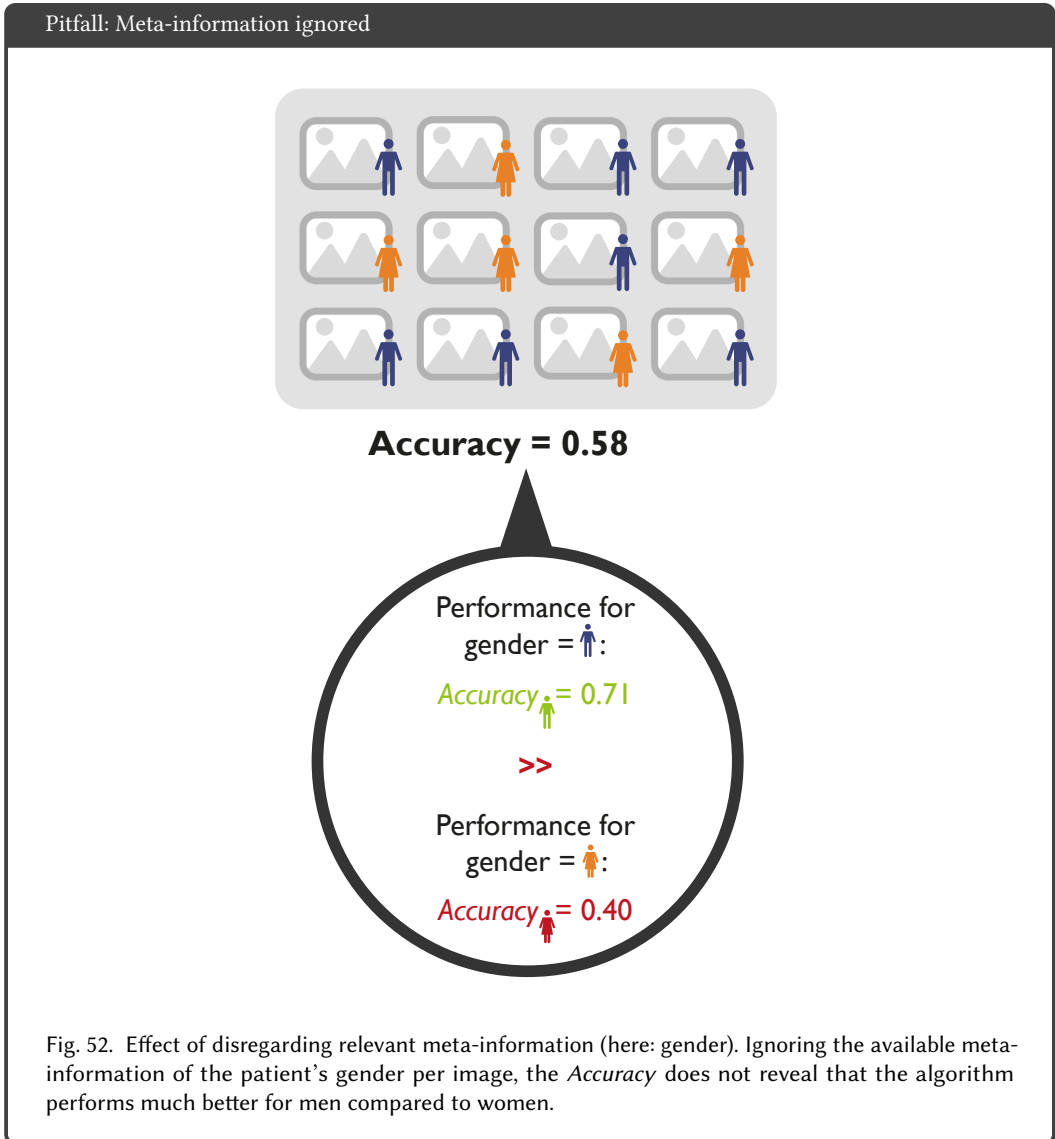


Fig. 50. Effect of unequal handling of classes. (a) Effect of using metrics that are not suitable for penalizing False Negative (FN)/False Positive (FP). The definition of the *Positive Predictive Value* (PPV) metric does not incorporate FN and is therefore not well-suited for penalizing FN, as required in cancer screening tasks, for example. Analogously, the *Sensitivity* is not well-suited for penalizing FP, as required in many retrieval tasks, for example. (b) Simple averaging (macro-averaging) of the *Accuracy* ignores the unequal importance of classes, given by pre-defined weights of classes. Incorrect predictions are indicated by a red square.

Interdependencies between classes. If multiple classes are visible in the data set, one should carefully account for interdependencies between the classes. Interdependencies can happen in cases of multi-colinearities in which two classes are correlated, either inherently, such as for the body mass index (BMI) and the body fat percentage, or in the case of dependent data settings, for example multiple images per patient or the presence of confounders. An algorithm aiming to classify the dark blue triangle class in Fig. 51 may result in a nearly perfect *Accuracy* of 0.94, but only because the dark blue triangle almost always appears in conjunction with the orange square. Computing the *Accuracy* for those images individually without the square class would lead to a much lower performance.

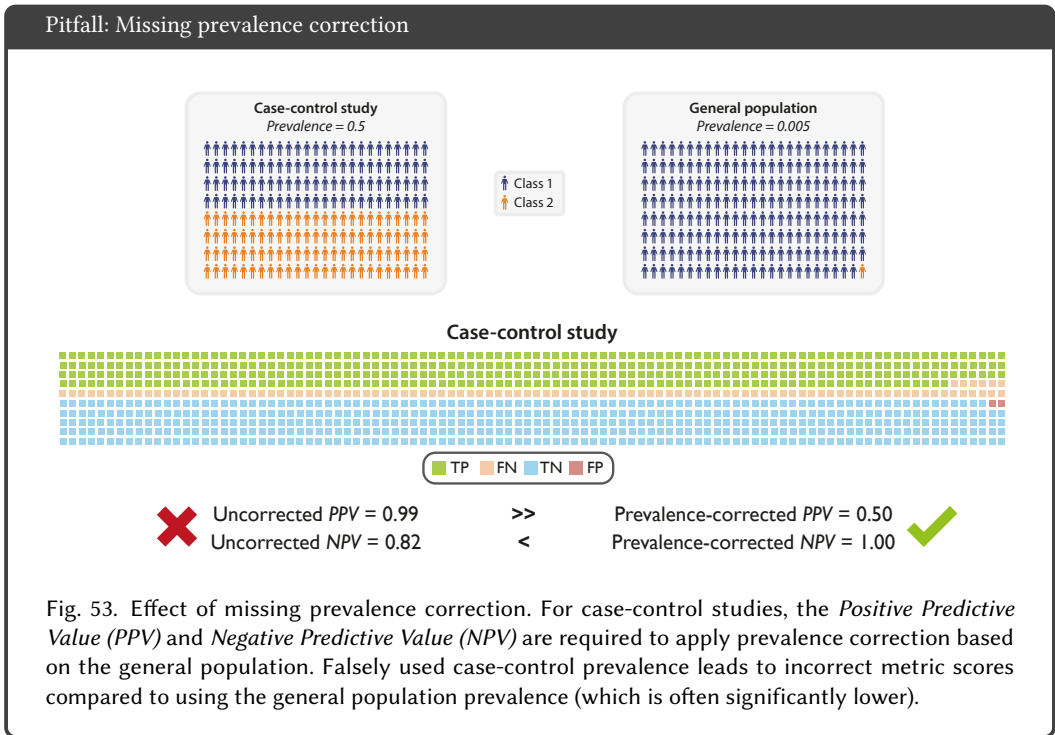


Stratification based on meta-information. Different kinds of meta-information may be available for a data set, including the presence and relevance of artifacts or artificial structures (e.g. metal artifacts in CT images or text overlay in endoscopic data) as well as specifics of acquisition protocols (e.g. acquisition angle or viewpoint) or grid size (cf. Fig. 67). Another typical example is the gender of a patient, as shown in Fig. 52. In this case, the *Accuracy* is computed over twelve cases, disregarding the available meta-information (gender). Stratification based on gender will reveal that the prediction performs much worse for women compared to men. These aspects are currently investigated in the fairness literature [8].



Missing prevalence correction. The *PPV* and the *Negative Predictive Value (NPV)* are common measures to validate classification performances. In many cases, binary classification is considered, for example presence or absence of a disease. In contrast to *Sensitivity* and *Specificity*, in case-control studies, *PPV* and *NPV* should be seen as the conditional probability of a disease being present based on a test result and the prevalence in a general population.

However, *PPV* and *NPV* are frequently used incorrectly. This is due to the fact that many practitioners assume the same prevalence in an analysed case-control study group as in the general population. However, a study group is often heavily biased, either due to the study design or due to the observation of patient groups from specialized clinics. Thus, the assumed disease prevalence in scientific literature is often higher than that found in the general population (cg. Fig. 53). This problem is amplified by default implementations (e.g. in *scipy* [98]) which disregard wider population prevalence and calculate prevalence from the study group. Without prevalence correction, this can lead to misleading results, confusion among patients and ill-informed policy-making.



Discrimination vs. calibration. A model's *discrimination* capability refers to how well it separates samples with and without the class of interest. If all predicted class scores for the samples with the class of interest are higher than for the others, the model discriminates perfectly, reflected in an AUROC score of 1. A *calibrated model* outputs predicted class scores that match the empirical success rate (e.g. outputs with score 0.8 for a specific class, empirically belong to this class in 80% of the cases). [25]. However, it may happen a perfectly discriminating model, such as the one presented in Fig. 54, is not well calibrated. The *Prediction* gives a confidence score of 0.52 for all samples of the positive class (orange circle) and a score of 0.51 for all samples of the negative class (blue triangle). Although this leads to a perfect discrimination, the calibration is very poor and the predicted probabilities would not be helpful in practice at all.

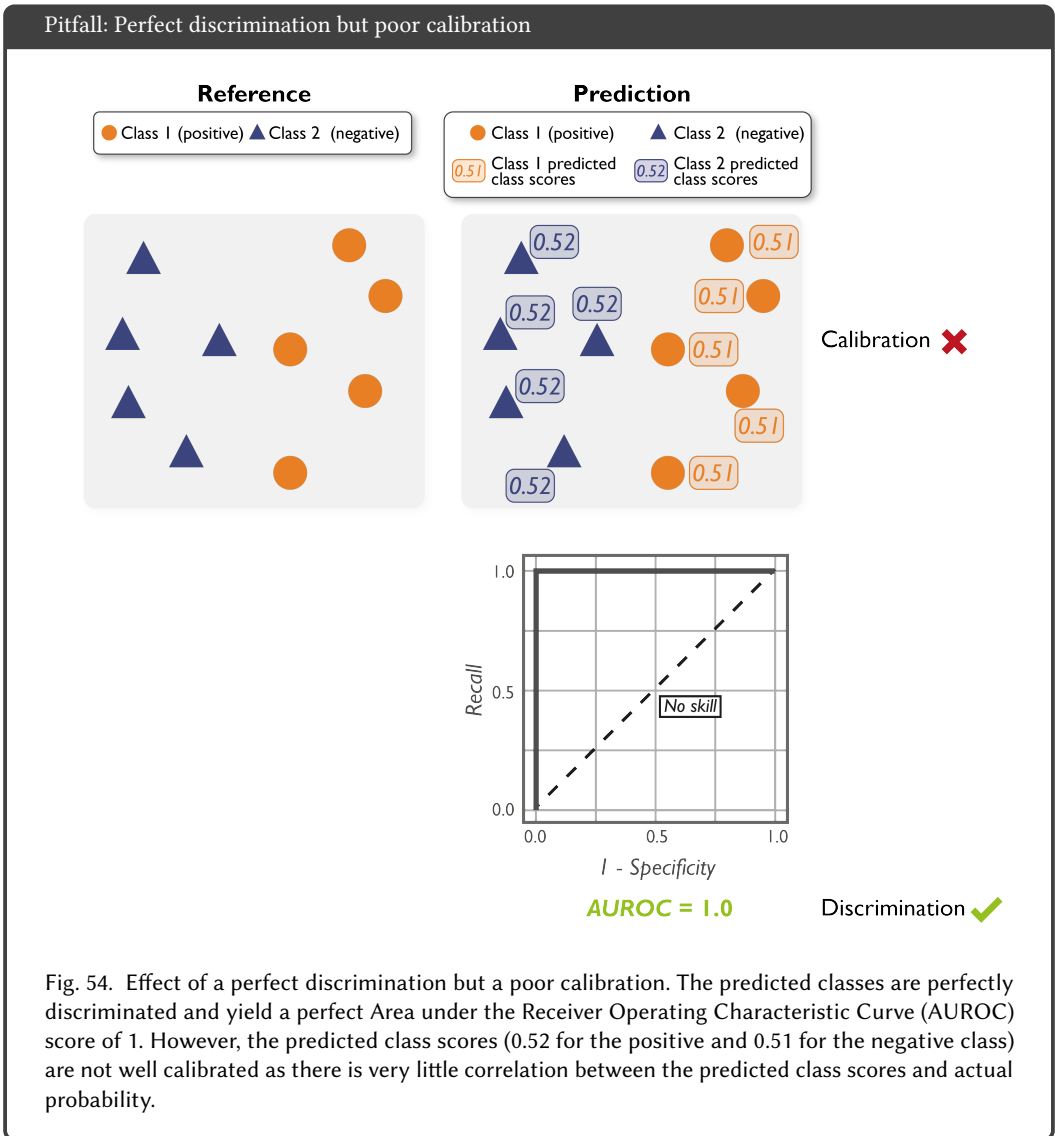


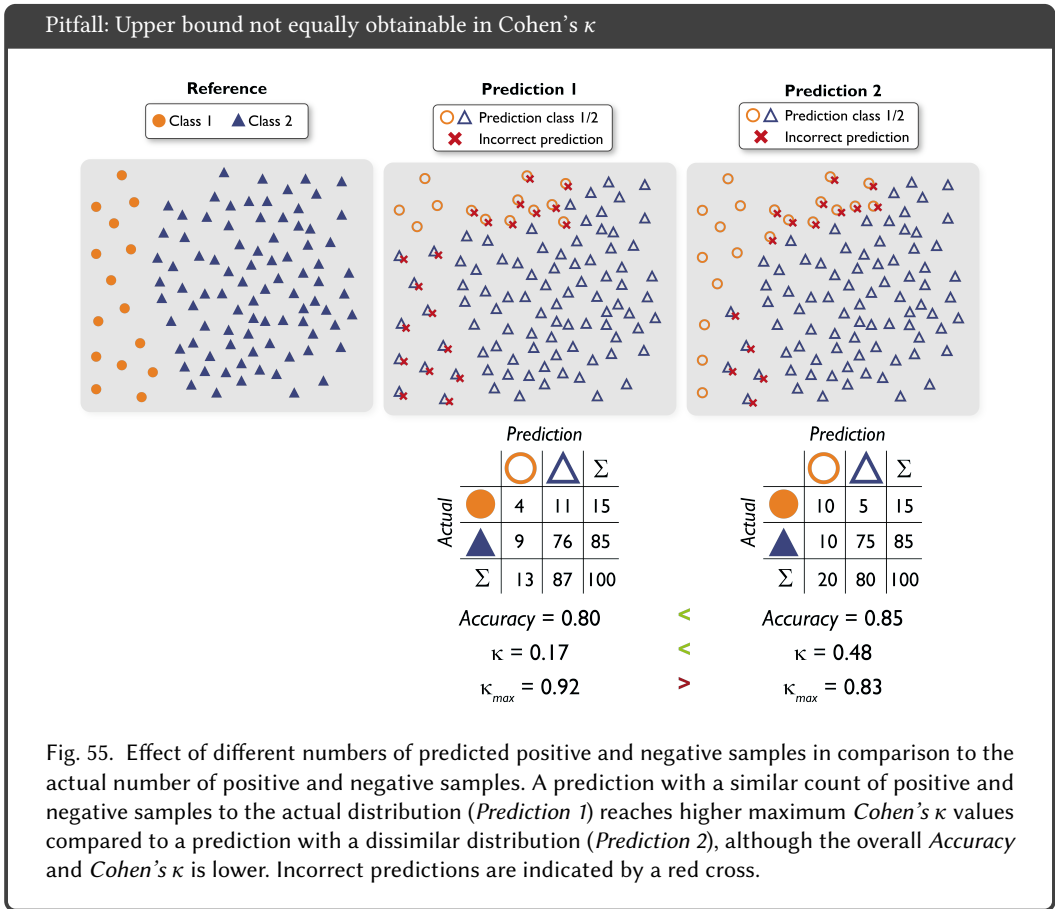
Fig. 54. Effect of a perfect discrimination but a poor calibration. The predicted classes are perfectly discriminated and yield a perfect Area under the Receiver Operating Characteristic Curve (AUROC) score of 1. However, the predicted class scores (0.52 for the positive and 0.51 for the negative class) are not well calibrated as there is very little correlation between the predicted class scores and actual probability.

Upper bound in Cohen's κ calculation. Cohen's κ measures the agreement between ratings while incorporating information on the *Accuracy* by chance. It therefore investigates how well a prediction follows the distribution of the actual class. The maximum *Cohen's κ* helps interpreting the calculated κ score by symbolizing the corner case in which either the FP or FN are equal to 0 [93]:

$$\begin{aligned} \kappa_{max} &= \frac{p_{max} - p_e}{1 - p_e}, \\ p_{max} &= \min \left(\frac{TP + FN}{TP + TN + FP + FN}, \frac{TP + FP}{TP + TN + FP + FN} \right) \\ &\quad + \min \left(\frac{TN + FN}{TP + TN + FP + FN}, \frac{TN + FP}{TP + TN + FP + FN} \right) \end{aligned} \quad (8)$$

The maximum *Cohen's κ* score will be lower as the number of the predicted positive and negative samples diverges more from the actual number of positive and negative samples. This is shown in Fig. 55 with two predictions. *Prediction 1* achieves lower *Accuracy* and *Cohen's κ* scores compared to *Prediction 2*, as it only predicts a very low number of TP. However, the predicted distribution of samples in *Prediction 1* is closer to the actual distribution of samples (13 circle predictions vs. 15 actual circles and 87 triangle predictions vs. 85 actual triangles). The distribution of samples of *Prediction 2* differs more from the actual distribution, yielding a lower *Cohen's κ_{max}* value¹⁰.

¹⁰<https://www.knime.com/blog/cohens-kappa-an-overview>



H.3 Pitfalls related to segmentation.

This section focuses on limitations for semantic segmentation, but some of them are also transferable to other problem categories, such as instance segmentation. Limitations of metrics are typically related to the following properties:

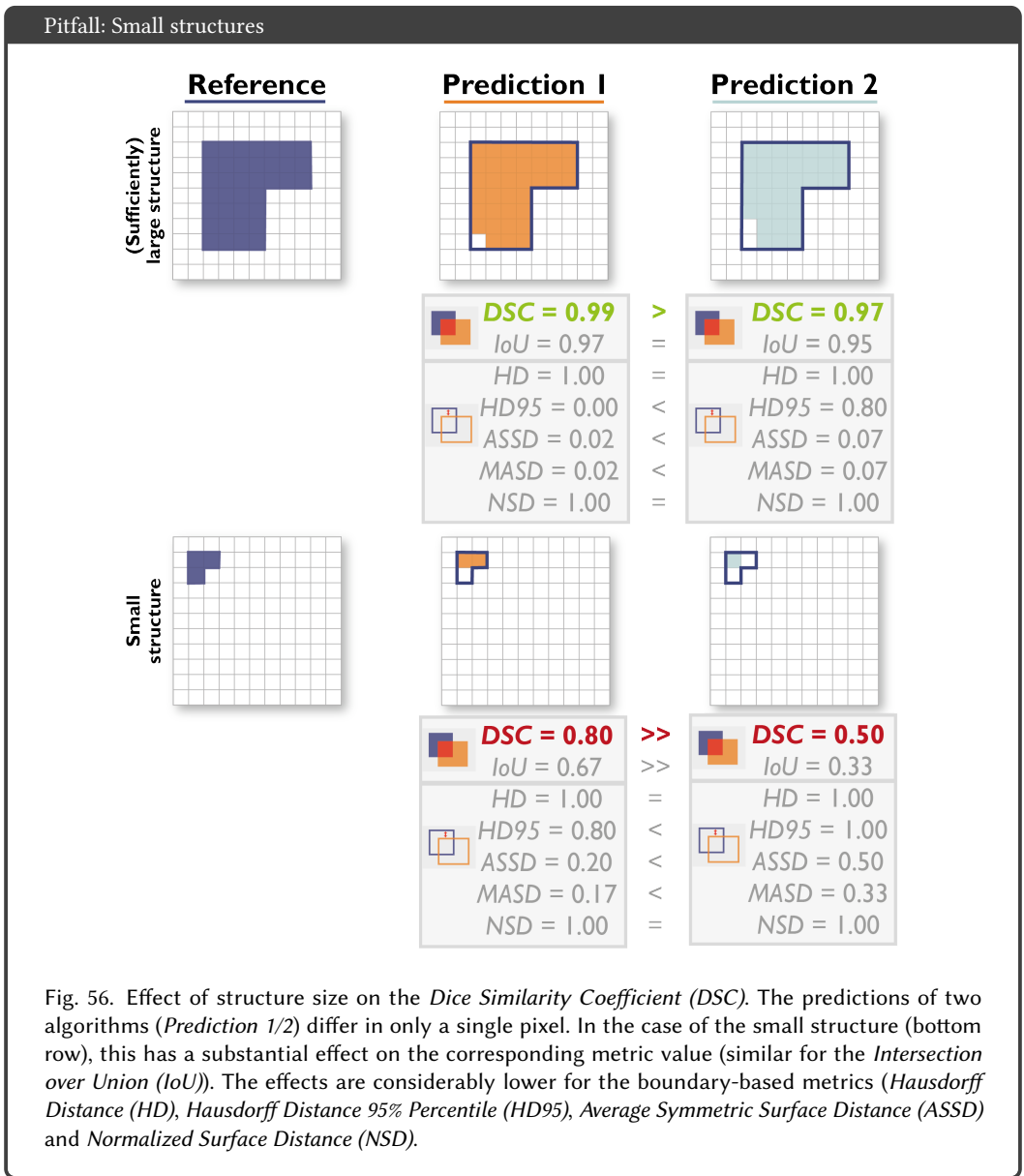
- Small size of structures relative to pixel size (Figs. 56 and 57, F3.1)
- High variability of structure sizes (Fig. 58, F3.2)
- Complex shapes of structures (Fig. 59, F3.3)
- Particular importance of structure volume (Fig. 60, F2.2)
- Particular importance of structure center (Fig. 61, F2.3)
- Particular importance of structure boundaries (Fig. 62, F2.1)
- Possibility of multiple labels per unit (Fig. 63, F3.4)
- High inter-rater variability (Fig. 64, F4.2.1)
- Possibility of spatial outliers in reference annotation (Fig. 65, F2.5.4 and F4.2.2)
- Possibility of reference or prediction without the target structure (Fig. 66, F4.5 and F5.2)
- Preference for over- vs. undersegmentation (Fig. 68, F2.5.2)

Further pitfalls are related to technical peculiarities, such as the choice of global decision threshold for creating the confusion matrix (Fig. 69, F2.6 and F5.1) and the image resolution (Fig. 67).

The limitations are presented for the most commonly used overlap segmentation metrics, namely *DSC*, *IoU*, and the most common boundary-based metrics, namely *HD*, *HD95*, *ASSD*, *MASD* and *NSD*. The *NSD* calculation is based on a user-defined threshold (cf. Fig. 34). Results differ for different thresholds. Unless stated otherwise, we set the threshold to $\tau = 1$.

To preserve clarity of the illustrations, specific values may only be highlighted for one metric from each metric family, if the other metrics share similar properties (e.g. *DSC* and *IoU* share the same properties). Green metric values correspond to a "good" value (e.g. a high *DSC* or a low *HD* score), whereas red values correspond to a "bad" value (e.g. a low *DSC* or a high *HD* score). Green check marks indicate metric scores reflecting the research question, red crosses show those that do not. Please note that a low *DSC* value (or similar) is not automatically a "bad" score. A metric value should always be put into perspective and compared to inter-rater variability. We only use the terms "good" and "bad/poor" for simplicity.

Small size of structures relative to pixel size. Segmentation of small structures, such as brain lesions or cells imaged at low magnification, is essential for many image processing applications. In these cases, the *DSC* or *IoU* may not be appropriate metrics, as illustrated in Fig. 56 (cf. [19]). In fact, a single-pixel difference between two predictions can have a large impact on the metric values. Given that the correct outlines (e.g. of pathologies) are often unknown and taking into account the potentially high inter-observer variability related to generating reference annotations [47], it is typically not desirable for few pixels to influence the metrics as much. This problem is particularly amplified in cases of large variability of structure sizes (cf. Fig. 58). The same problem arises for other versions of the *DSC* or *IoU*. For example, the *clDice* is often used in the case of tubular structures. Similarly to the original *DSC* metric, a single-pixel difference will have a larger influence on the *clDice* for small tube structures compared to larger ones. This pitfall also applies to object detection tasks. It should be noted that once a data set exclusively contains only very tiny structures, one may consider this problem to be an object detection rather than a segmentation problem.



Pitfall: Small tubular structures

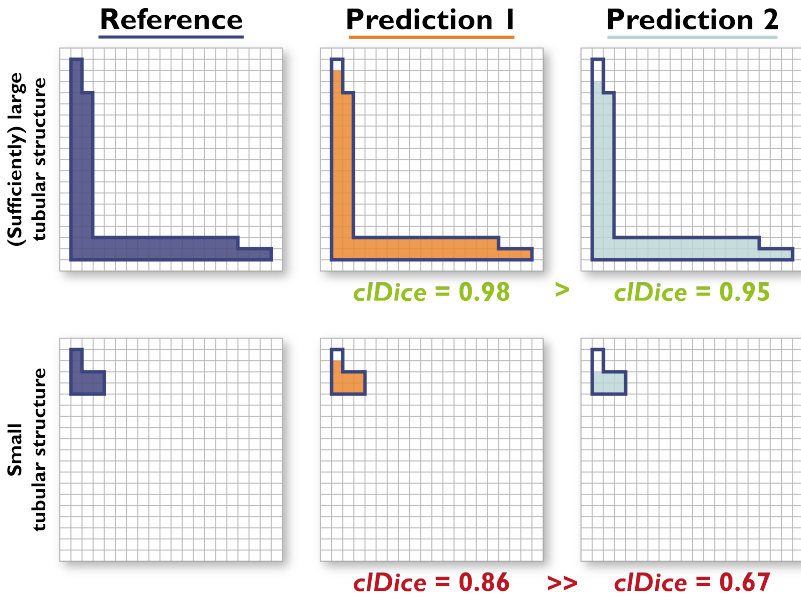
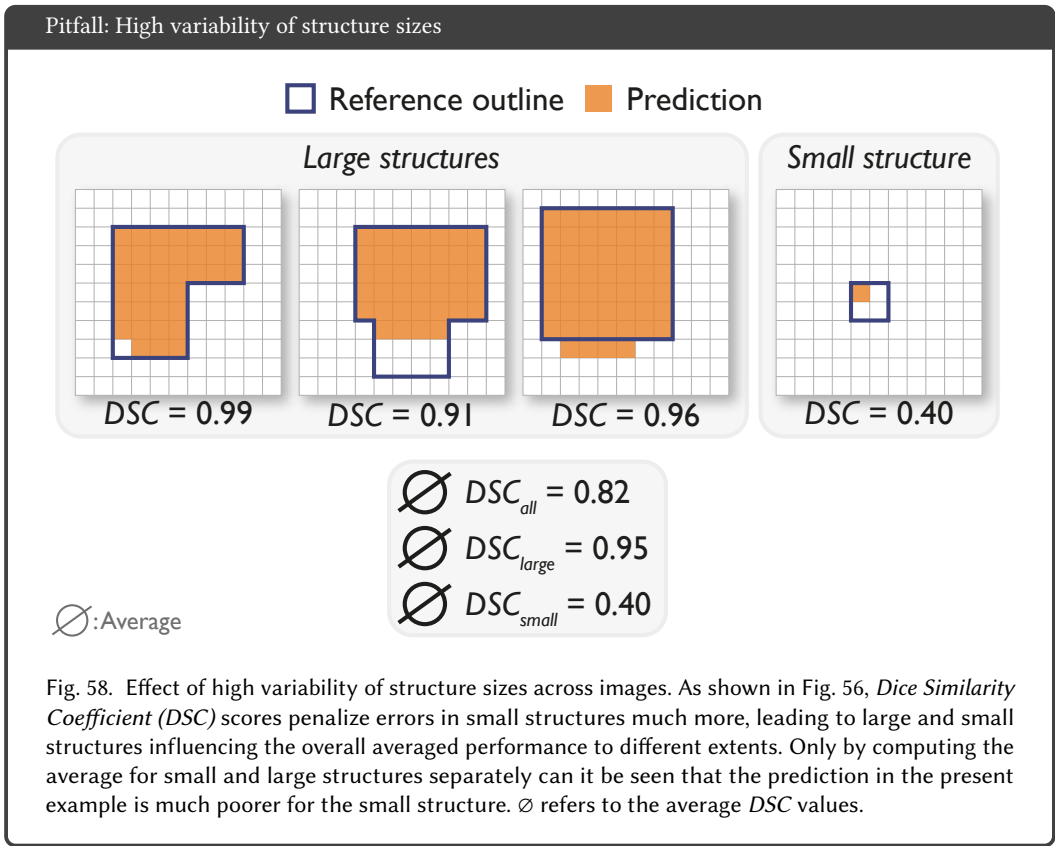


Fig. 57. Effect of structure size on the *Center line Dice Similarity Coefficient* (*cDice*). The predictions of two algorithms (*Prediction 1/2*) differ in only a single pixel. In the case of the small tubular structure (bottom row), this has a substantial effect on the corresponding *cDice* value.

High variability of structure sizes. The size of target structures may vary substantially, both within an image and across images. For example, in medical instrument segmentation in laparoscopic video data, an image frame may contain full-sized instruments as well as only the tip of an instrument just entering the scene [76]. In these cases, metrics need to be chosen carefully. As shown in the example above (Fig. 56), metrics such as the *DSC* or *IoU* are typically not well-suited for very small structures. Furthermore, size stratification – the aggregation of metric values for objects of similar sizes to uncover differences between them – should be employed. Fig. 58 shows an exemplary data set of four images, containing three large structures and one small structure. When aggregating over all *DSC* values, the average *DSC* is 0.82. Computing the average for large and small structures separately, however, shows that the performance is much lower for the small structures compared to the large ones, demonstrating the large influence of the low metric values of small objects. This pitfall also applies to object detection tasks and other metrics.



Complex shapes of structures. Metrics measuring the overlap between objects are not designed to uncover differences in shapes. This is an important problem in many applications such as radiotherapy, for which identifying and treating all parts of the tumor is essential to avoid recurrence [14]. Fig. 59 illustrates that completely different object shapes may lead to the exact same *DSC* and *IoU* values. Boundary-based measures are able to detect the changes in shapes [90]. Note that this pitfall also applies to object detection tasks.

Pitfall: Shape unawareness

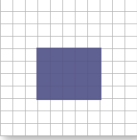
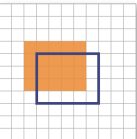
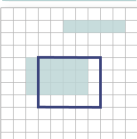
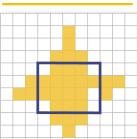
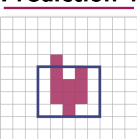
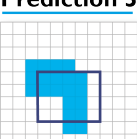
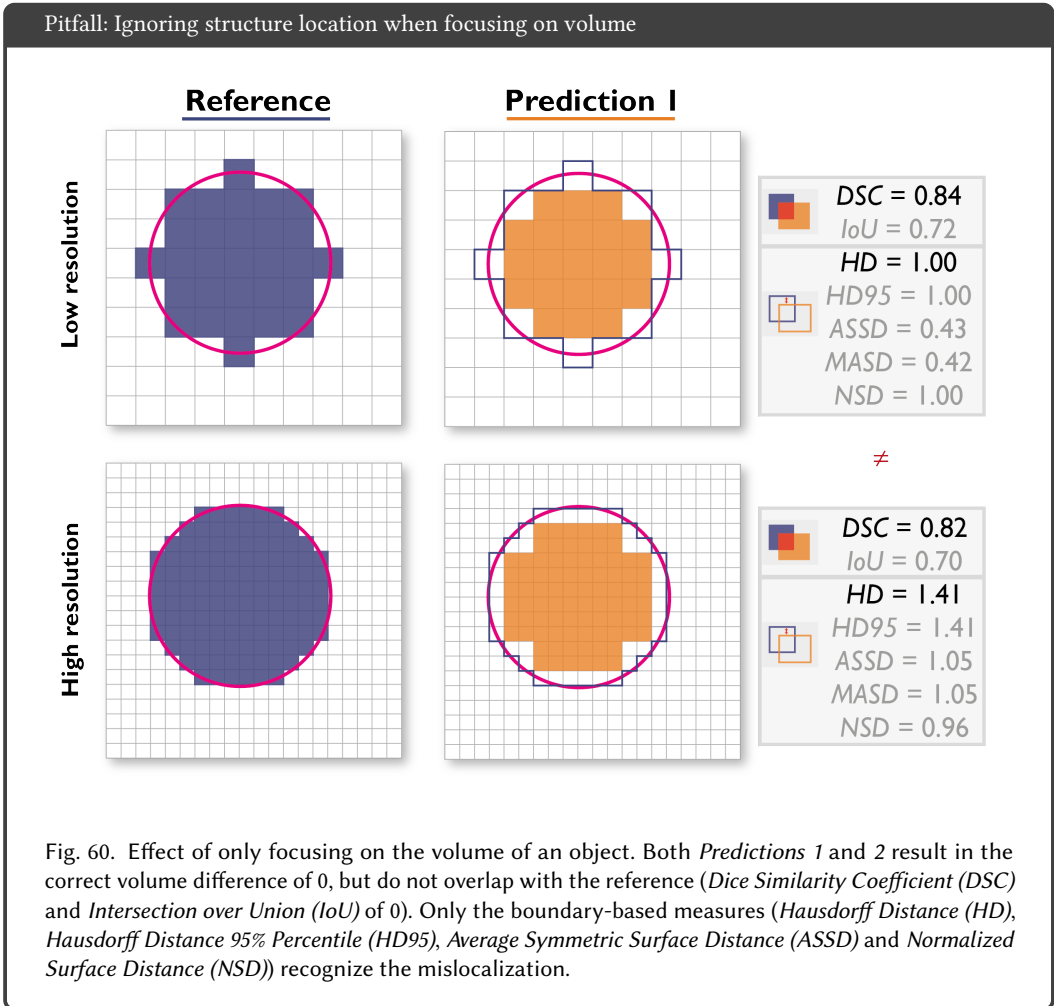
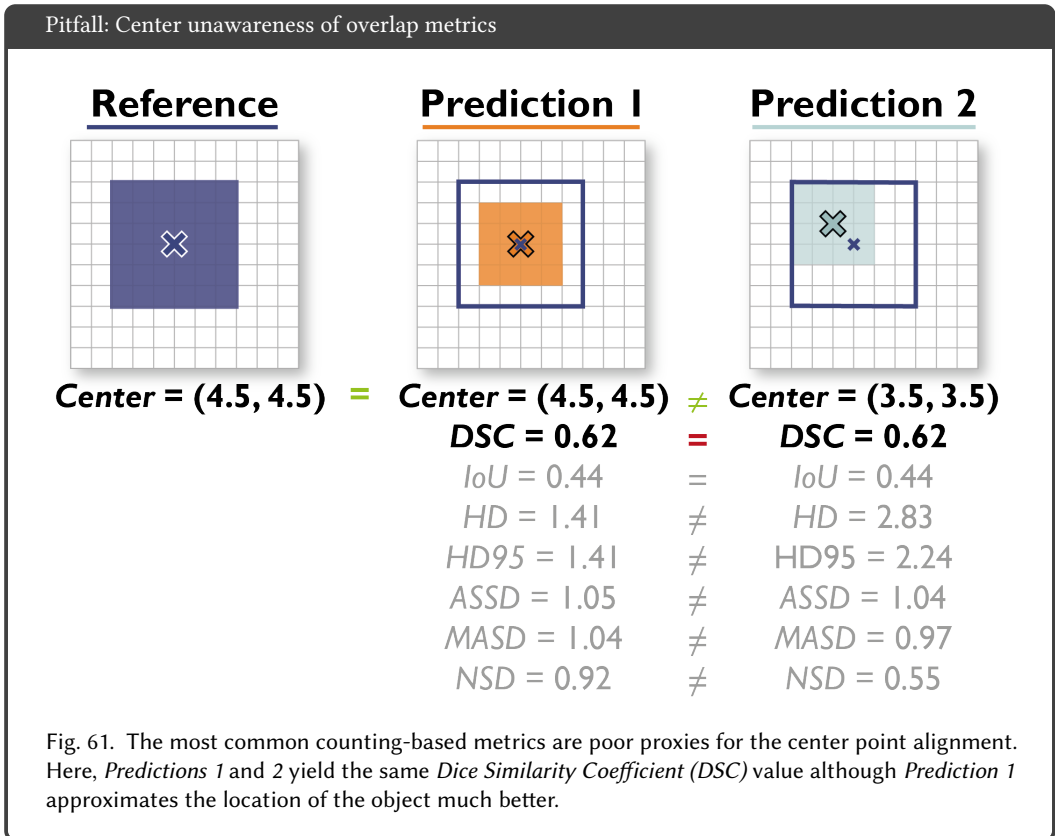
Reference	DSC	IoU	HD	HD95	ASSD	MASD	NSD
							
Prediction 1 	DSC = 0.6	IoU = 0.4	HD = 1.4	HD95 = 1.3	ASSD = 0.9	MASD = 0.9	NSD = 1.0
Prediction 2 	DSC = 0.6	IoU = 0.4	HD = 3.6	HD95 = 3.1	ASSD = 1.0	MASD = 1.0	NSD = 0.7
Prediction 3 	DSC = 0.6	IoU = 0.4	HD = 3.0	HD95 = 2.0	ASSD = 0.8	MASD = 0.7	NSD = 0.8
Prediction 4 	DSC = 0.6	IoU = 0.4	HD = 2.2	HD95 = 2.0	ASSD = 0.8	MASD = 0.7	NSD = 0.8
Prediction 5 	DSC = 0.6	IoU = 0.4	HD = 2.0	HD95 = 1.2	ASSD = 0.8	MASD = 0.8	NSD = 0.9

Fig. 59. Effect of different shapes. The shapes of the predictions of five algorithms (*Predictions 1-5*) differ substantially, but lead to the exact same *Dice Similarity Coefficient (DSC)* and *Intersection over Union (IoU)*, while boundary-based metrics (*Hausdorff Distance (HD)*, *Hausdorff Distance 95% Percentile (HD95)*, *Average Symmetric Surface Distance (ASSD)* and *Normalized Surface Distance (NSD)*) consider the shape differences.

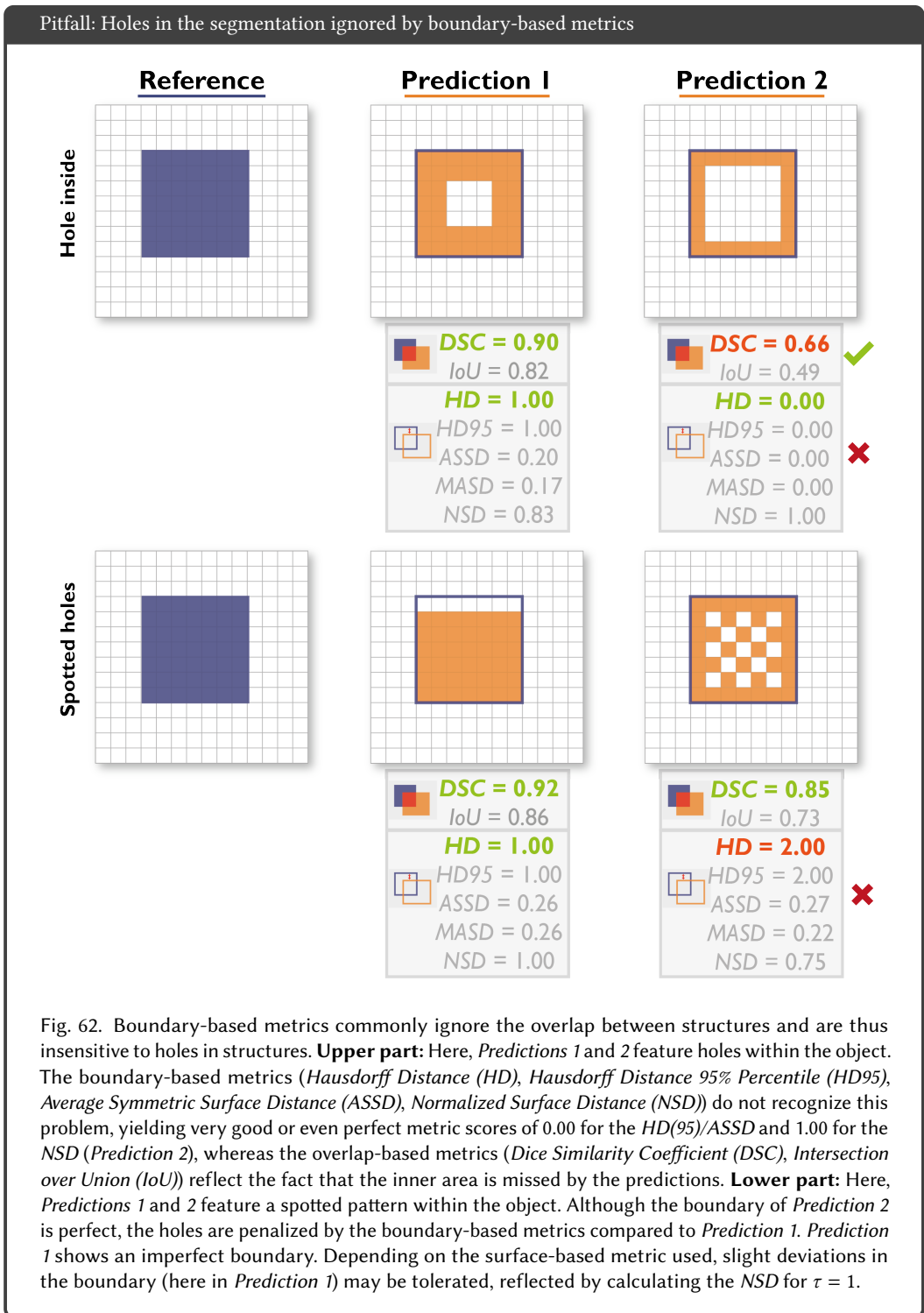
Particular importance of structure volume. Depending on the domain focus, a surgeon, radiologist or similar may be especially interested in the volume of a segmented structure. The most commonly used metrics may, however, result in predictions at entirely wrong locations if boundary or overlap are not considered. Fig. 60 shows two predictions of a 3x3 square structure, both of them being at the wrong position. While the volume difference is correct for both predictions, the overlap is zero. Only boundary-based metrics will indicate the magnitude of mislocalization of the predicted objects.



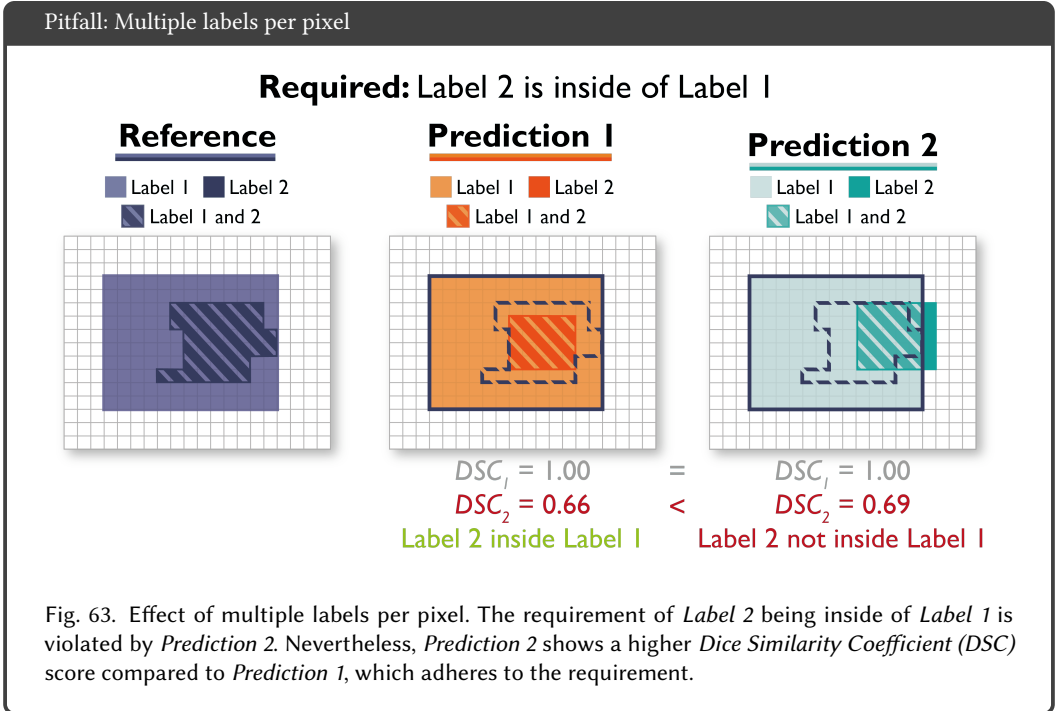
Particular importance of structure center. The structure center point or center line may be more important than an accurate boundary or overlap of the structure, as for example in nerve segmentation [63]. In these cases, the accuracy of the center point or line should be examined via an additional metric to make sure the center is correct for the prediction. Fig. 61 shows two predictions yielding the same *DSC* values, as they have the same overlap to the reference annotation. However, only *Prediction 1* is centered around the same point as the reference, while *Prediction 2* is shifted slightly towards the upper left corner and thus centered incorrectly. This pitfall also applies to object detection tasks. It should be noted that once the center location is of particular importance to the task, one may consider it an object detection rather than a segmentation problem.



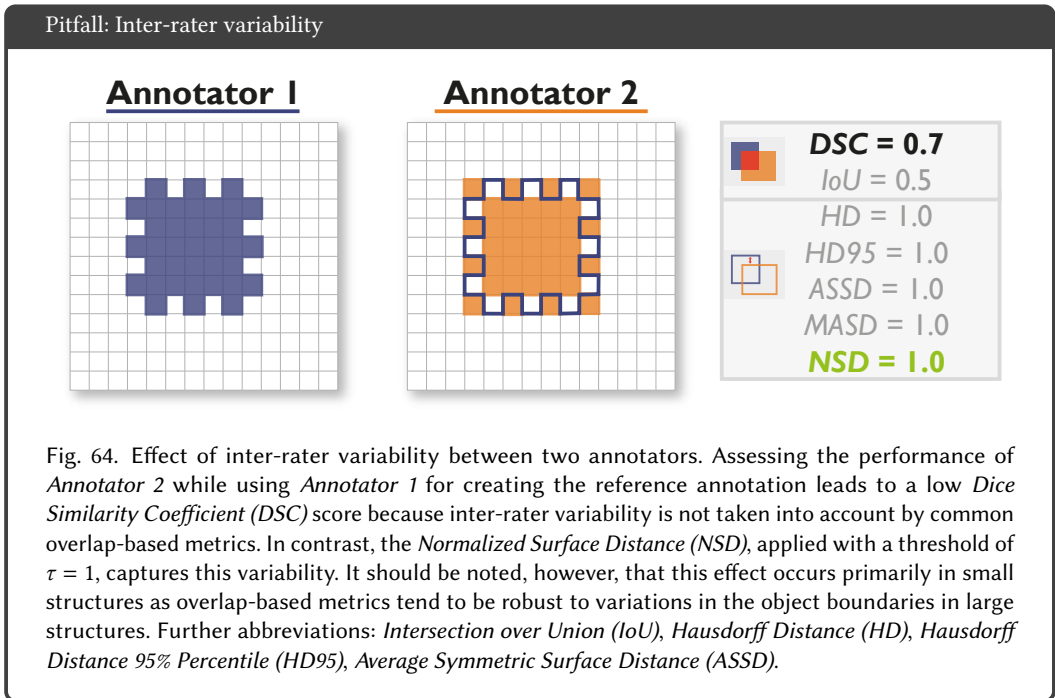
Particular importance of structure boundaries. While boundary-based metrics such as the $HD(95)$, $ASSD$ and others can help to detect shape differences between the reference and the predicted object, they do not focus on the object itself. As shown in Fig. 62(top), the boundary-based metrics do not recognize a prediction with a large hole inside as poor (*Prediction 2*). Furthermore, in Fig. 62(bottom) [90], those metrics do not punish the spotted pattern within the object. It should be noted that this behaviour may also be desirable. For example, it may be highly difficult to decide whether a necrotic core (hole) is present in a tumor or not. A boundary-based metric would not punish errors resulting from such annotation uncertainties.



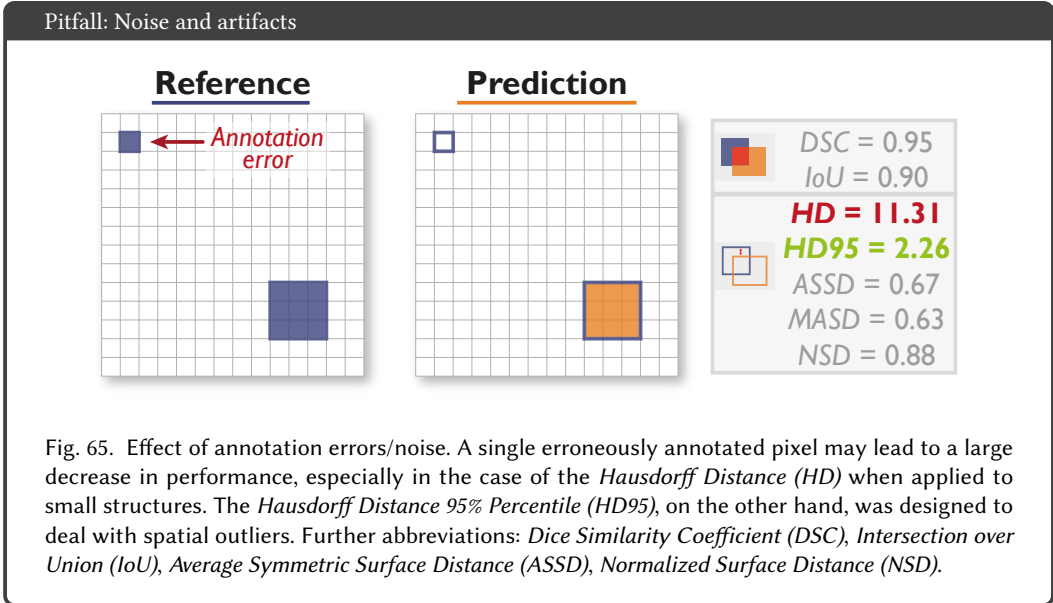
Possibility of multiple labels per unit. In several biomedical imaging scenarios, multiple labels per pixel may be possible. A prominent example would be the tumor core inside the tumor [62]. Often, however, prior knowledge related to such scenarios (e.g. a tumor core cannot lie outside the tumor) is not reflected by common metrics, which simply calculate the agreement of the reference and prediction per class. Fig. 63 shows two predictions for a multi-label example. The *DSC* value of *Label 2*, which is required to be inside of *Label 1*, is higher for *Prediction 2* although *Label 2* is also found outside the *Label 1* area. For simplicity, we only show the results for the *DSC* metric. This pitfall also applies to object detection tasks.



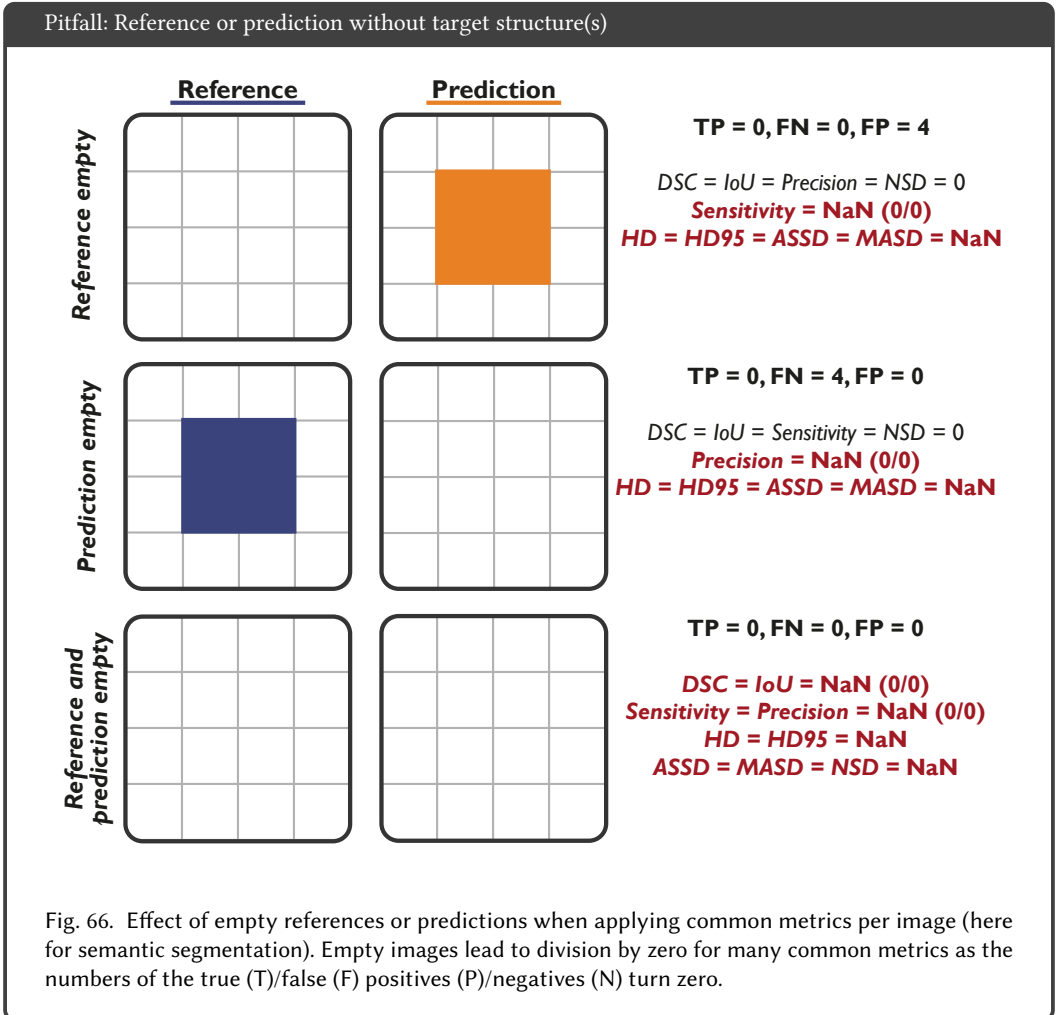
Noisy reference standard. A high quality reference annotation is crucial to determine the performance of a supervised learning algorithm. A prediction can be almost perfect, but low quality reference images will still result in a bad metric score. Especially in the medical domain, the inter-rater variability is often very high as domain knowledge is required and experts themselves often disagree [47]. Fig. 64 shows two masks from different annotators approximating the same structure. Although the annotations differ only slightly at the boundary, the *DSC* score is 0.7. With such inter-rater variability, a *DSC* score of 1 would not be achievable in practice. To address this issue, the *NSD* metric can be applied as an alternative or additional metric, as it is designed to allow a certain tolerance of outline pixels based on the threshold τ . This pitfall can also be translated to object detection and image-level classification tasks.



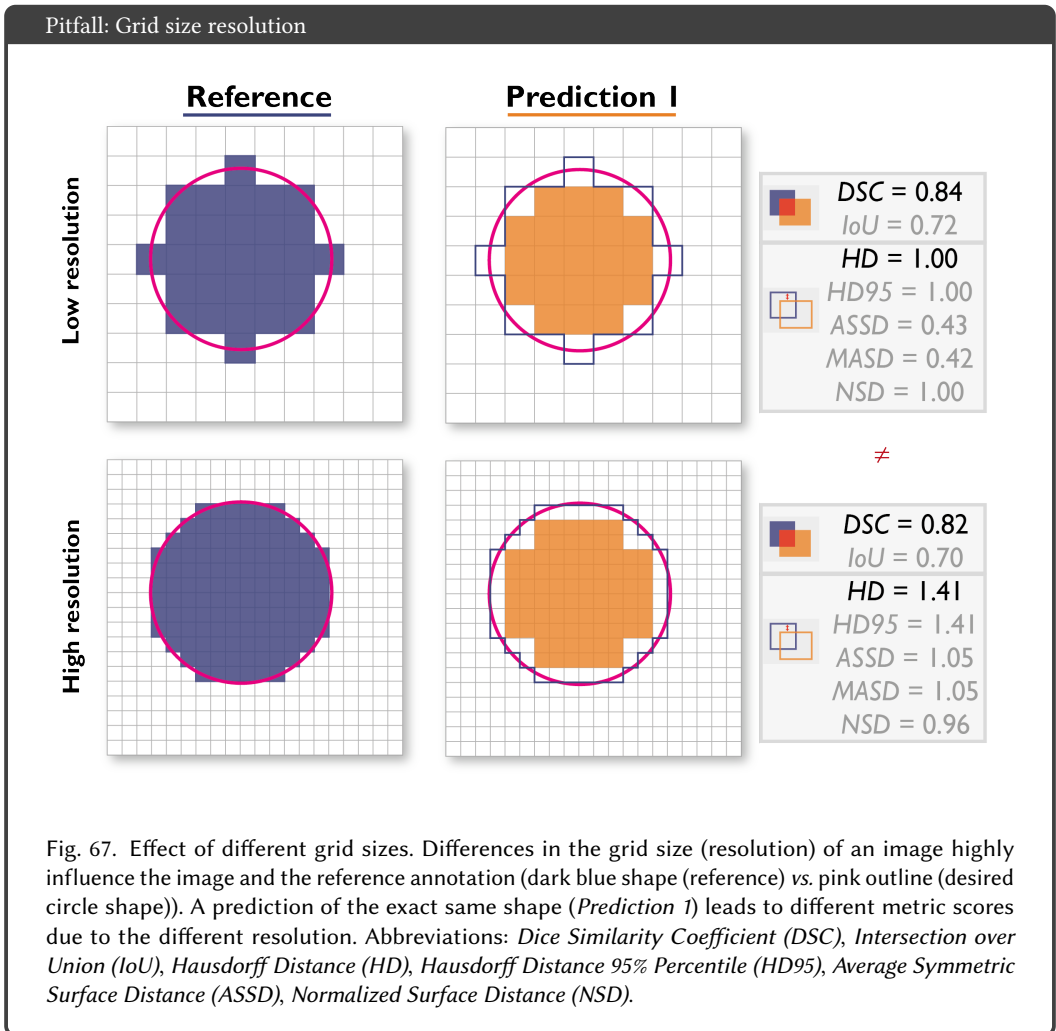
Possibility of outliers in reference annotation. The presence of spatial outliers, such as noise or reference annotation artifacts, may severely impact performance metric values. Fig. 65 demonstrates how a single erroneous pixel in the reference annotation (or the prediction) leads to a substantial decrease in the measured performance, especially in the case of the *HD*. Using the 95% percentile instead of the maximum (*HD95*) to compute the distance significantly improves the metric score as it can handle outliers. Please note that the presented example may also be seen vice versa, with a prediction including single pixel errors. It should further be noted that whether or not outliers should be considered depends on the respective research question.



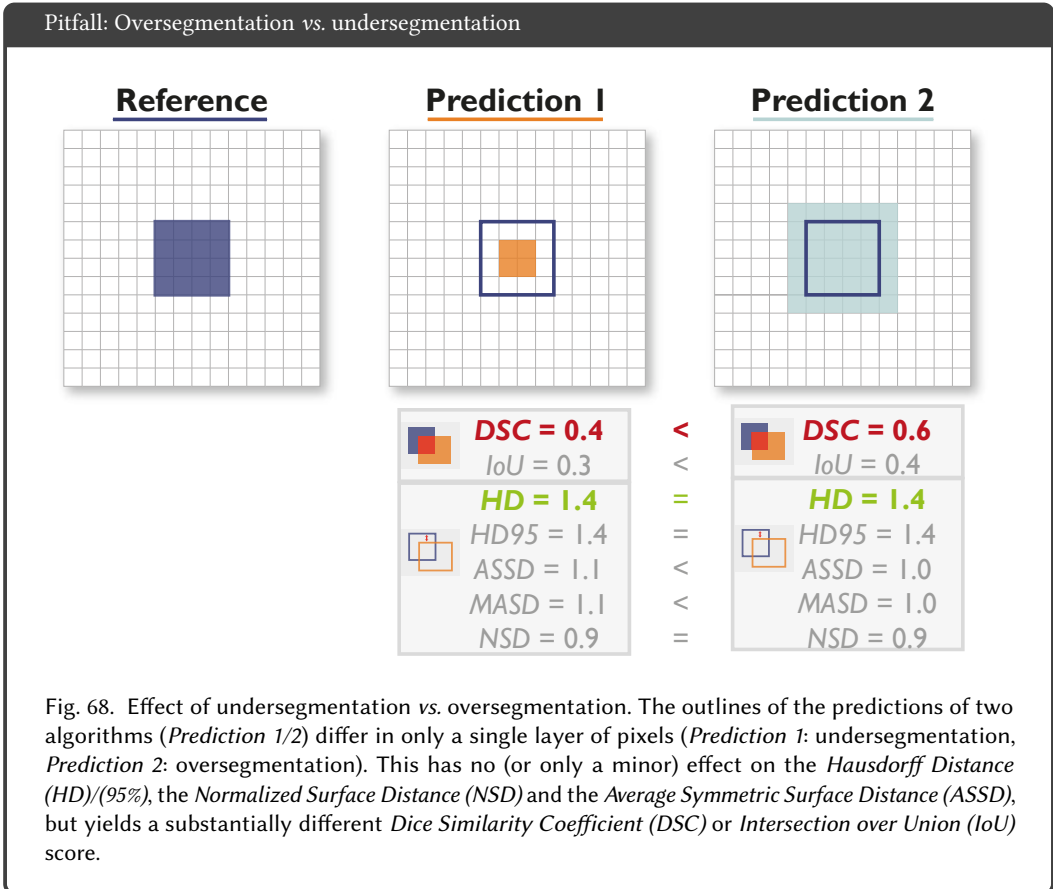
Possibility of reference/prediction without target structure(s). A given data set may contain reference annotations without the target structure(s). For example, the data set may consist of healthy and sick patients. A healthy patient will not have a tumor in the image, yielding an empty reference if the tumor is the targeted structure. An algorithm should be careful not to classify a healthy patient as tumourous as this may lead to unnecessary medical interventions. Similarly, a patient with a tumor should not be classified as healthy (empty prediction). These cases require special care to be taken in the validation, because some metrics may be undefined due to division by zero errors or similar. It is necessary to either choose appropriate metrics that consider empty references (or predictions) or account for it in the metric implementation. For example, boundary-based metrics such as the *HD(95)* and *ASSD* will be NaN if one of the structures is empty. Fig. 66 shows three examples, for which several counting- and boundary-based metrics were computed. The top row depicts the case of an empty reference and a prediction of an object. Given the number of TP and FN being 0, this will result in a division by zero in the *Sensitivity* calculation, yielding a NaN score. A similar case is given in the second row, showing an empty prediction for a given target structure in the reference annotation, yielding an undefined *Precision*. When both reference and prediction are empty (bottom row), all scores will be undefined. Please note that this example is shown for a validation per image, as done for segmentation tasks. For classification and object detection tasks, the validation is typically performed over the whole data set, which would possibly preclude this problem. The presented pitfall also applies to object detection tasks.



Technical peculiarities. Several technical peculiarities also have an impact on metric behaviour. For example, the image resolution and pixel sizes highly influence the reference annotation and the predicted shapes in image processing tasks. Fig. 67 illustrates how the reference annotation differs between a low resolution image (top) and a high resolution image (bottom) compared to a circle. The latter is more exact. A prediction of the same size will therefore lead to different corresponding metric values, independent of the type of the metric. This pitfall also applies to object detection tasks.



In some applications such as radiotherapy, it may be highly relevant whether an algorithm tends to over- or undersegment the target structure. The *DSC* metric, however, does not represent over- and undersegmentation equally [101]. As depicted in Fig. 68, a difference of a single layer of pixels in the outline yields different *DSC* scores (oversegmentation preferred) [90]. Other boundary-based performance values such as the *HD* are invariant to these properties.



Another technical peculiarity is the choice of global decision threshold. Most methods in modern image analysis output continuous class scores. While it is quite common to provide those scores in image-level classification and object detection tasks, segmentation architectures often do not output class probabilities per pixel. However, fuzzy segmentation masks are getting more and more common (for instance, see [1, 48, 67]) and the choice of a global decision threshold τ is very important for the algorithm's result. Fig. 69 (cf. [66]) shows the predicted class probabilities for a reference annotation. For a binarization typically required for segmentation outputs, a threshold needs to be defined based on which a pixel is assigned to a class (here: a pixel with class probability $< \tau$ corresponds to the background class, otherwise to the foreground class). The resulting segmentation masks are shown for the thresholds 0.2, 0.5 and 0.8. It can be seen that the respective masks completely differ across the thresholds. Consequently, metric values will also vastly change.

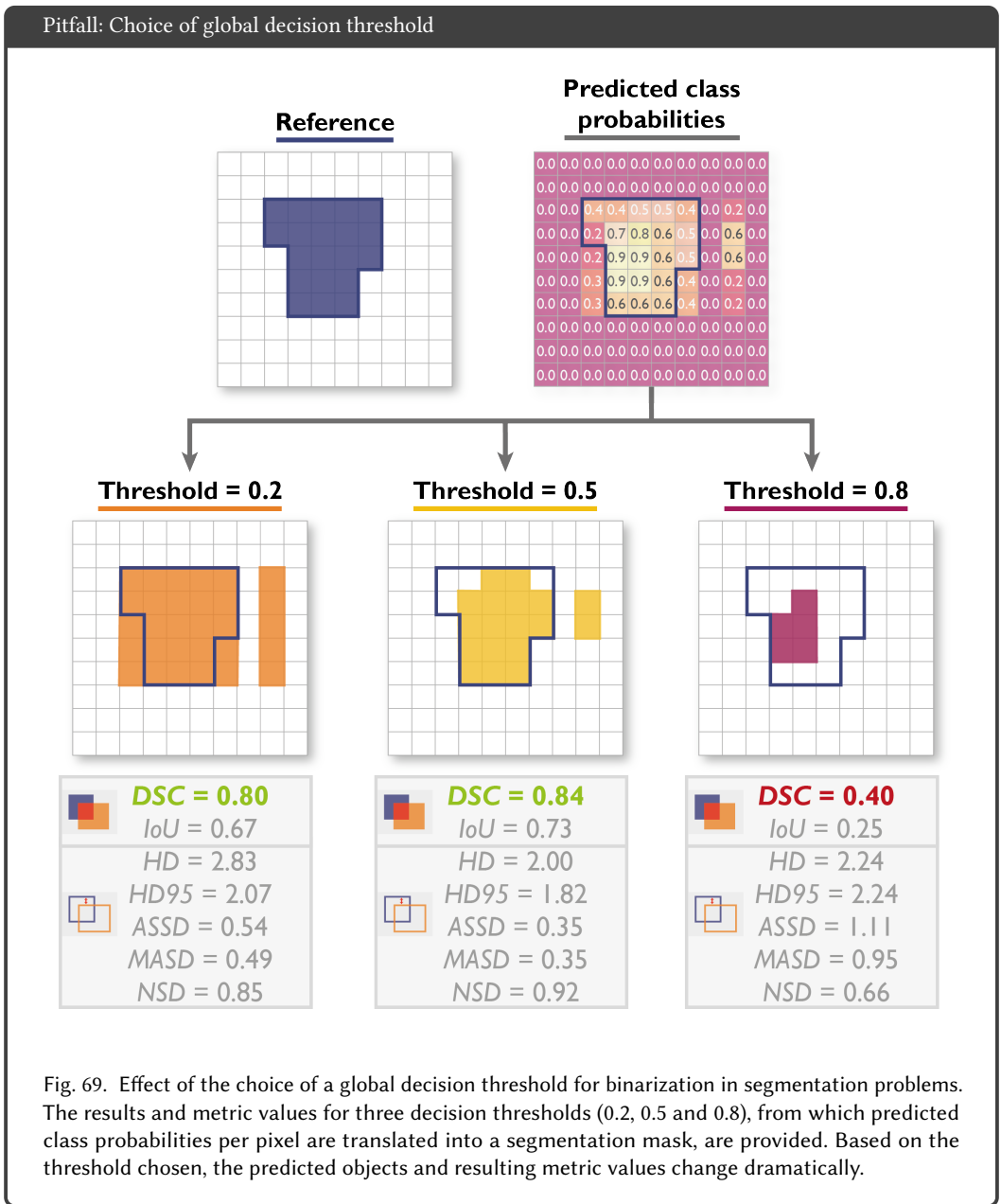
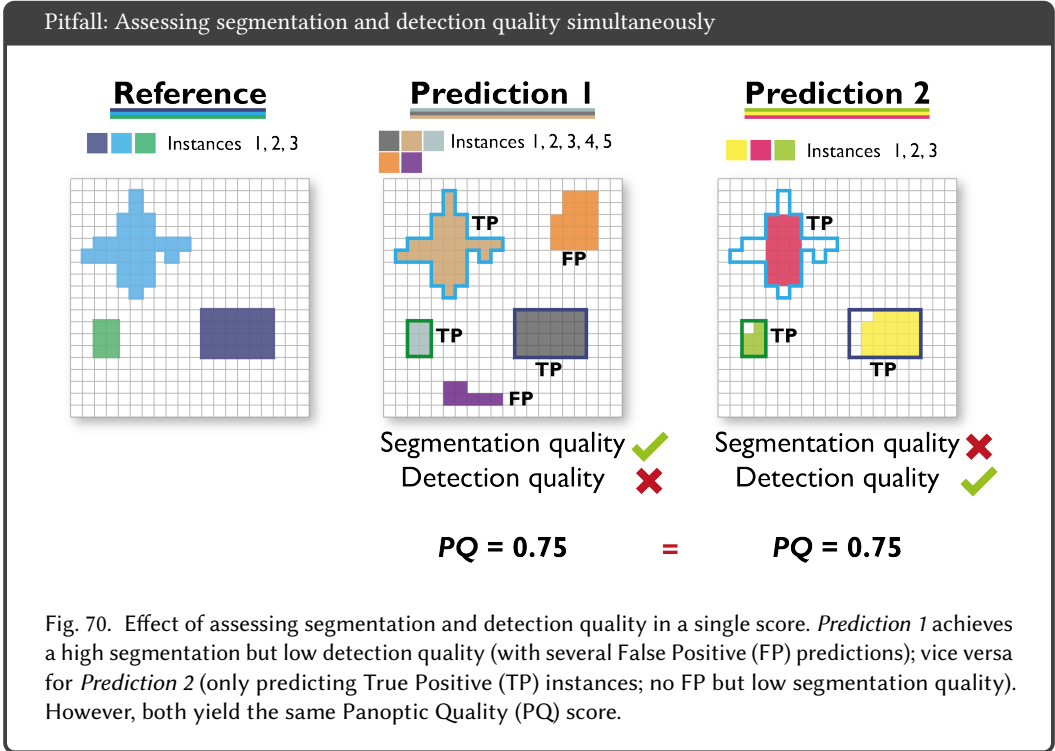


Fig. 69. Effect of the choice of a global decision threshold for binarization in segmentation problems. The results and metric values for three decision thresholds (0.2, 0.5 and 0.8), from which predicted class probabilities per pixel are translated into a segmentation mask, are provided. Based on the threshold chosen, the predicted objects and resulting metric values change dramatically.

When it comes to instance segmentation, the PQ is an attractive metric as it covers segmentation and detection quality in a single score. However, this can be misleading, as shown in Fig. 70. *Prediction 1* with a perfect segmentation and poor detection achieves a PQ score similar to that of *Prediction 2*, which detects all objects correctly (without any FP or FN), but only provides moderate segmentation results. If segmentation and detection quality should be assessed individually, two separate metrics - one for segmentation quality and one for detection quality - should be preferred.



H.4 Pitfalls related to object detection.

This section presents pitfalls relevant for object detection and instance segmentation. Note that these pitfalls equally apply to instance segmentation problems. While most issues related to the actual metric selection have already been mentioned in the previous paragraphs, this section is primarily dedicated to technical peculiarities related to the localization and assignment criteria. These include:

- Mathematical implications of center-based localization criteria (Fig. 71)
- Mathematical implications of *IoU*-based localization criteria (Fig. 72)
- Penalization of one prediction assigned to multiple reference objects requested (Fig. 73, F2.5.7)
- Effect of the provided annotations (Fig. 74, F2.4 F3.3.2 and F4.3)
- Effect of small structures on localization criterion (Fig. 75, F3.1)
- Perfect *Boundary IoU* for imperfect prediction (Fig. 76)
- Possibility of reference or prediction without the target structure and NaN handling (Fig. 77, F4.5 and 5.2)
- *Average Precision vs. Free-response ROC* score (Fig. 78)
- Effect of predicted class probabilities on multi-threshold metrics (Figs. 79, 80 and 81, F5.1)

Mathematical implications of center-based localization criteria. Before calculating metrics for object detection tasks, it is necessary to define what qualifies a detection as a *hit* (TP) or *miss* (FP). There are multiple ways to define a hit, all of which come with their specific limitations. Below, the most commonly used center-based localization criteria are presented¹¹.

- For the **center-cover criterion**, the reference object is considered a hit if the center of the reference object is inside the predicted detection. Fig. 71a shows how this criterion can be fooled by a model outputting very large boxes to maximize the chance of a correct detection.
- In the case of the **distance-based hit criterion**, a prediction is considered a hit if the distance d between the center of the reference and the detected object is smaller than a certain threshold τ . In Fig. 71b, both predictions have the same distance to their corresponding reference object centers. However, the prediction on the top right shows no overlap with the reference and should therefore not be counted as a hit.
- The **center-hit criterion** holds true if the center of the predicted object is inside the reference bounding box or contour. Given this definition, large reference objects are more likely to be hit, as shown in Fig. 71c. The left prediction is defined as a missed object (FP), the right detection as a hit because of its larger size.

¹¹For more details, please refer to the blogpost "Evaluation curves for object detection algorithms in medical images": <https://medium.com/lunit/evaluation-curves-for-object-detection-algorithms-in-medical-images-4b083fddce6e>.

Pitfall: Mathematical implications of center-based localization criteria

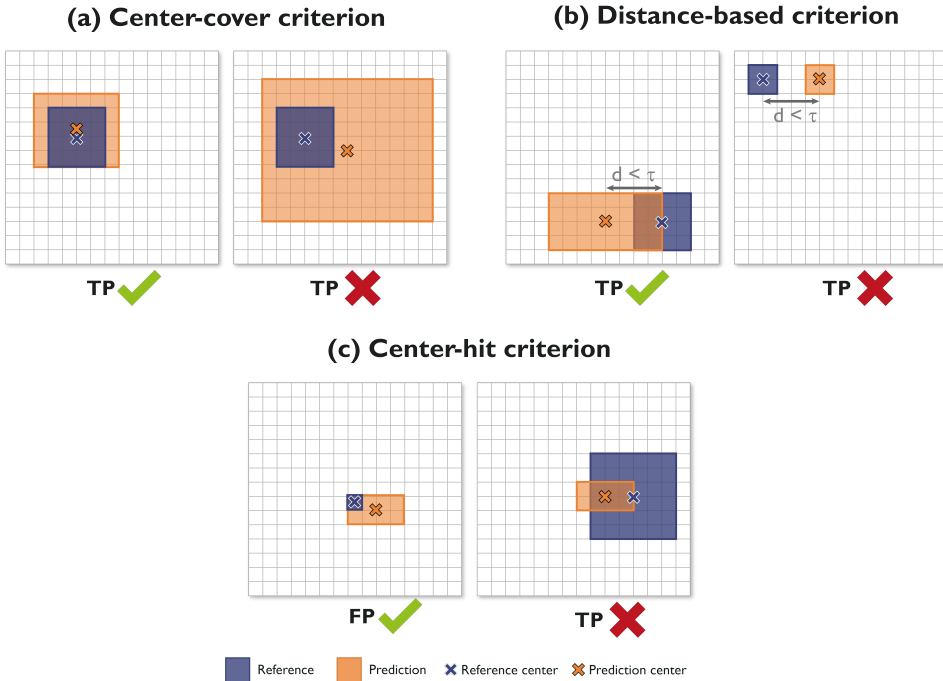


Fig. 71. Pitfalls for several center-based hit criteria in object detection. Reference objects are shown in dark blue, predictions in orange. The object centers are shown as blue/orange crosses. **(a)** The **center-cover criterion**, which requires the center of the reference to be inside the detection, can be fooled easily by predicting a very large bounding box/object. **(b)** Both predictions have the same distance to their corresponding reference center. The **distance-based criterion**, which requires the distance between center points not be exceeded, does not take into account the overlap between objects. However, the right prediction does not overlap with the reference and should, thus, not be considered a True Positive (TP). **(c)** The **center-hit criterion**, which requires the center of the prediction to be located inside the reference, favors large reference objects, as they are easier to detect. The left prediction is considered a False Positive (FP), as the reference center was not hit. The right prediction is considered a TP because of the larger size of the object.

Mathematical implications of IoU-based localization criteria. The most commonly used hit criterion is determined by computing the *IoU* between the predicted and the reference mask/bounding box/boundary. Pitfalls related to *IoU*-based criteria are mainly related to the setting of the threshold (Fig. 72). Many biomedical applications involve 3D rather than 2D images. When working with a higher dimension, it should be kept in mind that metrics may be affected. The additional dimension will lead to overlap errors being punished even more. Fig. 72a shows a comparison of the *IoU* for two rectangles (or bounding boxes) in 2D and 3D. Being mistaken by one voxel in the *z*-dimension will lead to a much lower *IoU* score in 3D compared to the 2D case.

As *IoU*-based criteria take the overlap between regions into account, it is only possible to cheat with very large boxes if the *IoU* threshold is set to a very small value (here: 0), as shown in Fig. 72b. However, special care should be taken when applying the *Box IoU* in the presence of highly concave or elongated structures, as illustrated in Fig. 72c. This is because bounding boxes may quickly grow for narrow and diagonally placed objects, such as medical instruments, and result in FP although visual inspection would indicate a correct prediction.

Pitfall: Mathematical implications of *IoU*-based localization criteria

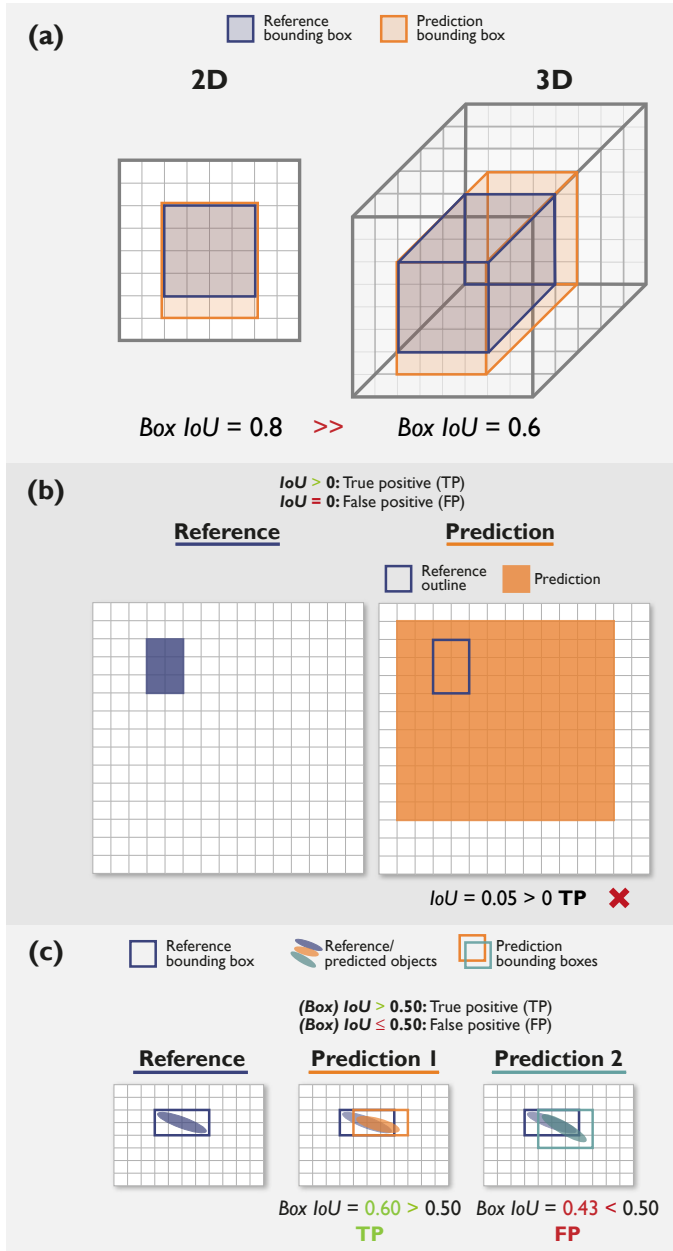


Fig. 72. The *Intersection over Union (IoU)* is a commonly used localization criterion in object detection. It comes with several limitations: **(a)** The image dimension should be considered when setting the *IoU* (here: *Box IoU*) threshold for object detection. In 3D settings, the additional z-dimension results in a cubical increase in erroneous pixels. **(b)** Effect of a loose *IoU* criterion for object detection. When defining a True Positive (TP) by an $IoU > 0$, the resulting localizations may be fooled by very large predictions. **(c)** Effect of defining TP based on the *IoU* (here: *Box IoU*) threshold of the reference and predicted bounding boxes. Especially for diagonal, narrow objects, the number of bounding box pixels may change quadratically. Although *Predictions 1* and *2* are very similar, their bounding boxes diverge and lead to one of them being defined as TP, the other as False Positive (FP).

Penalization of one prediction assigned to multiple reference objects requested. Object detection and instance segmentation algorithms typically involve the step of assigning predicted objects to reference objects. This may result in one prediction being assigned to multiple reference objects or vice versa. Using the $IoU > 0.5$ (or similar threshold) as assignment strategy may end up in a very strict penalty of two FN and one FP if the IoU for both reference objects is smaller than the threshold (as shown for two reference objects in Fig. 73). Using the IoR may result in a less strict penalization for what could be interpreted as only a single error with an additional step of penalizing the non-split errors (either directly in object detection or indirectly in instance segmentation).

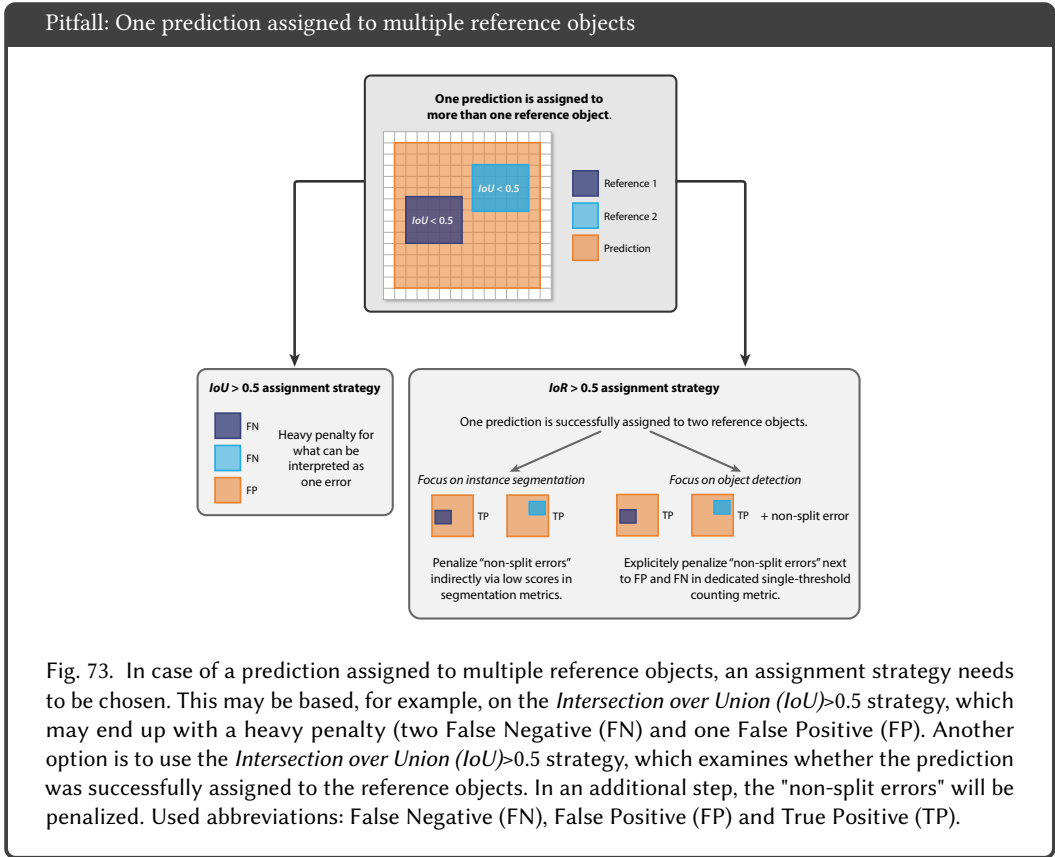
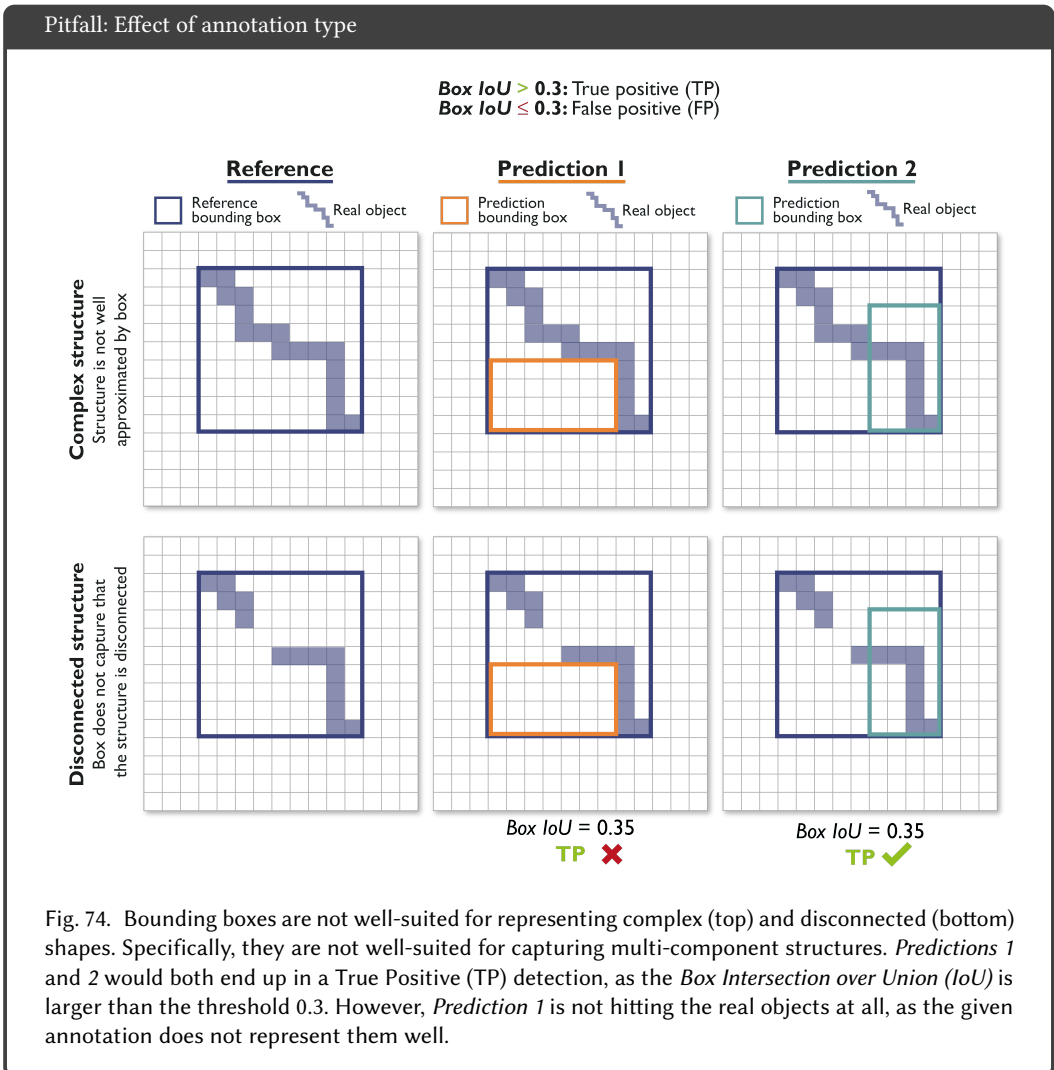


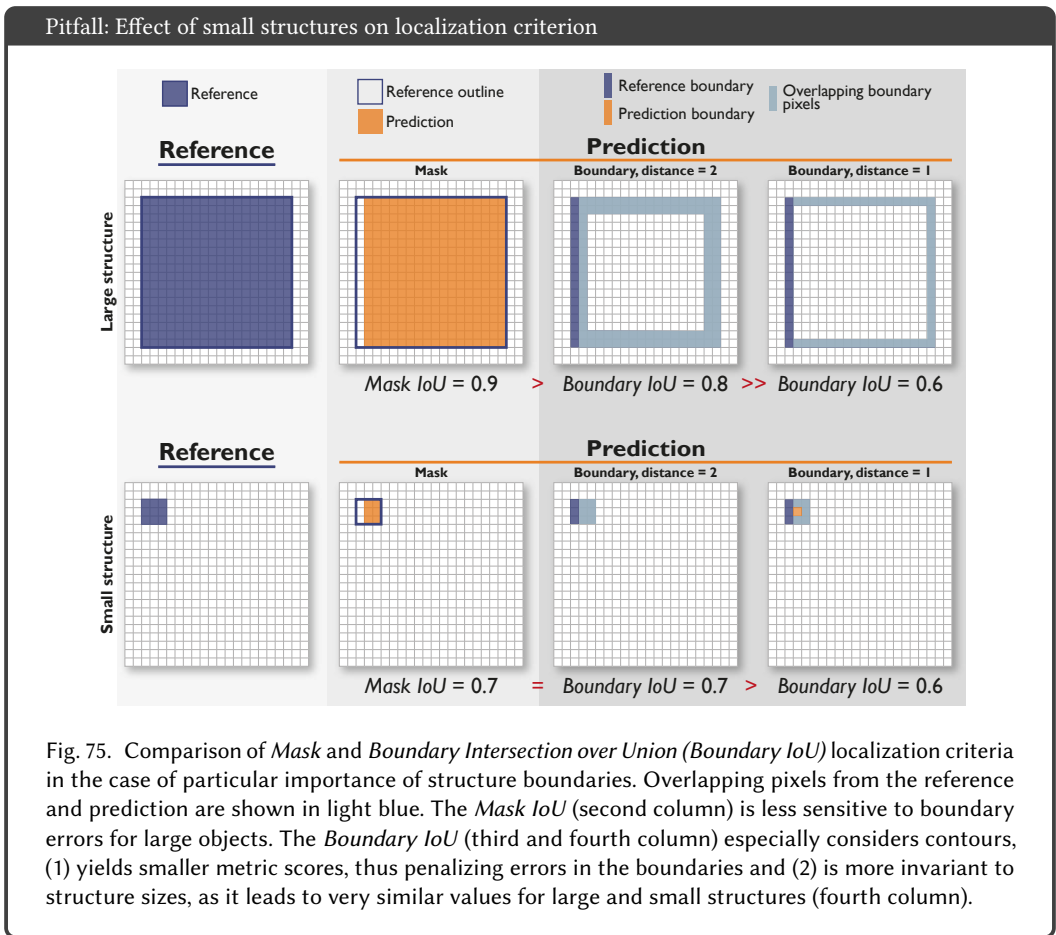
Fig. 73. In case of a prediction assigned to multiple reference objects, an assignment strategy needs to be chosen. This may be based, for example, on the *Intersection over Union* (IoU) >0.5 strategy, which may end up with a heavy penalty (two False Negative (FN) and one False Positive (FP)). Another option is to use the *Intersection over Union* (IoU) >0.5 strategy, which examines whether the prediction was successfully assigned to the reference objects. In an additional step, the "non-split errors" will be penalized. Used abbreviations: False Negative (FN), False Positive (FP) and True Positive (TP).

Possibility of disconnected structures. The *Box IoU* is sometimes employed despite access to pixel-mask annotations. A possible explanation is that researchers want to phrase their problem as an object detection problem and then apply the most commonly used validation methods. Such simplification might cause problems if structures are not well approximated by a box shape, or if structures yield multi-component masks, appearing to be disconnected. This may occur in the case of a tubular structure shown in a 2D tomographic image or a medical instrument occluded by tissue in an endoscopic image, for example. Fig. 74 provides examples of a complex diagonal (top) and a disconnected structure (bottom). Both box predictions yield a *Box IoU* larger than 0.3, and are thus counted as TP because of the chosen localization threshold. Nevertheless, *Prediction 1* is not hitting the actual object at all. This is due to the fact that the target structures are not well approximated by the bounding box, leaving many empty pixels in the boxes.

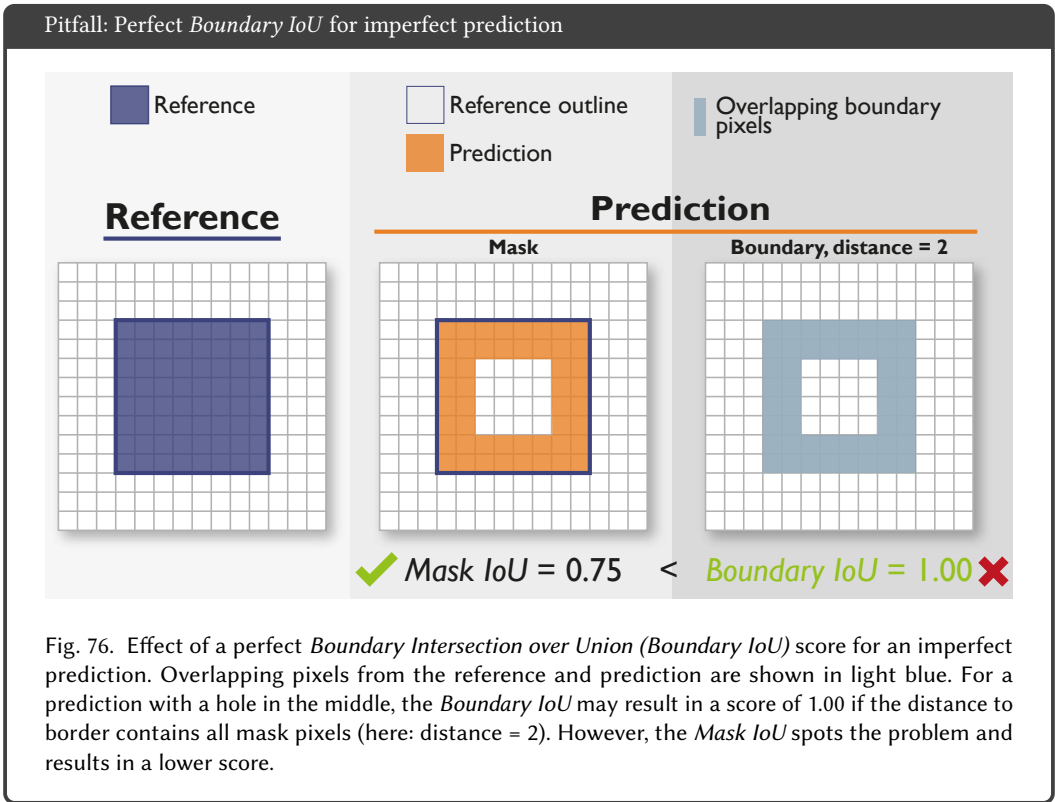


Effect of small structures on localization criterion. *Box IoU* and *Mask IoU* are not sensitive to structure boundary quality in larger objects (cf. Section H.3). This is due to the fact that boundary pixels will increase linearly (quadratically in 3D) while pixels inside the structure will increase quadratically (cubically in 3D) with an increase in structure size. In consequence, the *IoU*-scores tend to be higher for large objects compared to small objects. For this reason, localization criteria such as the **Boundary IoU** were designed.

Fig. 75 shows an example of *Mask IoU* and *Boundary IoU* for a large (top) and a rather small structure (bottom). In the case of the *Mask IoU*, the score drops substantially for the small structure, while the scores are more consistent for the *Boundary IoU* when comparing small and large structures. This pitfall also applies to segmentation problems in which the (*Mask*) *IoU* and *Boundary IoU* are applied as overlap-based metrics.



It should further be noted that the *Boundary IoU* is highly dependent on the chosen distance d , as illustrated in Fig. 75 (third vs fourth column). Similarly to the example provided in Fig. 62, the *Boundary IoU* can be fooled to result in a perfect value of 1.0. A prediction with a hole in the middle of the structure may result in a perfect metric score if the distance is chosen in a way that it incorporates all pixels of the predicted mask, as shown in Fig. 76 [19]. The *Mask IoU*, however, will be able to recognize the problem, as it completely measures the overlap between both structures. [19] propose to use the $\min(BoundaryIoU, MaskIoU)$ to resolve this issue. Please note that the same limitations also affect other distance-based measures, such as the *NSD* or *HD* metrics. This pitfall also applies to segmentation tasks.



Possibility of reference/prediction without the target structure and NaN handling. When validating an object detection problem per image rather than per data set, a reference or prediction image without the target structure(s) may become problematic as some metric values will turn into NaN due to division by zero errors (cf. Fig. 66). Fig. 77a shows potential scenarios for a validation per image categorized by the presence and absence of TP, FP and FN. Four occurrences of NaN are presented. To proceed with the validation, namely aggregating metric values for every image over the entire data set, a NaN strategy needs to be defined for every use case.

Pitfall: Not a Number (NaN) handling for empty reference/prediction

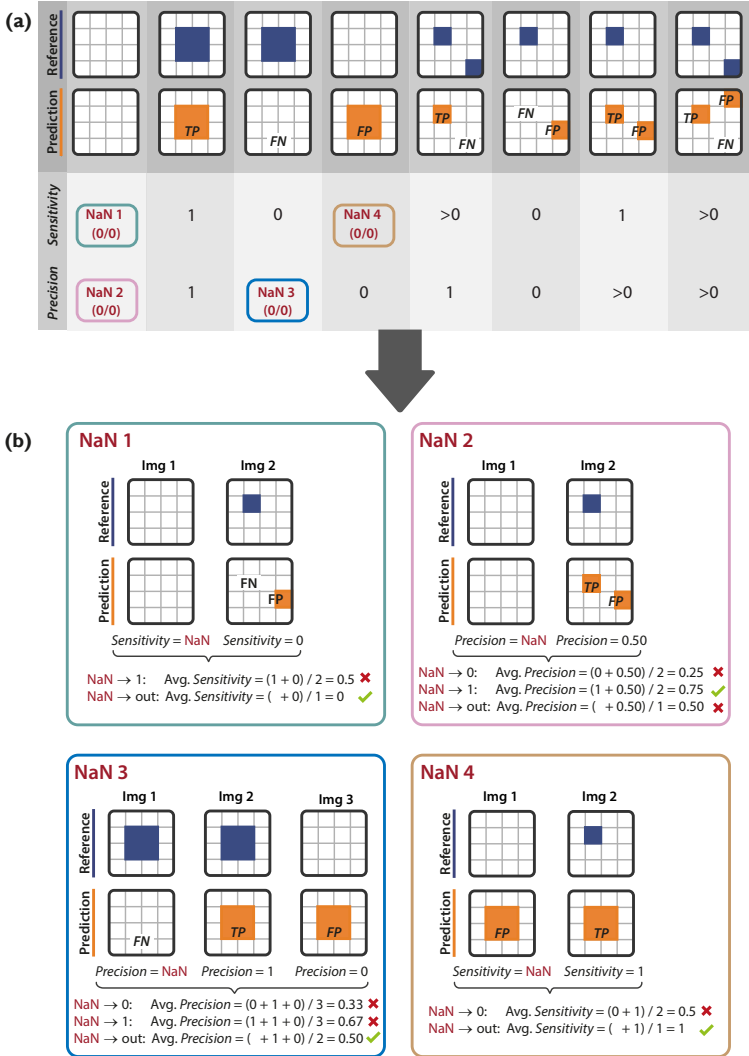


Fig. 77. Effect of handling a Not a Number (NaN) caused by reference or prediction without target structure(s) in object detection/instance segmentation problems validated per image. (a) Demonstration of how and when NaN can occur. Each column represents a potential scenario for per-image validation of objects, categorized by whether True Positive (TP), False Negative (FN), and False Positive (FP) are present ($n > 0$) or not present ($n = 0$) after matching/assignment. The sketches on the top showcase each scenario when setting "n > 0" to "n = 1". For each scenario, Sensitivity and Precision are calculated. (b) Effect of different NaN handling strategies based on different conventions for the aggregation across multiple images. Four examples are shown for the NaN scenarios from (a) (NaN 1-4). NaN 1 and 4: The intuitive penalization for FPs in "empty" images is already established by means of Precision scores (see NaN 4) and further penalization by means of Sensitivity is neither required nor appropriate. Instead, images without reference objects should be ignored when averaging Sensitivity scores over images. NaN 2: The intuitive penalization for FP in "empty" images is established when assigning a Precision of 1. NaN 3: The intuitive penalization for FP is established when removing images with FN and no FP from the aggregation of Precision scores.

Average Precision vs. Free-response ROC score. While the AP constitutes the standard metric for object detection and instance segmentation in the computer vision community, the *FROC* score is often favoured in the clinical context. In contrast to the AP, the *FROC* score takes into account the total number of images in the data set. As can be seen from Fig. 78, both data sets D1 and D2 will yield the same AP score, although data set D1 contains two images and D2 contains four images. The *FROC* score, however, will reflect that the number of images is different for both data sets and that data set D2 contains two images that do not contain any FP. Thus, the *FPPI* will be lower in data set D2, yielding a higher *FROC* score.

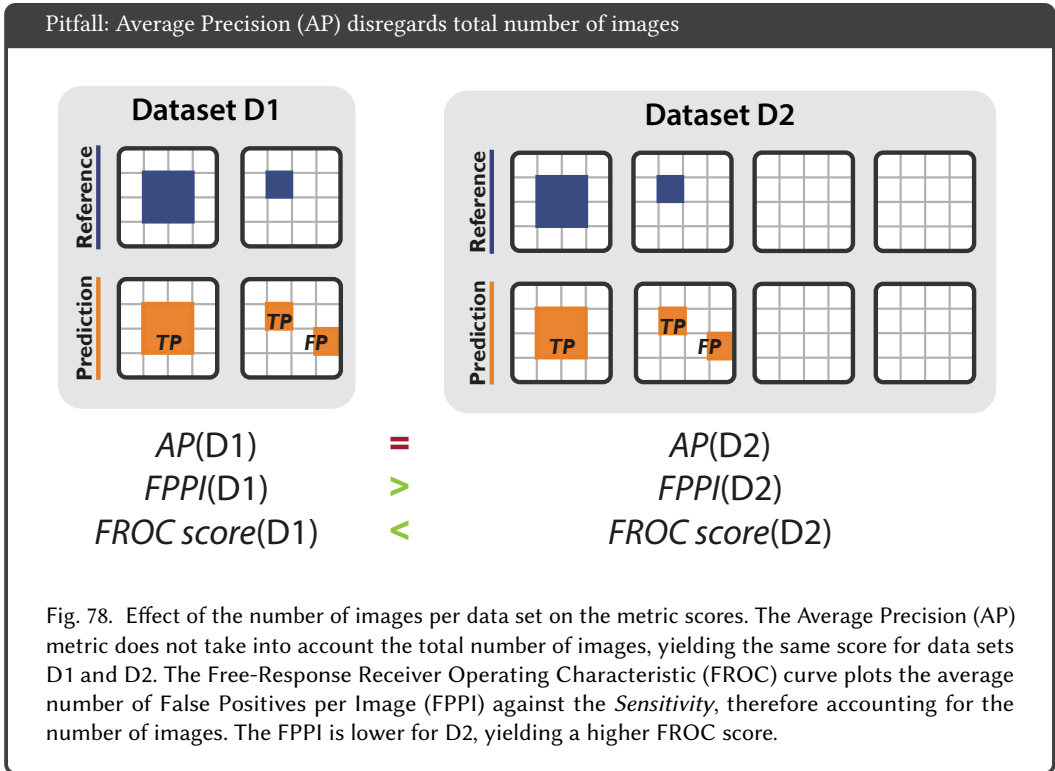


Fig. 78. Effect of the number of images per data set on the metric scores. The Average Precision (AP) metric does not take into account the total number of images, yielding the same score for data sets D1 and D2. The Free-Response Receiver Operating Characteristic (FROC) curve plots the average number of False Positives per Image (FPPI) against the *Sensitivity*, therefore accounting for the number of images. The *FPPI* is lower for D2, yielding a higher *FROC* score.

Multi-threshold metric-related properties. In the next paragraphs, we highlight some limitations of the multi-threshold metrics, exemplarily for the AP metric, which can be transferred to other multi-threshold metrics, such as the $AUROC$ [69]. By definition, multi-threshold metrics are ranking metrics, which rank the predicted class probabilities or confidence scores (cf. Fig. 39). They are not designed to reflect the calibration of confidence or class scores, as shown in the following examples. Please note that we disregard the concrete choice of the localization criterion here for simplicity.

Predicted class probabilities. The PR curve and the resulting metric score AP highly depend on the ranking of predictions, based on their predicted class probabilities or confidence scores. Small changes in the scores can therefore significantly change the metric value, as shown in Fig. 79. On the other hand, as long as the ranking remains unchanged among predictions, the predicted class probabilities themselves are not important for the result, although they should be (see Fig. 80).

Pitfall: Large effects of small changes in predicted class probabilities

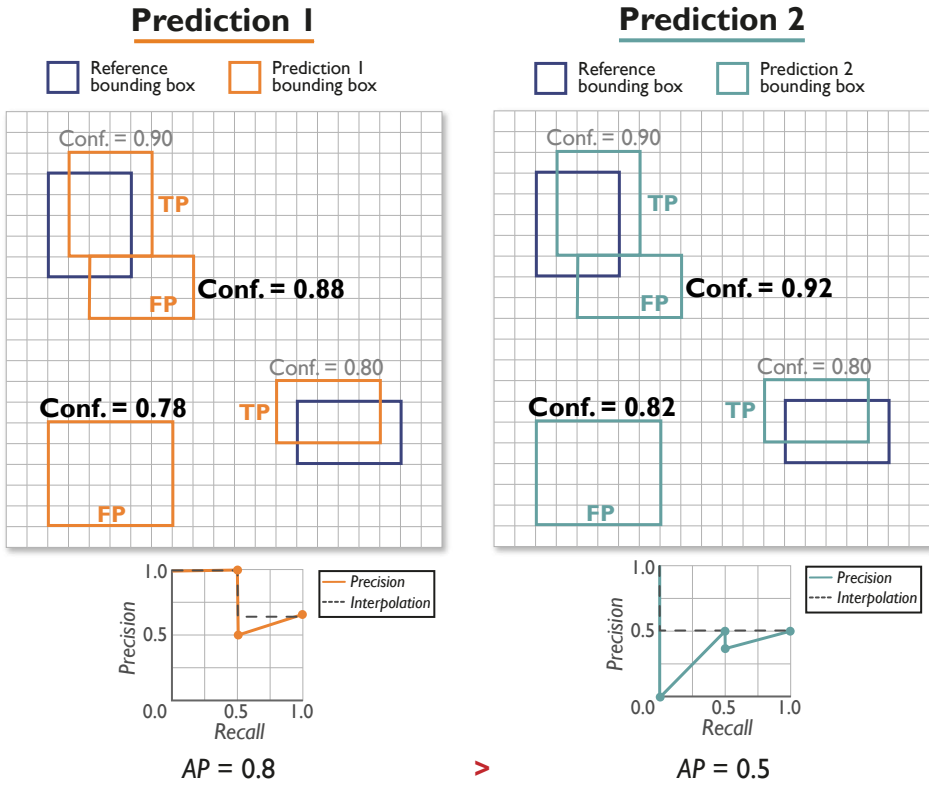
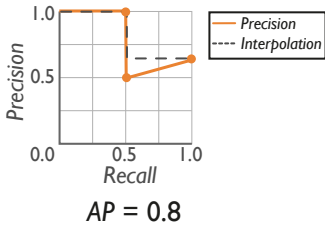
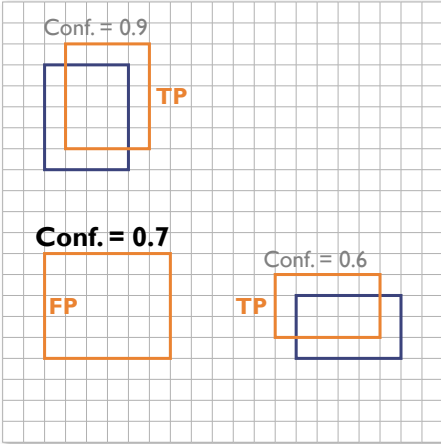


Fig. 79. Effect of small changes in predicted class probabilities. Reference bounding boxes are shown in dark blue. Predictions 1 and 2 detect the exact same bounding boxes with minor variations in their predicted class probabilities (represented by the confidence scores (conf.)). This leads to a different ranking and therefore varying Precision-Recall (PR) curves, curve interpolations (dashed grey lines) and resulting Average Precision (AP) scores.

Pitfall: Predicted class probabilities neglected within ranking

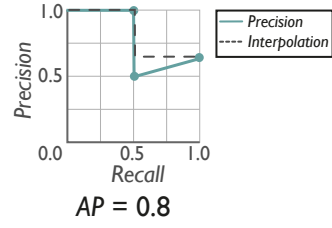
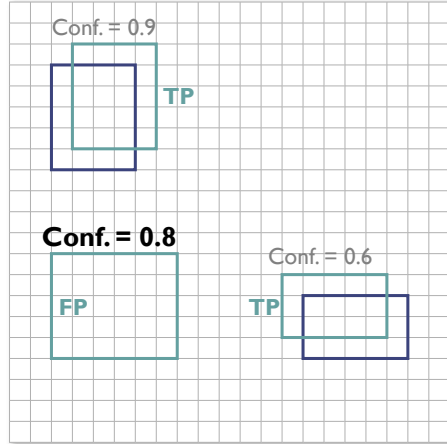
Prediction 1

Reference bounding box
 Prediction 1 bounding box



Prediction 2

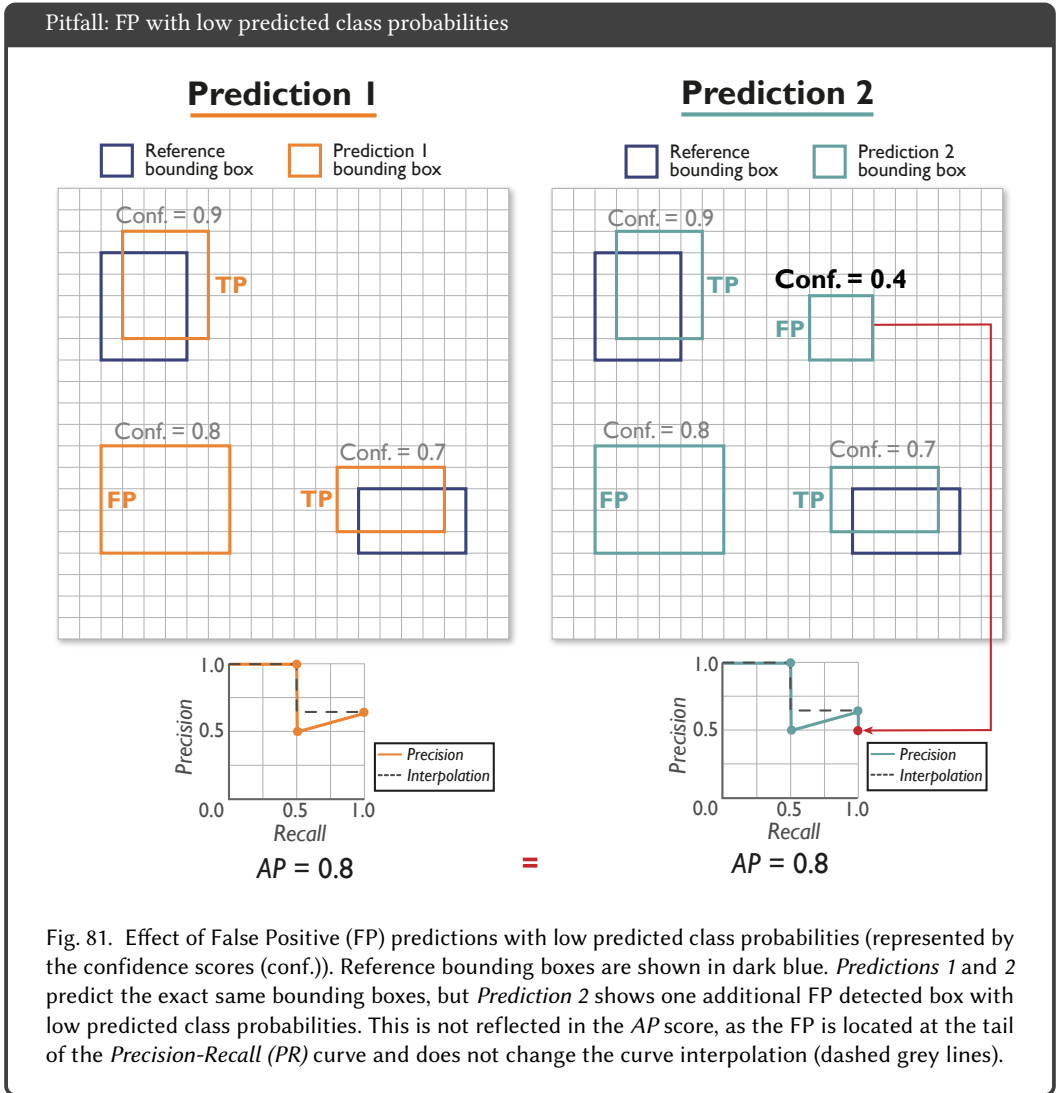
Reference bounding box
 Prediction 2 bounding box



=

Fig. 80. Effect of neglecting (the absolute values of) predicted class probabilities within the ranking. Reference bounding boxes are shown in dark blue. *Predictions 1* and *2* detect the exact same bounding boxes with variations in their predicted class probabilities (represented by the confidence scores (conf.)) that do not affect the ranking. Therefore, the *Precision-Recall (PR)* curves, curve interpolations (dashed grey lines) and resulting *Average Precision (AP)* scores are the same; the predicted class probabilities are hence unimportant within the ranking.

FP with low predicted class probabilities. False positive predictions with lower predicted class probabilities than the last correctly predicted reference, corresponding to the end of the *PR* curve, do not affect the *AP* scores. Fig. 81 shows two examples that are very similar, only differing in the number of wrongly predicted objects. *Prediction 2*, with two FP, performs worse than *Prediction 1* with only one FP. Nevertheless, the *AP* scores are the same for both models, given the low confidence of the second FP of *Prediction 2*.

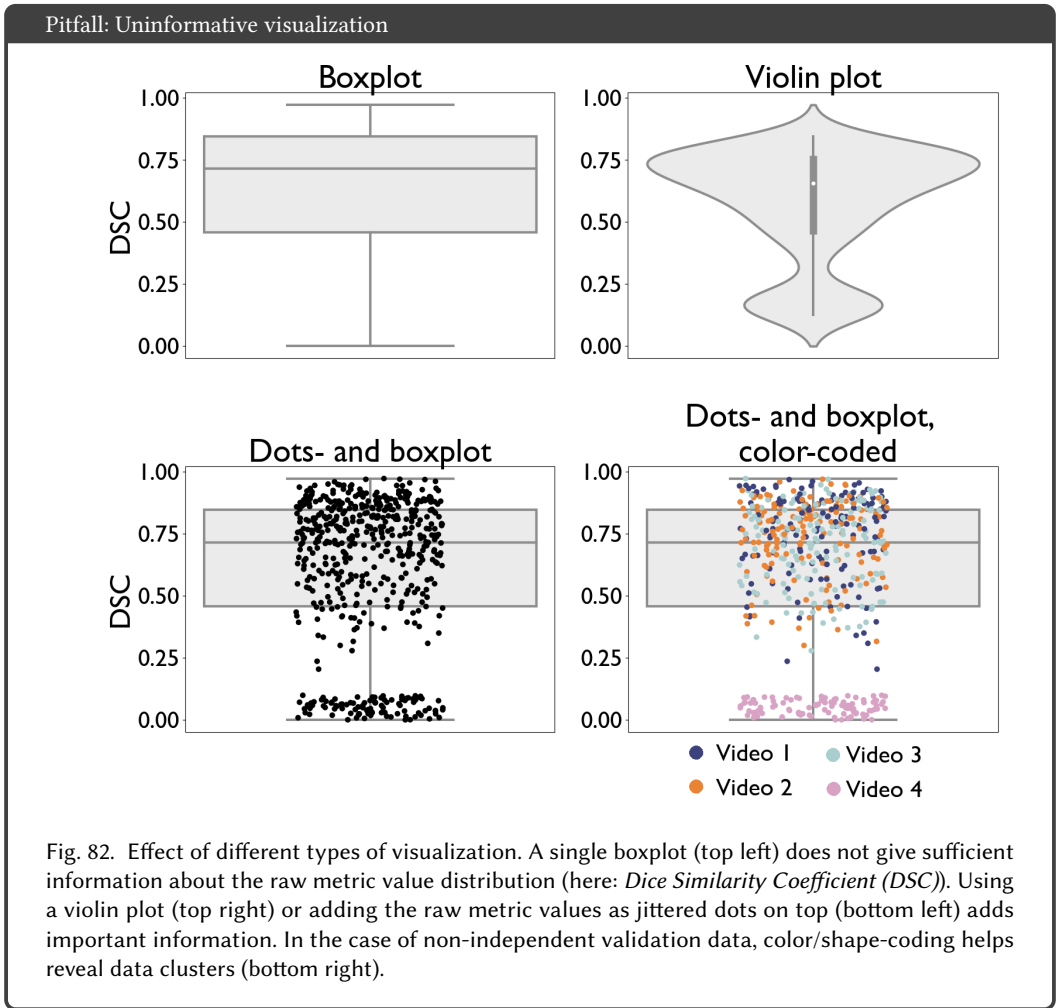


H.5 Pitfalls related to analyses and post-processing.

A data set typically contains several hundreds or thousands of images. When analyzing, aggregating and combining metric values, a number of factors need to be taken into account. Pitfalls in this step are primarily related to the following aspects:

- Uninformative visualization (Fig. 82)
- Metric aggregation for invalid algorithm output (e.g. NaN) (Figs. 83 and 84, F5.3)
- Hierarchical data aggregation (Fig. 85, F4.4)
- Aggregation in the presence of multiple classes (Fig. 86)
- Combination of related metrics (Fig. 87)

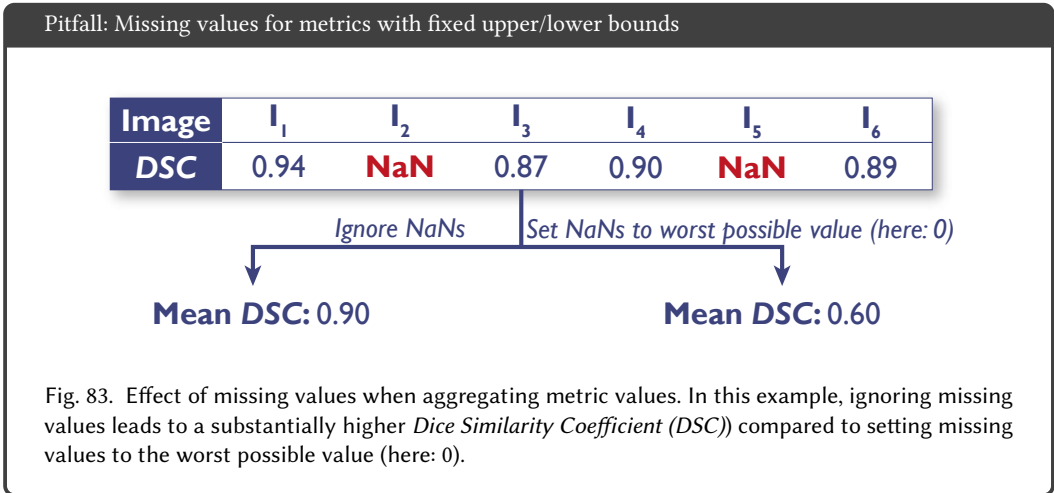
Uninformative visualization. Relying on only reporting aggregated metric scores may result in missing essential information on algorithm performance. Therefore, raw metric values (e.g. per image) should always be shown, for example in the shape of boxplots, as depicted in the top left of Fig. 82. However, boxplots will only provide information on some key descriptive statistics, like median or 1st and 3rd quartiles. Another choice can be violin plots, which further visualize the raw data distribution. The top right of Fig. 82 illustrates the multimodal distribution of the underlying data, invisible in the boxplot. Furthermore, using a violin plot and/or plotting the raw metric values for each data point on top (Fig. 82, top right and bottom left) will reveal the complete data distribution. In the example below, many values lie below the 3rd quartile, although the box looks tight. Nevertheless, even these two visualizations may hide important information. Assume a data set with metric values of four different videos. Color- or shape-coding the metric values by the video type (Fig. 82 bottom right) reveals a huge cluster of extremely low *DSC* values only affecting Video 4 (pink), which would have been hidden by the other two types of visualization.



Metric aggregation for invalid algorithm output (e.g. NaN). In challenges or benchmarking experiments, metric values are often aggregated over all test cases to produce a challenge ranking [57]. Missing data plays a crucial role when aggregating metric values and occurs primarily due to two reasons: invalid output of the algorithm or metric routine output resulting in NaN, and non-submission of single cases (by accident or even for cheating [72]). Figs. 83 and 84 illustrate why a strategy on how to handle missing values may be crucial.

In the case of metrics with fixed boundaries, such as the *DSC* or the *IoU*, missing values can easily be set to the worst possible value (here: 0). For spatial distance-based measures without lower/upper bounds, the strategy of how to treat missing values is not trivial. In the case of the *HD*, for example, one may choose the maximum distance of the image or normalize the metric values to [0, 1] and use the worst possible value (here: 1). Another possibility is to employ a case-based ranking scheme [57] and assign the last rank for every missing submission. Furthermore, aggregating with the mean may not be a good choice as results are unlikely to be normally distributed. Crucially, however, every choice will produce a different aggregated value (Fig. 84), thus potentially affecting the ranking. Another way of handling missing values would lie in rejecting the entire submission in a challenge.

However, metric values may also be undefined (NaN) if either reference or prediction or both are empty. In the case of empty reference and prediction, an undefined metric value (e.g. *DSC*) may be a desirable outcome and should therefore not necessarily be penalized.



Pitfall: Missing values for metrics without fixed upper/lower bounds

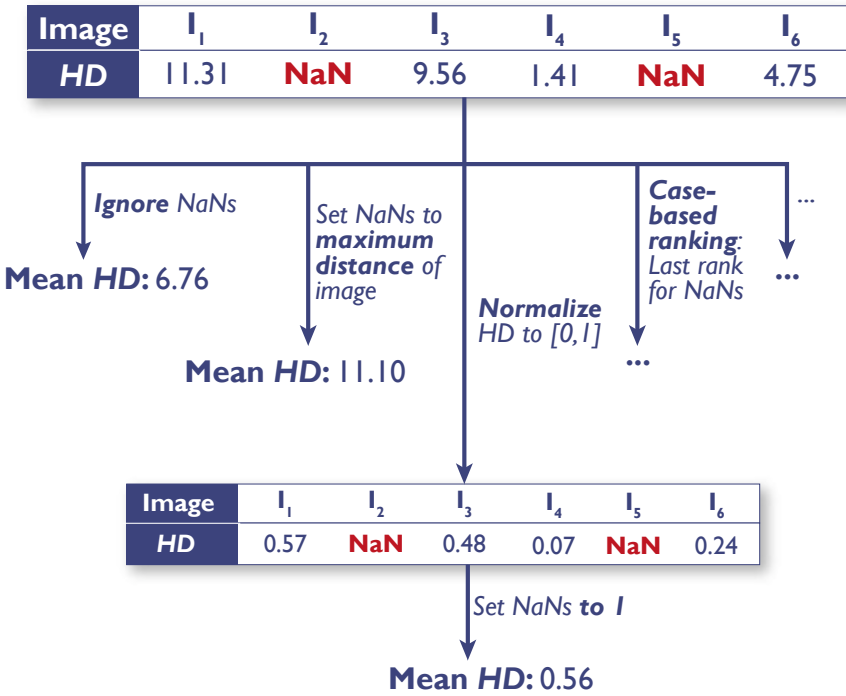


Fig. 84. Effect of missing values when aggregating metric values for metrics without fixed boundaries (here: Hausdorff Distance (HD)). In this example, ignoring or treating missing values in different ways leads to substantially different HD values.

Hierarchical data aggregation. Nowadays, most data sets are inherently hierarchically structured, meaning that the test cases are not independent. Data may, for example, come from several centers or hospitals, and for every center or even within one, different devices may be used for image acquisition, and images may be drawn from different subjects or patients. This should be kept in mind when visualizing and aggregating data points, especially if the individual tree nodes end in a large variation in the size of images. Fig. 85 shows an example of five patients with an unequal number of images associated with them. Just averaging all metric values for every image would result in a high average DSC of 0.8. Averaging metric values per patient reveals that the DSC values are much higher for *Patient 1*, overruling the other patients due to the high number of samples for this patient. Aggregating per patient first and averaging subsequently will resolve this issue.

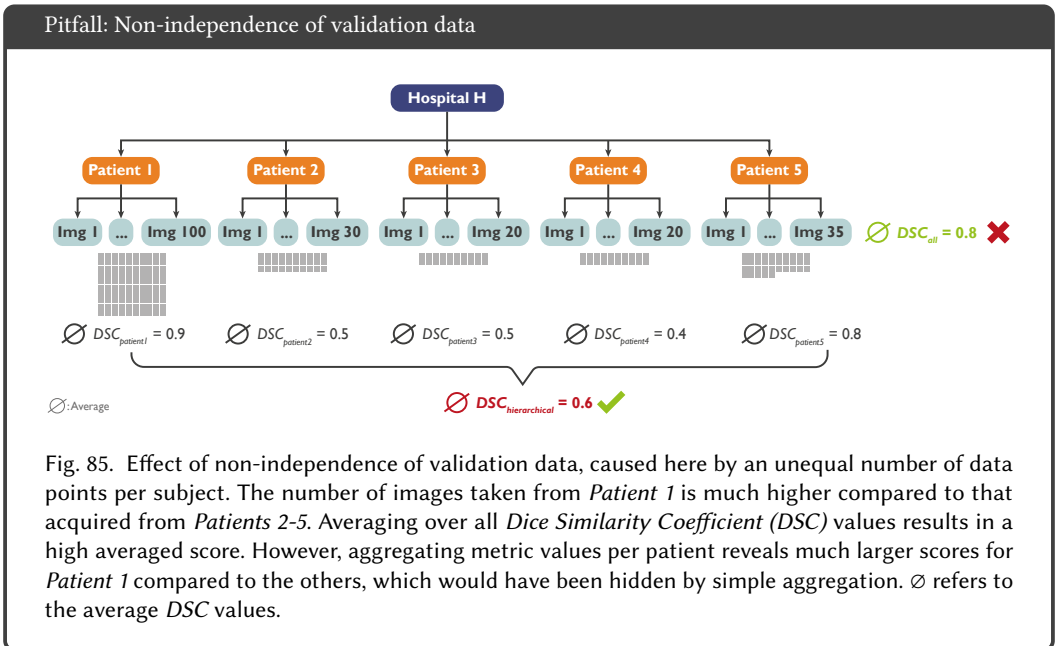
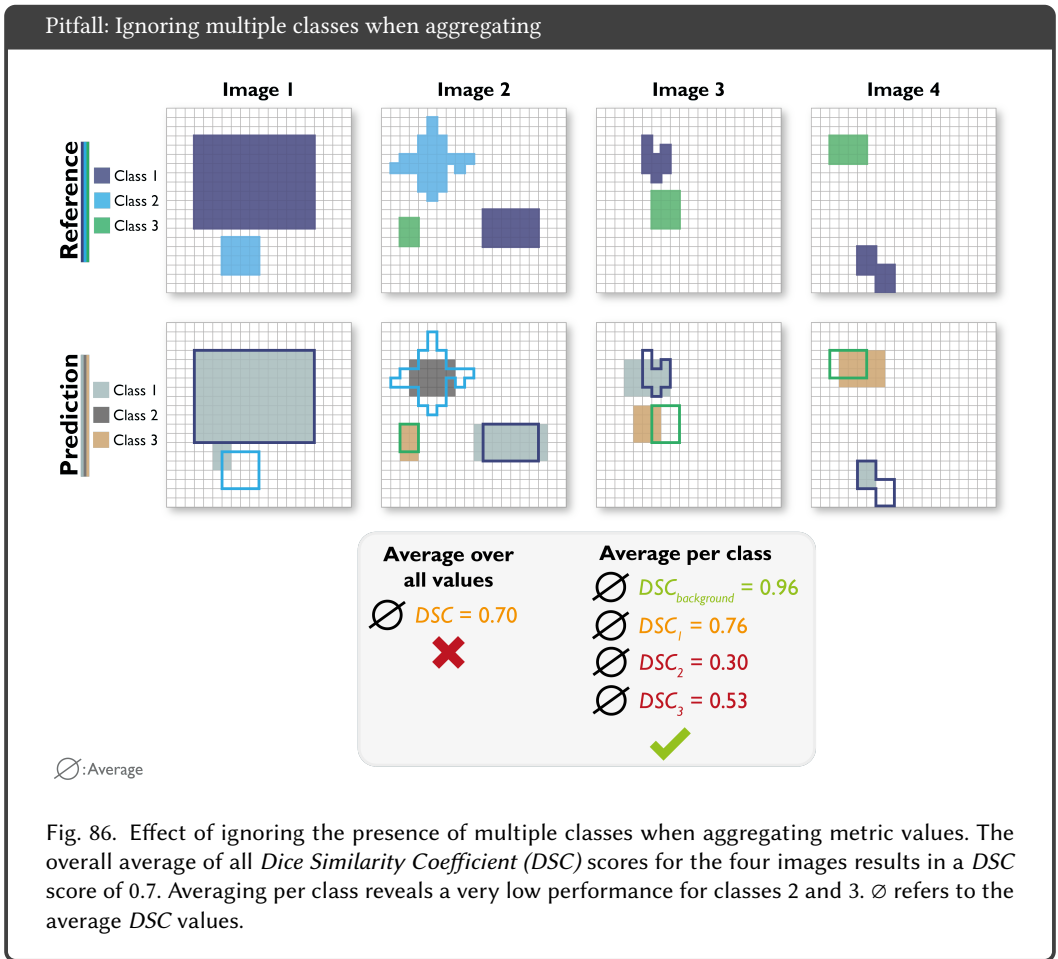


Fig. 85. Effect of non-independence of validation data, caused here by an unequal number of data points per subject. The number of images taken from *Patient 1* is much higher compared to that acquired from *Patients 2-5*. Averaging over all *Dice Similarity Coefficient (DSC)* values results in a high averaged score. However, aggregating metric values per patient reveals much larger scores for *Patient 1* compared to the others, which would have been hidden by simple aggregation. ∅ refers to the average DSC values.

Aggregation per class. Similar approaches should be chosen in the presence of multiple classes in a data set. The performance may differ significantly for the individual classes, as shown in Fig. 86. The background class in particular will result in a nearly perfect averaged *DSC* value, whereas the average scores for classes 2 and 3 are much lower. Aggregating over all values, not considering the class, would hide this information. An alternative approach to the problem lies in the application of metrics that explicitly handle class balance, such as using the *Generalized DSC* [88].



Metric combination. A single metric typically does not reflect all aspects that are essential for algorithm validation. Hence, multiple metrics with different properties are often combined. However, the selection of metrics should be well-considered as some metrics are mathematically related to each other [90, 91]. A prominent example is the *IoU* – the most popular segmentation metric in computer vision – which highly correlates with the *DSC* – the most popular segmentation metric in medical image analysis. In fact, the *IoU* and the *DSC* are mathematically related (see App. G.2) [90].

Combining metrics that are related will not provide additional information for a ranking. Fig. 87 illustrates how the ranking can change when adding a metric that measures different properties.

